1 OF 2

23234 UN

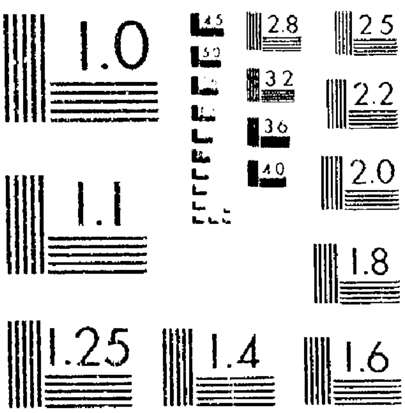

MICROCOPY RESOLUTION TEST CHART

NI

NASA CONTRACTOR REPORT 166186

Determination of Wind Tunnel Constraint Effects by a Unified Pressure Signature Method

Part 1: Applications to Winged Configurations

(NASA-CR-166186) DETERMINATION OF WIND TUNNEL CONSTRAINT EFFECTS BY A UNIFIED PRESSURE SIGNATURE METHOD. PART 1: APPLICATIONS TO WINGED CONFIGURATIONS Final Report, Oct. 1980 - (Lockheed-Georgia Co., N82-23234

Unclas G3/05 09847

J.E. Hackett
S. Sampath
C.G. Phillips

Lockheed-Georgia Company

CONTRACT NAS2-9883(Mod 3)
June 1981

NASA

NASA CONTRACTOR REPORT 166186

Determination of Wind Tunnel Constraint Effects by a Unified Pressure Signature Method

Part 1: Applications to Winged Configurations

J.E. Hackett
S. Sampath
C.G. Phillips

Lockheed-Georgia
Marietta, Georgia 30060

Prepared for
Ames Research Center
under Contract NAS2-9883(Mod 3)

NASA
National Aeronautics and
Space Administration

Ames Research Center
Moffett Field, California 94035

PRECEDING PAGE BLANK NOT FILMED

CONTENTS

Page

LIST OF FIGURES

LIST OF SYMBOLS

A	Least-Squares Influence Coefficient
$A_{R/F}$	Matrix of Influence Coefficients, (Roof-Floor)
A_{CL}	Matrix of Influence Coefficients, for the Determination of Tunnel Center-Line Interference Velocities.
B	Tunnel Breadth
B	Least Squares Column Vector (Sec. 2.5)
b	Vortex `an
C_L	Lift Coefficient
C_D	Drag Coefficient
$C_{M_{C/4}}$	Moment Coefficient about Quarter Chord Point
C_μ	Knee-blowing Jet Momentum Coefficient for KBF Model
D	Drag
H	(Fig 4.4) Total Head
H	(elsewhere) Tunnel Height
L	Lift
N	Total Number of Singularities
$\mathcal{N}$	Number of Observation Points
P_o	Free Stream Total Pressure
Q	Source Strength
q	Dynamic Pressure
U_∞, U_o	Free Stream Velocity
u, v, w	Velocity Components
v_{ij}	Influence Coefficient. Velocity Induced at j^{th} Observation. Point due to i^{th} Singularity.
v_j	Total Velocity Induced at j^{th} Observation Point.
V_j	Measured Velocity at j^{th} Observation Point

x,y,z	Cartesian Co-ordinate System
α	Angle of Attack
Γ	Vortex Circulation Strength
δ_j	Difference Between Measured and Calculated Velocity at j^{th} Observation Point
ρ	Density
σ_i	Strength of i^{th} Singularity

Subscripts:

G	Implies Ground
tot	Implies Total

Operators:

Δ	Demotes a Difference or Increment

Abbreviations:

BLC	Boundary Layer Control
CP	Center of Pressure
KBF	Knee-Blown-Flap
LV	Laser Velocimeter

Note: Symbols used in Section 2.6 are explained locally.

SUMMARY

A new, fast, non-iterative version of the "Wall Pressure Signature Method" is described and used to determine blockage and angle-of-attack wind tunnel corrections for highly-powered jet-flap models. The correction method is complemented by the application of tangential blowing at the tunnel floor to suppress flow breakdown there, using feedback from measured floor pressures. This tangential blowing technique was substantiated by subsequent flow investigations using an LV.

The basic tests on an unswept, knee-blown, jet flapped wing were supplemented to include the effects of slat-removal, sweep and the addition of unflapped tips. C_μ values were varied from 0 to 10 and free-air C_L's in excess of 18 were measured in some cases. Application of the new methods yielded corrected data which agreed with corresponding large tunnel "free air" results to within the limits of experimental accuracy in almost all cases. A program listing is provided, with sample cases.

The present report is the first of two parts: Part Two describes an extension to include jet-in-crossflow effects. A copy of the present report is retained in the Lockheed-Georgia Company Engineering Report Files. The identifying number is LG81ER0166.

PRECEDING PAGE BLANK NOT FILMED

ACKNOWLEDGEMENTS

The authors wish to express their sincere thanks to

Sherry Bartley, who prepared the figures;

Shelby Christophers and Louise Ballew, who typed the text;

Doug Lilley, for his help with data handling;

John Malone, for advice on inverse methods;

Bill Stevens, for the initial theoretical work and programming;

Rebecca White, for her help with data plots;

Derek Wilsden, who reviewed the text and who acted as a 'sounding board' on numerous occasions.

1.0 INTRODUCTION

1.1 Background

In any wind tunnel test, the basic requirement is to create a flow field around a test model which properly represents either free air conditions or, on occasion, the condition of flight near the ground. For conventional models, nominal tunnel velocity must be corrected in magnitude and direction to compensate for the presence of the tunnel walls. For V/STOL models these corrections are likely to be large enough to require special correction methods and the further complication arises that separation may be induced on a tunnel surface. If an in-ground condition is to be simulated the relative ground motion must also be considered: in flight, this motion will usually reduce the extent of a ground separation (if present) but will not necessarily eliminate it.

Within the above terms-of-reference, three distinct but related test needs may be identified:

(a) the need for improved correction methods, particularly for blockage effects, including the effects of highly three dimensional powered flows.

(b) the need to understand and either correct for or remove the effects of tunnel flow breakdown during tests to determine free air data.

and (c) The need firstly to understand and then to properly simulate the effects of ground motion during ground effects testing.

References 1 through 10 represent some ten year's work at Lockheed-Georgia on the above questions. As a result of this and the present work, the flow physics is now well understood and practical solutions are almost complete. To place the present work in perspective a review is presented below covering blockage experiments, software development, angle-of-attack correction and ground or tunnel floor separation phenomena as studied at Lockheed-Georgia during the 1970's.

Experiments on Wind Tunnel Blockage

The history of wall-pressure based tunnel blockage correction research at Lockheed is represented chronologically by References 5 through 10, or parts of these.

When conducting an investigation of ground effects on a knee-blown flap model (Ref 2) a substantial static pressure drop was noticed between the test section entry and the tunnel breather slots at the test section exit. The calibrated velocity, at the test section entry, was evidently significantly below the effective value at the model implying that the conventionally calculated model coefficients were too high. An obvious 'fix' was to define a model station reference static pressure equal to the mean of the test section entry and exit values.

This approach was applied to pressure data from new tests on a knee-blown flap model in the 30" x 42" tunnel and comparisons were made with datum tests in the Lockheed 16¼' x 23¼' tunnel (Ref 5). In the absence of balance data, C_L-values were estimated from pressure integrations. Only a basic, straight winged, slats-on configuration was tested. These pilot studies showed significantly improved C_L correlations, between tunnels, when the new reference static correction procedure was employed.

A fuselage containing a three-component balance and optional, unflapped wing tip extensions were added to the knee-blown flap model for the next test series (Ref 6). Test conducted in the 30" x 42" tunnel and datum tests in the NASA/AAMRDL 7' x 10' tunnel included wake flow as well as balance measurements. With the slats fitted, the flow measurements showed little wake distortion, relative to a corrected mainstream vector, and good force and moment correlations were obtained. However, with the slats removed the drag behavior in the small tunnel was totally different from that in the large tunnel, though the lift performance was comparable. Slats-off flow data were not taken but analysis of the drag data suggested that flow breakdown in the short test section of the small tunnel interacted in some way with the separated main wing flow and caused the jet sheet to separate prematurely from the flap upper surface. In addition to this problem, it was recognized in Reference 6 that the revised reference static method responded primarily to wake blockage and was inherently incapable of responding to solid or separation-bubble-induced blockage.

Reference 7 describes early Lockheed-funded work on what has become known as the "wall pressure signature method." As the name indicates, a series of pressures along the test section length is used to characterize the tunnel flow. Analysis of this "signature" yields not only individual estimates of solid/bubble and wake blockage but also corresponding axial velocity interference increments anywhere in the test section. The feasibility of the approach was established by means of tests on normal flat plates of various sizes tested in the Lockheed 16¼' x 23¼' tunnel. The data of Reference 7 were analyzed entirely by 'hand' methods, using look-up charts: it was a considerable time before the corresponding computerized version was ready for 'production' use.

From the work of References 6 and 7 it became clear that the 4-foot test section length of the 30" x 42" tunnel was insufficient. The tunnel test section was therefore reworked to 7-foot total length. Rows of permanent wall pressure orifices were added.

Reference 8 closely parallels Reference 6 but describes tests on a swept wing variant of the knee-blown-flap model. The straight winged model was retested, in the longer test section, and the 'drag flip back' anomaly disappeared. The correlations for the straight wing improved and those for the swept wing were good for attached-flow cases. Wall pressure signatures were measured but were not used for correction purposes. Nonetheless, they gave important insight into tunnel interference and tunnel flow breakdown phenomena.

Other, Lockheed IRAD-sponsored, tests at this time included work on spheres of two sizes in two tunnels and on flat plate wings of four sizes tested in the (now) 30" x 43" tunnel. Automation of the wall pressure signature method was completed in 1977 and its usefulness in application to automobile testing in the 16¼' x 23¼' tunnel was becoming appreciated. However, it could be used only off-line because its operation was somewhat slow.

Reference 9 collects together most of the previous data and analyzes it using the automated program, which it also documents. Data for normal flat plates, spheres, and idealized automobile, flat-plate wings and the unswept knee-blown flap model are all included.

Software Development

The initial objective of the computer program is to locate a source-sink pair, representing solid/bubble blockage and a wake-source, all on the tunnel axis, and determine their strengths so as to provide the best curve fit to the observed wall pressure signatures. This is essentially an inverse problem and the solution must be found iteratively with regard to the source and sink locations. A developed version of the previous look-up charts (Reference 7) is used, in tabular form, during this iteration. Having solved this inverse problem, the determination of tunnel interference effects is straightforward.

The period from 1975 to 1978 saw substantial improvements in program capability with regard to increased robustness and reduced run time. It was found that a good deal of data reviewing is required to reject 'bad' points, to interpret unusually shaped signatures properly and to achieve the best theoretical match to observed data. The earliest program ran about 30-seconds per data point, which is totally unacceptable for on-line use. The Reference 9 program requires about 3-seconds on a minicomputer and is much more robust than the early programs. A practical limit appears to have been reached in development of the method in its iterative form.

Reference 10 describes the most recent Lockheed research on the wall pressure signature method. An alternative approach to the iterative method is introduced in which multiple sources or sinks are employed at fixed positions. This method avoids iteration and a constant influence matrix may be used. A least-squares fit to the wall pressure signature may be achieved, when using the new program, by choosing fewer singularities than pressure data points. The direct method is an order-of-magnitude faster than the best iterative program. It can also accommodate unusually-shaped wall signatures for which the previous method must make approximations.

Angle-of-Attack Corrections

The sensitivity to angle-of-attack correction is either zero or weak in most of the correlations described above. It has been found sufficient to employ the methods of Williams and Butler (Reference 11) for the powered model tests or the classical, Glauert correction as quoted in Reference 12 in other cases. However as is pointed out in Reference 10, the development of a wall pressure signature method for angle-of-attack is desirable to afford consistency with the blockage corrections.

Reference 10 describes intitial studies of angle-of-attack correction by the wall pressure signature method. The general feasibility is established and a number of sensitivity studies are described. However, only limited examples are quoted which involve test data.

Ground or Tunnel-Floor Separation

References 1 through 6 deal predominantly with ground simulation in the wind tunnel. It is clear the the most realistic simulation should include the ground motion, using a moving belt or some alternative means of controlling the flow immediately above the tunnel floor. It is shown in Reference 3 that tangential blowing along the ground, from just ahead of the model, may be used successfully to simulate a moving belt. The criterion for blowing quantity, based upon the physics of the flow, is that skin friction at the ground shall be positive or zero everywhere. Reference 6 describes the development of a ground blowing system which employs feedback from ground skin friction sensors to determine the level of tangential blowing.

A blowing rig designed for ground simulation by tangential blowing (e.g. Ref. 4) may also be used to control tunnel flow breakdown. However, there is an important distinction between the two applications. It is shown in Reference 3 that, even with a moving ground, a spanwise vortex may be trapped between the wing and the ground. The appearance of a floor vortex during center-tunnel testing heralds the onset of tunnel flow breakdown and can never be a "correct" flow condition. We shall see later in this report that such a vortex can distort the flow seriously in the vicinity of the model and render the data uncorrectable. When used during center tunnel testing, we shall see that ground blowing should be used to destroy the floor vortex, if it occurs.

1.2 Some Theoretical Considerations

Selection of Flow Model

It is possible, if only in principle, to exploit the non-iterative, matrix approach described above by defining three-dimensional arrays of sources and vortices clustered in the vicinity of the model and its wake and solving for boundary conditions derived from wall pressures. (In the present work, the normal velocity condition is satisfied by using an appropriate image system.) However, such an approach would almost certainly encounter matrix conditioning problems.

The number of unknown source or vortex strengths is reduced greatly if knowledge of the model geometry - location, wing sweep, angle-of-attack etc - is exploited. This relieves the matrix conditioning problem significantly though, as indicated in Reference 10, some difficulties remain. The problem becomes more one of limiting the number of influence matrices which must be held ready for use.

Even after reducing the number of singularities, there are constraints on their geometry which must be recognized. For example, if measured axial velocity at the tunnel wall mid height is used as a boundary condition, the strength of a vortex at mid height can not be determined because it cannot affect the boundary points' axial velocity. Sources Q_1 and Q_2 or vortices Γ_1 and Γ_2 placed at altitudes $\pm h$ cannot be resolved separately because the boundary velocity depends only upon $(Q_1 + Q_2)$ and $(\Gamma_1 - \Gamma_2)$ respectively For this reason the inclusion of a vortex on the centerline or the inclusion of sources or vortices equally spaced above and below the centerline results in a singular influence matrix for mid-wall orifice locations. These considerations suggest some necessary rules for valid singularity arrangements.

Other rules are probably needed to complete a set which is also sufficient: further work is needed to identify these.

Uniqueness of the Interference Flow Field

The constraints above reduce the permissible number of singularities, they restrict their location to the general area of the model and it's wake, they introduce some geometric properties related to the model itself and they introduce certain restrictions intended to avoid singular influence matrices. Even within these constraints a considerable number of possible arrangements of singularities remains, particularly with regard to their number and spacing. The details of the configuration selected will affect the singularity strengths but the implications in relation to the calculated interference velocities are not immediately clear.

Experience suggests that the interference flow field may be relatively insensitive to the fine details of the flow model. For example, a study is reported in Reference 10 in which the original source-source-sink, variable geometry formulation of the present problem was set up in non-linear equation form. A range of solutions was found, with widely varying geometry, and an interference velocity profile along the tunnel axis was calculated for each. Though the interference curve certainly was not unique, the spread between the individual solutions was acceptable in engineering terms.

Interpretation of the Interference Flow Field

Having solved the inverse problem, as indicated previously, and having defined interference velocities at locations of interest on the model, what remains is to determine their effects. This subject is discussed in detail in Reference 10. If the maximum benefit is derived from the wall pressure signature method, wind tunnel models may be sufficiently large that interference gradient corrections need to be considered. If the pressure gradients are nearly constant it usually will be possible to use standard gradient correction ("buoyancy") methods. If only surface pressure measurements are to be corrected, a "local mainstream" concept has been found to be effective in correcting for blockage (Ref 10). Beyond these, a method must be found for distributing the forces over the model so that moment corrections, in particular, may be made on the basis of the local conditions which apply to individual model components. Though an experimental approach is a candidate for this, and is used occasionally, a better choice is probably a simple analytical model of the configuration concerned.

Once a high-induced-gradient field has been defined - by whatever method - it is highly desirable to seek out and exploit such flow models as are available for the configuration concerned. A close interface with the "customer" is likely to be very beneficial in this regard.

Impingement Cases for Powered Flows

Even if the vortex which occurs ahead of floor impingement is removed by floor blowing boundary layer control, as described in sub-section 1.1, there may still be sufficient flow distortion to make data correction difficult, if not impossible. However, with the floor vortex removed, there is at least a reasonable change of defining the interference flow field over the model volume.

The calculation of the interference flow field for an impinging jet includes the determination of the effects of truncation as well as the effects of images. The vortex pair which might represent an impinging jet-in-crossflow bends sharply at the floor. To complete the interference calculation a contribution from the "missing" part of the plume downstream of this, must be added to the image effects corresponding to the section of plume within the tunnel. For flow continuity a further source effect, at the tunnel floor itself, may be needed to provide an appropriate envelope around the impinged jet fluid there.

With the interference flow field defined, a final consideration concerns jet path distortion. To first order, this will be a jet velocity ratio effect which should be adequately accommodated when the corrected mainstream velocity is defined at the model location. As the plume of an impinging jet is likely to be aerodynamically "stiff" the distortion due to gradients between the model and the tunnel floor are likely to be insignificant to within a short distance from impingement.

1.3 Layout of the Present Report

This is the first volume of a two-part report. The present volume deals with conventional, winged configurations and includes computer program listings relevant to the baseline, wall pressure signature program. It should be noted that the baseline program is not restricted to unpowered cases: it will accommodate jet-flapped configurations, for example. Volume II deals with the special topic of jet-in-crossflow modeling, as it affects wall pressure signature analyses.

Section 2 of the present report comprises a description of the new, direct version of the wall pressure signature method. This repeats some Reference 10 material, but this is included for ready reference in connection with the corresponding program listings.

Test hardware for recent knee-blown-flap (KBF) model tests is described in Section 3: jet-in-crossflow hardware details may be found in Volume II. The application of tangential blowing at the tunnel floor in KBF tests is described in Section 4.

Most of Section 5 comprises a presentation of results for several configurations of the knee-blown flap model and shows the correlations between 30" x 43" tunnel corrected data and constraint-free data. The main text of this report is completed by Discussion, Conclusion and References in Sections 6, 7 and 8, respectively. The Appendices include the appropriate program listings, user guides and data tables.

The present report is intended to complement and update Reference 9 which includes more detail on how the basic wall pressure signature method works together with practical details concerning its implementation.

2.0 THE GENERALIZED METHOD FOR WALL PRESSURE SIGNATURE ANALYSIS

2.1 Review

Reference 7 includes the original formulation of the problem of determining wind tunnel blockage via the solution of an inverse problem, starting with measured wall pressures. The general approach is to find the strengths of an array of line sources and sinks, located on the horizontal center plane of the tunnel, which when acting with the appropriate wall image set, produces the observed wall pressures. Having solved this inverse problem, tunnel blockage is determined by considering the image set acting alone. This approach is retained for the present work. An iterative solution which has been the standard approach to date is described, in its most developed form, in Reference 10. The more recent generalized, or matrix solution is also described in Reference 10 and sensitivity studies, to source or vortex span, phase etc. are also described.

The algorithms for influence coefficient calculations were relatively straightforward in the Reference 7 and 10 programs, since only spanwise line sources were involved. However the geometric requirements for swept wing and for jet-in-crossflow models are more demanding and a generalized, skewed, line-singularity algorithm has been prepared. The formulation for sources, horseshoe vortices and doublets and the corresponding algorithms are documented in Reference 14.

In the sub-section which follows, some of the more important characteristics of the matrix approach will be reviewed. Some recent findings concerning the choice of pressure sensing points will be discussed in sub-section 2.3. The effects of model offset and sweep, on measured signatures are reviewed in subsection 2.4 and a least-squares formulation of the basic problem is given in sub-section 2.5. The section concludes with a mathematical description of the generalized method.

2.2 Properties of the Influence Matrices and Their Inverses.

Figure 2.1 shows influence matrices for five-element line-source and five-element horseshoe vortex systems. The source matrices are, in fact, the sum of two others, corresponding to the direct influence of the line sources (an antisymmetric matrix) and the influence of matching, but opposite-sign, sources situated far downstream which are needed to satisfy continuity. Every element in the downstream source matrix equals 0.5. Each of the constituent matrices is singular, but their sum is not. Inspection of the tunnel floor and roof source coefficients (Figure 2.1) shows that, to avoid repeated rows in the influence matrix (which would make it singular) mean values of supervelocity increment must be determined from floor and roof orifices having the same x-location. However, sidewall data will generally be used for blockage estimation.

The vortex influence coefficients include vertical velocity components at the tunnel sidewalls, as denoted by arrows in the upper right portion of Figure 2.1. Though these components could, in principle, be measured and used to determine vortex strengths this is less practical than measuring solely static pressures. However, we shall see later that these velocities may influence pressures significantly and hence may represent a lift-dependent interference upon the blockage signature in some cases. The roof and floor vortex coefficients are of opposite sign, at a given x-location. When solving for lift interference, differences must be taken between supervelocity data determined at corresponding roof and floor orifice locations.

Figure 2.2 shows a wall influence matrix for sources (upper left) and a roof/floor influence matrix for vortices (upper right) together with their respective inverses, below them. In both cases the inverses include alternating-sign elements, indicating that the influence matrices are ill-conditioned. Though it has been demonstrated that correct singularity strengths are returned from computer-generated wall pressure signatures, it may be anticipated that, for 'noisy', real data, oscillating singularity strengths will be returned. Application of the method to tunnel data confirms this (see Ref. 10).

To complete a tunnel interference calculation, the source or vortex effects at the tunnel centerline are determined, with the central system removed. This step may be combined with the previous one by multiplying the center-tunnel interference matrix by the inverse matrix already determined. The product matrices are shown in the lower part of Figure 2.2. As before, the elements have alternating signs. Nonetheless, it is found that smooth interference distributions are generally obtained from experimental data.

Figure 2.3 shows results from pilot tests on an interim program, designated "MATCH", which employs the new matrix method. Corresponding results are also shown using the previous iterative program. The wall pressure signature fitted by "MATCH" passes through every experimental point: the iteratively obtained signature must approximate because it has fewer degrees of freedom. Though the source-sink geometries differ considerably, the two methods predict remarkably similar distributions of interference velocity.

2.3 Geometrical Considerations

Singularity Spacing and Location

In early studies, solutions were obtained using arrays like those shown in Figure 2.1. Though good interference prediction was possible (Fig. 2.3), wildly oscillating singularity strengths were obtained which were obviously unrelated to the flow physics. Closing up the arrays and placing them around the model location would, in principle, relieve this problem but in practice did not because the matrix became increasingly ill-conditioned. It is evident from Figure 2.3 that a satisfactory solution is obtained with a reduced number of singularities, provided that their placement recognizes the model and flow geometry appropriately. To satisfy the greater number of boundary conditions a least-squares approach is therefore required.

In addition to the downstream sink, matching each source in the test section matrix, a single, upstream source is also provided, explicitly, to allow the overall signature to shift vertically. This helps to achieve a better match to the experimental upstream asymptote.

Singularity Span

It has been found that the present, generalized method is fairly forgiving with regard to errors in estimating vortex or source span. It is stated in Reference 10 that span-solution within ±0.10B will hold errors to an acceptable level. This tolerance is fairly coarse and should not be too difficult to attain in practice. An exception, found recently, occurs when wall signatures measured in the tunnel corners are employed. These locations are significantly more span-sensitive than the central ones.

Wall Pressure Orifice Location - Peripheral Direction

Both theoretical and practical considerations arise in selecting the peripheral locations for wall pressure orifice rows. Figure 2.4 shows theoretical wall pressures, as a function of peripheral location in the bound vortex plane and far downstream of a horseshoe vortex in a wind tunnel. As expected, center-roof and center-floor locations give the largest pressure signals due to lift and so are good candidates, from a theoretical standpoint, for upwash interference predictions. The tunnel corner locations, 5 and 13, are much less sensitive*. While roof locations are usually very practical, there may be difficulties with floor orifices. In large tunnels there is the obvious problem of foot traffic but in all tunnels powered models may involve jets or jet sheets which impinge on the tunnel floor. Even if tunnel floor separation is controlled (see Section 4), jet-impingement may compromise the floor pressure signature.

Wall Pressure Orifice Location - Axial Direction

As indicated in Reference 9, Section 4, a test section length of about 1.5 times tunnel width is desirable to obtain adequate asymptotes to the pressure signatures. Orifice spacing should be smallest opposite to the model and it's immediate wake and may increase towards the test section ends where pressure gradients are less.

A generous number of orifices should be provided on the floor at and ahead of likely jet impingement locations, for monitoring ground boundary layer control. In jet-impingement situations, only the forward part of a floor-orifice row may be usable for tunnel interference estimation. In other situations a less dense selection from the whole row will be useful.

Vortex-Induced Upwash Effects at the Tunnel Sidewall

In broad terms, floor and roof orifice rows may be thought of as responsible for sensing vortex-induced flows and thereby providing data for upwash interference corrections. The sidewall orifices are used for estimation of blockage corrections.

Far downstream of the bound vortex, Figure 2.4 shows that upwash induced by the trailing vortex systems can have a significant effect upon sidewall pressures. This could affect the downstream asymptote of the sidewall pressure signature and cause an apparent increase in wake blockage. However the implicit assumption of Figure 2.4, that the trailing vortex remains horizontal, must be reviewed before any legitimate comment can be made regarding corrections for such cross flow effects.

*Note, however, that 13 becomes the proper location for the "sidewall" row in ground-effect tests. It is also needed for semi-span model tests.

In Reference 13, vortex roll-up calculations are described for wings situated in tunnels of various relative sizes and shapes. Though the central vortex sheet deflected significantly in some cases, the vortex centers drifted downwards very little. A more extreme, experimental result is presented in Figure 5.2 of Reference 8 concerning flow measurements behind a partial-span jet-flapped model. In this case the tip vortex path was horizontal and the flap vortex moved down significantly only at high C_μ. On this basis, it appears reasonable to assume that the trailing system remains essentially horizontal and to consider correcting sidewall pressure signatures for trailing vortex-induced upwash. Since there is no corresponding source effect on floor/roof increments due to lift, for centrally mounted models, it is possible to analyze these first and then correct the wall signature for vortex-induced crossflow, prior to setting up the blockage analysis. No iteration is required and the lift and blockage problems remain essentially uncoupled for unswept configurations.

2.4 Effects, on Measured Signatures, of Sweep, Angle-of-Attack and Model Offset

At zero angle of attack the addition of sweep to the source and vortex lines only affects the shapes of the velocity distributions at the tunnel surface and there are no "cross" effects such as vortex-induced apparent blockage or source-induced apparent lift. However, on pitching the swept system, these effects appear and must be considered. To interpret them, a relationship must be established between Q/BH and $\Gamma/\sqrt{BH}$, the respective normalization velocities for source and vortex-induced effects.

We may find the ratio of total drag to total lift for a line-source, line-vortex system as follows:

Lift = $\rho U_\infty \Gamma b$ where b is vortex span

Induced Drag = $\frac{\pi}{8} \rho \Gamma^2$

Profile Drag = $\rho U_\infty Q$

$$\text{Thus } \frac{D_{tot}}{L} = \frac{\frac{\pi}{8}\rho\Gamma^2 + \rho U_\infty Q}{\rho U_\infty \Gamma b} = \frac{\pi}{8}\frac{\Gamma}{U_\infty b} + \frac{Q}{\Gamma b} \qquad 2.1$$

At $(L/D)_{MAX}$ induced and profile contributions are equal so

$$\left(\frac{D}{L}\right)_{MIN} = \frac{\pi}{4}\frac{\Gamma}{U_\infty b} = \frac{2Q}{\Gamma b}$$

$$\text{Thus } \frac{2Q}{\Gamma b} = \left(\frac{D}{L}\right)_{MIN} \qquad 2.2$$

This permits us to interpret the source-strength, vortex strength relationship in terms of $(L/D)_{MAX}$. After some algebra, we obtain

$$\frac{Q}{\Gamma\sqrt{BH}} = \frac{1}{2}\,\frac{\left(\frac{b}{B}\right)\sqrt{B/H}}{(L/D)_{MAX}} \qquad 2.3$$

For the basic, knee-blown flap model, tested in the 30" x 43" tunnel, $b/B = 0.465$, $B/H = 1.433$

$$\text{so that } \frac{Q}{\Gamma\sqrt{BH}} = \frac{1}{2}\,\frac{.4651 \times 1.1972}{(L/D)_{MAX}} = \frac{.2784}{(L/D)_{MAX}}$$

$$= .0928 \text{ for } (L/D)_{MAX} = 3$$

$$= .0398 \text{ for } (L/D)_{MAX} = 7 \qquad 2.4$$

In a typical test case, for the knee blown flap model at $C_\mu = 2$ and low angle-of-attack, it was found that

$$\text{total } Q/U_\infty BH = 0.0338$$

$$\text{and total } \Gamma/U_\infty\sqrt{BH} = 0.5527$$

$$\text{so that } Q/\Gamma\sqrt{BH} = 0.0612$$

which is within the range in Equation 2.4.

Effects of Sweep and Angle-of-Attack on Wall Signatures

To demonstrate these effects, an example has been selected which is based upon the geometry of the swept, knee-blown flap model in the no-tips configuration. Effects at the tunnel wall are shown in Figure 2.5. Sweep and angle-of-attack effects will be discussed first.

Figure 2.5(a) shows that adding sweep to the line-source system shifts the axial velocity signature downstream. This is expected, since the same value of root (X/B) is used. The shift is insensitive to angle-of-attack, which is a welcome feature.

Vortex-induced axial velocities at the sidewall (Figure 2.5(b) are entirely dependent upon angle-of-attack. For typical relative strength values (Equation 2.4) it is apparent that peak "cross"-induced velocities at high angle-of-attack may be comparable with the direct, source-induced velocities. This probably explains the over-corrections for blockage noted in Reference 9 for swept-wings.

Vortex-induced upwash at the sidewall (Figure 2.5(c)) is comparable, in normalized units, with the source induced horizontal velocities (Figure 2.5(a)) - as might be expected. It is appropriate to relate the upwash to the mainstream velocity: this may be accomplished via the lift parameter C_{Lhb} (i.e. lift coefficient normalized on model span times tunnel half-height, in the present case). As a C_{Lhb} value of 2.0, which corresponds to incipient tunnel flow breakdown (see Reference 8) the maximum value in Figure 2.5(c) of 0.60 represents an upwash equal to about 25% of mainstream. When added vectorially to a unit mainstream, an increase of only about 3% occurs in the total vector. This would increase somewhat at the higher C_{Lhb} values permissible when ground-blowing is used; correction for the effect on blockage is probably desirable at this point.

Figure 2.5(d) shows that source-induced upwash at the sidewall location is an order-of-magnitude smaller than the source-induced axial velocity (Figure 2.5(a). When combined vectorially with the total axial velocity the effects of source-induced upwash will be negligible

Effects, at the Sidewall, of Change to Model Pivot Location

Curves are included in Figure 2.5 which show the effect of changing from the standard, mid-semi-span α-center to one at the wing root. The latter was used for swept KBF model tests. At 25-degrees angle-of-attack, this places the entire model approximately 7½% nearer to the tunnel floor. In most of the cases in Figure 2.5, the effects of this change are small. For Figure 2.5(d) this is also true because the overall effects are small (see above). However the effect on vortex-induced horizontal velocity is noticeable and it is apparent that offset effects must be included when calculating this correction to the blockage signature. This feature could be troublesome because it is angle-of-attack dependent.

Effects on Roof-Minus-Floor Signature

Figure 2.6(a) shows that the sum of the roof supervelocity and the floor countervelocity, induced by the vortex system, is substantial. Sweep reduces the peak velocity differences ($u_R - u_F$). It is found that the swept vortex curve, at zero angle-of-attack, is essentially unchanged by adding 25-degrees of incidence. The pivot location is consequently immaterial.

Source "cross" effects, on the "lifting" (roof-minus-floor) signature (Figure 2.6(b)) are small when relative vortex/source strength is considered. The fact that the forward pivot case produces less "cross" effect is, at first sight, surprising. This arises because the tunnel roof and floor centerlines are most affected by the central region of the source system, which remains on the tunnel axis for the forward pivot, but which moves towards the roof, with increase in α, for the mid semi-span pivot.

Ground Effects Testing

For in-ground-effect testing, either the tunnel floor ("ground") or the first ground image may be regarded as part of the model under test. The true "center-sidewall" orifice row is now situated at the foot of the tunnel sidewall and, strictly speaking, the blockage sensing orifice row should be located here. The roof orifice row remains correctly located but, in impingement-free cases, the tunnel floor row senses pressures which correspond to the with-blockage double-tunnel centerline velocity distribution.

Though it would be possible to set up the necessary computation schemes on the above, somewhat idealistic basis, it is more practical to consider the in-ground configuration as a below-center test when recovering source/sink and vortex strengths from the measured pressure signatures. In the second-stage analysis, interference velocities are then calculated at the tunnel floor location, rather than at the true tunnel centerline. Both the in-tunnel vortex/source arrays and their first ground images are omitted when calculating blockage and upwash interference.

Offset Models

Sometimes, the need arises to conduct a "center-tunnel" test with the model displaced vertically from the tunnel centerline. One reason for doing this would be to increase 'ground' clearance so as to reduce the severity of impingement problems for powered models. Ground-effects testing would, of course, involve below-center models. An orifice row situated at mid-sidewall "sees" not only the desired blockage effect associated with (for example) an above-center model but also a bound-vortex-induced counterflow which, wrongly interpreted, would appear as a negative solid blockage component. Distortion of the tunnel roof and floor signatures would also occur because of offset effects for both vortex and source systems.

A swept-wing model at angle-of-attack has several similarities to the off-center model. The front of the model, situated above-center, has some of the properties just described while the tips, below center, yield increments of opposite sign and shifted aft. The net effects are illustrated in Figures 2.5 and 2.6.

2.5 Use of Least-Squares Smoothing

Though the results of the pilot study (Figure 2.3) were encouraging, doubts remained about the response of the alternating inverse elements (Figure 2.2) to severe data scatter. Figure 2.7 explores this problem. A single point on a smooth, 'standard' wall pressure signature, designated 'A' in Figure 2.7(a), was perturbed upward and downward as indicated at 'B' and 'C'. Though the interference results from case A agreed quite well with those derived via the older, iterative method (Figure 2.7(c)), the consequence of perturbations 'B' and 'C' were serious (see Figure 2.7(b)). This provided strong motivation towards a least-squares approach.

Derivation of Least-Squares Equations

We define v_{ij} as the velocity induced at the j th observation point by the i th singularity and it's image system in the tunnel walls. Due to the complete set of N singularities the total velocity induced at the j th point is given by

$$V_j = \sum_{i=1}^{N} v_{ij} \, \sigma_i$$

where σ_i are the required individual singularity strengths. If the corresponding measured velocity $\mathcal{V}_j$ differs from the calculated value $\mathcal{V}_j$ by a residual amount δ_j we may write

$$\delta_j = | \mathcal{V}_j - V_j |$$

or

$$\delta_j = | \mathcal{V}_j - \sum_{i=1}^{N} v_{ij} \, \sigma_i |$$

The objective of the least squares approach is to minimize the net area between the $\mathcal{V}_j$ and the V_j curves as determined at the $\mathcal{N}$ observation points. To do this we minimize

$$\sum_{j=1}^{\mathcal{N}} \delta_j^2 \, .$$

i.e minimize

$$\sum_{j=1}^{\mathcal{N}} \delta^2{}_j = \sum_{j=1}^{\mathcal{N}} [V_j - \sum_{i=1}^{N} v_{ij} \sigma_j]^2 \tag{2.1}$$

To minimize this sum for a particular member k of the singularity set N, differentiate (2.1) with respect to σ_k and equate to zero. Thus:

$$\frac{\partial}{\partial \sigma_k}\left[\sum_{j=1}^{\mathcal{N}} [V_j - \sum_{i=1}^{N} v_{ij} \sigma_j]^2\right] = 0$$

or

$$\sum_{j=1}^{\mathcal{N}} 2[V_j - \sum_{i=1}^{N} v_{ij} \sigma_i] \ (-v_{kj} \cdot 1) = 0$$

which leads to

$$\sum_{i=1}^{N} \sigma_i \sum_{j=1}^{\mathcal{N}} v_{ij} v_{kj} = \sum_{j=1}^{\mathcal{N}} V_j v_{kj} \tag{2.2}$$

for

$$1 \leqslant k \leqslant N$$

The previous $\mathcal{N} \times \mathcal{N}$ equation set used to obtain an exact match at every observation point j is now replaced by an N x N set. N, the number of singularities, may be greater than, equal to or (more usually) less than $\mathcal{N}$, the number of observation points. The case $N = \mathcal{N}$ is not equivalent to the "MATCH" procedure described previously because the theoretical curve is fitted to the experimental data in a least-squares sense. On writing equation (2.2) in the form

$$[A_{ik}] \ [\sigma_i] = [B_k]$$

we notice that the elements of A_{ik} no longer can be identified simply as influence coefficients. The B_k elements are no longer simply observed velocity increments at k but are now weighted sums of all $\mathcal{N}$ increments.

Figure 2.8 is the least-squares equivalent of Figure 2.2, which generates an exact match. It is evident that the least-squares process has caused the upper source-sink matrix to become symmetrical about the leading diagonal and the largest element is now only 16-times the smallest, rather than almost 300-times. However the 'chequerboard' plus and minus pattern in the inverse matrix (center table) still remains. The lowest matrices, used to obtain centerline interference directly from wall velocity increments, do have a changed structure, however. It may be seen that, rather than the previous 'chequerboard' plus-minus structure (Figure 2.2), signs now alternate by column. However, the significance of this must be appraised via studies of some typical cases.

Examples of the Least-Squares Approach

Figure 2.9 repeats the example shown in Figure 2.7, which demonstrated the sensitivity of the "MATCH" approach to data scatter, but applies the above, least-squares solution to it. It is evident that the previous sensitivity to "noise" in the data has been largely eliminated.

Figure 2.10 is an example of a complex, double-peaked wall pressure signature, measured under tunnel flow breakdown conditions with no tunnel boundary layer control applied. Though the example is somewhat artificial for this reason, it shows that the restriction of the previous, iterative method to simple, single-peaked pressure signatures have been removed. This flexibility, the data smoothing capability and the reduction of maxtrix size afforded by the least-squares approach represent a significant advance over the previous approaches.

2.6 Mathematical Summary

Having reviewed the physics of vortex and source variables in the previous sections, we are in a position to set up the equations from which source and vortex strengths may be obtained. In the interests of clarity, these will be set up as direct influence rather than least-squares equations.

Notation

Subscript	i is the index for the source or vortex. j is the index for the sensing point.
Summations	I_Q is the number of source variables, equal to the number of wall X-locations. I_Γ is the number of vortex variables, equal to the number of roof/floor X-locations.
Superscripts	R Roof F Floor RF Roof value - Floor value W Sidewall
U,V,W	"Direct" influence coefficients, due to unit singularity i.e. due to Γ for rod/floor sensing points and due to Q for wall points.
u,v,w	"cross" influence coefficients including both axial and normal-to-mainstream effects.
C_p	Measured static pressure coefficient

Influence Equations

Equating measured and theoretical roof-minus-floor axial velocity components, we obtain

$$U_\infty \left(\sqrt{1 - C_{p_j}}^{\,R} - \sqrt{1 - C_{p_j}}^{\,F}\right) = \sum_{i=1}^{I_\Gamma} U_{ij}^{RF}\,\Gamma_i + \sum_{i=1}^{I_Q} u_{ij}^{RF}\,Q_i \tag{1}$$

Fig 2.6(a) Fig 2.6(.)

Equating measured and theoretical sidewall pressure coefficients taken as the mean of the two sides, we obtain:

$$U_\infty^2\, C_{p_j}^{w} = U_\infty^2 - \left[\left(\sum_{i=1}^{I_Q} U_{ij}^{w}\,Q_i + \sum_{i=1}^{I_\Gamma} u_{ij}^{w}\,\Gamma_i\right)^2 + \left(\sum_{i=1}^{I_\Gamma} w_{ij}^{w}\,\Gamma_i\right)^2 + \left(\sum_{i=1}^{I_Q} w_{ij}^{w}\,Q_i\right)^2\right] \tag{2}$$

Fig 2.5(a) Fig 2.5(b) Fig 2.5(c) Fig 2.5(d)

We note that equations (1) and (2), which will be needed to find Γ_i and Q_i are coupled and, because of terms four and five of Equation (2), nonlinear. However, we saw previously (Figure 2.5(d) and related discussions) that the fifth term is very small. Dropping this term makes (2) linear in Q_i and permits us to write (1) and (2) as:

$$\Gamma_i = \left[U_{ij}^{RF}\right]^{-1}\left[U_\infty\left(\sqrt{1-C_{p_j}}^{\,R} - \sqrt{1-C_{p_j}}^{\,F}\right) - \sum_{i=1}^{I_Q} u_{ij}^{RF}\,Q_i\right] \tag{3}$$

$$= \left[U_{ij}^{RF}\right]^{-1}\left[T_1 + T_2\right] \tag{3a}$$

and

$$Q_i = \left[U_{ij}^{w}\right]^{-1}\left[\left\{U_\infty^2\left(1 - C_{p_j}^{w}\right) - \left(\sum_{i=1}^{I_\Gamma} w_{ij}^{w}\,\Gamma_i\right)^2\right\}^{\frac{1}{2}} - \sum_{i=1}^{I_\Gamma} u_{ij}^{w}\,\Gamma_i\right] \tag{4}$$

$$= \left[U_{ij}^{w}\right]^{-1}\left[\left\{T_3 + T_4\right\}^{\frac{1}{2}} + T_5\right] \tag{4a}$$

If the w_{ij}^{w} term is also negligible, as for small span or low lift cases, (3) and (4) may be combined as

$$
\begin{bmatrix} \Gamma_i \\ Q_i \end{bmatrix} = \begin{bmatrix} U^{RF}_{ij} & u^{RF}_{ij} \\ u^{W}_{ij} & U^{W}_{ij} \end{bmatrix}^{-1} \begin{bmatrix} U_\infty \left(\sqrt{1 - C_{p_j}}^{R} - \sqrt{1 - C_p}^{F} \right) \\ U_\infty \sqrt{1 - C_{p_j}}^{W} \end{bmatrix} \tag{5}
$$

Solution of Influence Equations

For the general, large Γ, case the four sub influence matrices U^{RF}_{ij}, u^{RF}_{ij}, U^{W}_{ii} and u^{W}_{ij} and the upwash matrix W^{W}_{ij} are required. The form of equation (5) is less useful than it appears, not only because it lacks the w^{W}_{ij} correction but also because data is taken from two distinct populations (the roof/floor and sidwall signatures) which violates an underlying assumption of least-squares theory. For these reasons an iterative scheme has been adopted. This is illustrated in Figure 2.11. For convenience of layout the pressure terms, which are dominant, are shown last in the equations given in the figure.

3.0 TEST MODELS, RIGS AND PROCEDURES

3.1 General Comments

Many of the tests which will be described are essentially repeats of earlier tests (Reference 8) with augmented wall pressure instrumentation and, in appropriate cases, floor blowing to suppress tunnel flow breakdown. Since detailed descriptions of the models concerned have been given previously, particularly in Reference 8, only the main dimensions and details of any relevant changes will be presented here.

The models and rigs to be described comprise a simple, semi-span wing (subsection 3.2), the unswept and swept knee-blown-flap models (subsection 3.3) and wind tunnel instrumentation. All tests were conducted in the 30" x 43" low speed wind tunnel (the "MTF") at Lockheed-Georgia. The tests on the simple wing were conducted as part of an in-house, pilot program on upwash interference determination by the wall pressure signature method. Selected results are included in the present report for illustrative purposes.

3.2 The Simple Wing

Figure 3.1 shows a floor-mounted semi-span wing having a whole-wing aspect ratio of 3.0. It has an NACA0012 section and body-of-revolution tips. At the quarter-chord location, a 1-inch diameter bar extends downward through a clearance hole in the floor and attaches to a 3-component platform balance via a turntable which is used to set angle-of-attack. The bar may be replaced by a cylindrical balance which adds wing normal force, normal bending and end load to the lift drag and pitching moment measured by the platform balance. There is a clearance of approximately 0.10" between the wing root and the tunnel floor. The wing root is immersed in the tunnel floor boundary layer which is uncontrolled. Nonetheless, checks between data from the present wing and established finite wing theory show minimal performance degradation due to wing root effect.

The photograph of Figure 3.1 was taken through a new, laser velocimeter window which now comprises the back wall of the 30" x 43" test section. Part of the laser velocimeter may be seen at the right.

3.3 The Unswept and Swept Knee-Blown-Flap Models

Figure 3.2 was also taken through the new back window/wall of the test section. Though the swept knee-blown-flap model is the object of the photograph, a good view of the sting, model air supply, tunnel wall pressure orifice strips and the floor blowing slot are also obtained. Though the sting appears quite massive in this view, it should be noted that it is only about 2-inches wide. Most of it disappears into the floor at high angle-of-attack, as shown in Figure 3.3.

Figures 3.4 and 3.5 show the principal dimensions of the unswept and 25-degrees-swept knee blown flap models. For both models the tips and the slats are removable. The flaps are integral with the model, however and have upper surface angles of 76- and 60-degrees to the wing reference line respectively for the unswept- and swept-wing models. Further dimensional and sectional details are given in TABLE I.

3.4 Floor Boundary Layer Control

The boundary layer control rig used for ground blow-ng in previous tests (References 3, 6 and 8) was modified for the present test series by providing the capability to control three spanwise slot segments independently. Separate controls were provided for a central 8-inch span slot and two 6-inch segments to each side of this, for a 20-inch total, equal to the powered span as recommended in Reference 8. (Previous tests employed a 30-inch span slot). The change in supply arrangements made it necessary to revise the blowing slot detail to the form indicated in Figure 3.6. The slots had been situated above the middle of each plenum in earlier tests. Spacers were used at regular spanwise intervals to maintain the 0.067-inch slot height. More were required than previously because of a change from stainless steel to aluminum plenum covers.

Slot calibration procedures were as documented in Reference 3. As before, blowing rate was monitored using plenum static pressure taps.

3.5 Wall Pressure Instrumentation

Figure 3.7 shows details of wall pressure orifice locations used for tests on the knee-blown flap models. It should be noted that, for these tests, rows 3 and 5 were located on the upper and lower side walls and not on the roof and floor as shown in Figure 3.2. The orifice strips were moved after completion of the main tests to accommodate the laser velocimeter window.

Previous instrumentation comprised the sidewall orifice rows, 2 and 4 and the floor rows, 7 and 8. The latter rows were augmented for the present tests to give better resolution for identifying the ground vortex and hence flow breakdown. Rows 1, 3 and 5, in the tunnel corners, are new. Rows 1, 3, 5, 6 and the aft parts of 7 and 8 were made from aluminum strips, as may be seen in Figure 3.2. This, newer arrangement is preferable to orifices installed directly in the tunnel walls. General comments about pressure orifices, their location and their use may be found in Section 4 of Reference 9.

3.6 Tunnel Speed Control

The desirability of running at "corrected-q" during powered model tests is well known. In previous tests in the present series (References 6 and 8) this was achieved by sensing wall pressures upstream and downstream of the model at suitable locations and using a voltage divider network (Figure 3.5 of Reference 6) to interpolate for an effective pressure at the model location. Though this approach was quite successful, the fact that it relies upon only two pressures, rather than a whole pressure signature, is an obvious weakness. A specific shortcoming is that solid or separation bubble-induced blockage is likely to be underestimated.

For the present tests, the matrix method for blockage was available in time to permit on-line, whole-signature analysis to be used for speed control. A combined inverse and centerline interference matrix (similar to Figure 2.2, lower part) was applied to supervelocity data derived from the sidewall orifice rows. Tunnel 'q' and thereby C_μ was determined at the model using the on-line data reduction program and the tunnel speed control was adjusted until the desired C_μ was obtained. At the time of testing, no swept-bound vortex capability had been developed, so a straight wing matrix was used for the swept wing tests.

4.0 USE OF TUNNEL-FLOOR BLC TO SUPPRESS FLOW BREAKDOWN

4.1 Effects of Tunnel Blockage and Flow Breakdown.

The major problems confronting the test engineer in a powered model test have been, in order of decreasing importance: the difficulty in running "whole" C_μ's, the related difficulty in correcting forces for blockage effects on 'q', the difficulty in recognizing when flow breakdown effects have become excessive, the impossibility of correcting for them and, finally the problem of angle-of-attack correction with curved, powered wakes present.

It is believed that the studies described below represent the first successful attempt to solve the overall problem and identify the specific contributions, to model forces, attributable to the various effects mentioned above. The general approach will be to start with uncorrected lift data for the unswept knee-blown flap model, at high C_μ, and illustrate the effects of first correcting for blockage and then applying floor blc to suppress tunnel flow breakdown.

Blockage and Angle-of-Attack Corrections

Figure 4.1 shows $C_L \sim \alpha$ curves measured using on-line blockage corrections, as described in Section 3, at 'whole' C_μ values of 4.0 and 10.0. For comparison, "free air" curves are included (broken lines) which represent data measured in the 7' x 10' tunnel at NASA-Ames. The crosses in Figure 4.1 show C_L-values which employ nominal tunnel-q and uncorrected α values. Since corrected - C_μ is held constant, uncorrected C_μ values vary with α and are greater than the set values.

The circles represent data corrected for blockage, by the matrix method and for angle-of-attack, by the Williams and Butler method (see References 11 and 6 - section 5). We shall see in Section 5 that use of pressure signatures to determine angle-of-attack correction procedures almost identical results in many cases. Chained lines in Figure 4.1 connect corresponding uncorrected (crosses) and corrected data points. It is evident that although corrections are reasonably successful at lower angles-of-attack and C_μ-values, significant errors remain at high α's.

Use of Tunnel-Floor Blowing

The first tests on the unswept knee-blown flap model in the present series were used to develop ground-blowing strategy, recognizing that, in distinction to previous tests, the objective is to remove the ground vortex entirely, if possible. For the previous, ground-effect tests the objective was to establish a zero-skin friction condition at the ground.

Several candidate criteria were considered for determining the tunnel-floor BLC setting. However, it rapidly became apparent that the best procedure, was to eliminate entirely the negative pressures upstream of the jet impingement, as illustrated in Figure 4.2. Line printer symbol plots were made routinely of the center-floor static pressure signature and blowing was increased until the suction peak disappeared. No attempt was made to prevent jet impingement. At this point, no force correlations had been made and no flow field measurements had been attempted.

Figure 4.3 shows that the use of floor-blowing to suppress flow breakdown was remarkably successful in removing the residual errors in the Figure 4.1 lift curves. The errors in the previous blockage and incidence corrected data (circles), were virtually eliminated when floor-blowing was applied (triangles). Only for the last two points at C_μ = 10 was floor-blowing not fully effective: for these the limit of blowing capability evidently had been reached.

Figure 4.3 also demonstrates the significance of the distinction between ground boundary conditions appropriate to ground-effects as opposed to center-tunnel testing. The moving-ground points (pluses in Figure 4.3) give the correct result for a ground-effects case. It is evident that, for this case, a floor vortex should be present, rolling just above the moving ground. Because of this, some lift degradation would occur, relative to the corresponding free air case, in flight near the ground.

Magnitudes of correction and ground blowing quantities

Figure 4.4 shows typical blockage corrections, angle-of-attack corrections and ground-blowing C_μ values as a function of angle-of-attack at typical model C_μ values.

In the most extreme case, the tunnel-q setting was only 65% of the q experienced by the model. Angle-of-attack corrections appear to be less sensitive to C_μ and peak at about 4-degrees. Some scatter is evident in the ground-blowing C_μ settings but the general trends are clear. Through values of the order of 0.6, for the C_μ = 10 case, seem high they are a small fraction of the corresponding model blowing momentum coefficients. The blowing pressure ratio scale, to the right of the ground C_μ plot in Figure 4.4 does not apply to the C_μ = 10 case because this was obtained via a reduction in tunnel-q at constant model mass flow.

4.2 Flow Measurements Using the Laser Velocimeter

At the end of the planned test series on the knee-blown flap models, tunnel modifications were made to install the large window in the back wall of the test section. The laser velocimeter was then installed, in preparation for another test. The opportunity was taken to investigate the flow breakdown phenomena just described by making LV flow traverses near to the model center plane. To reduce "shadowing", the straight-winged model was reinstalled.

Figures 4.5 and 4.6 provide vivid evidence of flow breakdown, ahead of the model, at extreme model C_μ's and angles of attack. These are fixed-floor cases with no blc applied. It will be noted that the incident flow angles, just ahead of the model are quite low in Figure 4.5 and 4.6. Figures 4.7 and 4.8 show the same model conditions with blowing applied at the tunnel floor; The floor vortex has been pushed back almost to the impingement point in both cases and it's size has been reduced markedly. Just ahead of the model, the incident flow angles are much greater and the flow vectors are longer. These changes are consistent with the lift increases observed when floor blowing was applied.

The data of Figures 4.5 through 4.8 confirm the choice of the criterion, discussed previously, of increasing floor blowing until suctions below the floor vortex vanish.

4.3 Interpretation of Wall Pressure Signatures

Wall supervelocity data, derived from pressure signatures for the previous $C_\mu = 6.0$, $\alpha = 28°$ case, are shown in Figures 4.9 and 4.10. With no floor blowing (solid points) the floor vortex peak is readily identifiable in rows 7 and 5 and may contribute to the row 2 and 4 (i.e. sidewall) peaks. However, it appears that row 3 is not affected: its peak is too far forward to be vortex-related.

On applying blowing through the 20-inch slot (+ symbols), the suction peak disappears entirely at the center floor row 7 (by definition), but is not entirely removed at row 5, the lower sidewall, where there is no blowing to suppress it. It is also very likely that the second peak in rows 2 and 4 also marks the path of the "floor" vortex in the 20" blown-floor case.

Data with the slot-width reduced to 8 inches (triangles) shows that this is less effective than the standard, 20-inch slot. This is confirmed by force measurements.

Effects on Tunnel Corrections

It is disturbing that, under high-C_μ, high-α conditions, the main suction peak measured at the sidewalls (rows 2 and 4) may include a significant component caused by the passage of the floor vortex across the tunnel sidewall orifice row. However, the application of floor blowing shifts the vortex aft leaving what is probably the correct, solid/bubble-blockage induced first peak. Nonetheless, the wall pressure signature input to the tunnel blockage correction program still includes a second peak which is directly induced by a vortex, rather than being a true reflection of tunnel blockage.

Figure 4.11, taken from Reference 10, explores the effect of a dominant second peak upon tunnel centerline blockage interference. The experimental case (circles) is compared with an idealized case (triangles) with the second peak removed. As might be expected, there are significant changes in interference opposite to the second peak itself. However, the effect of the peak on the interference at the model location is surprisingly small.

Another effect of floor blowing, indicated to some degree in the row 3 data of Figure 4.10, is a general reduction in blockage interference. This is especially noticeable on applying BLC to the $C_\mu = 10$ case illustrated in Figure 4.12. In this case, it is speculated that, with no BLC applied, the separation streamline, from ahead of the floor vortex, rises to perhaps half the model altitude at its crest. Though the pressure signature blockage prediction method probably responds to this with appropriately located corrections of the proper sign, the total flow is far too distorted for any such corrections to be taken seriously. It is obviously better to get rid of the floor vortex, by applying blowing blc, than to try to correct for it's effects.

Additional Floor-Vortex Data

Figures 4.13 and 4.14 show the development of floor centerline pressure distributions, with angle-of-attack, at $C_\mu = 2.0$ and $C_\mu = 4.0$ respectively, with no floor blc applied. Figure 4.15 summarizes the data for $C_\mu = 4.0$ in terms of vortex and impingement location. Corresponding pressure data, at both C_μ's are presented in Figure 4.16.

The impingement point moves forward, as expected, with angle-of-attack (Figure 4.15). The maximum suction point remains an almost-constant distance ahead of impingement which suggests that vortex size is not very dependent upon model angle-of-attack. The first positive pressure peak gives a general indication of the location of the ground separation point, however the peaks are not well defined at the high angles of attack.

The development of peak pressures is shown in Figure 4.16. At $C_\mu = 2$ this plot gives a good definition of the angle-of-attack for the onset of floor separation, i. e. where the vortex and impingement curves diverge from the single, first positive peak, line.

Application of floor blowing eliminates the vortex suction lines in Figure 4.16. However there is very little change in the impingement pressure curves.

5.0 FORCE AND MOMENT CORRELATIONS

5.1 Checkout for a Simple Wing

Before embarking upon an investigation of powered-model corrections, it appeared desirable to test the new, wall pressure signature-based angle-of-attack correction procedure on a simple model. Appropriate tunnel pressure and model force data were therefore obtained in tests on the wing shown in Figure 3.1.

Figure 5.1 compares $C_L \sim \alpha$ curves corrected by the classical, Glauert method (+-symbols) and by the new wall pressure signature method (circles). Wall pressure signature - derived blockage corrections, which were small, were applied in both cases. It is evident that the new method provides angle-of-attack correction estimates slightly smaller than those determined via the 'Glauert' approach. However the generally good agreement gave confidence that the new method works properly.

5.2 Selection of Singularity Geometry and Iteration Procedure

Geometry of Vortex and Source Elements

The effects of sweep and angle-of-attack on tunnel influence coefficients were discussed in some detail in Section 2 from a theoretical standpoint. Figure 5.2 shows results from a practical application to the swept-wing, knee-blown, jet-flap model in a test at $C_\mu = 2$. Influence matrices corresponding to two different element geometries were used in Figure 5.2(a) to correct measured data (chain lines) for comparison with "free air" data (circles) measured in the NASA-Ames 7' x 10' wind tunnel.

The broken lines show corrections based upon the "correct" swept element geometry set at 15-degrees angle-of-attack for both bound vortices and sources. For the full lines, simple, unswept elements were used. the influence of geometry is clearly very minor for this model and tunnel combination.

Effect of "cross" terms

Figure 5.2(a) displays over-correction of the lift curve. It has already been mentioned that previous blockage over-correction may have been a consequence of neglecting the effects of vortex-induced upwash "cross" effects on the sidewall signature. The broken lines in Figure 5.2(b) show the results of a full iteration, as outlined in Figure 2.11, applied to the previous example. The differences between the broken lines and the full lines are the effects of "cross" terms. As anticipated, the over-correction of the lift curve has been almost eliminated.

Further examination of the "cross" terms revealed that w-squared term - i.e. wake upwash at the tunnel wall centerline is by far the largest. It is also found that the effects of these terms become excessive beyond $C_L = 2$ (see Figure 5.2(c)). This suggests that the horizontal trailing vortex model starts to fail because its' geometry is fixed. It may be shown that incremental C_L-corrections due to the effect of w-squared on blockage are proportional to C_L-cubed for a fixed-geometry wake. The system is very sensitive, at high C_L, to small changes in wake location.

5.3 Analysis of Angle-of-Attack Corrections

The corrections for the knee-blown-flap models are dominated by blockage effects and the sensitivity to errors in angle-of-attack corrections is quite small when plotted in conventional lift curve and drag polar form. The present angle-of-attack corrections will therefore be assessed in comparison with other predictions.

The wall pressure signature method provides a continuous distribution of $\Delta\alpha$ along the tunnel axis and an effective model position must be selected which characterizes its aerodynamics. In the present case, a fixed location at x = 0 has been selected for both unswept and swept wings, recognizing that other locations - such as varying load centers derived from C_M and C_L - could be considered.

For the swept wing, the choice of the correction location at the root quarter-chord could be questioned. However an aft shift in C.P. location on adding sweep did not occur because a lower flap angle was also introduced, during design, to improve the drag polar. In fact, the measured swept-wing C.P. lay slightly forward of that for the straight wing in most cases. Both lay between the quarter and three-quarter root chord locations and moved forward or aft depending upon the balance between wing and flap lift.

Figure 5.3 shows angle-of-attack corrections, $\Delta\alpha$ for the basic swept wing as a function of blockage-corrected C_L. The three parts correspond to a) unpowered or low-C_μ (i.e. BLC) conditions, b) moderate C_μ's with no floor impingement and c) cases with floor impingement, with floor blowing used. In all cases full-length roof and floor pressure signatures were employed, recognizing that errors arise from impingement regions.

Figure 5.3(a) shows that, as for the simple wing, wall-signature derived angle-of-attack corrections are slightly lower than the classical Glauert method but increase, per C_L, during and after stall. The hook-shaped $\Delta\alpha$ curves occur because the wing center-of-pressure moves back less rapidly with C_L after stall than it had moved forward prior to stall. It is known that the flap separates before the leading edge does at zero and low C_μ values.

At moderate C_μ values, with no floor impingement, Figure 5.3(b) shows smaller angle-of-attack corrections than both the Glauert (straight-wing) and the Williams-Butler estimates, even though the latter include a C_μ-related attenuation factor. However the increase with C_L is more rapid for the signature-based estimates than for the others. Though the C.P. does move forward with angle-of-attack in both the cases shown, the streamwise angle-of-attack gradients are insufficient for this to be the full explaination. Changing flow geometry may also be partly responsible. This is almost certainly true in the impingement cases, at C_μ = 4.0 and 6.0, shown in Figure 5.3(c). Here, the trends are generally similar to those of the previous figure but the levels are in better agreement with the other estimates.

Angle-of-attack corrections for the unswept KBF model (not shown) are generally greater than for the swept geometry as should be expected, and lie above the Glauert values increasingly up to $C_\mu = 2$. Above this, difficulties in signature analysis obscured the trends.

Comments

In the non-impinging cases described above, the $\Delta\alpha$ estimates by various methods are generally within a spread of about one-degree. Within this range, there is no experimental basis for saying which result is correct. Further refinement would probably require investigations of surface pressures - particularly leading edge suction peaks, in large and small tunnels. As mentioned previously, the consequences of these differences to the present force and moment data are not of major importance.

For impinging cases, the signature method indicates quite large $\Delta\alpha$ values at high C_L compared with the simpler theories. However, the theoretical model used in these cases is clearly inadequate because it fails to recognize impir nt. Improvement to the correction procedure is also required in these cases with regard to the roof/floor part of signature analysis.

5.4 Force and Moment Correlations for Unswept- and Swept-winged knee-blown jet-flap models.

Figures 5.4(a) through 5.7(c) show "free air" (broken lines) and corrected small tunnel force and moment data (points) for the four model configurations tested. In analyzing the data, 'whole' floor signatures were used in all cases except the straight wing at C_μ's of 4 and above, which failed to converge using this procedure. In these cases, the roof signature only was used for angle-of-attack correction, after removing blockage effects and doubling the roof perturbations. For the same reason, computation was stopped after the first pass for all configurations when C_μ was 4 or greater. All uncoupled solutions (i.e. independent angle-of-attack and blockage solutions) are designated by an asterisk in the C_μ table.

NASA CR 152,241 (Ref 9) documents the first attempt to apply the wall pressure signature method to the present configurations. Relative to the earlier, 'q-pot' corrections of CR 152,032 (Ref 8) the Ref 9 pressure signature results were disappointing because the correlation with "free air" data was significantly worse for high-C_μ cases. This occurred largely because of flow breakdown itself but also to some degree because the signature analysis of the Ref 9 iterative method can respond adequately only to classical, single-peaked pressure signatures.

Straight-Wing, With and Without Slats

The previous over-correction tendency of the iterative, Reference 9 method has been largely overcome as a result of the better flexibility of the present method. The chance for success is increased further by ground blowing, as was seen in Section 4. Figures 5.4 and 5.5 show that the present method improves upon both the Ref 9 and the Ref 8 approaches. The latter had a tendency to over-correct at high C_μ and under-correct at low C_μ. The overall agreement is now within the limits of experimental error.

Selected unblown ground data have been added to Figure 5.4 (flagged points) to supplement Figure 4.3 which is based upon interim blockage corrections and includes Williams-Butler angle-of-attack corrections.

The crosses in Figure 5.4, at $C_\mu = 1$, correspond to an "overblown" ground-blowing case in which the blowing was set as for $C_\mu = 6$, $\alpha = 30$. The $C_\mu = 1$ case does not include impingement, so the results show that blowing maybe left operative at a "set and forget", worst-case level without significant change to other data. Any q-changes, due to excessive floor blowing, are accommodated automatically via the wall pressure signature blockage correction procedure.

Swept Wing With and Without Tips Fitted

Relative to previous methods for correction the present swept wing corrections, Figures 5.6 and 5.7, show definite improvements in the drag polar correlations. However, lift curve slope still appears to have been over-corrected at or above $C_\mu = 4$, particularly for the with-tips case (Figure 5.7(a)). Pitching moments are less well corrected at $C_\mu = 6$ and 10 with the tips added (Figure 5.7(c)) but continue to agree well for the basic swept case (Figure 5.6(c)).

With the above relatively few qualifications it appears that the differences between the corrected and the free air data are not only within the experimental error band but have reached the point where possible corrections to the large-tunnel data should be reviewed. Rough calculations indicate that a large-tunnel C_L-value of 10 would be reduced by approximately 0.2 on correcting for blockage effects. This is of the same magnitude as the anticipated experimental error.

6.0 DISCUSSION

6.1 Aerodynamics

Overview

The methods described above bring to the wall pressure signature method new, more powerful and more comprehensive capabilities. These include an order-of-magnitude reduction in run time and angle-of-attack correction capability. During development, an effort has been made to make an effective trade between flexibility and ease of use. Some typical simplifications which have been included are the use of "whole" tunnel floor pressure signatures knowing that they contain impingement spikes, and the use of a constant effective model location, rather than one which responds to known changes in C. P. location. Despite these self-imposed restrictions the present methods have achieved good successes.

There were major questions, at the start of the present work, concerning the sensitivity of the wall pressure signature method to model geometry, particularly to sweep and angle-of-attack effects. Strong sensitivity would have made the method much less useful. In most respects insensitivity has been found not only to sweep and angle-of-attack but also to singularity spacing. Sensitivity has been found, however, to vortex wake location under high lift conditions. This will be discussed below.

Cases with jet-impingement and floor-blowing were the subject of an extension to the work planned originally. The use of floor tangential blowing and wall pressure signature based blockage corrections is a prerequisite to several of the discussions of impingement effects at high-C_μ which appear elsewhere in this report. However, theoretical modeling for cases with impingement is currently much less advanced than for cases without it. It is anticipated that jet-in-crossflow experience (see Part II) will help significantly when improving impinged-jet flow models. Further discussion of impingement modeling and its problems will follow that for non-impinging cases, below.

Wake Modeling for Non-Impinging Cases

AGARD Report 692 is a country-by-country review of wind tunnel correction methods for high angle-of-attack models. Repeated reference is made to the fact that tunnel-induced wake distortion must be considered, even for unpowered models, during the correction process. This appears to contradict the assertion, in sub-section 2.3, that wake vortex movement is not significant for the present KBF tests. While the present very high-C_L test results support the AGARD 692 assertions, an apparent paradox remains in the lower ranges, including most of the region of practical interest.

A vortex fair shed to the 50-percent semi-width positions in a rectangular wind tunnel, at mid-height, possesses the special property of being in equilibrium in the cross-plane. This may be confirmed by considering image vortices which give cancelling induced velocities at say, the right-hand trailer (see Figure 6.1). Members of a vortex pair shed near to these special points in the tunnel orbit them at a rate determined by vortex strength. This appears to be the situation for the basic KBF models, which span 46.5% of the width of the 'MTF' tunnel. This choice of model size may explain the paradox mentioned above.

The above special result for 50% semi-span models is not new, but it may have new significance for sizing and positioning models in tests at very high lift. For example, if a powered model's span must exceed 50% of the tunnel width, consideration of near-wake distortion could be used to locate an optimum, above-center location in the wind tunnel. This would also relieve the impingement problem. Further work in this area appears worthwhile.

Wake Modeling for Impinging Cases

The most significant property of an impinging flow of the present type is probably that the circulation and span of the downstream vortex wake no longer define the total lift on the model. This is because the existence of the floor stagnation point permits vortex lines to link to the tunnel floor. Mathematically, the connectedness of the region is changed by floor stagnation and closed circuits can no longer be drawn which define the model's bound vorticity. It is partly for this reason that an obvious step, of linking total vortex strength to model lift, was not incorporated as part of the angle-of-attack correction procedure in the present work.

The first problem encountered in setting up an impingement model is to determine how much of the bound vorticity trails downstream and how much joins to the tunnel floor via the jet. In unblown-floor cases, the standing floor separation vortex (Figure 4.5 etc.) tends to confuse the issue. Some tentative trials have been made using tunnel surface pressures, in blown floor cases. Tests with several combinations of model-to-floor and trailing vortex systems gave disappointing results. Tests at C_μ = 6 and 10, and usually 4.0, (Figures 5.4 through 5.7), include impingment, but were corrected using flow models which ignore it entirely, except via the fact that tunnel surface boundary conditions are satisfied. The success of the corrections is difficult to explain. While some necessary conditions for this success certainly can be identified in the present studies (for example, the use of floor blowing and signature-type methods) additional conditions are needed to complete a sufficient set. These are difficult to identify: the topic requires further work.

6.2 Signature Analysis

Inverse Methods

Recognizing that the first stage of signature analysis comprises the solution of a three-dimensional inverse problem, the methods in Section 2 were reviewed by a researcher in inverse wing design. It was found that conventional inverse techniques could be applied to the present problem. A paneled shape corresponding to the model and its wake might be found using tunnel wall pressures as the objective function, leading eventually to interference velocities. Further review reveals, however, that this approach would neither be sufficiently compact, nor sufficiently fast for practical use in routine wind tunnel correction work.

Flow Model Geometry

Though the insensitivity of the overall method to most model details, mentioned above, is interesting aerodynamically, its predominant importance lies in the simplifications it affords when the new methods are applied. If significant sensitivity to sweep and/or angle-of-attack (in particular) had been found, individual influence matrices might have been needed for (at worst) every data point. As it has transpired, relatively few matrices will be needed for any particular test.

While introduction of "cross"-term capability (Sections 2 and 5) lead to the above result, it also revealed sensitivity to wake location as discussed above. Within the present framework, the effect has been to limit quite severely the use of "cross"-terms to improve the results. New experimental and/or theoretical techniques are needed, to locate the vortex wake, before the capabilities of the present methods can be exploited fully.

Data 'Conditioning'

As for the previous, iterative method, the main task of data preconditioning is to subtract empty tunnel wall supervelocities from corresponding model-present data (see NASA CR152, 241, Section 4). A subsequent conditioning task, in the preent case, will be the removal of jet-in-crossflow induced velocity components when appropriate. The last conditioning stage, which concerns data smoothing, is embedded in the signature analysis itself both for the previous, non-iterative and for the present method. Though the latter employs a least-squares procedure for signature fitting, recent experience has shown this to be insufficient to prevent a blocked pressure orifice at the 'wrong' location from spoiling otherwise good data. A bad-point rejection filter, similar to that used in the earlier algorithm, is needed.

The impingement-case floor-signature is a heavy candidate for data conditioning. Currently, it is either accepted in full, at user option, or it is rejected in favor of 'doubled-up' tunnel roof data. This is not always a good alternative. However, there are a number of unanswered questions concerning how an impingement 'spike', for example, should be treated (e.g.: Is it theoretically correct to fair it out?). The answers to such questions should become more apparent as impingement modeling becomes better understood

7.0 CONCLUSIONS

Recent advances in wall pressure signature methods are described and used to estimate angle-of-attack and blockage constraint effects for several powered models in low-speed tunnel tests. Tunnel floor BLC was employed at high C_μ, to control flow breakdown. The combined techniques permitted successful testing well beyond usually accepted limits.

Use of Tunnel-Floor BLC to Control Flow Breakdown

Control of tunnel flow breakdown was accomplished using tangential blowing, along the tunnel floor, from a point just ahead of the model (Figure 3.6). Floor pressures were monitored to determine blowing settings. Subsequent flow measurements, with an LV anemometer, showed that the floor BLC had destroyed the vortex ahead of jet impingement.

Other observations include:

(1) Elimination of the floor vortex resulted in a large increase in upwash at the model location.

(2) Lift loss relative to 'free-air' conditions at high C_μ was eliminated.

(3) There was a significant reduction in tunnel blockage when floor BLC was used.

(4) Floor pressures may be used to monitor vortex destruction: floor blowing is increased until the suction peak ahead of impingement is eliminated.

(5) Overblowing is not harmful. An entire test may be performed, without detriment, with blowing set for "worst-case" conditions.

(6) The span of the blowing slot must be no less than the powered span of the model.

(7) The BLC needed in the present tests significantly exceeded that which would be provided by a moving ground matched to tunnel speed.

Use of Wall Pressure Signatures for Angle-of-Attack Correction

Tunnel roof and floor pressures were used to determine the strengths of horseshoe vortices, used to represent model lift effects, and thence angle-of-attack corrections. The technique was very successful for a simple wing but the corrections for powered models were less easy to interpret because in many cases strong blockage effects and floor impingement were also present. Some specific observations:

(8) $\Delta\alpha$ estimates for unpowered cases and for low-range powered cases were generally slightly lower than the classical 'Glauert' predictions.

(9) In the low- to medium-C_μ range, $\Delta\alpha$ values were comparable with Williams/Butler estimates (Ref. 11) at low angle-of-attack but increased more rapidly with α.

(10) At high-C_μ, $\Delta\alpha$ values determined from roof/floor pressures were generally high. Other tendencies were as just noted.

It is not possible to judge, from the present experiments, which of the $\Delta\alpha$ estimates was 'correct'. It is possible that the 'changing-δ' effect is related to changes in jet-sheet geometry as angle-of-attack is increased.

Combined Blockage and Angle-of-Attack Correction Program

New developments in the wall pressure signature method include:

o Angle of attack correction capability (see above).

o Use of fixed geometry, multi-singularity solutions which replace the previous, iterative moving-singularity procedure (Ref. 9).

o Application of a least-squares approach which gives both smoothed fits to experimental data and reduced matrix size.

o Use of a generalized singularity routine to generate influence coefficients for swept geometries at angle-of-attack, including "cross" effects for non-planar cases. The latter are also applicable to offset models.

o Generation of a combined blockage and angle-of-attack algorithm capable of handling non-planar "cross" effects (see Figure 2.11).

The following facts have emerged:

(11) The matrix method is almost an order-of-magnitude faster than the previous iterative method when applied to a given problem.

(12) The least-squares approach works well for smoothing 'local noise' but an additional point-rejection scheme is required for "rogue" points (blocked orifices, electrical 'spikes' etc). This has not been implemented.

(13) The least-squares approach cannot and should not be used when combining blockage and angle-of-attack solutions: iteration between these is effective.

(14) The use of swept singularities, at angle-of-attack produced little change relative to corresponding straight-wing results in the present applications (Figure 5.2(a)).

(15) For the cases investigated, the only significant coupling between lift and blockage solutions was via trailing-vortex-induced upwash on sidewall blockage signatures.

(16) The above coupling is significant at high C_L: incremental C_L's, due to wall upwash, are proportional to C_L-cubed.

(17) The coupling term is very sensitive to wake geometry. This was a limiting factor in the present application.

Application to Unswept and Swept-Wing Knee-Blown, Jet Flap Model Data

Application of the above methods gave generally improved correlations of corrected small-tunnel data with large-tunnel, free-air data. The level of disagreement is now comparable with experimental error. The following qualifications should be noted:

(18) Fully coupled solutions gave improved results, particularly in reducing overcorrection for blockage, only for C_μ less than or equal to 2.

(19) Above $C_\mu = 2$, the inclusion of the sidewall upwash term reduced the blockage correction too much. It is suspected that the assumption of an undeflected vortex wake may be responsible for this at mid-range C_μ's. Improved impinging-jet flow models are required for high-C_μ cases.

(20) The tendency to overcorrect lift curves at high C_μ, noted previously for the configuration with tips fitted (Figure 5.7(a)), has been reduced but not eliminated by the present methods. Drag polar and pitching moment correlations are quite good.

PRECEDING PAGE BLANK NOT FILMED

8.0 REFERENCES

1. Hackett, J. E.; and Justice, J. L.: The Aerodynamics of a Fixed Ground Plane for a Powered STOL Wind Tunnel Model. AIAA Paper 71-266 and *J. of Aircraft*, March 1973.

2. Hackett, J. E.; and Praytor, E. B.: Ground Effect for V/STOL Aircraft Configurations and Its Simulation in the Wind Tunnel, Part I - Introduction and Theoretical Studies. NASA CR 114,495. November 1972.

3. Hackett, J. E.; Boles, R. A.; and Praytor, E. B.: Ground Effect for V/STOL Aircraft Configurations and Its Simulation in the Wind Tunnel, Part II - Experimental Studies. NASA CR 114,496, November 1972

4. Hackett, J. E.; Praytor, E. B.; and Caldwell, E. O.: Ground Effect for V/STOL Aircraft Configurations and Its Simulation in the Wind Tunnel, Part III - Application to the NASA-Ames 40- by 80-foot Wind Tunnel. NASA CR 114,497, November 1972.

5. Hackett, J. E.; and Boles, R. A.: High Lift Testing in Closed Wind Tunnels. AIAA Paper No. 74-641, July 1974 (also see *J. Aircraft*, August 1976).

6. Hackett, J. E.; Boles, R. A.; and Lilley, D. E.: Ground Simulation and Tunnel Blockage for a Jet-Flapped, Basic STOL Model Tested to Very High Lift Coefficients. NASA CR 137,857, March 1976.

7. Hackett, J. E.; and Wilsden, D. J.: Determination of Low Speed Wake-Blockage Corrections via Tunnel-Wall Static Pressure Measurements. Presented at AGARD Wind Tunnel Design and Testing Techniques Conference, October 1975, in London, England. AGARD CP 174, Paper 23, October 1975.

8. Hackett, J. E.; and Boles, R. A.: Ground Simulation and Tunnel Blockage for a Swept, Jet-Flapped Wing Tested to Very High Lift Coefficients. NASA CR-152032, June 1977.

9. Hackett, J. E.; Wilsden, D. J.; Lilley, D. E.: Estimation of Tunnel Blockage from Wall Pressure Signatures: A Review and Data Correlation. NASA CR 152,241, March 1979.

10. Hackett, J. E.; Wilsden, D. J.; Stevens, W. A.: A Review of the "Wall Pressure Signature and Other Tunnel Constraint Correction Methods for High Angle-of-Attack Tests." Presented to the AGARD Fluid Dynamics Panel in Munich, FRG, May 1980. See also AGARD Report No. 692.

11. Williams, J.; and Butler, S. F.: Experimental Methods for Testing High Lift BLC and Circulation Control Models. In *Boundary Layer and Flow Control* by Lachman (ed), Vol. I, Pergamon Press, 1961, p. 395.

12. Pope, A.; and Harper, J. J.: *Low Speed Wind Tunnel Testing*. Published by John Wiley and Sons, 1966.

13. Hackett, J. E.; Evans, M. R.: Vortex Wakes Behind High Lift Wings. *Journal of Aircraft*, May 1971, pp 334-340.

14. Base, T. E.; and Hackett, J. E.: A Generalized Program for u, v and w Velocities Induced by 3-D Line-Source, Vortex and Doublet Element. Lockheed-Georgia Engineering Report No. LG80ER0138.

TABLE I

MODEL DIMENSIONS

Fuselage:		
length	31.55 cm	(12.42 in)
maximum width	4.46 cm	(1.76 in)
maximum height	7.76 cm	(3.06 in)
maximum cross-section	30.30 cm^2	(4.70 in^2)
equivalent diameter	6.21 cm	(2.44 in)
nose location	FS 0.00 cm	(FS 0.00 in)
fineness ratio	5.08	5.08
balance centerline location:		
water line	40.64 cm	(16.00 in)
butt line	0.00 cm	0.00 cm
reference point:		
fuselage station	0.00 cm	(0.00 in)
water line*	0.00 cm	(0.00 in)
butt line	0.00 in	(0.00 in)
Straight Wing:		
sweep	0°	0°
quarter chord MAC location:		
fuselage station	1.27 cm	(0.50 in)
water line	38.10 cm	(15.00 in)
butt line	12.70 cm	(5.00 in)
Swept Wing:		
sweep	25°	25°
quarter chord MAC location:		
fuselage station	6.64 cm	(2.71 in)
water line	38.10 cm	(15.00 in)
butt line	12.70 cm	(5.00 in)
Straight and Swept Wings:		
wing:		
area	517.00 cm^2	(0.556 ft^2)
aspect ratio (on nominal chord)	5.00	
span	50.80 cm	(20.00 in)
nominal chord (constant)	10.16 cm	(4.00 in)
quarter chord water line	38.10 cm	(15.00 in)
twist	0°	0°

Water line 0.0 is small tunnel floor with model on tunnel centerline.

TABLE I - Continued

MODEL DIMENSIONS

wing and tips:		
area	968.00 cm^2	(1.042 ft^2)
aspect ratio (on mominal chord)	6.00	
span	76.20 cm	(30.00 in)
nominal chord	12.70 cm	(5.00 in)
leading edge slat:		
area (projected onto maximum chord):		
wing only	103.00 cm^2	(0.111 ft^2)
wing and tips	155.00 cm^2	(0.167 ft^2)
span:		
wing only	50.80 cm	(20.00 in)
wing and tips	76.20 cm	(30.00 in)
chord (maximum)	2.03 cm	(0.80 in)
slot width	0.127 cm	(0.050 in)
deflection	80.00	
trailing edge flap:		
area (projected onto maximum chord)	234.00 cm^2	(0.252 ft^2)
span	50.80 cm	(20.00 in)
chord (maximum)	4.60 cm	(1.81 in)
slot width	0.041 cm	(0.016 in)
deflections (wing chord to flap upper surface)		
straight wing	76.00°	76.00°
swept wing	60.00°	60.00°

FIGURES

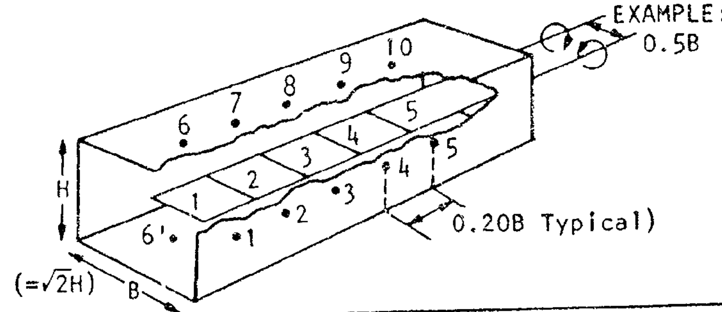

Location		Source Coefficients					Vortex Coefficients				
		1	2	3	4	5	1	2	3	4	5
SIDEWALL	1	0.5000	0.1440	0.0388	0.0115	0.0023	+.4033	+.2016	+.0895	+.0379	+.0154
	2	0.8560	0.5000	0.1440	0.0388	0.0115	+.6052	+.4033	+.2016	+.0895	+.0379
	3	0.9611	0.8560	0.5000	0.1440	0.0388	+.7160	+.6052	+.4033	+.2016	+.0895
	4	0.9885	0.9611	0.8560	0.5000	0.1440	+.7691	+.7160	+.6052	+.4033	+.2016
	5	0.9967	0.9885	0.9611	0.8560	0.5000	+.7939	+.7691	+.7160	+.6052	+.4033
ROOF	6	0.5000	0.0832	-.0081	-.0082	-.0034	0.4113	0.2755	0.1176	0.0458	0.0175
	7	0.9168	0.5000	0.0832	-.0081	-.0082	0.2755	0.4113	0.2755	0.1176	0.0458
	8	1.0081	0.9168	0.5000	0.0832	-.0081	0.1176	0.2755	0.4113	0.2755	0.1176
	9	1.0082	1.0081	0.9168	0.5000	0.0832	0.0458	0.1176	0.2755	0.4113	0.2755
	10	1.0034	1.0082	1.0081	0.9168	0.5000	0.0175	0.0458	0.1176	0.2755	0.4113
FLOOR	6'	0.5000	0.0832	-.0081	-.0082	-.0034	-.4113	-.2755	-.1176	-.0458	-.0175
	7'	0.9168	0.5000	0.0832	-.0081	-.0082	-.2755	-.4113	-.2755	-.1176	-.0458
	8'	1.0081	0.9168	0.5000	0.0832	-.0081	-.1176	-.2755	-.4113	-.2755	-.1176
	9'	1.0082	1.0081	0.9168	0.5000	0.0832	-.0458	-.1176	-.2755	-.4113	-.2755
	10'	1.0034	1.0082	1.0081	0.9168	0.5000	-.0175	-.0458	-.1176	-.2755	-.4113

Figure 2.1 Influence matrices for source and vortex arrays

Matrix	SOURCE-SINK SYSTEM					HORSESHOE VORTEX SYSTEM				
$A_{R/F}$	0.5000	0.0832	-.0081	-.0082	-.0034	0.4113	0.2755	0.1176	0.0458	0.0175
	0.9168	0.5000	0.0832	-.0081	-.0082	0.2755	0.4113	0.2755	0.1176	0.0458
	1.0081	0.9168	0.5000	0.0832	-.0081	0.1176	0.2755	0.4113	0.2755	0.1176
	1.0082	1.0081	0.9168	0.5000	0.0832	0.0458	0.1176	0.2755	0.4113	0.2755
	1.0034	1.0082	1.0081	0.9168	0.5000	0.0175	0.0458	0.1176	0.2755	0.4113
$A^{-1}_{R/F}$	+3.295	-0.947	+0.231	-0.028	+0.015	+4.915	-4.470	+2.066	-0.818	+0.246
	-7.507	+5.422	-1.434	+0.254	-0.028	-4.470	+8.968	-6.308	+2.707	-0.818
	+8.630	-9.931	+5.956	-1.434	+0.231	+2.066	-6.308	+9.700	-6.308	+2.066
	-8.426	10.590	-9.931	+5.422	-0.947	-0.818	+2.707	-6.308	+8.968	-4.470
	+6.576	-8.426	+8.630	-7.507	+3.295	+0.246	-0.818	+2.066	-4.470	+4.915
$A^{-1}_{R/F} * A_{\mathcal{C}}$	+0.398	+0.116	+0.228	-0.131	+0.181	+0.409	+0.173	-0.191	+0.079	-0.056
	-6.855	+3.254	-0.165	-0.128	+0.273	-1.391	+2.049	-0.750	+0.187	-0.072
	+4.725	-6.216	+3.466	-0.743	+0.493	-0.165	-0.145	+0.948	-0.206	-0.049
	-9.653	+8.663	-5.958	+2.201	+0.429	-1.011	+1.940	-1.596	+1.507	-0.354
	+3.997	-7.672	+8.045	-6.080	+2.819	-0.763	+1.079	+0.218	-0.523	+0.701

Figure 2.2 Application of influence matrices

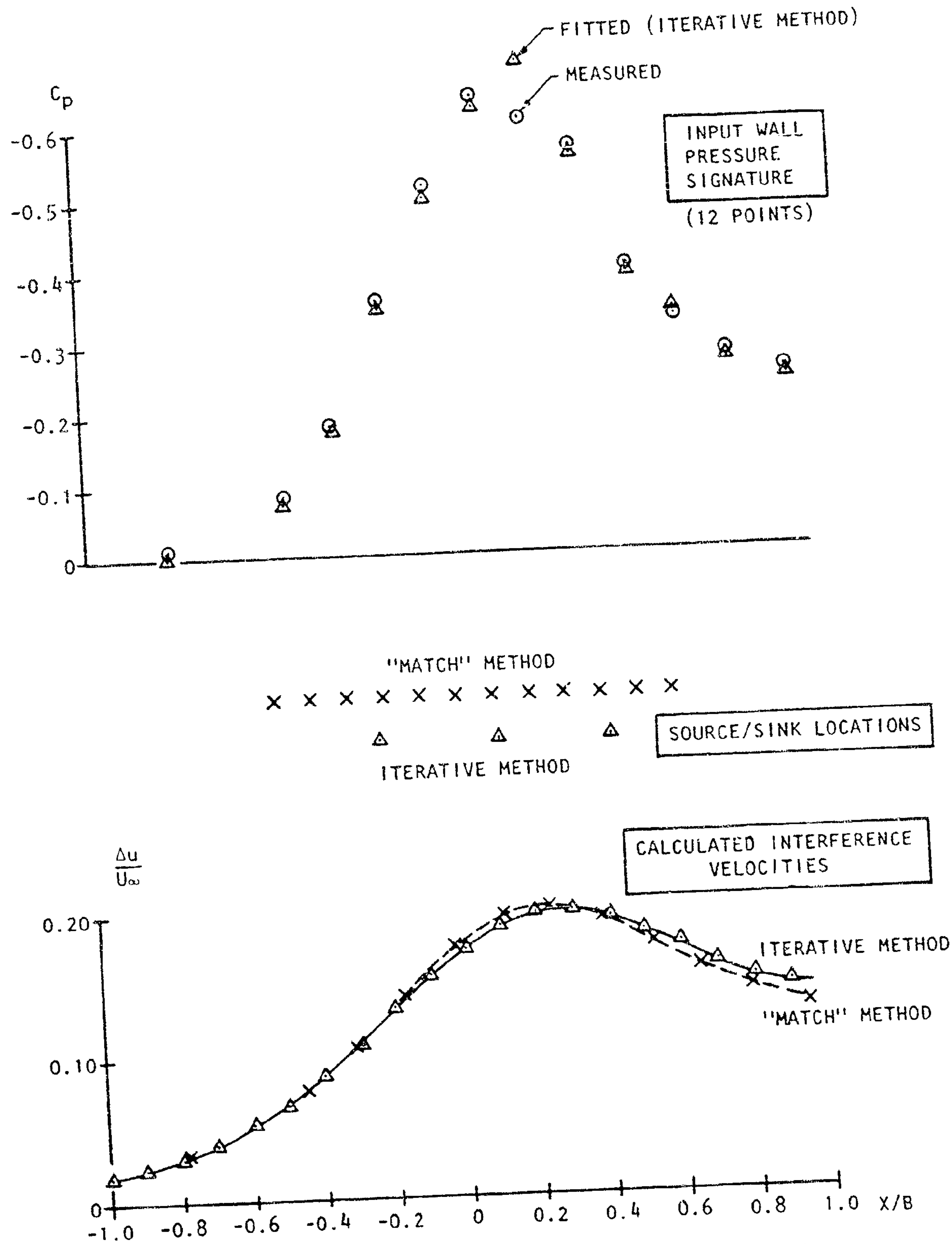

Figure 2.3 Performance of "match" and iterative methods (6' x 6' normal plate in 16¼' x 23¼' tunnel).

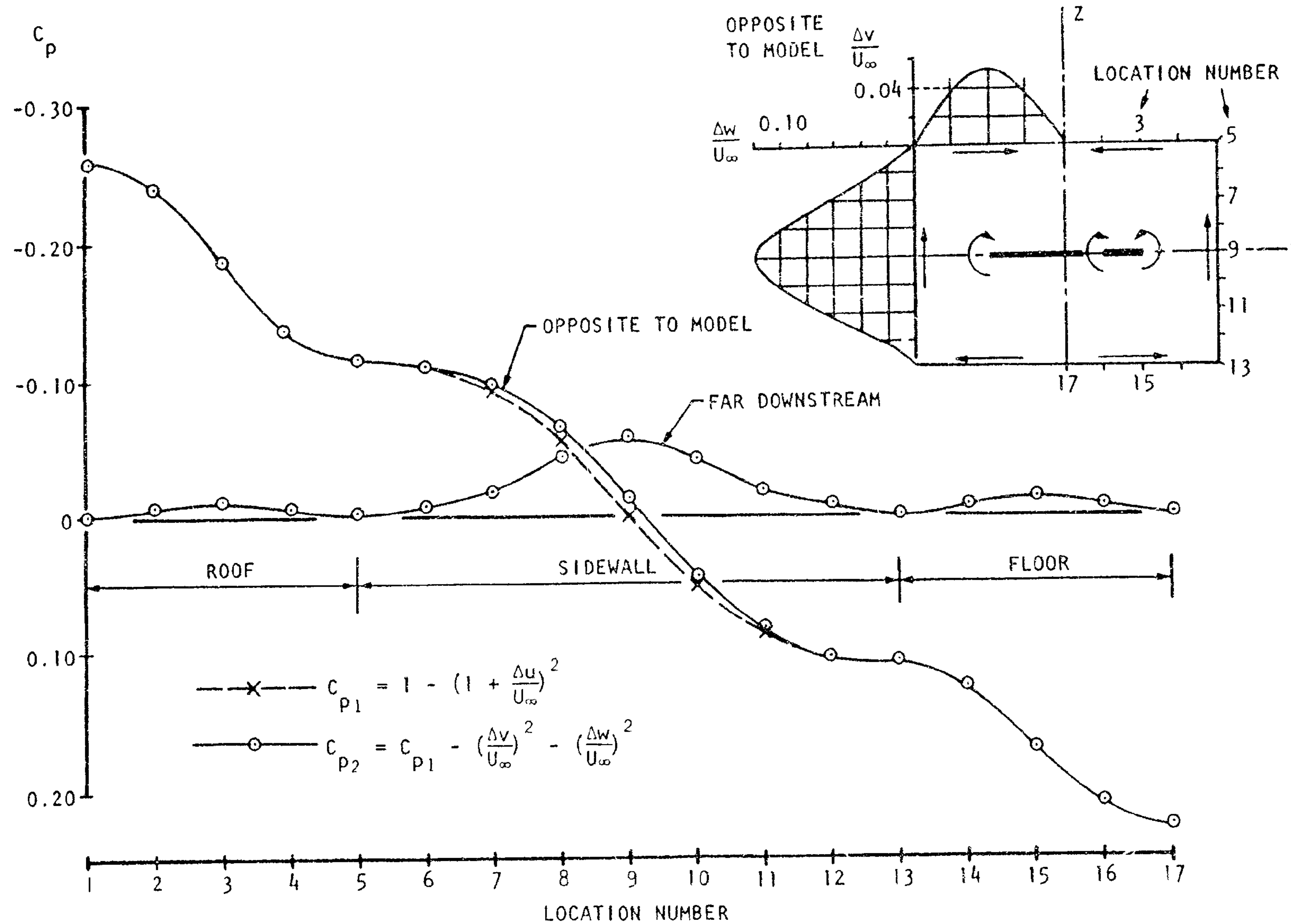

Figure 2.4 Tunnel surface pressures for a horseshoe vortex, $(C_L/AR = 1.0)$

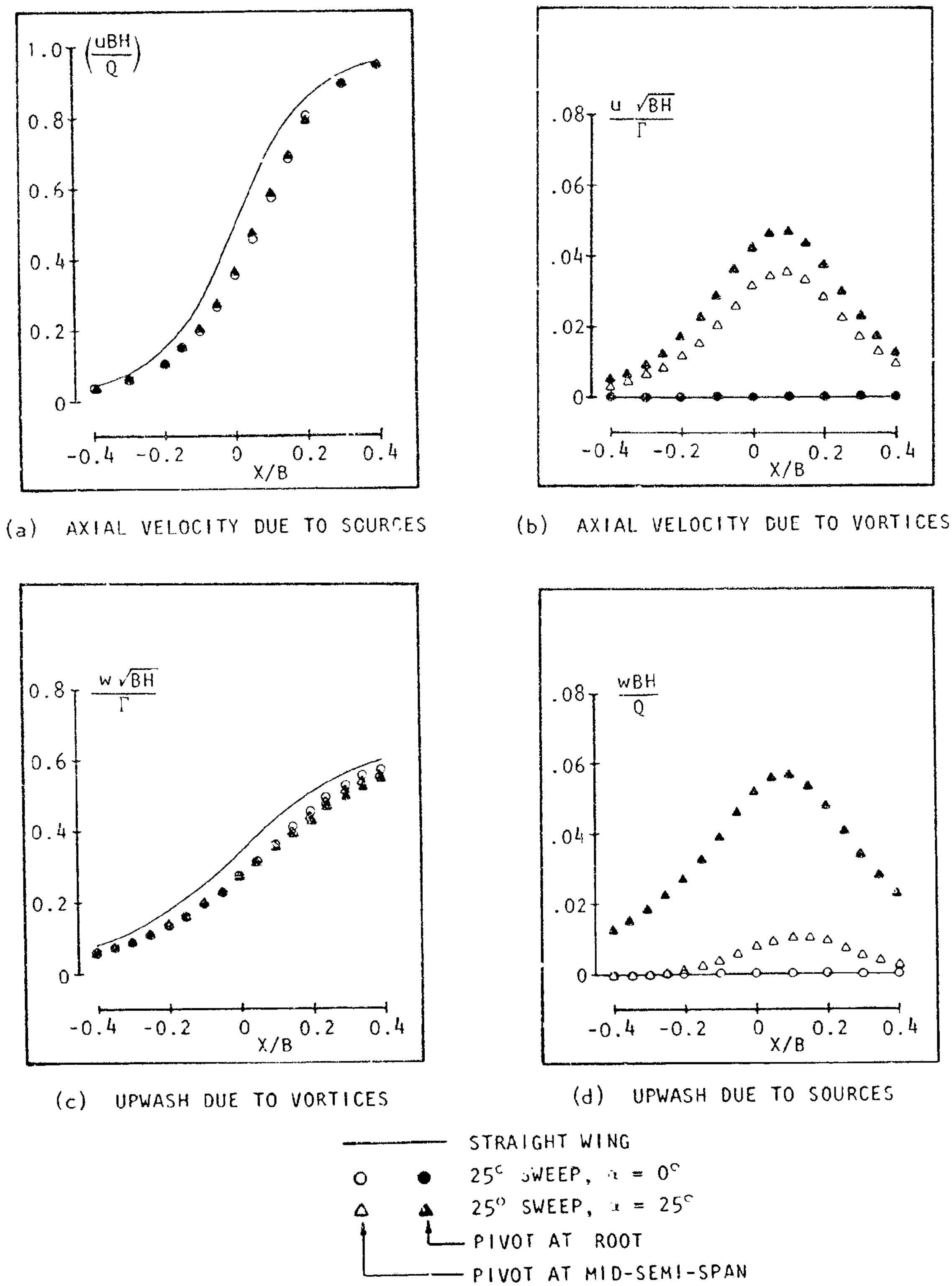

Figure 2.5 Effect of combined sweep and angle-of-attack on influence curves for tunnel sidewall

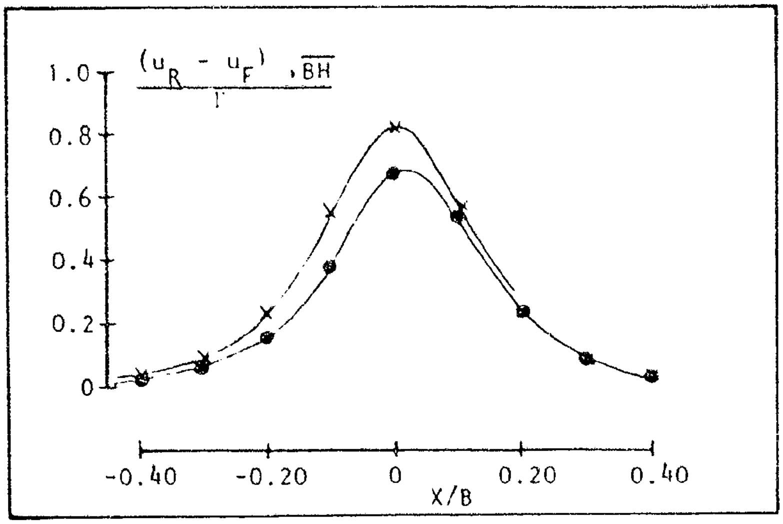

(a) AXIAL VELOCITY DUE TO VORTICES

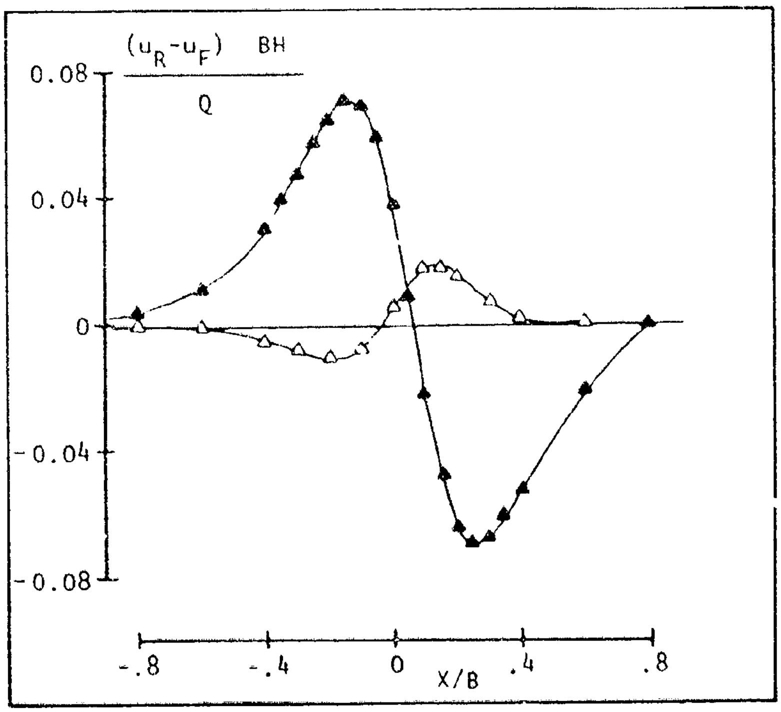

(b) AXIAL VELOCITY DUE TO SOURCES

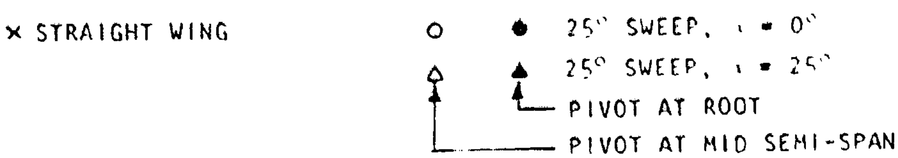

Figure 2.6 Effect of combined sweep and angle-of-attack on roof-minus-floor influence curves

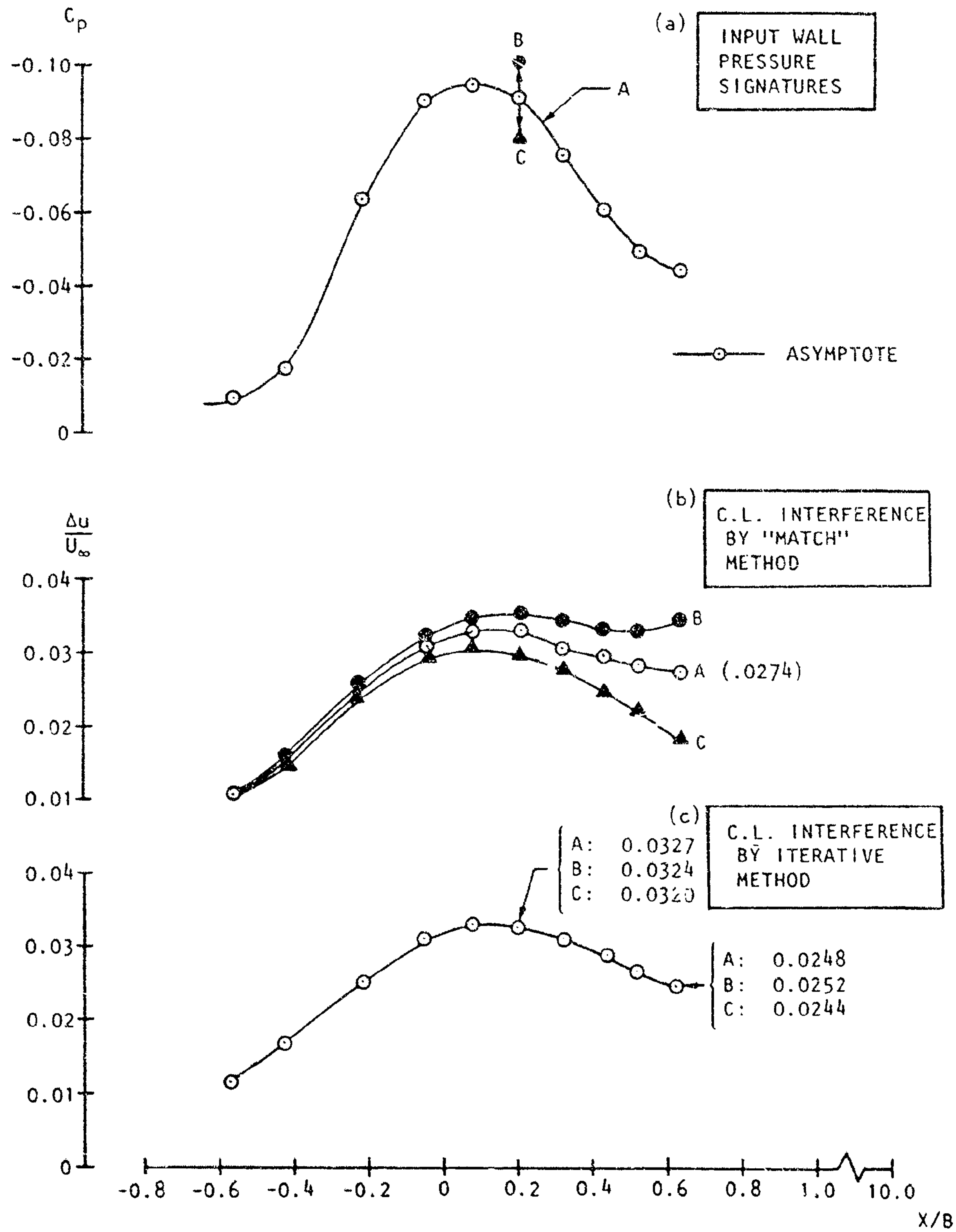

Figure 2.7 Sensitivity of "MATCH" and iterative methods to data scatter ("SAS" car model in 16¼' x 23¼' tunnel)

SOURCE-SINK SYSTEM

$A_{R/F}$	4.1301	3.4523	2.5121	1.4963	0.5681
	3.4523	3.1302	2.4400	1 4999	0.5761
	2.5121	2.4400	2.1138	1.4236	0.5756
	1.4963	1.4999	1.4236	1.0976	0.4994
	0.5681	0.5761	0.5756	0.4994	0.2571
$A_{R/F}^{-1}$	11.819	30.239	39.304	40.297	31.928
	-30.239	87.972	-127.700	136.490	-109.550
	39.304	-127.700	210.970	-245.350	203.600
	-40.297	136.490	-245.350	312.460	-274.470
	31.928	-109.550	203.600	-274.470	256.170
$A_{R/F}^{-1} * A_{C_L}$	1.4358	-3.7245	5.9404	-7.7723	7.2772
	1.5511	-4.2895	7.5369	-10.3330	9.8603
	1.9638	-6.1057	11.4460	-15.7330	15.0590
	2.9241	-9.6820	18.2290	-24.8560	23.9840
	4.6633	-15.8120	29.7270	-40.7450	39.6700

HORSESHOE VORTEX SYSTEM

$A_{R/F}$	0.18152	0.18400	0.12964	0.07420	0.03720
	0.18400	0.23387	0.20578	0.13690	0.07420
	0.12964	0.20578	0.24192	0.20578	0.12964
	0.0742	0.13690	0.20578	0.23387	0.18400
	0.0372	0.07420	0.12964	0.18400	0.18152
$A_{R/F}^{-1}$	69.57	-109.44	90.29	-52.91	19.64
	-109.44	209.03	-205.39	134.72	-52.91
	90.29	-205.39	25.68	-205.39	90.29
	-52.91	134.72	-205.39	209.03	-109.44
	19.64	-52.91	90.29	-109.44	69.57
$A_{R/F}^{-1} * A_{C_L}$	3.2593	-4.0683	2.7926	-1.4665	0.45240
	3.5767	-4.0744	2.8261	-1.5108	0.44508
	3.4637	-3.8549	3.0208	-1.5972	0.42590
	3.4428	-3.9375	3.2108	-1.3740	0.31090
	3.4323	-3.9746	3.2352	-1.3723	0.62470

Figure 2.8 Matrices for a least-squares solution.

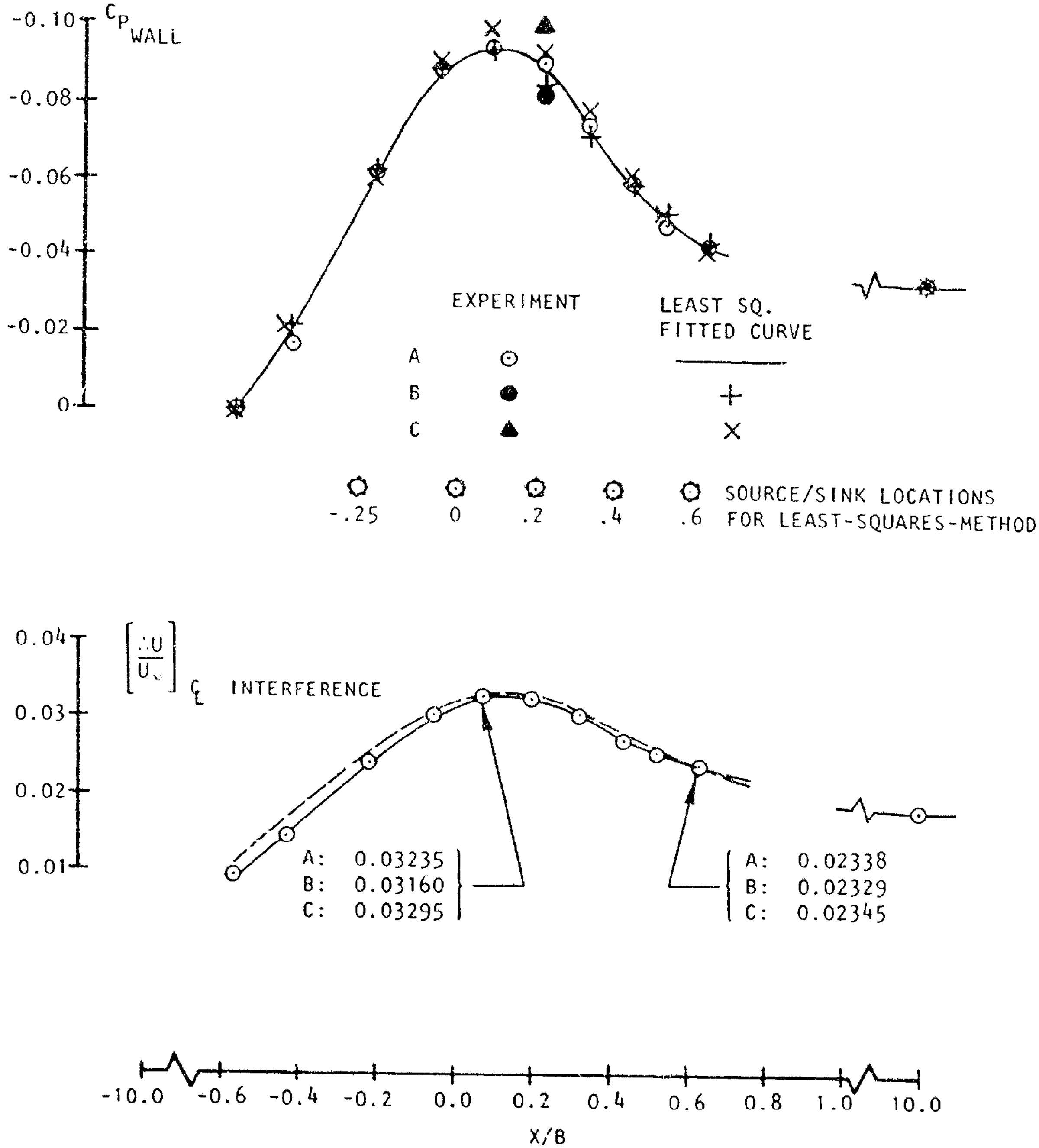

Figure 2.9 Application of the "Least-Squares" Approach to "noisy" Data (SAS Car Model in 16¼' x 23¼' Tunnel)

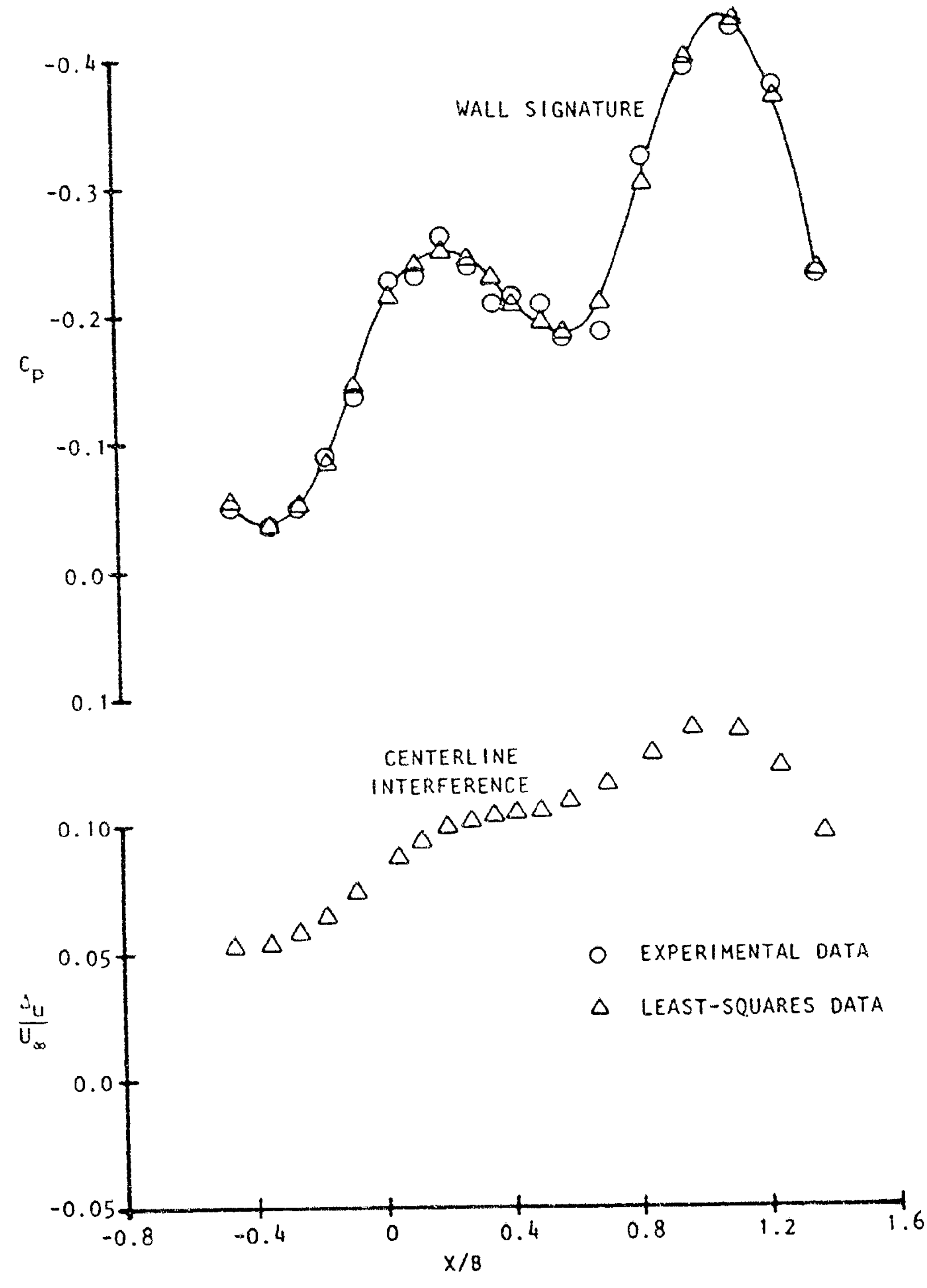

Figure 2.10 Application of least-squares approach to a complex signature (knee-blown flap model, at high Cu and angle-of-attack in the 30" x 43" tunnel).

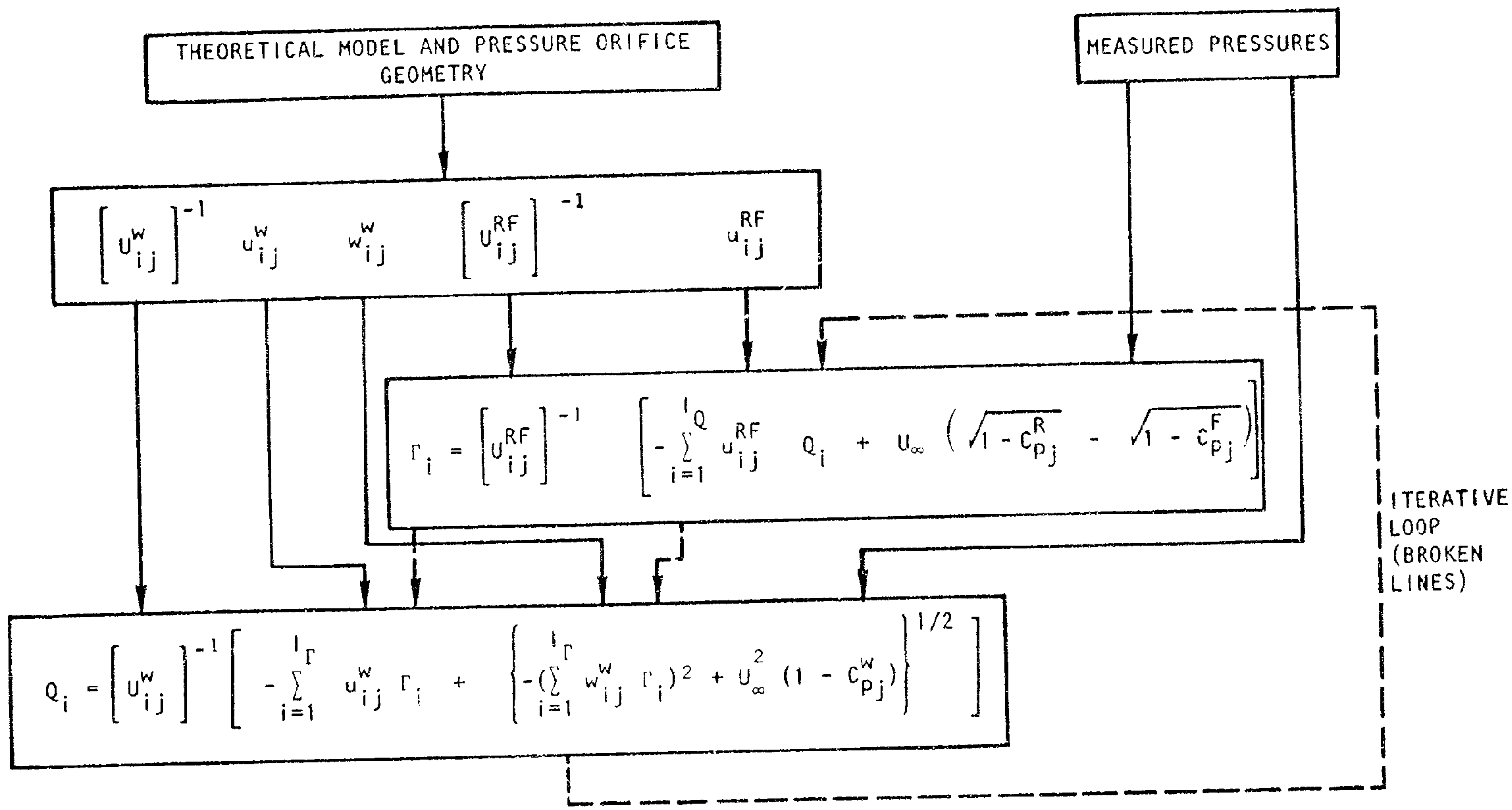

Figure 2.11 Iterative scheme for solving equations 3 and 4

ORIGINAL PAGE
BLACK AND WHITE PHOTOGRAPH

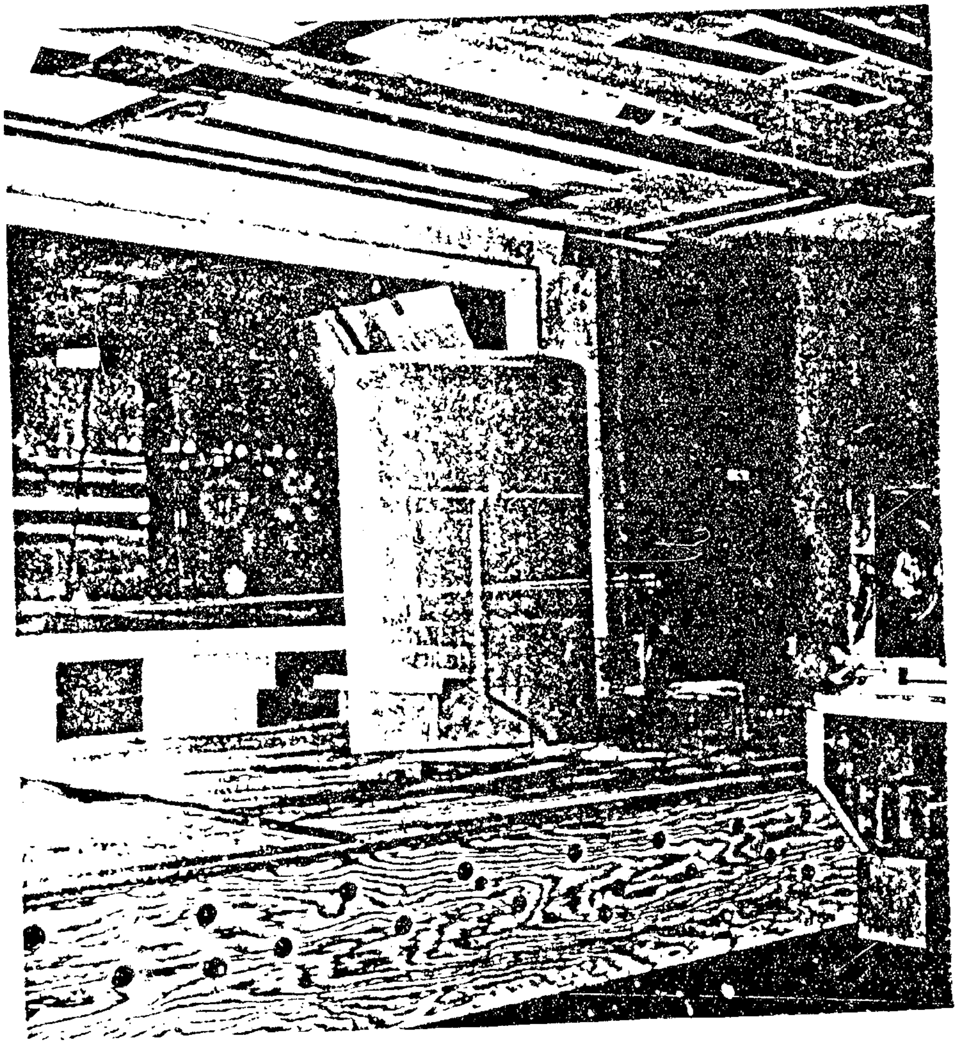

Figure 3.1 18-inch semispan, 12-inch chord half wing model in the 30" X 43" wind tunnel.

Figure 3.2 Basic swept knee-blown-flap model in the 30" X 43" test section (view through the LV window from the 'back' platform).

ORIGINAL PAGE
BLACK AND WHITE PHOTOGRAPH

ORIGINAL PAGE
BLACK AND WHITE PHOTOGRAPH

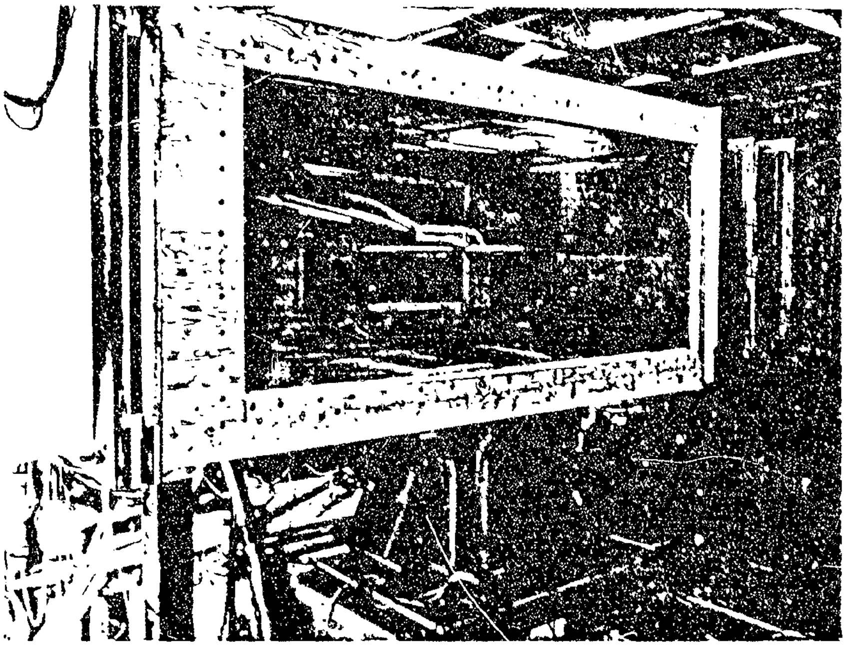

Figure 3.2(a) Continued

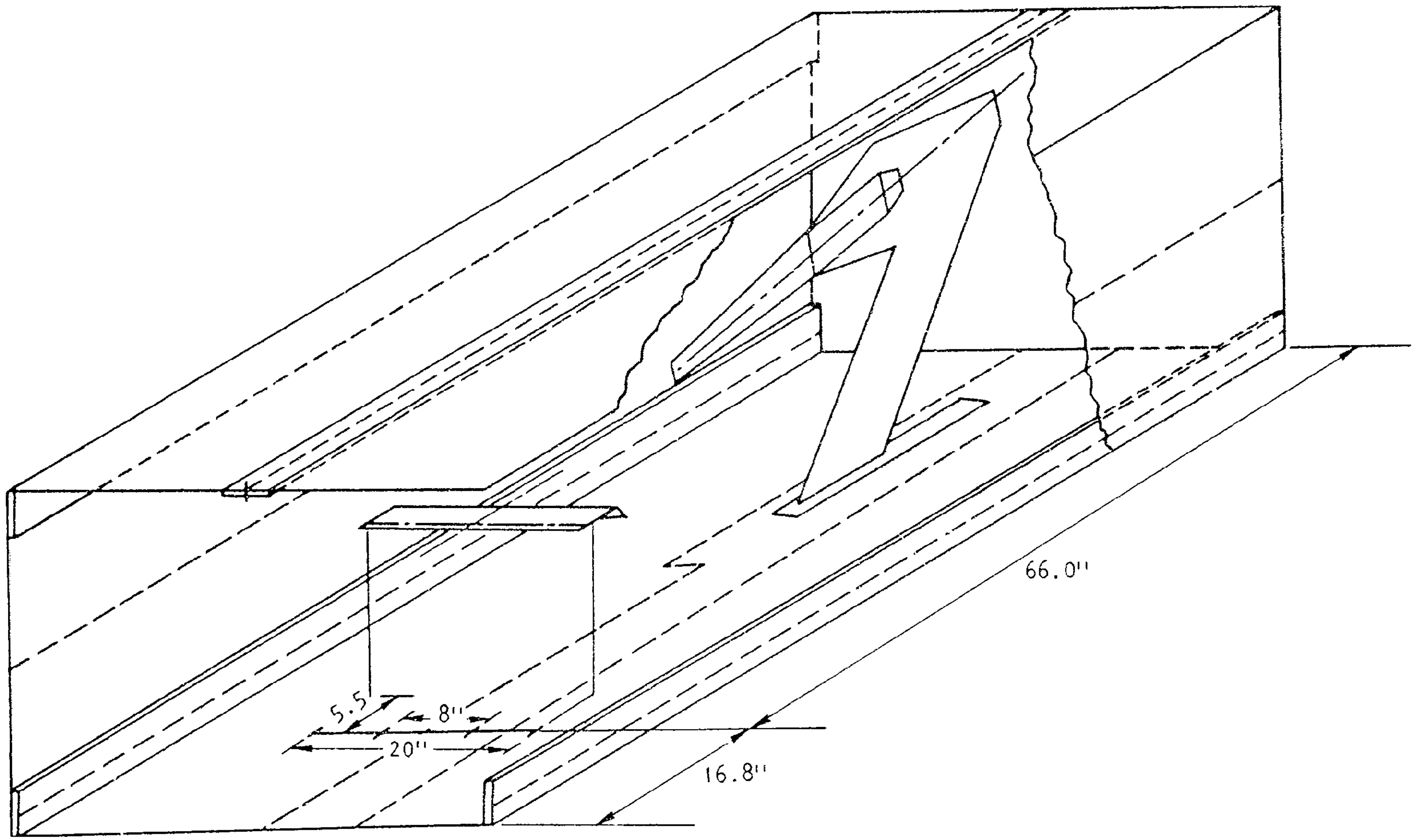

Figure 3.3 Model, sting and instrumentation layout in the 30" X 43" wind tunnel.

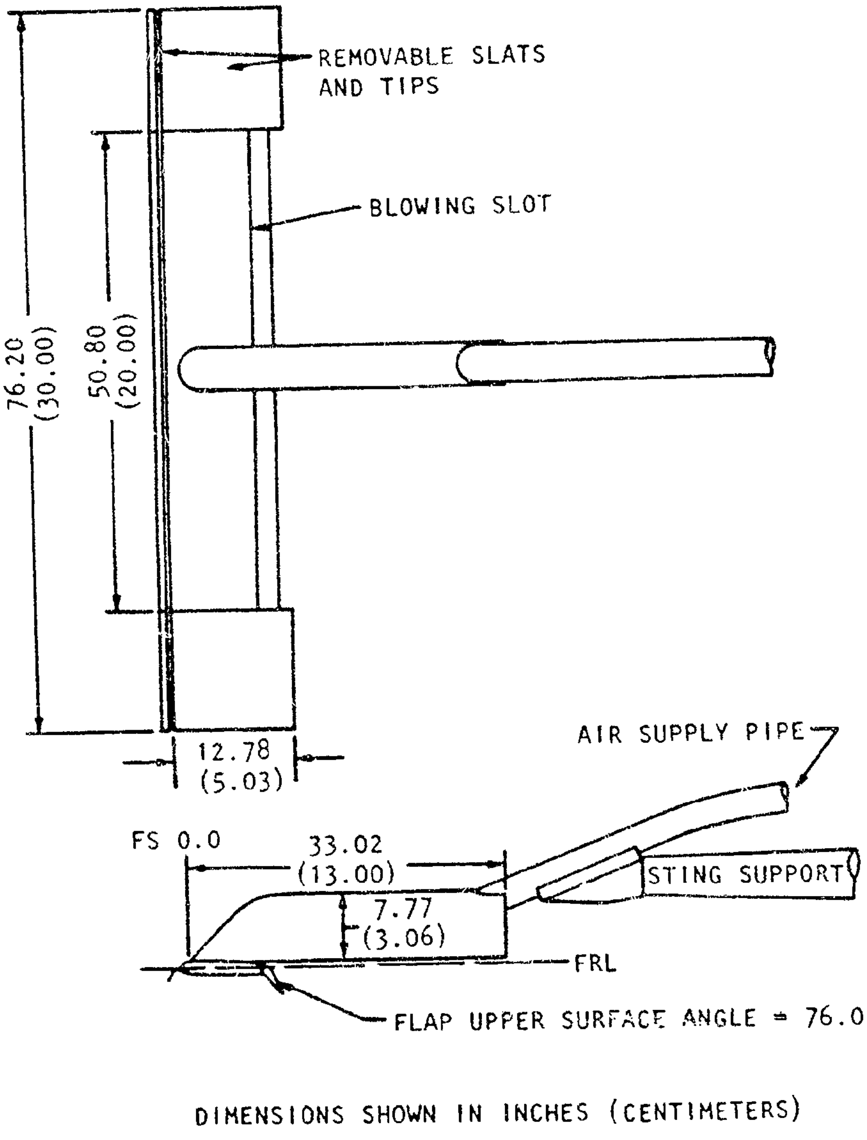

Figure 3.4. Principal Dimensions of the Unswept Knee-Blown Flap Model

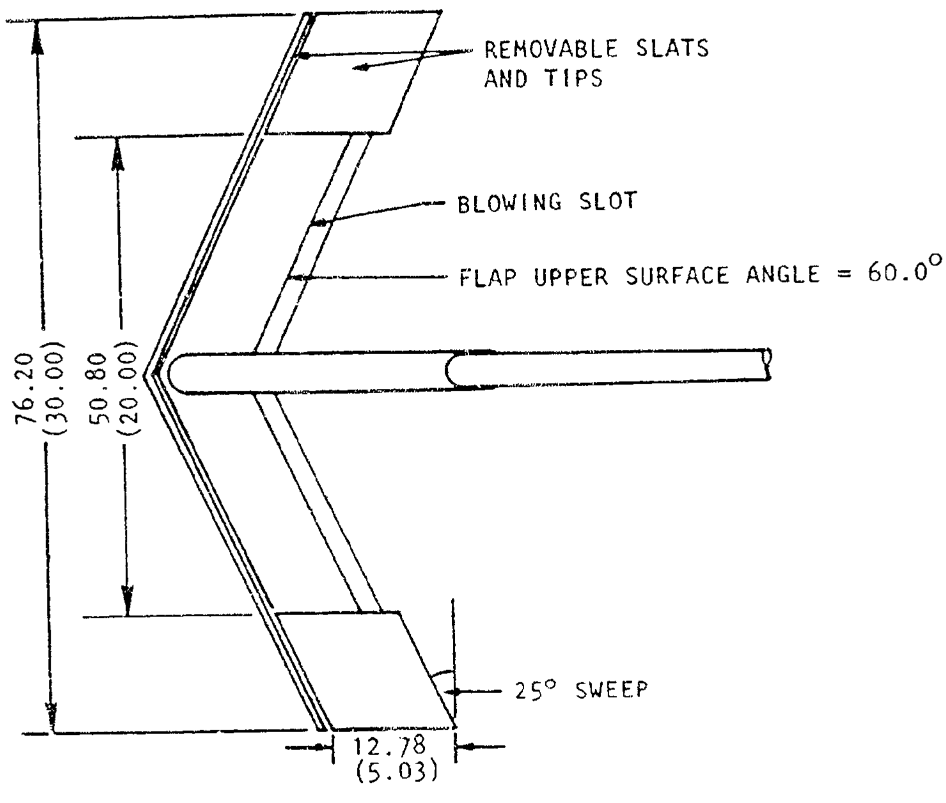

NOTE: SIDE VIEW IS SIMILAR TO UNSWEPT MODEL, FIGURE 3.4

Figure 3.5 Principal Dimensions of the Swept Knee-Blown Flap Model

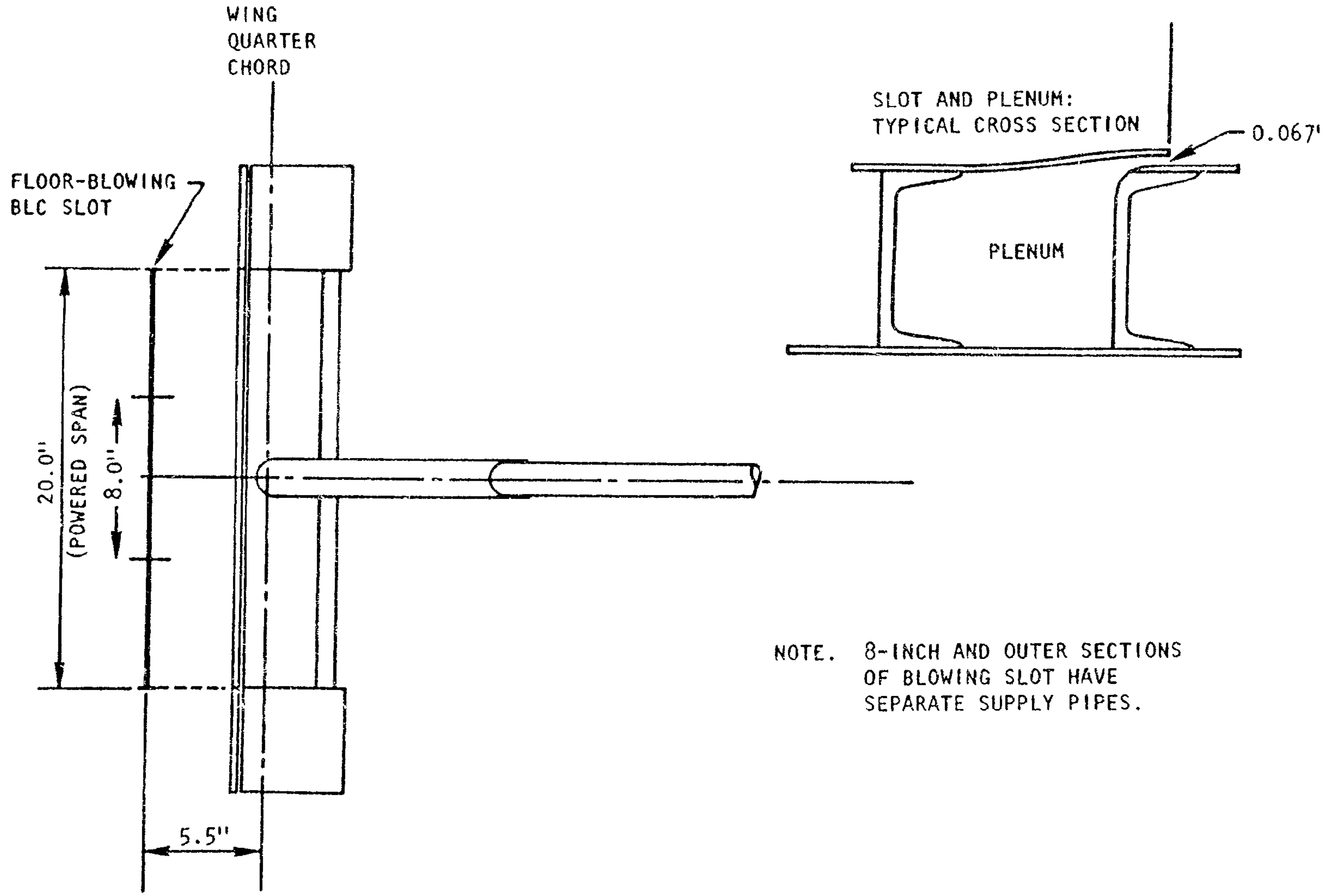

Figure 3.6 The Floor-Blowing BLC Slot

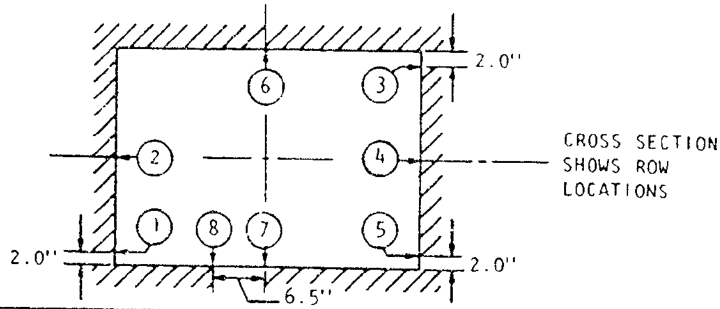

#	ROWS 1 THRU 6	#	ROW 7	#	ROW 8
1	-0.814	1	-0.814	1	-0.814
		2	-0.514	2	-0.514
2	-0.465	3	-0.426	3	-0.426
3	-0.372	4	-0.333	4	-0.333
4	-0.279	5	-0.237	5	-0.237
5	-0.186	6	-0.144	6	-0.144
6	-0.093	7	-0.051	7	-0.051
7	0.000	8	+0.019		
		9	0.042	8	0.042
8	0.070	10	0.065		
		11	0.088	9	0.088
9	0.140	12	0.112		
		13	0.158	10	0.158
10	0.209	14	0.209	11	0.209
11	0.279	15	0.251	12	0.251
		16	0.298	13	0.298
12	0.349	17	0.349	14	0.349
13	0.419	18	0.419	15	0.419
14	0.488	19	0.488	16	0.488
15	0.587	20*	0.558	17	0.558
16	0.698	21*	0.698	18	0.698
17	0.837	22*	0.837	19	0.837
18	0.977	23*	0.977	20	0.977
19	1.116	24*	1.116	21	1.116
20	1.256	25*	1.256	22	1.256
21	1.395	26*	1.395	23	1.395

← TUNNEL REFERENCE STATIC (row # 1)

TABLE SHOWS X/B VALUES (B = 43.0'')

*OFFSET 3.5'' RIGHT TO AVOID STING

Figure 3.7 Wall pressure orifice locations for experiments with the knee-blown flap models.

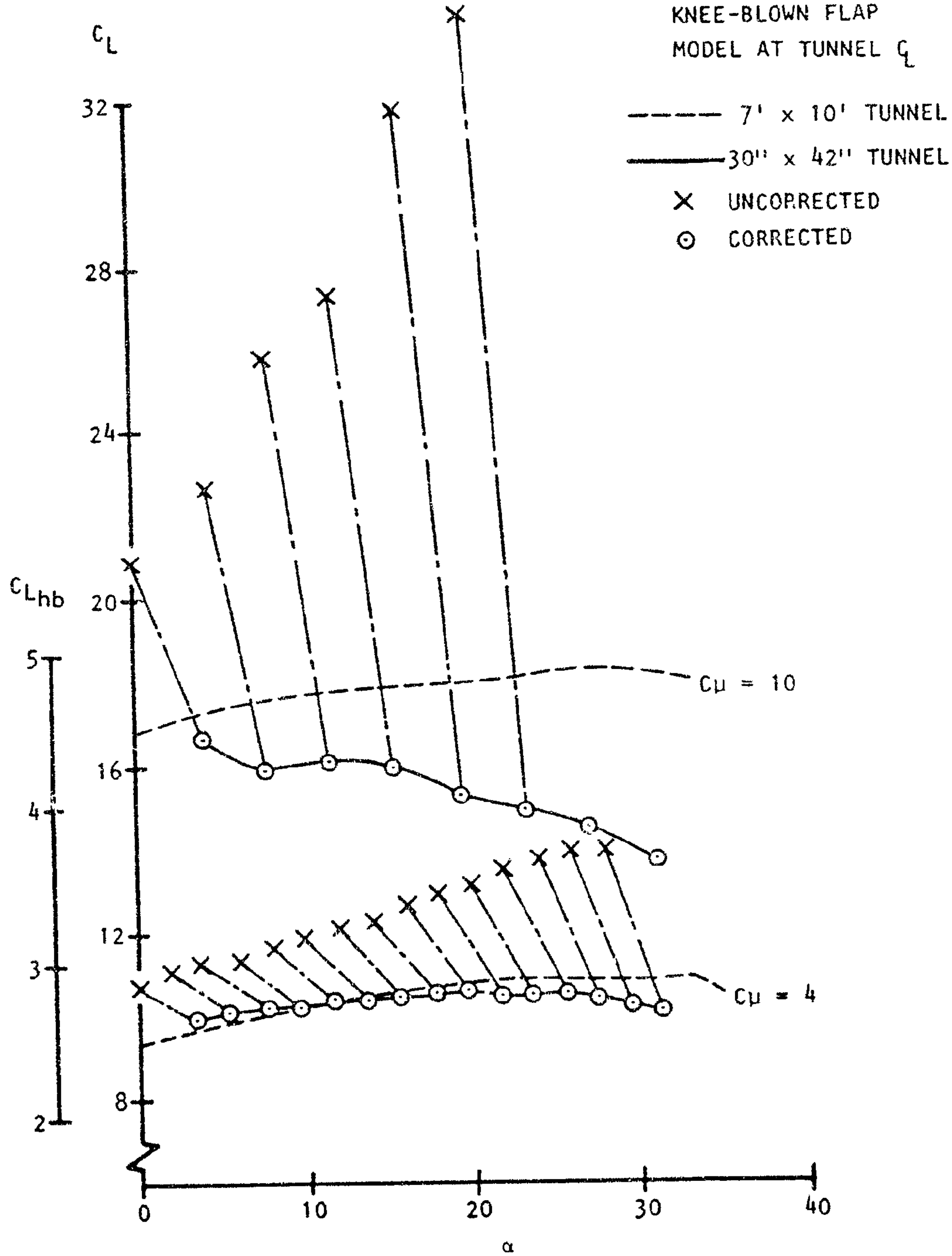

Figure 4.1 Implied corrections for "true-q" tests

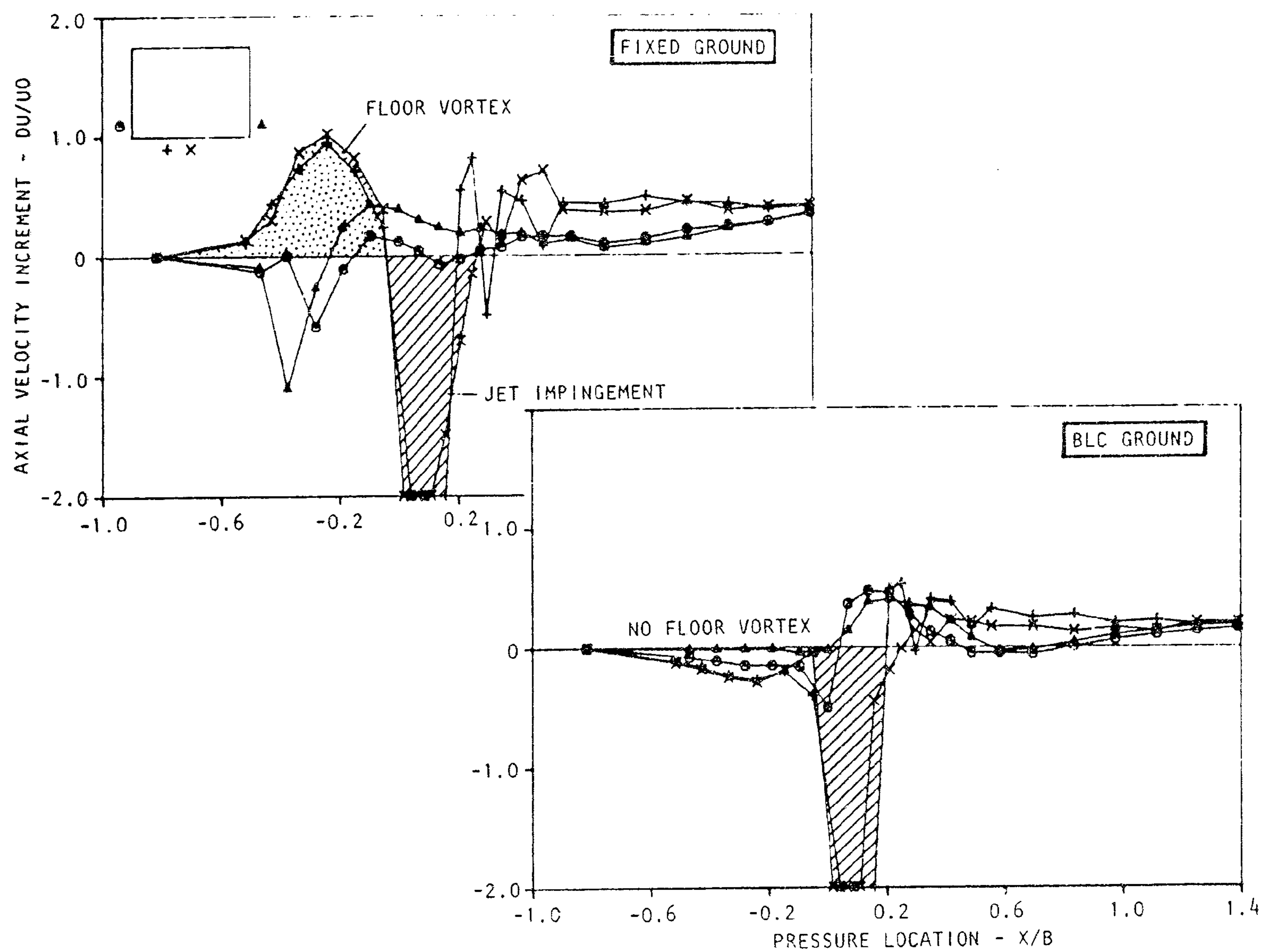

Figure 4.2 Use of ground pressures for BLC feedback

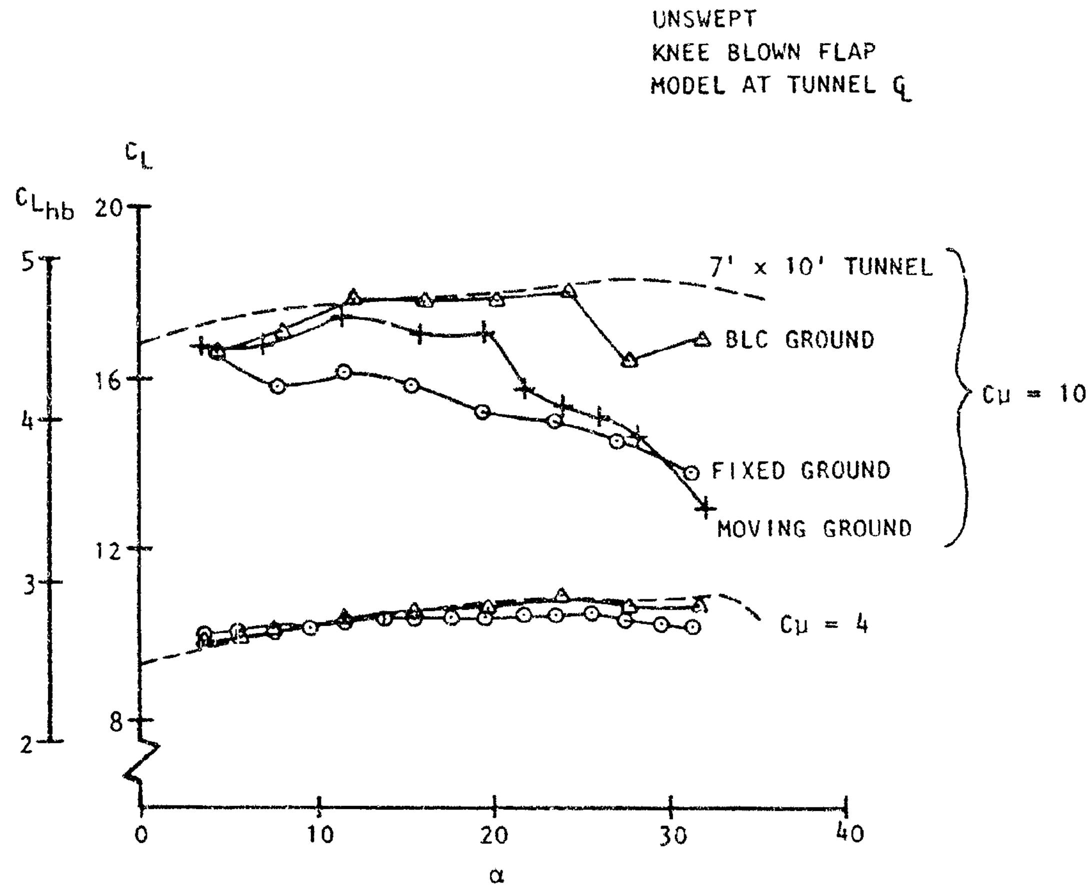

Figure 4.3 Effect of ground-blowing BLC on lift-loss due to the floor vortex

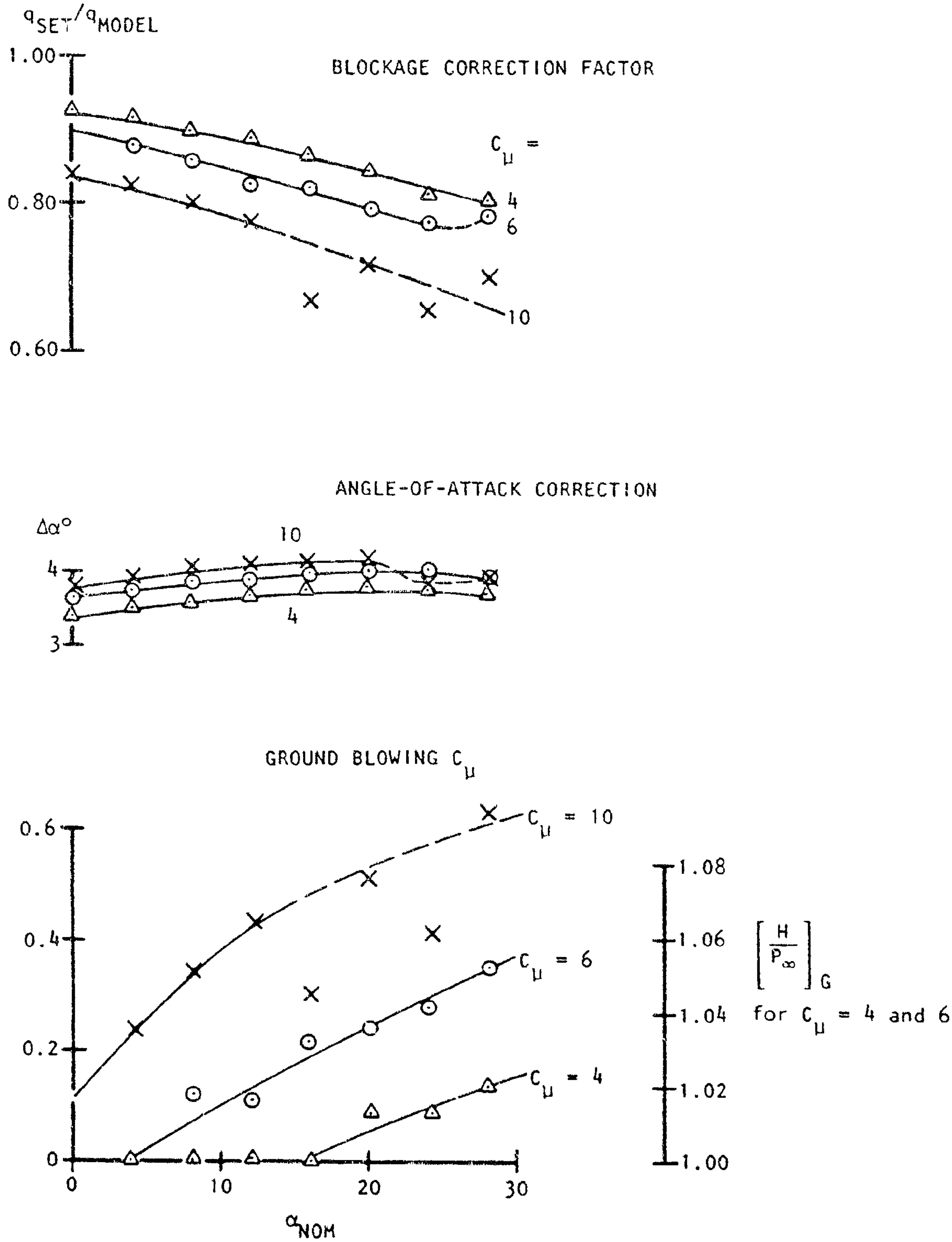

Figure 4.4 Test details for straight wing KBF runs

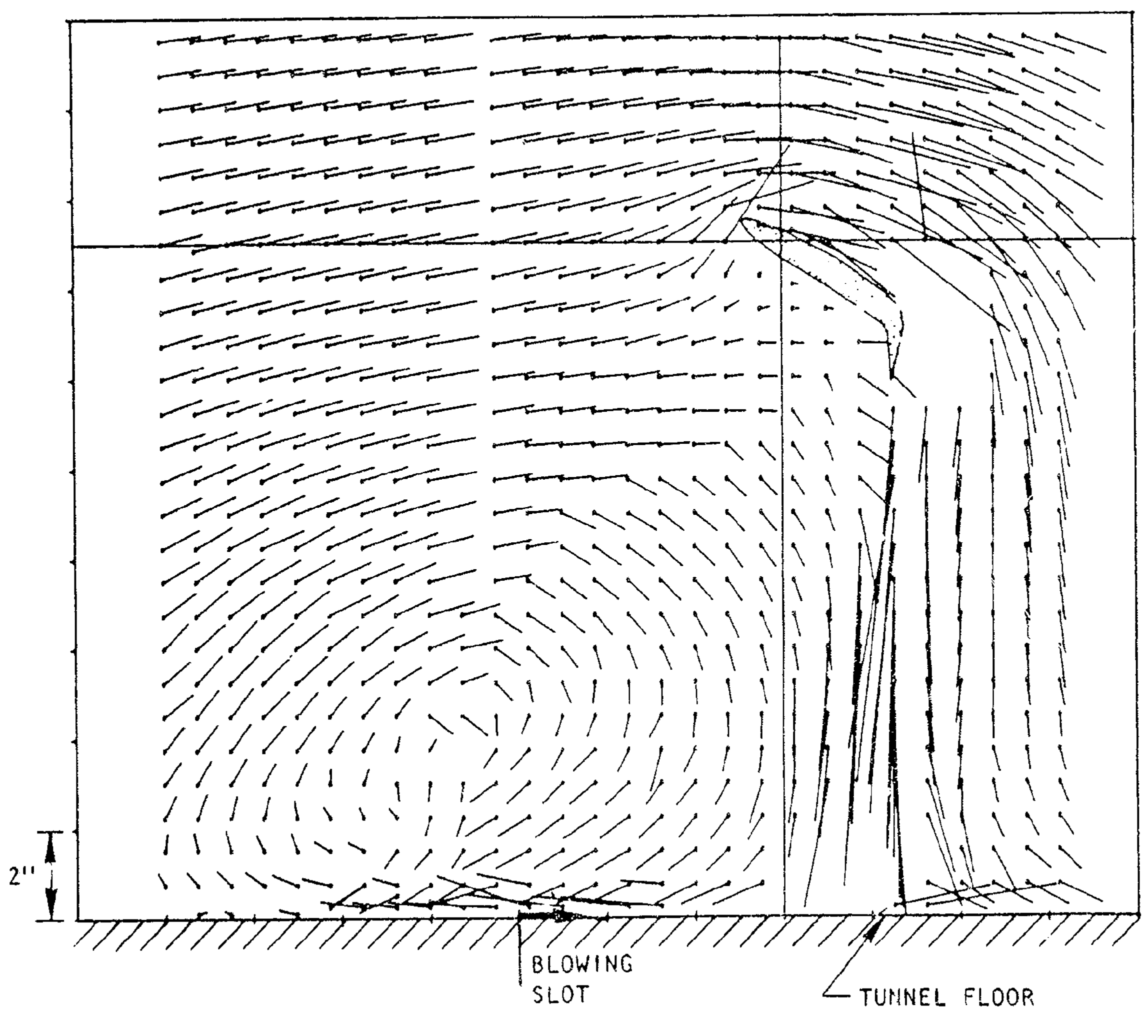

Figure 4.5 Laser velocimeter measurements of tunnel flow breakdown condition. $C_\mu = 6$, $\alpha = 28°$.

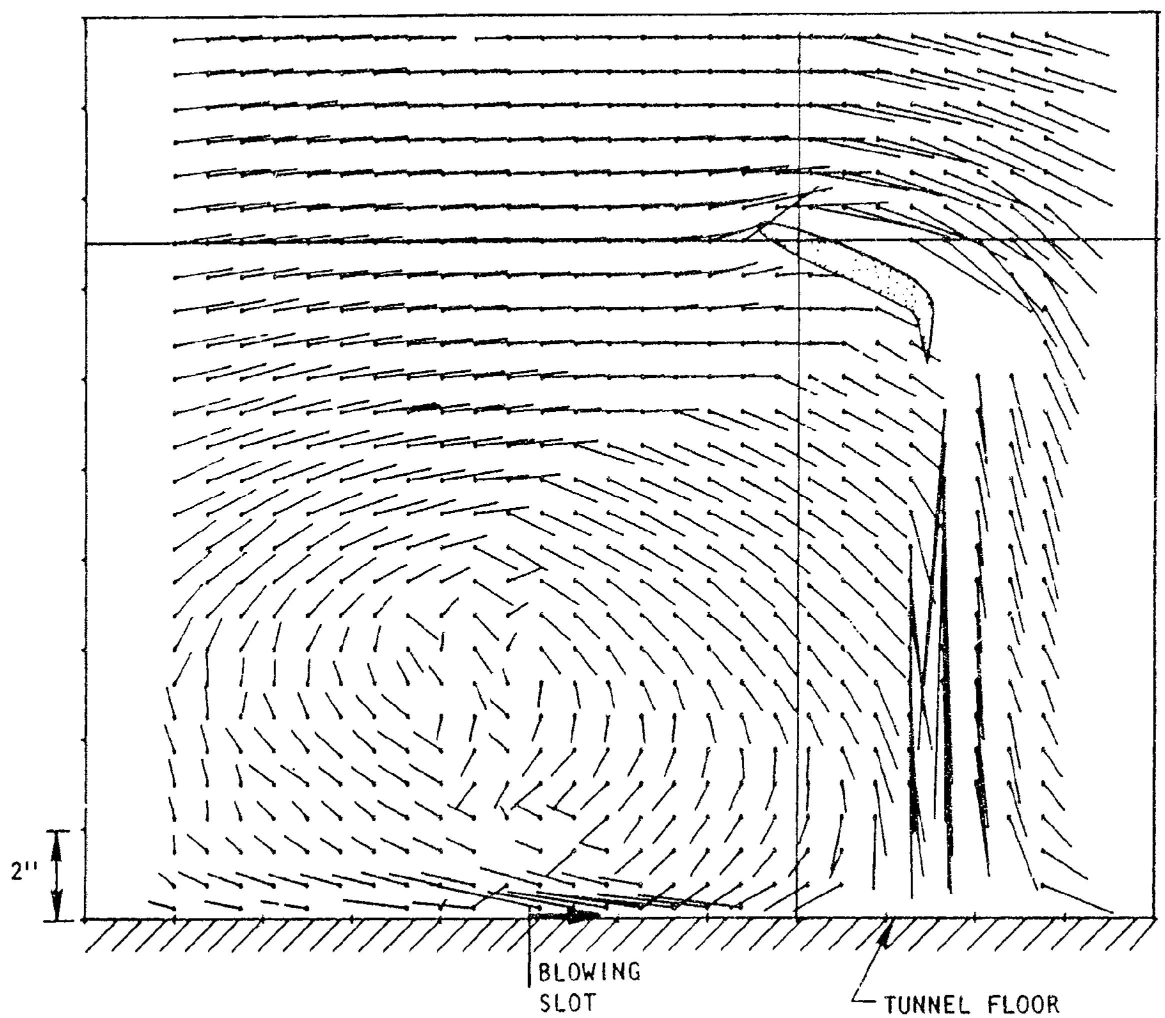

Figure 4.6 Laser velocimeter measurements of tunnel flow breakdown condition, $C_\mu = 10$, $\alpha = 20°$.

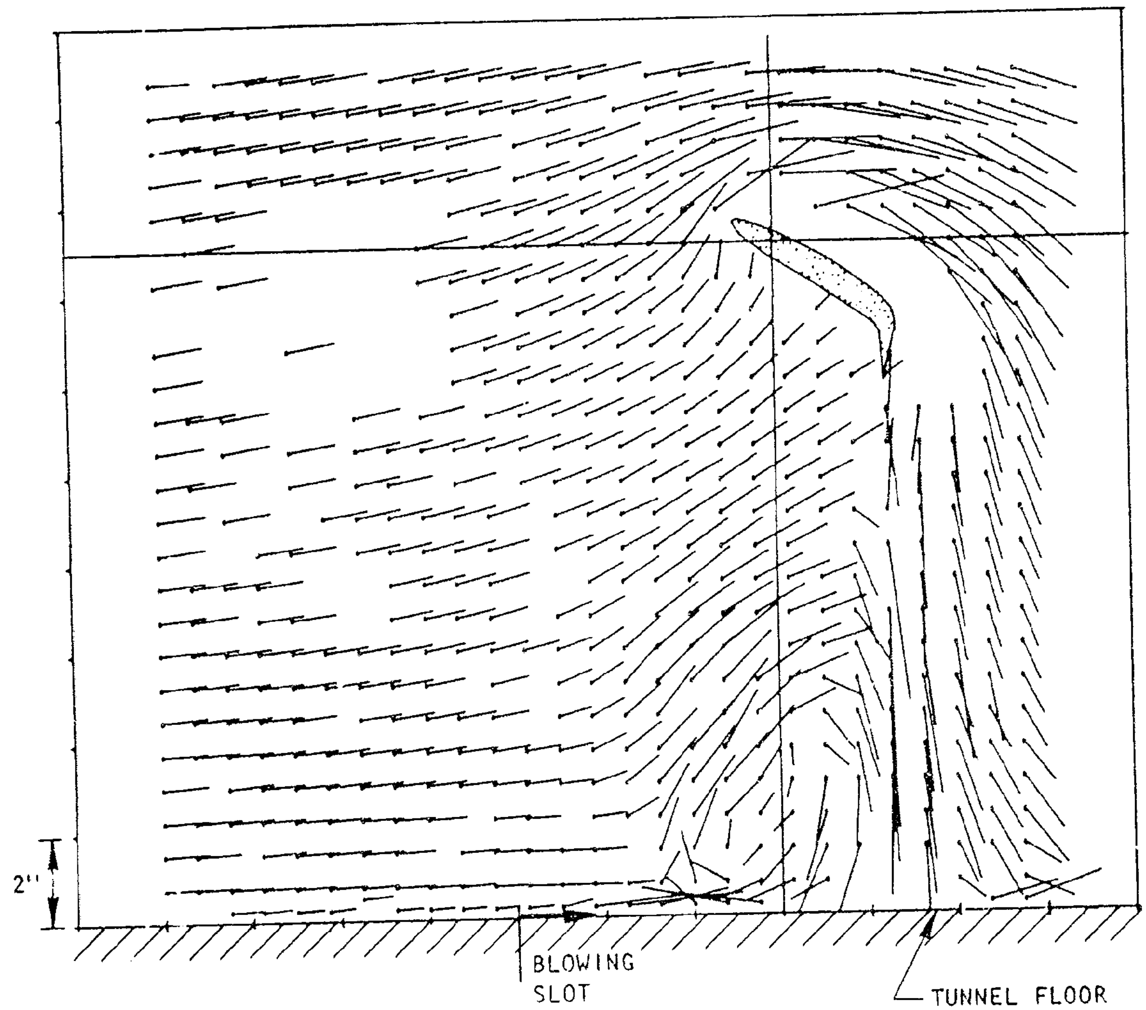

Figure 4.7. Laser Velocimeter measurements with floor blowing BLC Applied, $C_\mu = 6$, $\alpha = 28^\circ$.

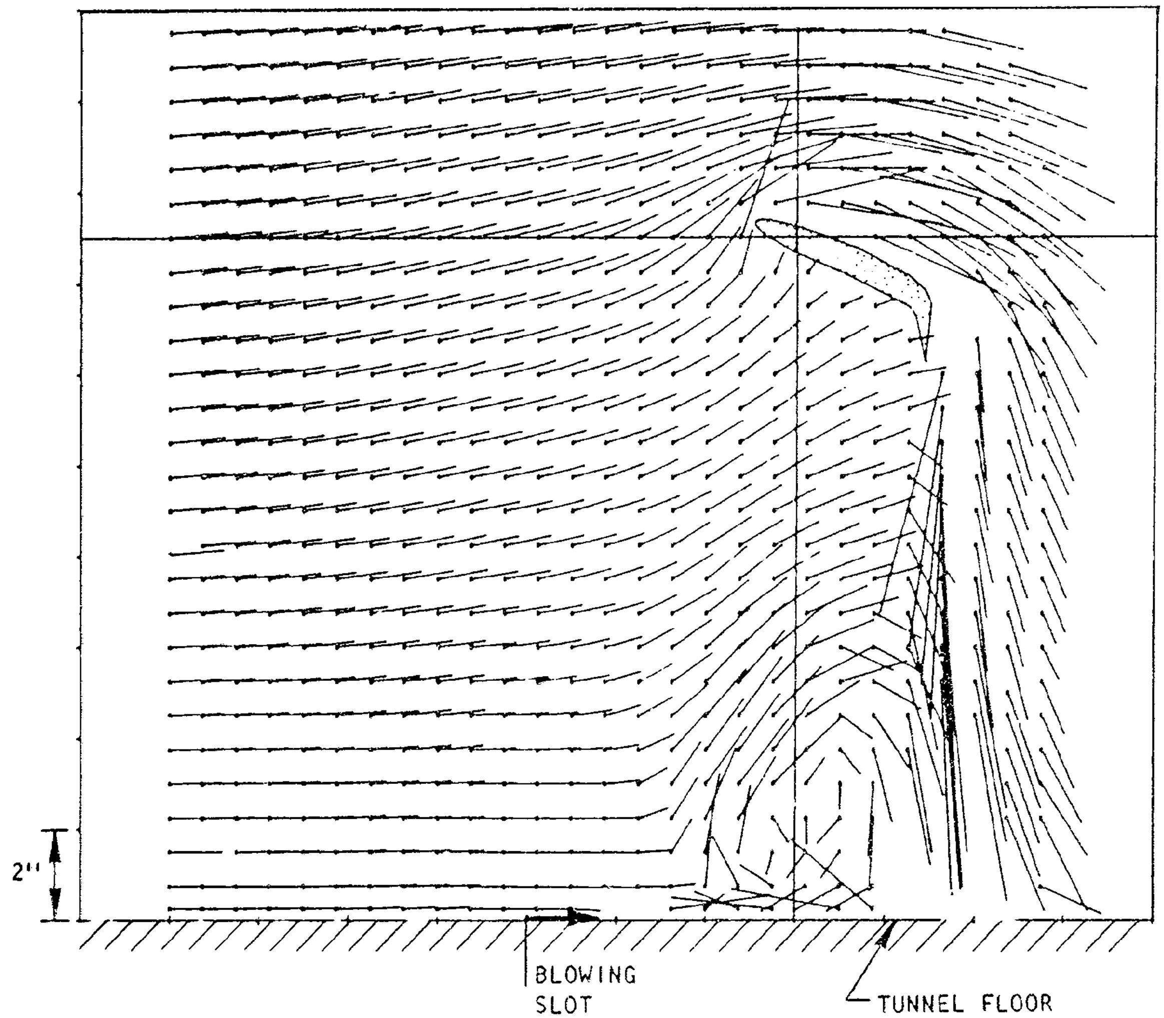

Figure 4.8. Laser Velocimeter measurements with floor blowing BLC Applied,
$C\mu = 10$, $\alpha = 20^{\circ}$.

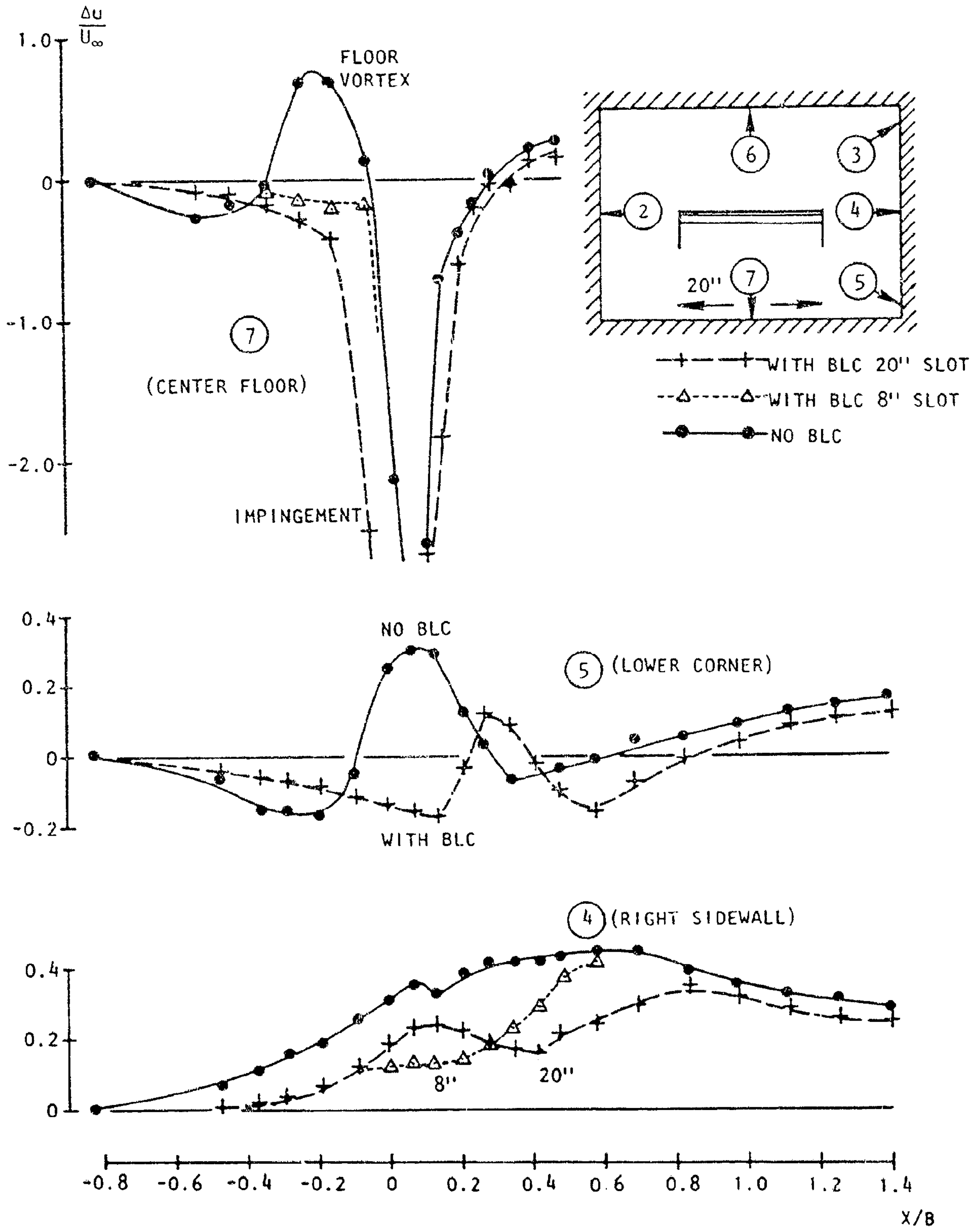

Figure 4.9 Effect of ground BLC on floor and sidewall signatures. Cu = 6.0 α = 28°.

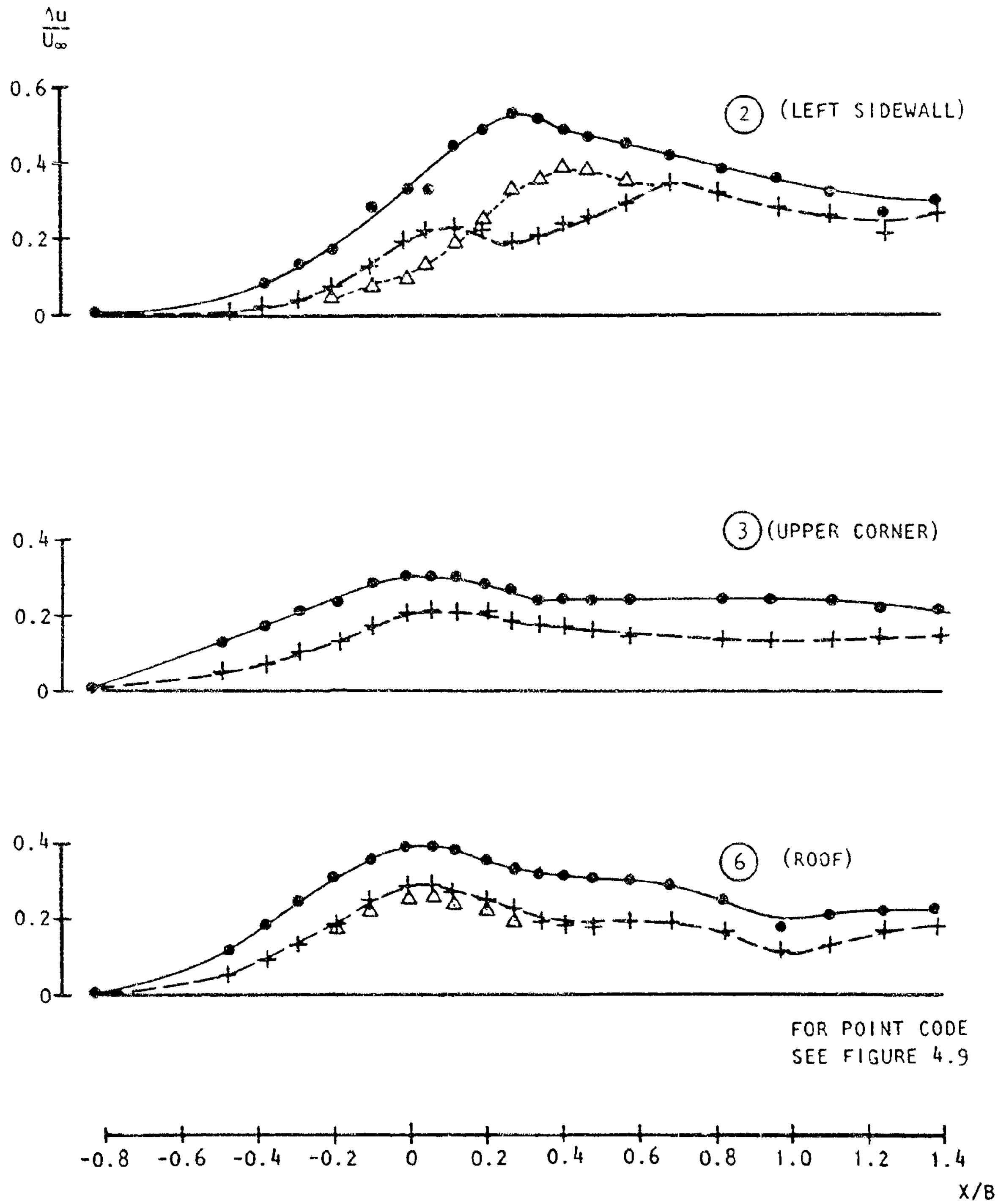

Figure 4.10 Effect of ground BLC on sidewall and roof signatures. $C_\mu = 6.0$ $\alpha = 28°$

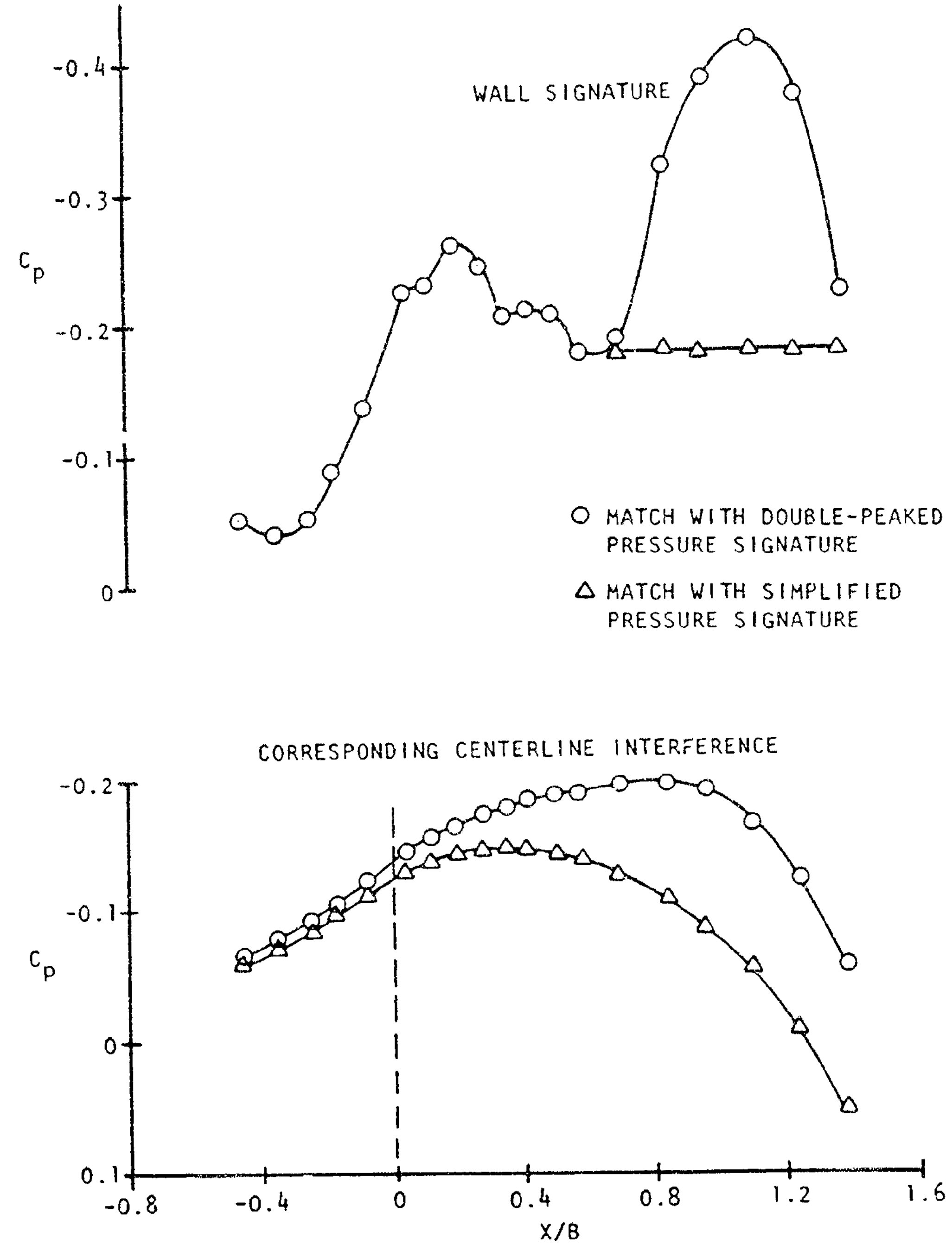

Figure 4.11 Effect of the second peak on predicted blockage. (Unswept KBF model, C_μ = 4.0 X = 12" from Figure 6.2 of Reference 8).

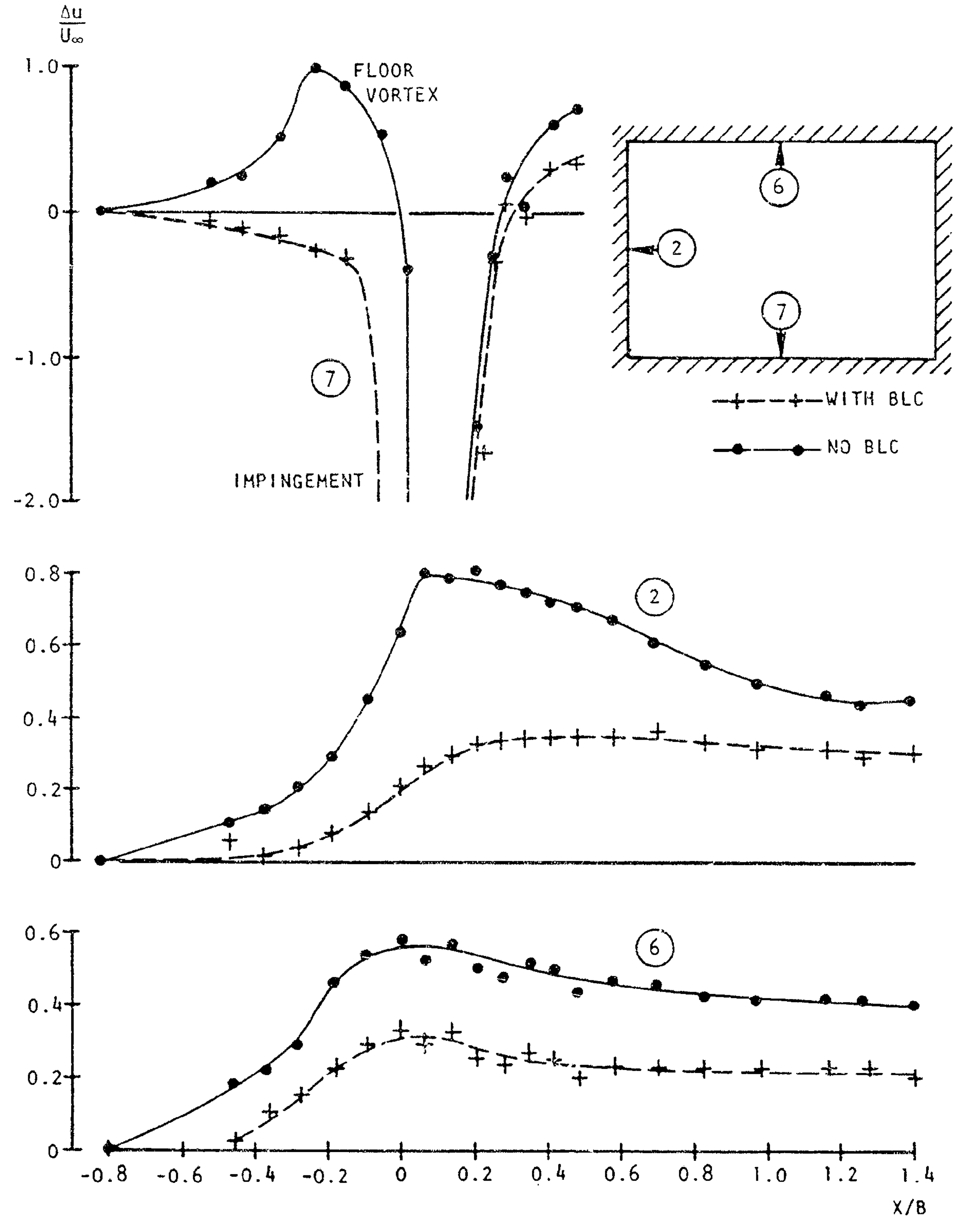

Figure 4.12 Effect of ground BLC on typical signatures
$C_\mu = 10.0 \quad \alpha = 20^\circ$

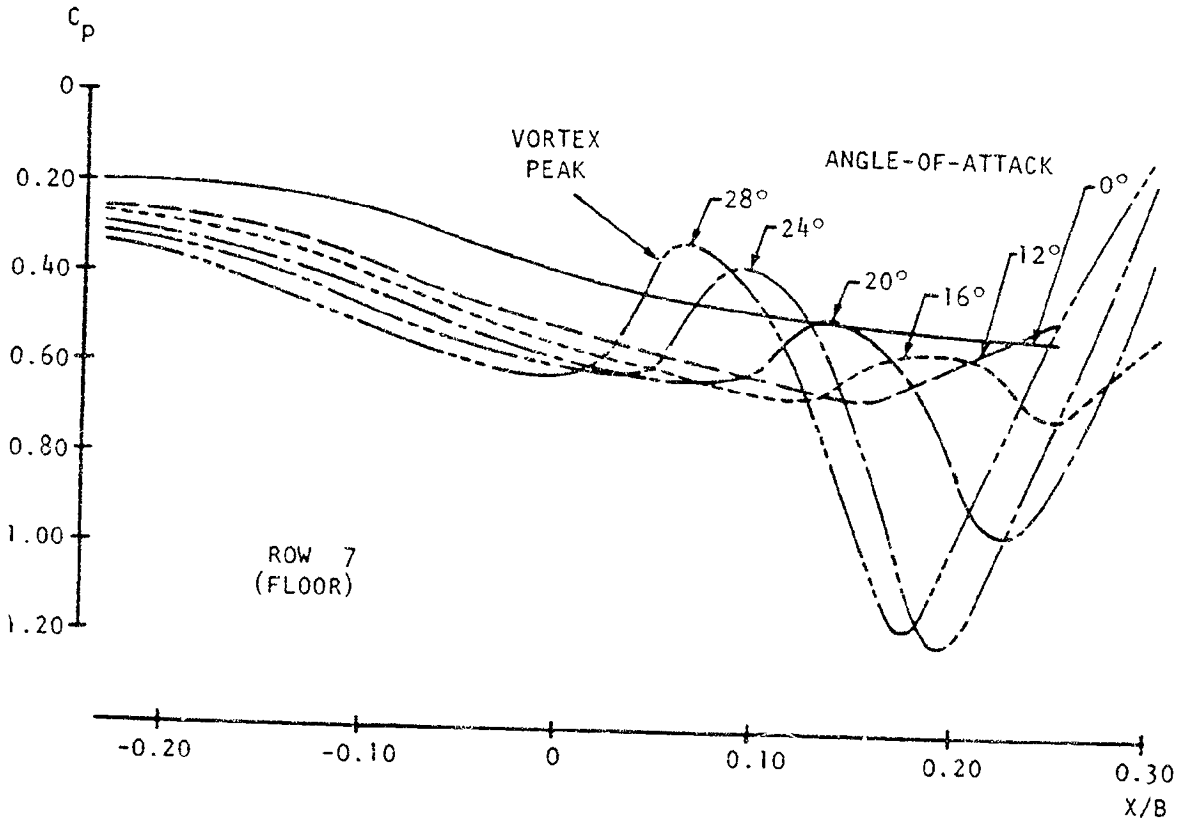

Figure 4.13 Development of floor vortex with increasing α: $C_\mu = 2.0$.

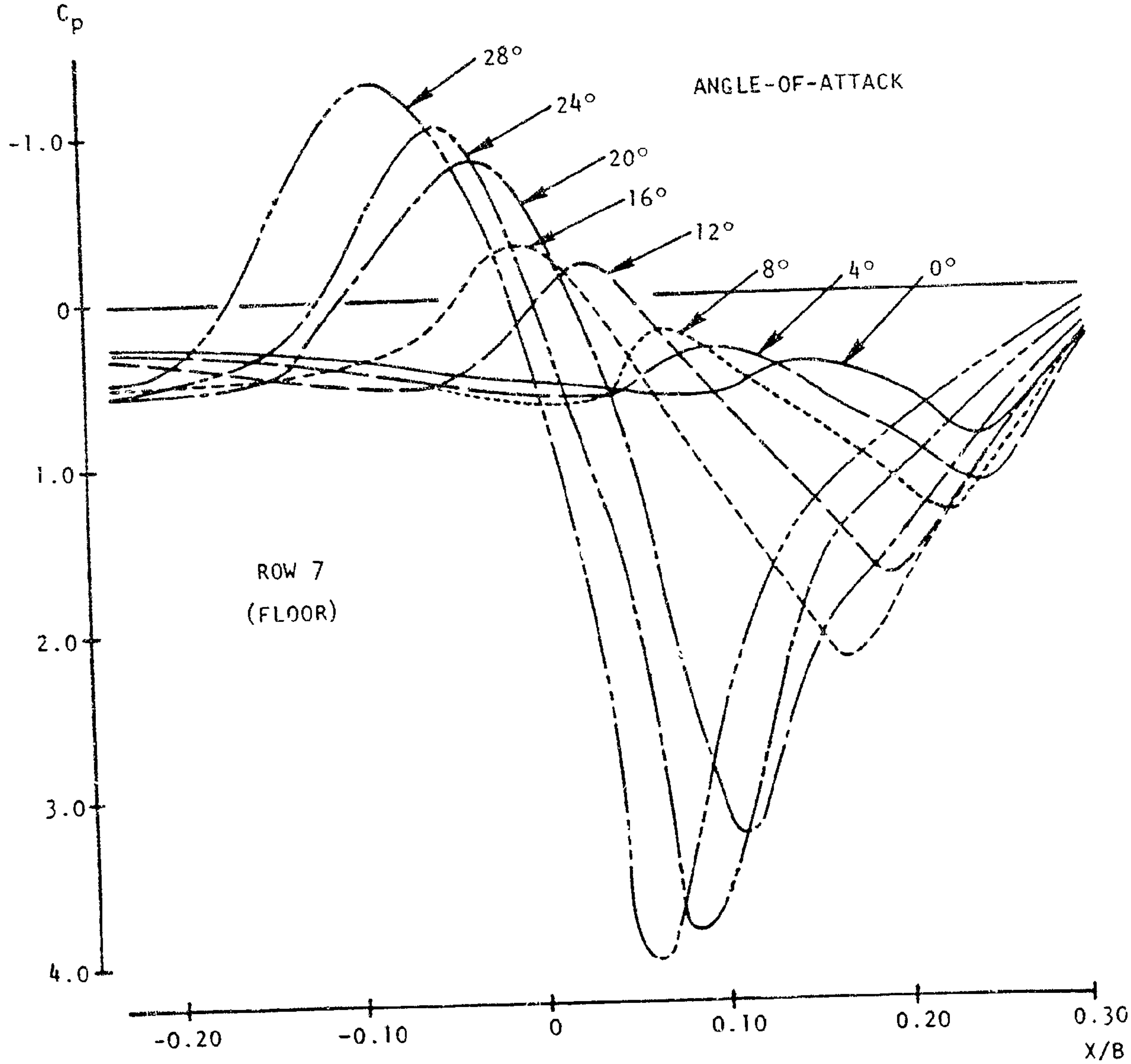

Figure 4.14 Development of floor vortex with increasing α: C_μ = 4.0

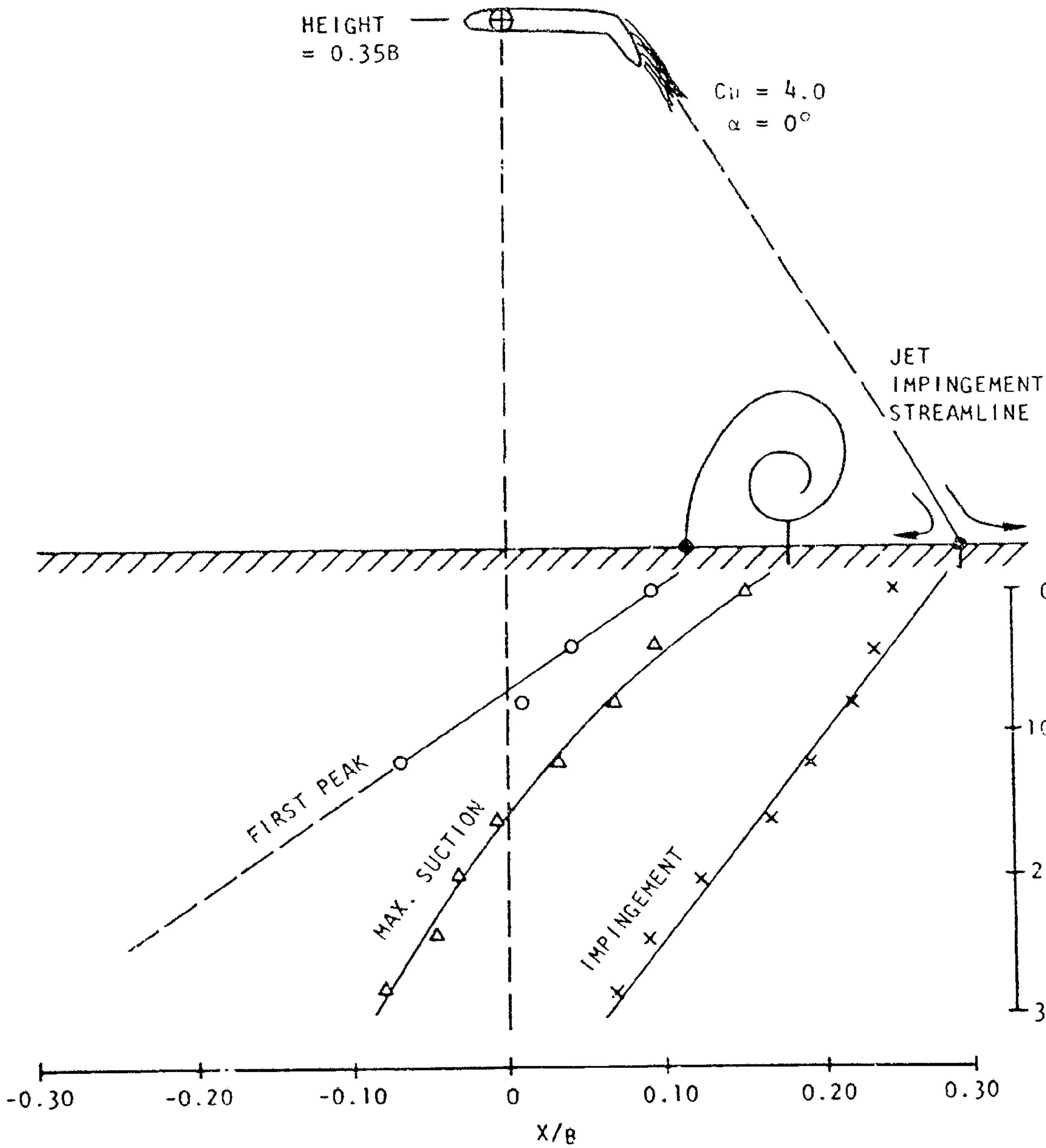

Figure 4.15 Dimensions of floor separation for $C_\mu = 4.0$.

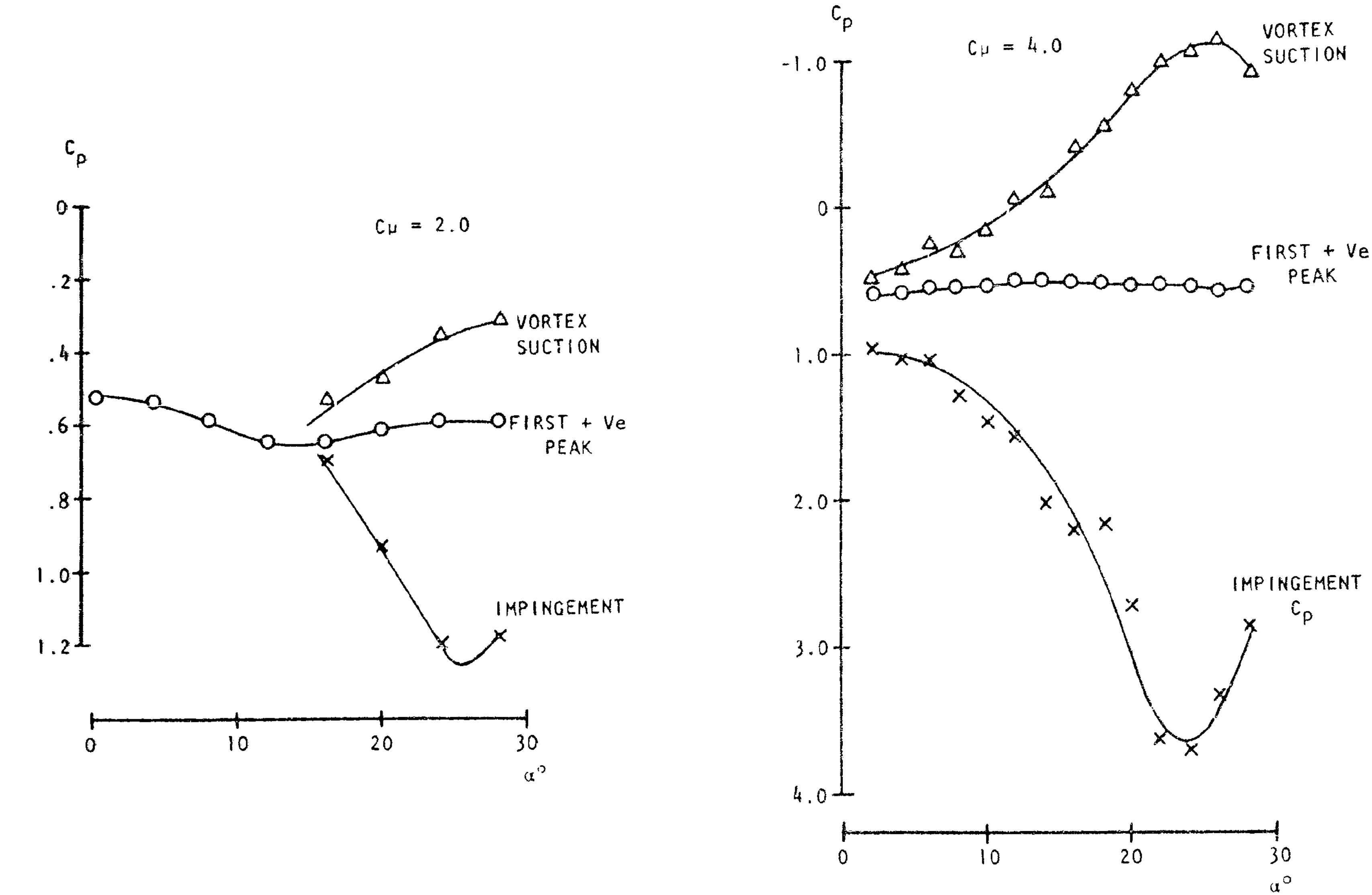

Figure 4.16 Development of floor vortex in terms of peak pressures. (No BLC applied)

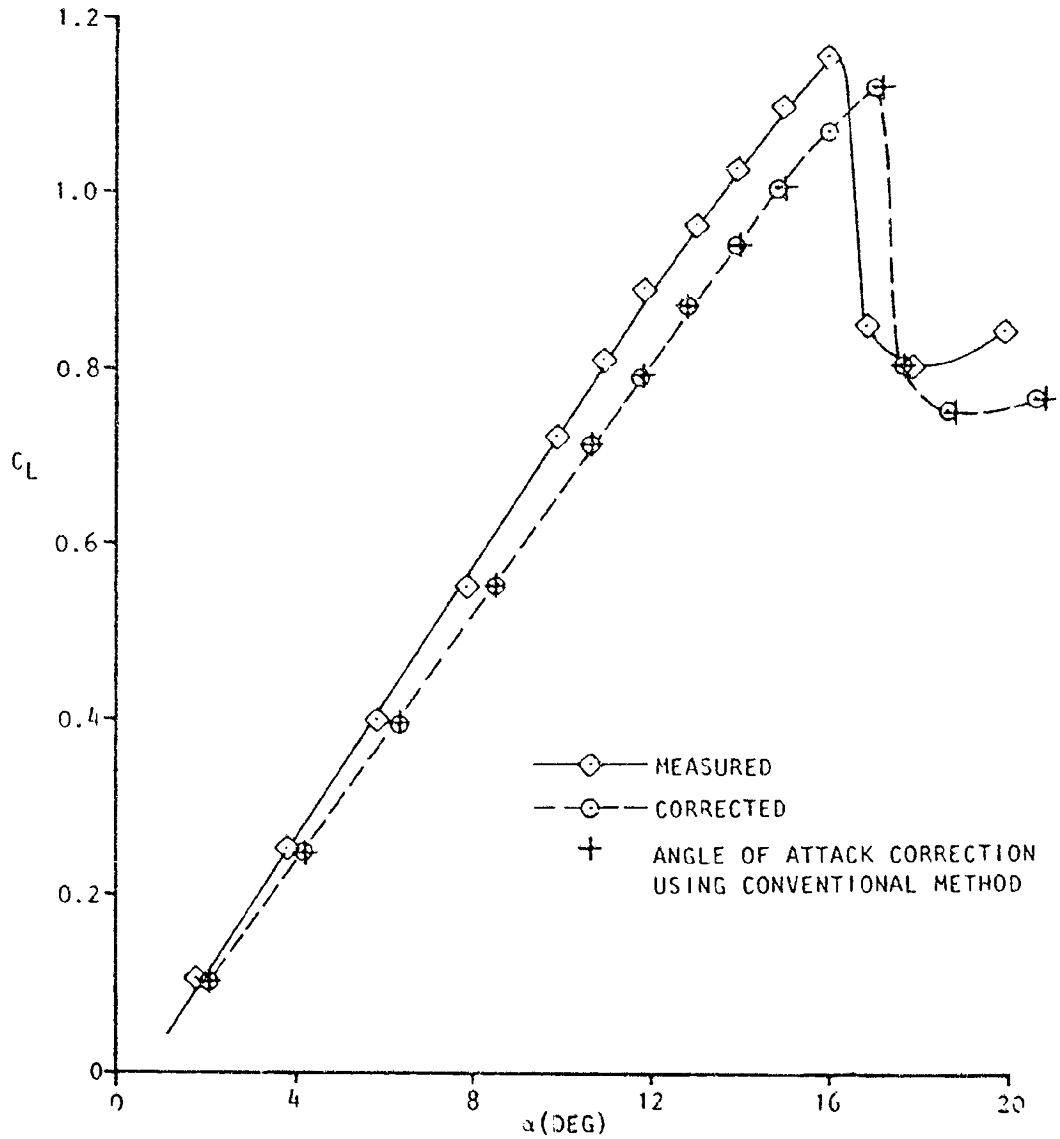

Figure 5.1 Angle-of-attack corrections for a simple wing using the wall pressure signature method

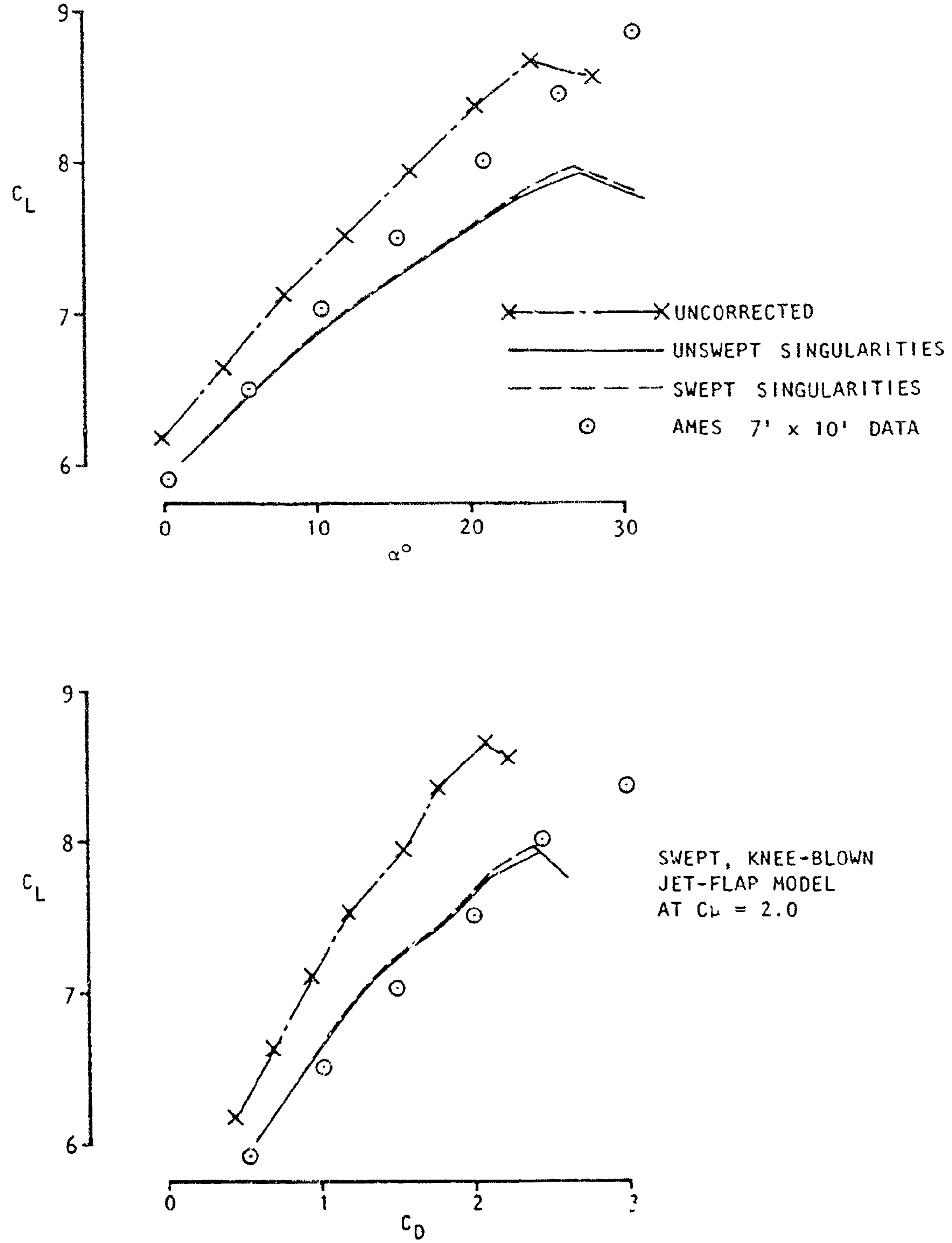

Figure 5.2 Correction of lift and drag data for the swept, knee-blown, jet-flap model.
a) Sensitivity to sweep of line singularities ("cross" effects included)

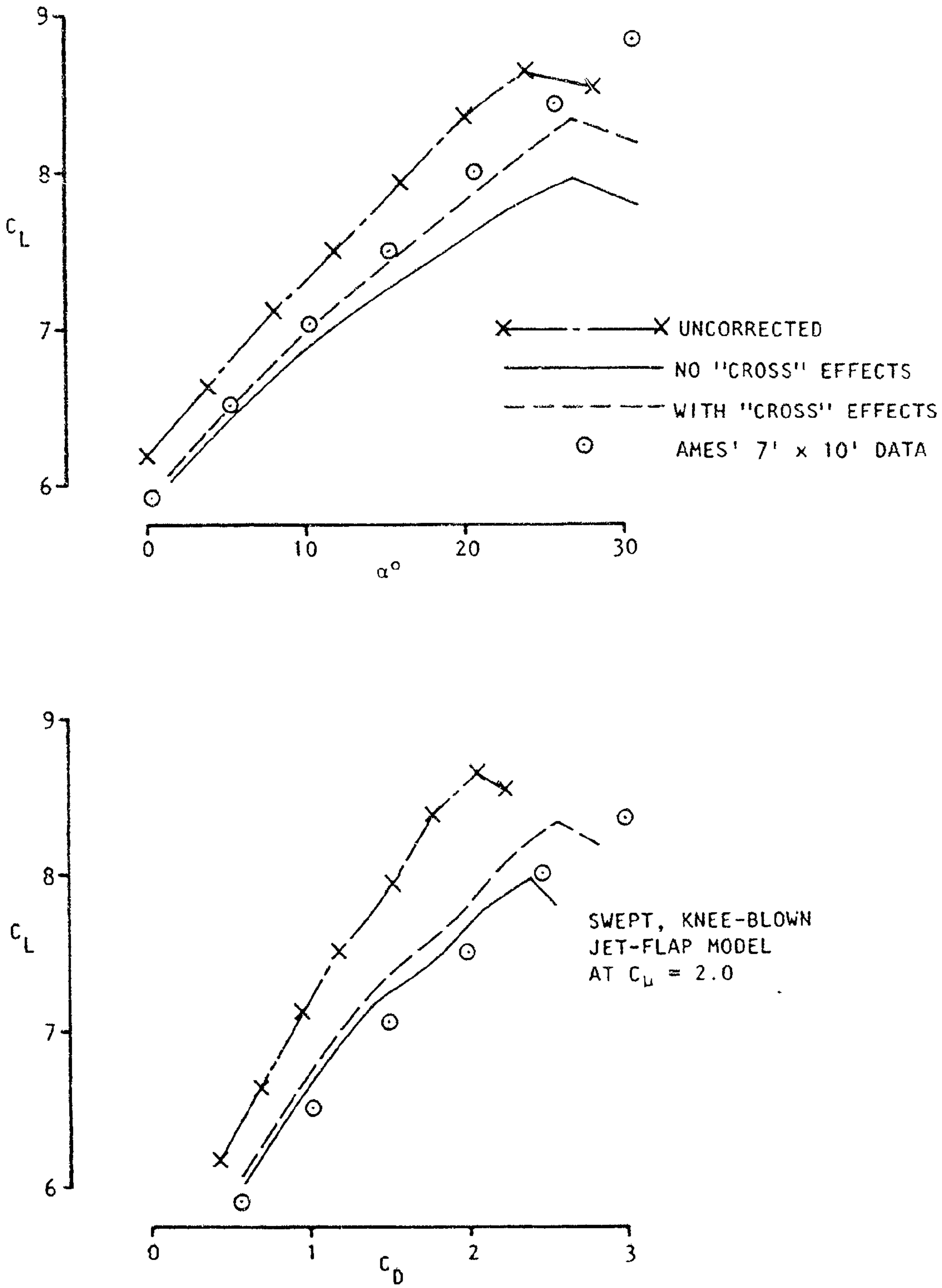

Figure 5.2 (continued) Correction of lift and drag data for swept, knee-blown, jet-flap model
b) Sensitivity to 'cross' effects.
(Swept singularities used set at 15° angle of attack)

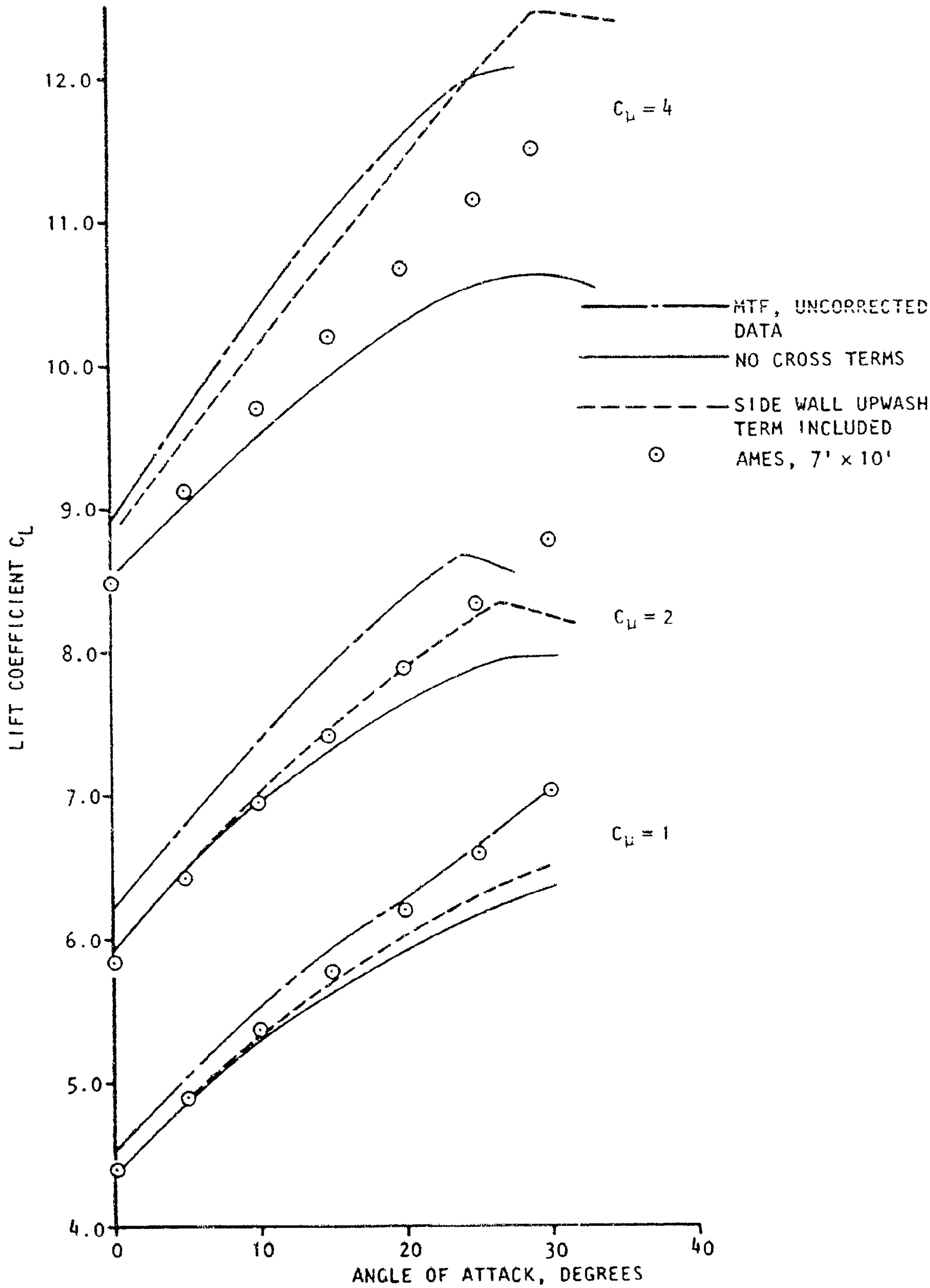

Figure 5.2 (concluded) Correction of lift and drag data for a swept, knee-blown, jet-flap model.
(c) Sensitivity to the side wall upwash term.

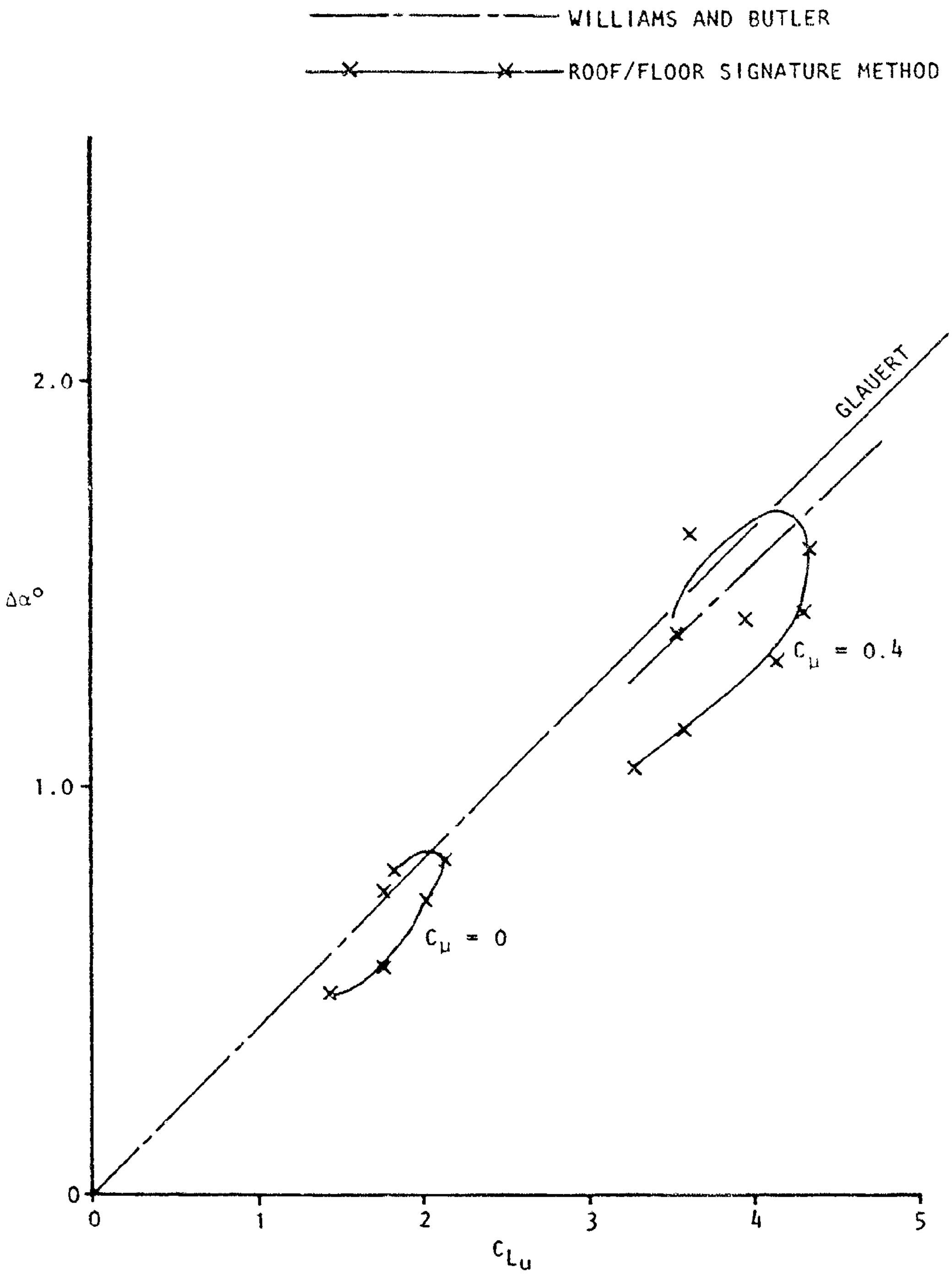

Figure 5.3 Angle-of-attack corrections for the swept, knee-blown jet-flap model
a) C_μ = 0 and 0.40

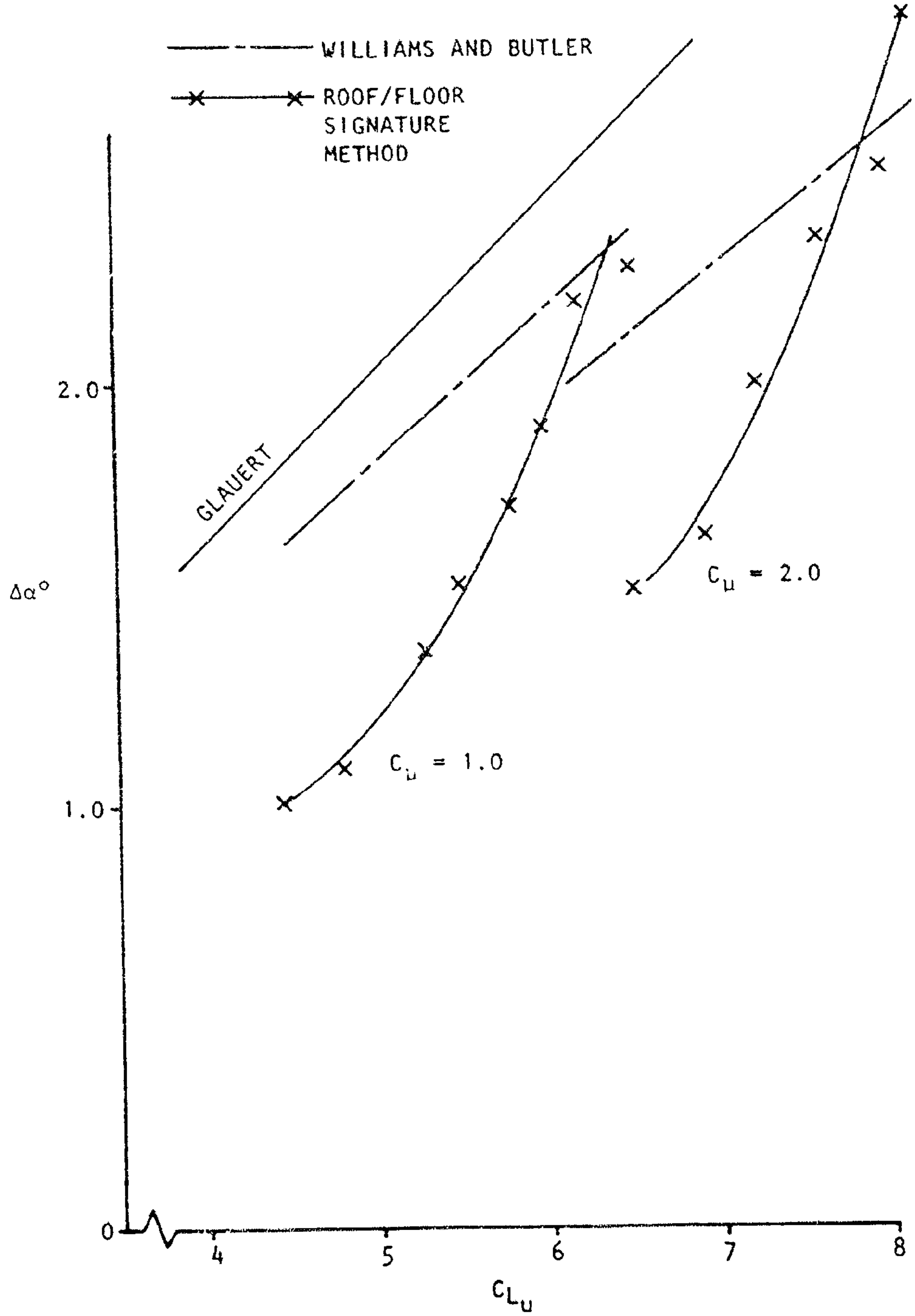

Figure 5.3 (continued) Angle-of-attack corrections for the swept, knee blown, jet-flap model
b) $C\mu$ = 1.0 and 2.0

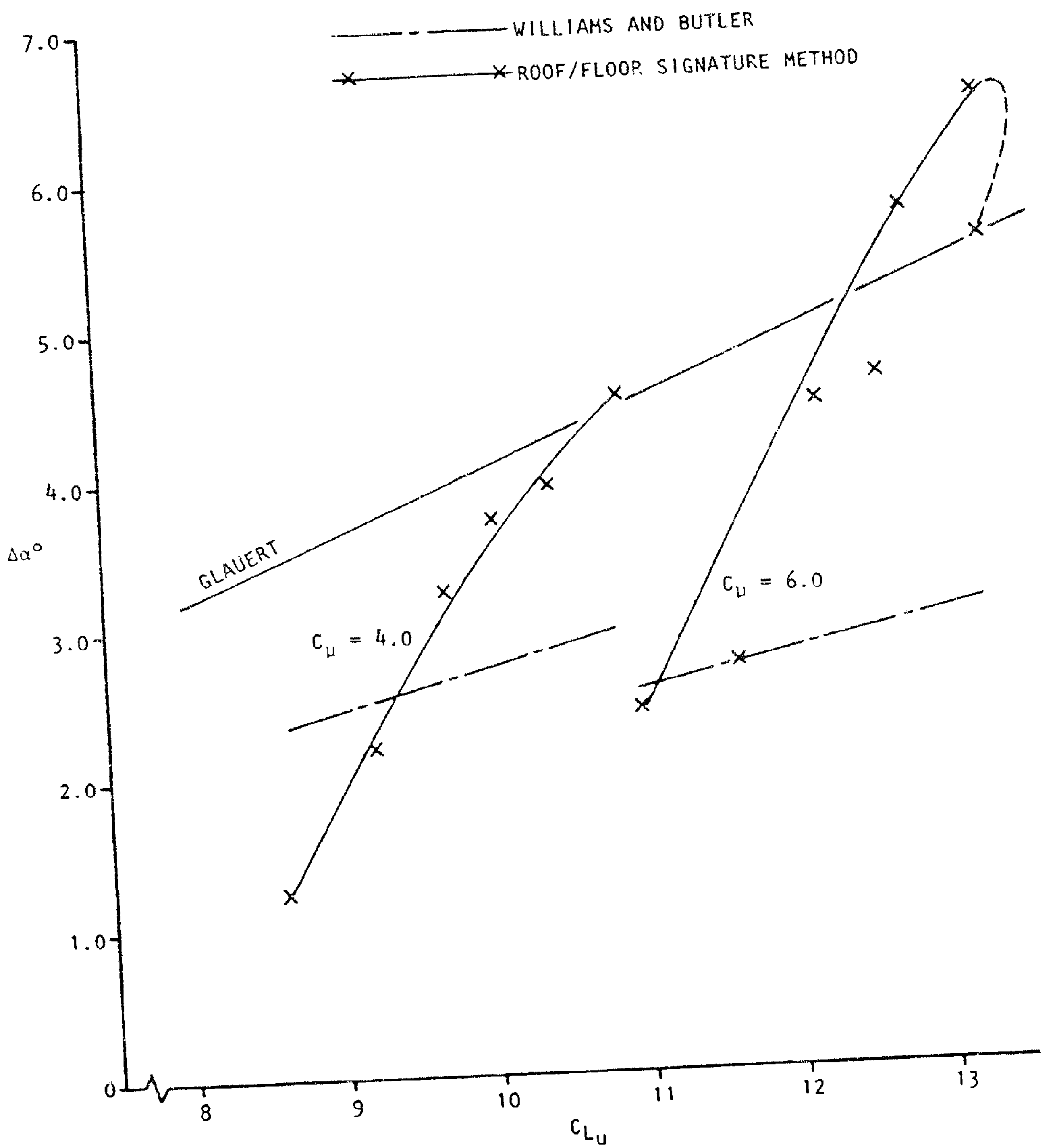

Figure 5.3 (concluded) Angle-of-attack corrections for the swept, knee-blown, jet-flap model
c) C_μ = 4.0 and 6.0

ORIGINAL PAGE IS
OF POOR QUALITY

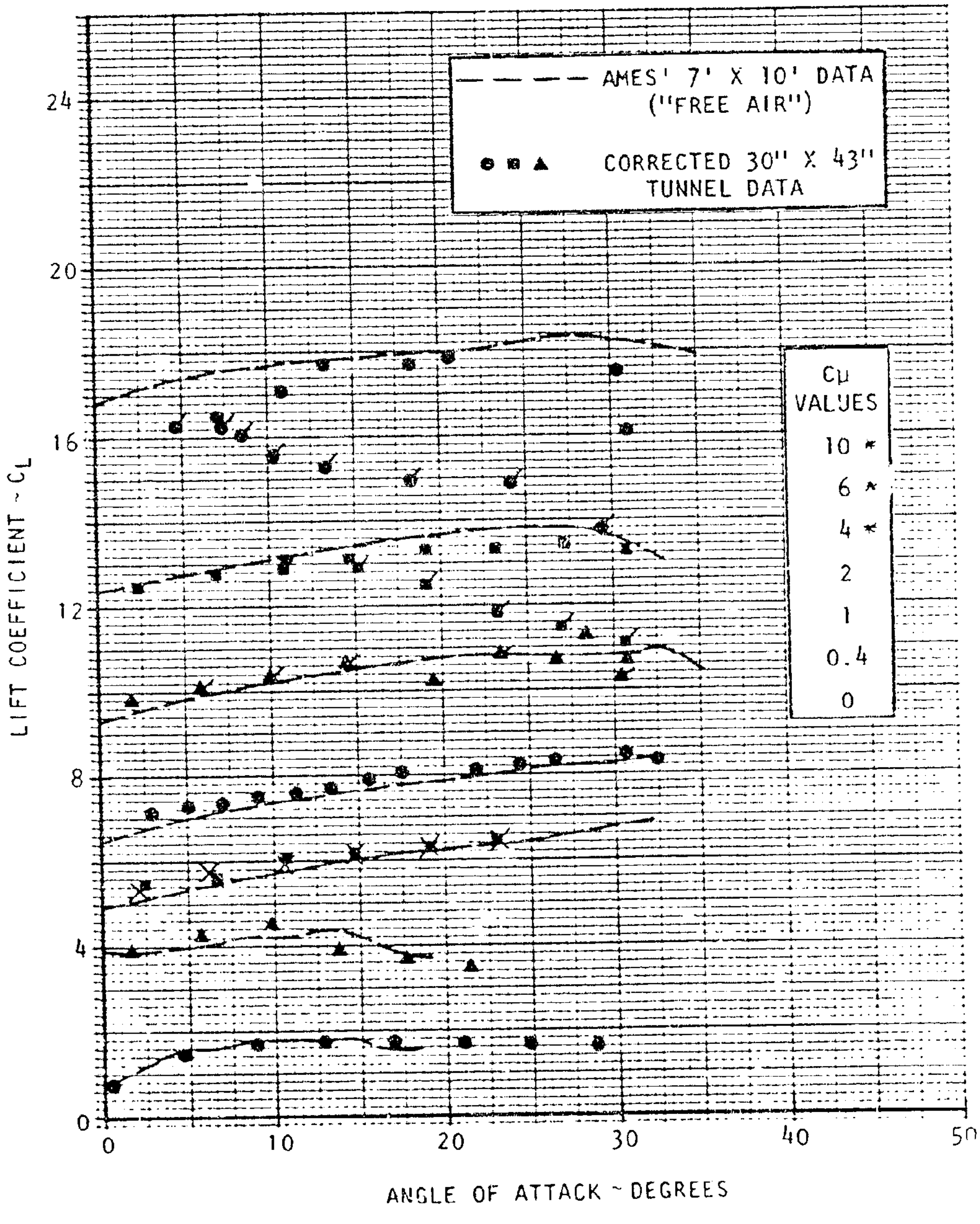

Figure 5.4(a) Basic Lift Data, Straight Wing With Slats

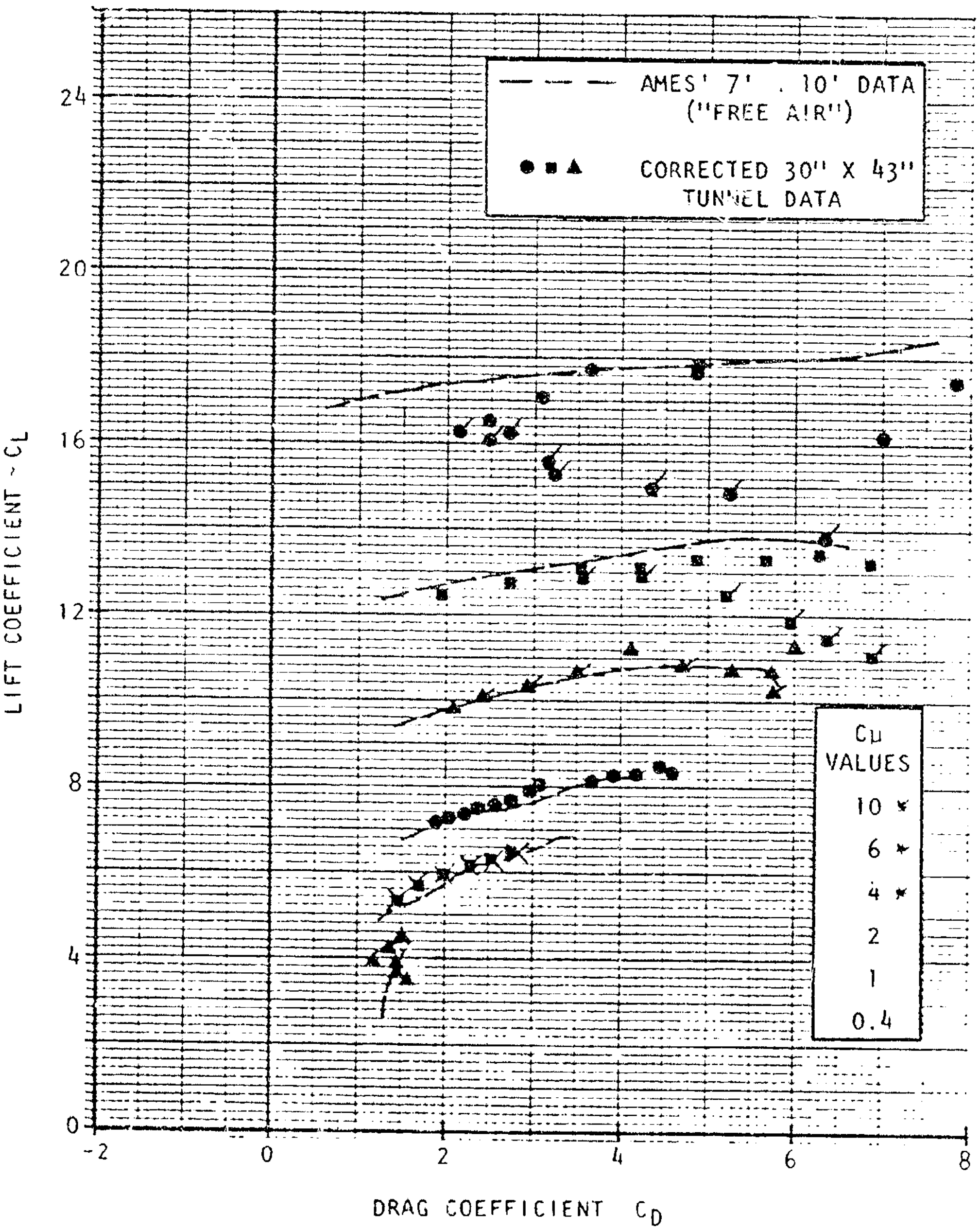

Figure 5.4(b) Basic Drag Data, Straight Wing With Slats

ORIGINAL PAGE IS
OF POOR QUALITY

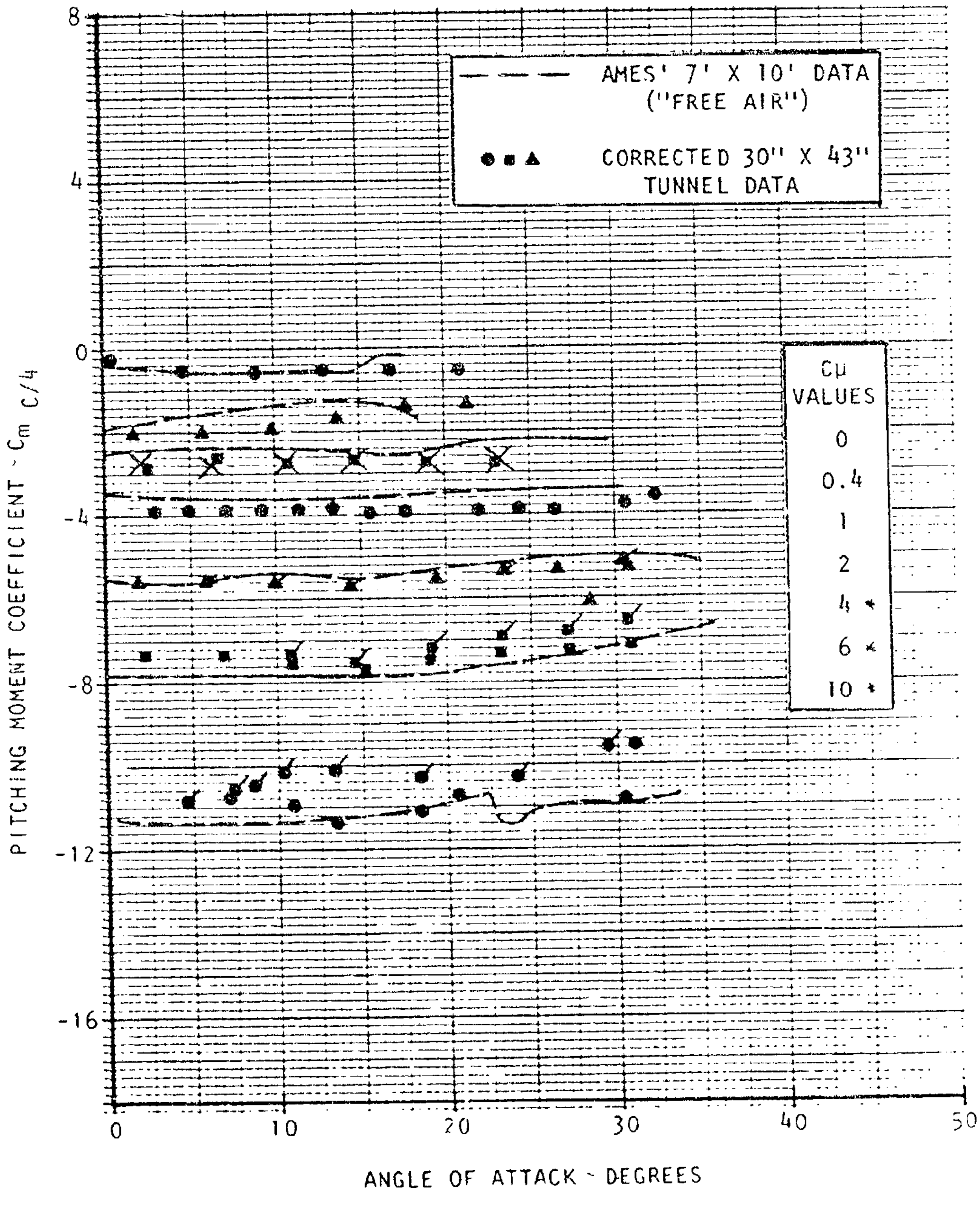

Figure 5.4(c) Basic Pitching Moment Data, Straight Wing With Slats

ORIGINAL PAGE IS
OF POOR QUALITY

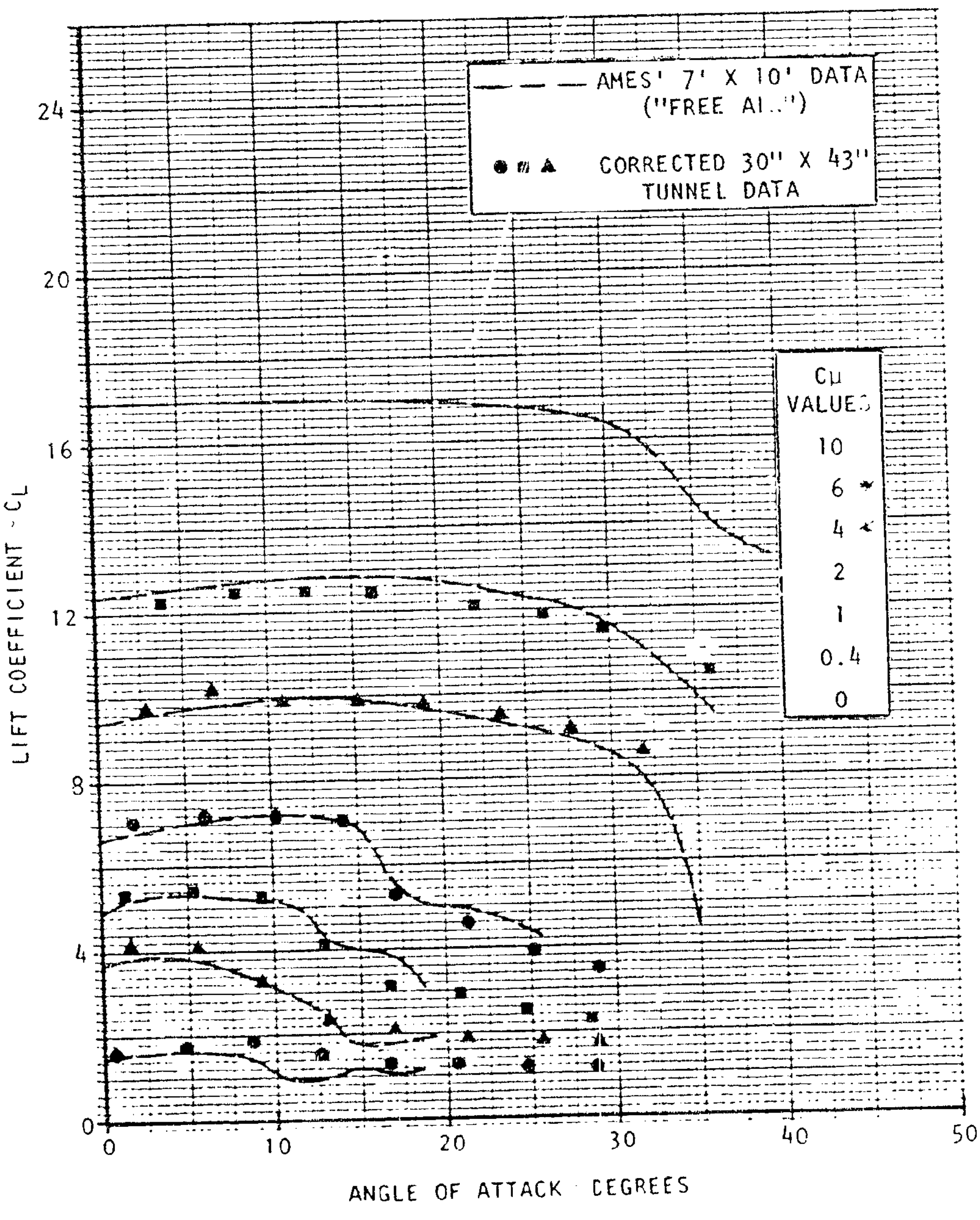

Figure 5.5(a) Basic Lift Data, Straight Wing, No Slats

2 OF 2

23234 UN

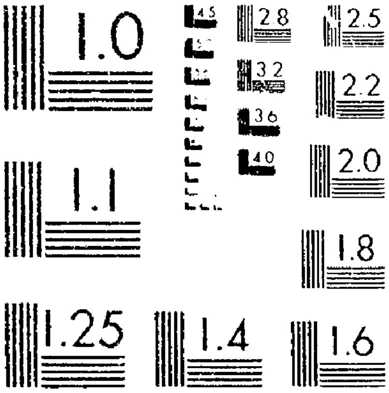

MICROCOPY RESOLUTION TEST CHART

NATIONAL BUREAU OF STANDARDS 1963 A

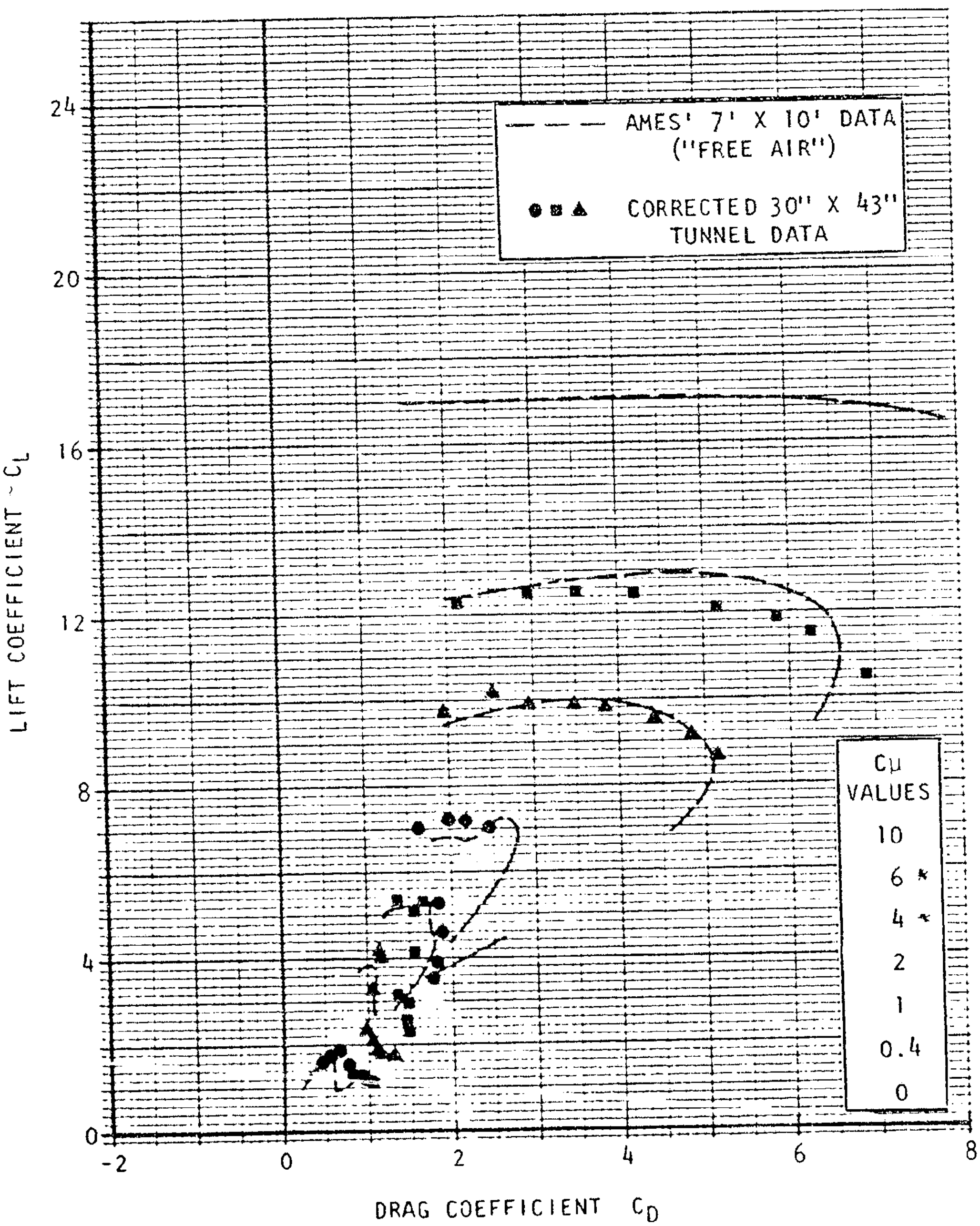

Figure 5.5(b) Basic Drag Data, Straight Wing, No Slats

C-2

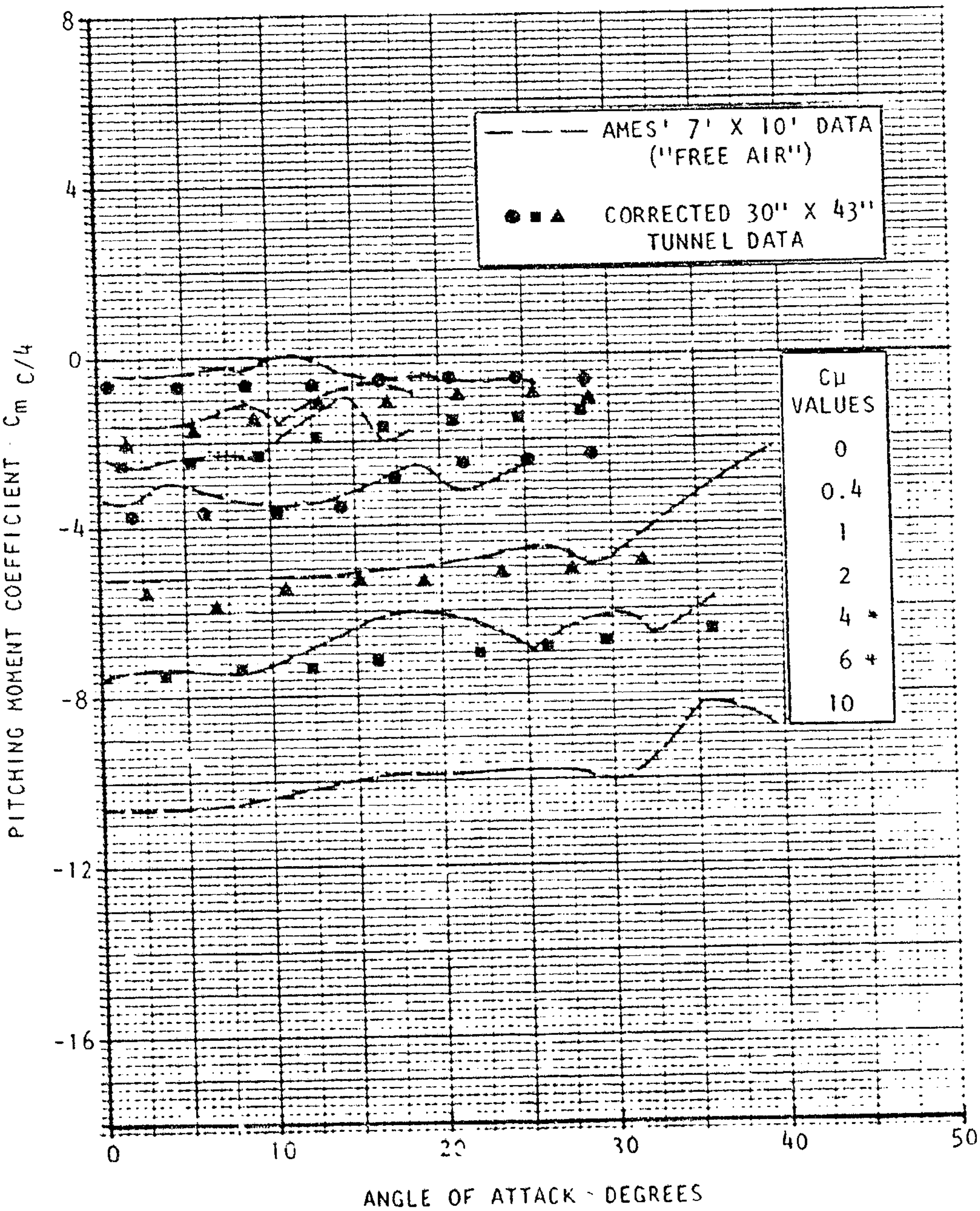

Figure 5.5(c) Basic Pitching Moment Data, Straight Wing, No Slats

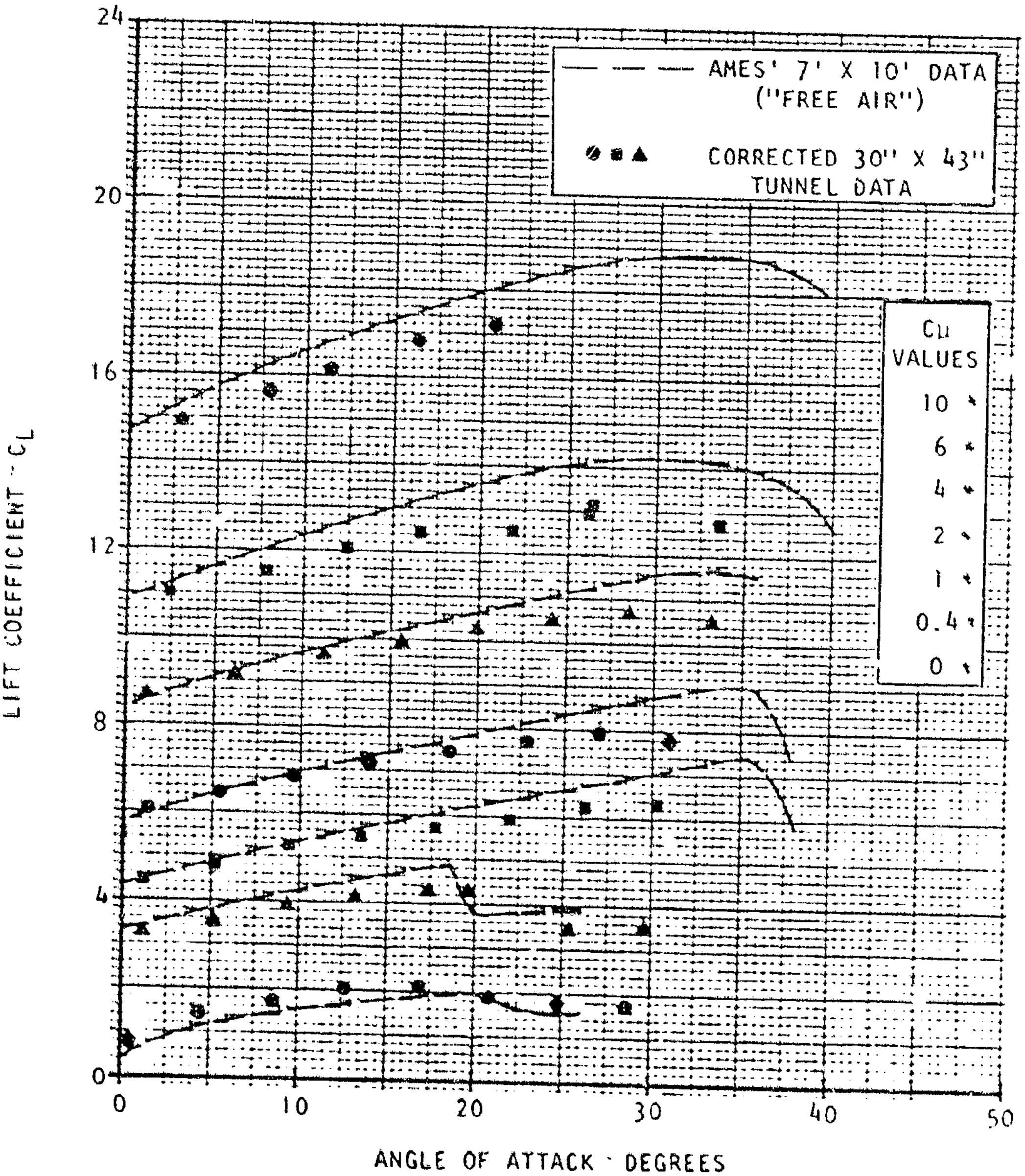

Figure 5.6(a) Basic Lift Data, Swept Wing With Slat.

ORIGINAL PAGE IS
OF POOR QUALITY

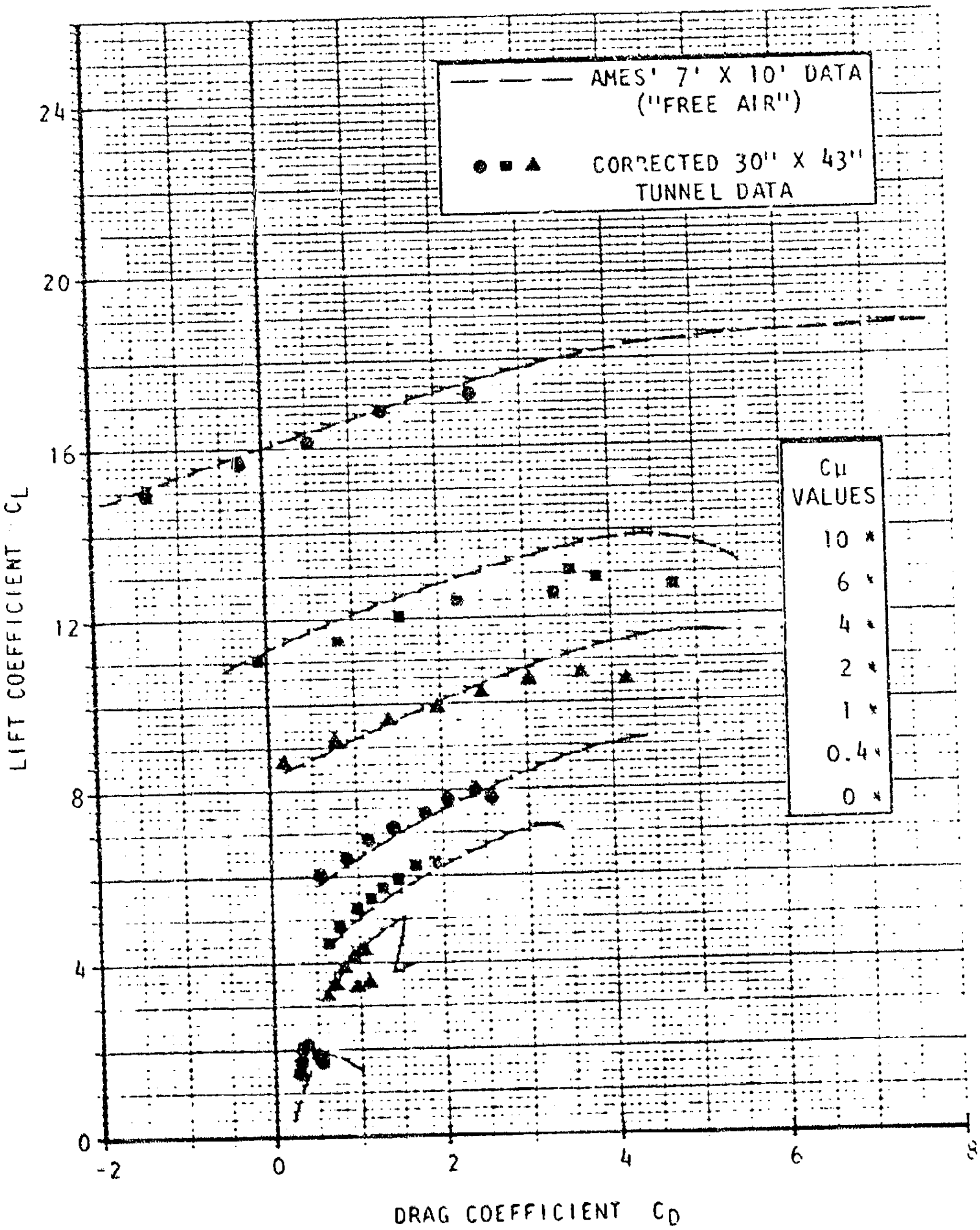

Figure 5.6(b) Basic Drag Data, Swept Wing With Slats

ORIGINAL PAGE IS
OF POOR QUALITY

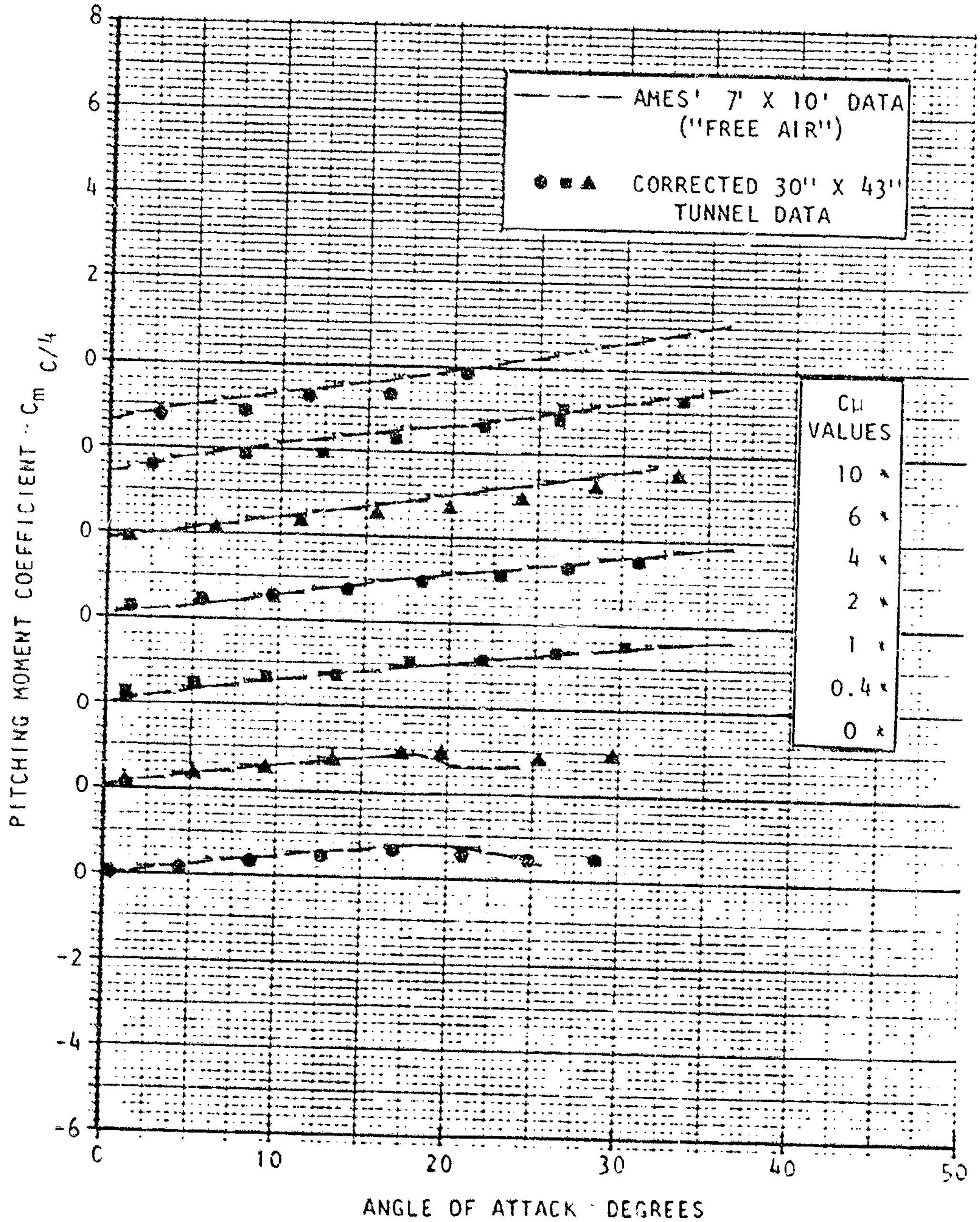

Figure 5.6(c) Basic Pitching Moment Data, Swept Wing With Slats

ORIGINAL PAGE IS
OF POOR QUALITY

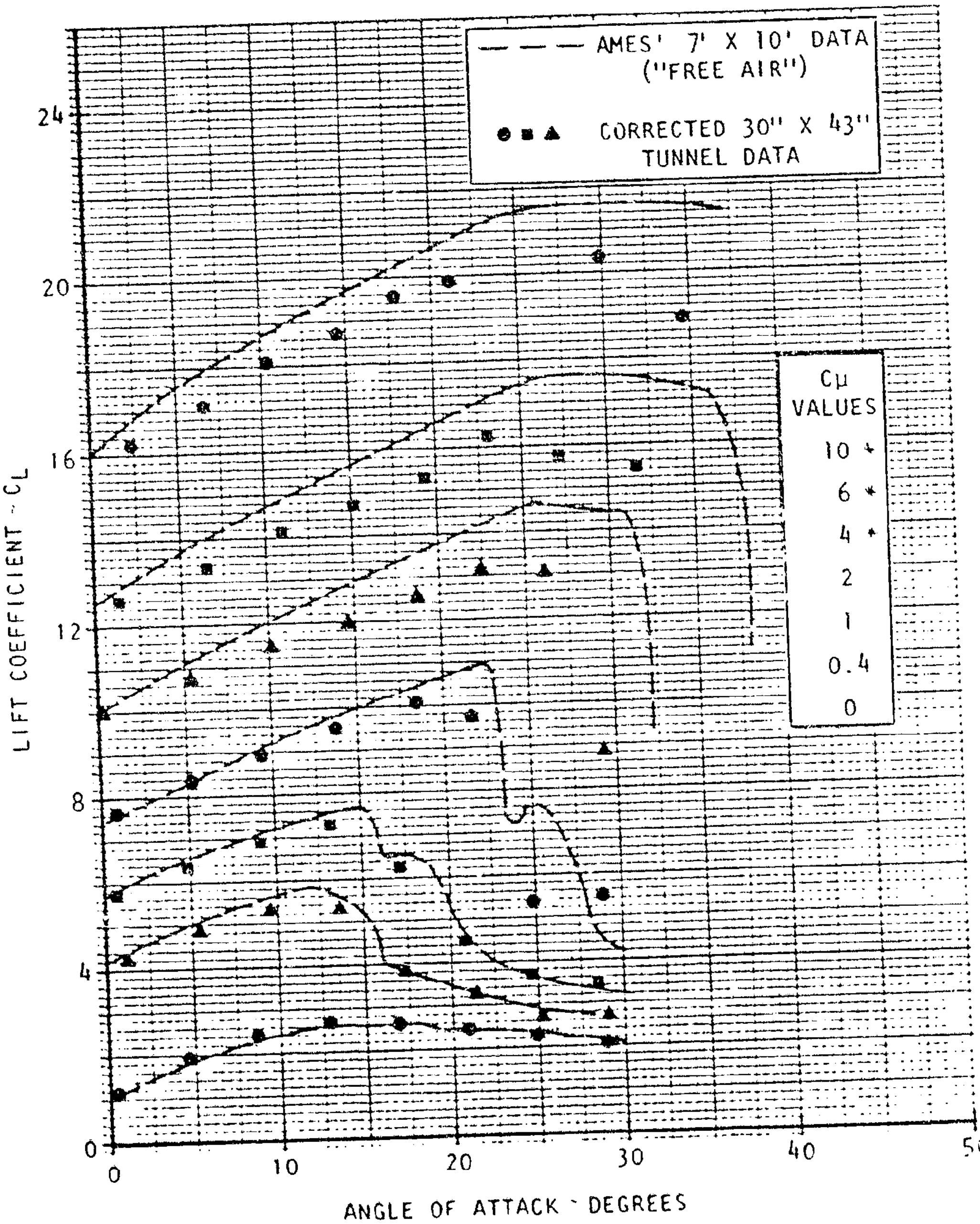

Figure 5.7(a) Basic Lift Data, Swept Wing With Tips and Full-Span Slats

ORIGINAL PAGE IS
OF POOR QUALITY

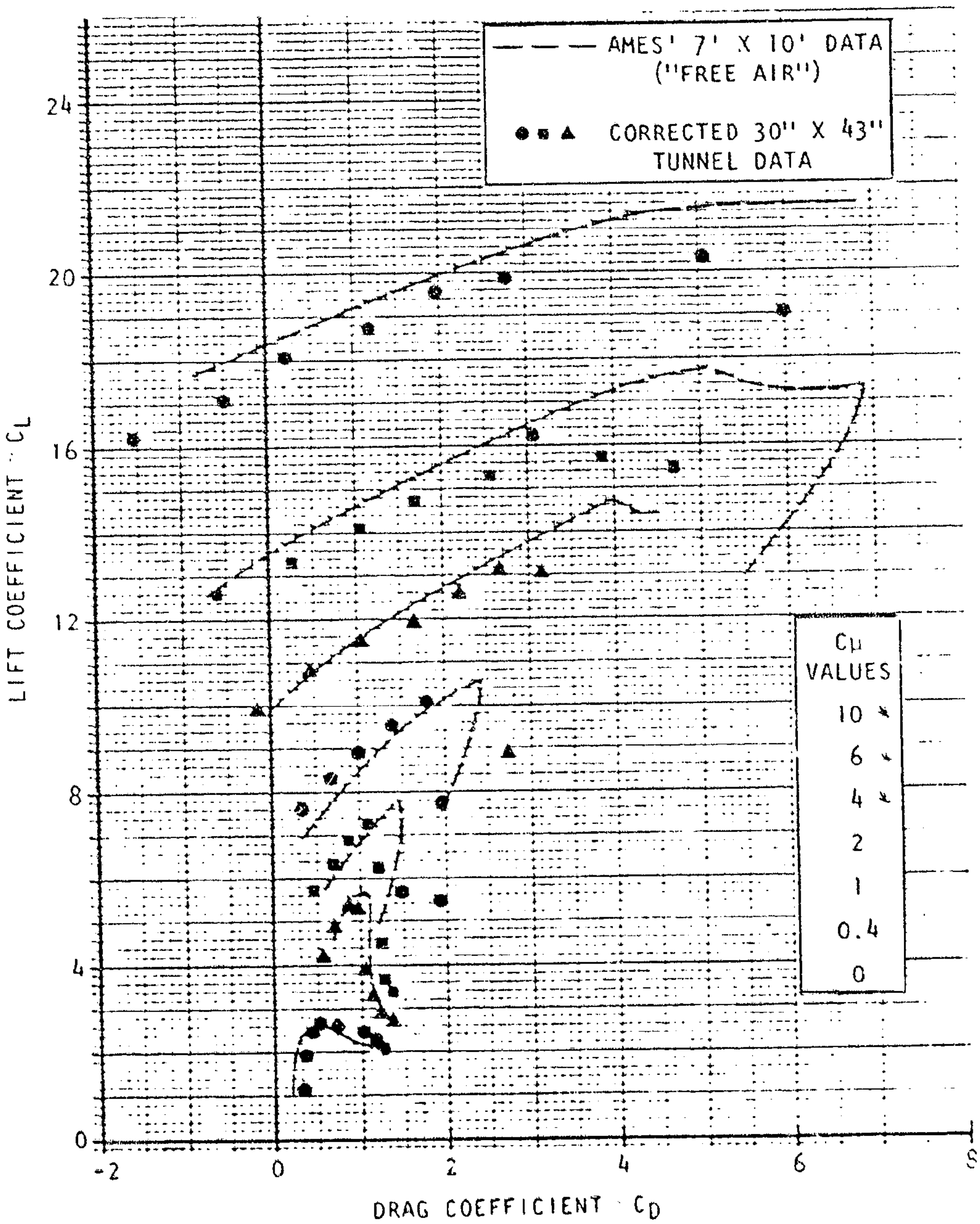

Figure 5.7(b) Basic Drag Data, Swept Wing With Tips and Full-Span Slats

ORIGINAL PAGE IS
OF POOR QUALITY

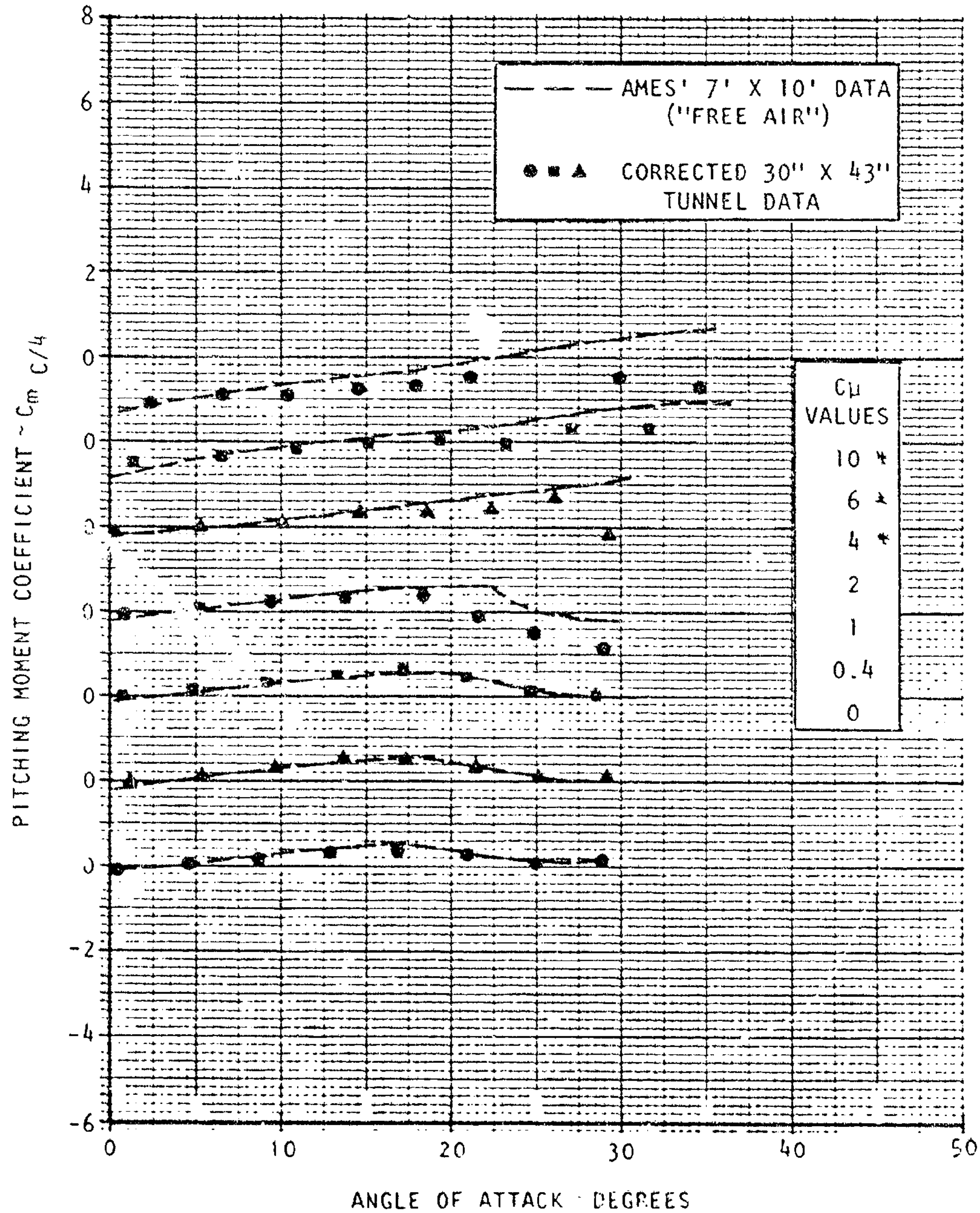

Figure 5.7(c) Basic Pitching Moment Data, Swept Wing With Tips and Full-Span Slats

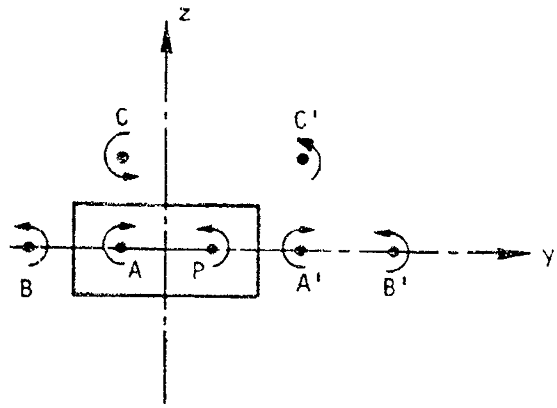

Upwash at P, due to A, B, C etc, is neutralized by downwash due to A', B', C' etc.

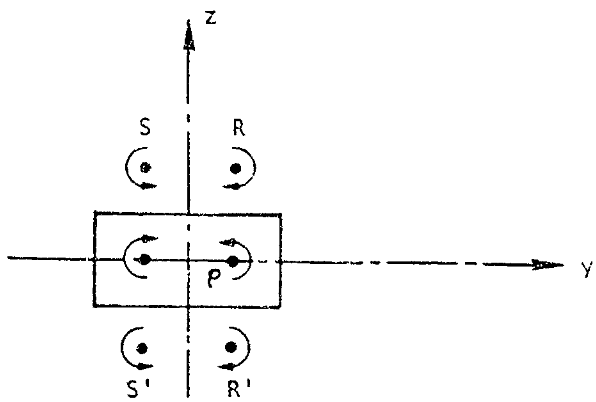

Sidewash at P, due to R, S etc, is balanced by sidewash due to R', S' etc.

Figure 6.1 Occurrence of 'neutral' points in a wind tunnel cross section.

APPENDIX 1

PROGRAM DESCRIPTION

APPENDIX - 1

PROGRAM DESCRIPTION

Capabilities:

The tunnel-wall-effect correction program is a generalized version to handle complex pressure signatures arising from powered model tests. It essentially solves an inverse problem of determining the strengths of potential singularities, the geometry of which has been specified, to satisfy the measured pressure signatures on the tunnel boundaries. The number of singularities can be fewer than the number of pressure signature points since the present approach satisfies the boundary condition in least squares sense.

It is possible for the user to specify arbitrary orientations and geometry for the potential singularities to model the actual flow as closely as possible. In the present version of the program, no assumptions regarding the symmetry or anti-symmetry of the influence coefficients are made to resolve the signature into vortex-related and source-sink-related parts. This resolution is done iteratively during the numerical computations. At present, the tunnel geometry however is restricted to rectangular shapes, since the computational procedure uses imaging technique to ensure zero-normal-flow through the tunnel walls. However, alternative arrangements are made for cases involving the 40' x 80' tunnel cross section (see below).

Normally, the difference between the observed supervelocity on the roof and the one on the floor is used as boundary condition for obtaining the vortex strengths. However, with powered models involving jet impingement on the floor, it may not be desirable to use the floor signature in the calculations. In such cases a flag, IRF, can be set to handle only the roof signature. Note that this requires that the cross term flags (KROSG and KROSQ) should be turned on and that the number of iterations (ITERMAX) should be set larger than unity even if all singularities are placed symmetrically with respect to the tunnel cross-section.

The program coding was developed using a VAX-16 computer. FORTRAN statements that may cause problems in other systems are identified by the characters VAX in columns 73 - 75 of those statements. When using other systems these statements should be appropriately replaced.

The present coding is written with the assumption that the pressure signatures and load coefficients to be corrected are made available in a mass storage file. The subroutine READCP reads in these values using FORTRAN I/O unit number 10. This subroutine is written to handle specifically the KBF model data of Lockheed-Georgia. In this case, eight rails of tunnel wall signature data were available in a mass storage file in the form of super-velocities rather than C_p-values. Also, since the x-wise locations of pressure points for rail No. 7 was different from the rest of the rails, a subroutine INTER is employed to linearly interpolate the rail-7 data to the standard x-wise locations. Since the general user's data structure will be different from that of Lockheed's KBF tests, these subroutines and their calling sequences in the driver program might have to be replaced.

Preparation of Input Data

The overall sequence of computations and the effects of different flag settings are shown in the flow chart given in figure A1. The meaning of all input variables are explained in the next section. A typical run of the program involves one of the two cases: (1) The required matrices are all

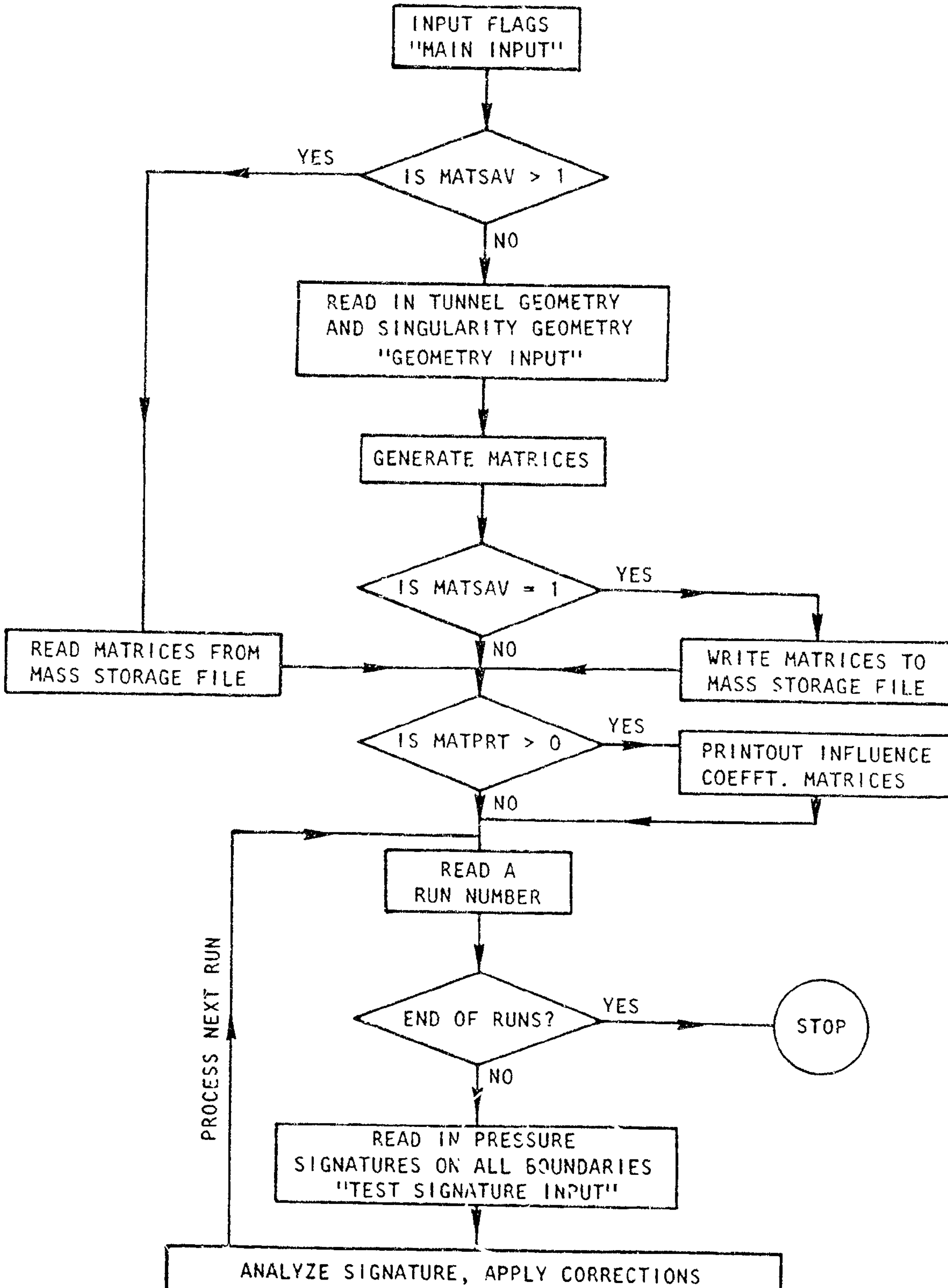

Figure A1. Flow chart for wall-pressure signature-based tunnel interference program.
a) Pre-analysis routines

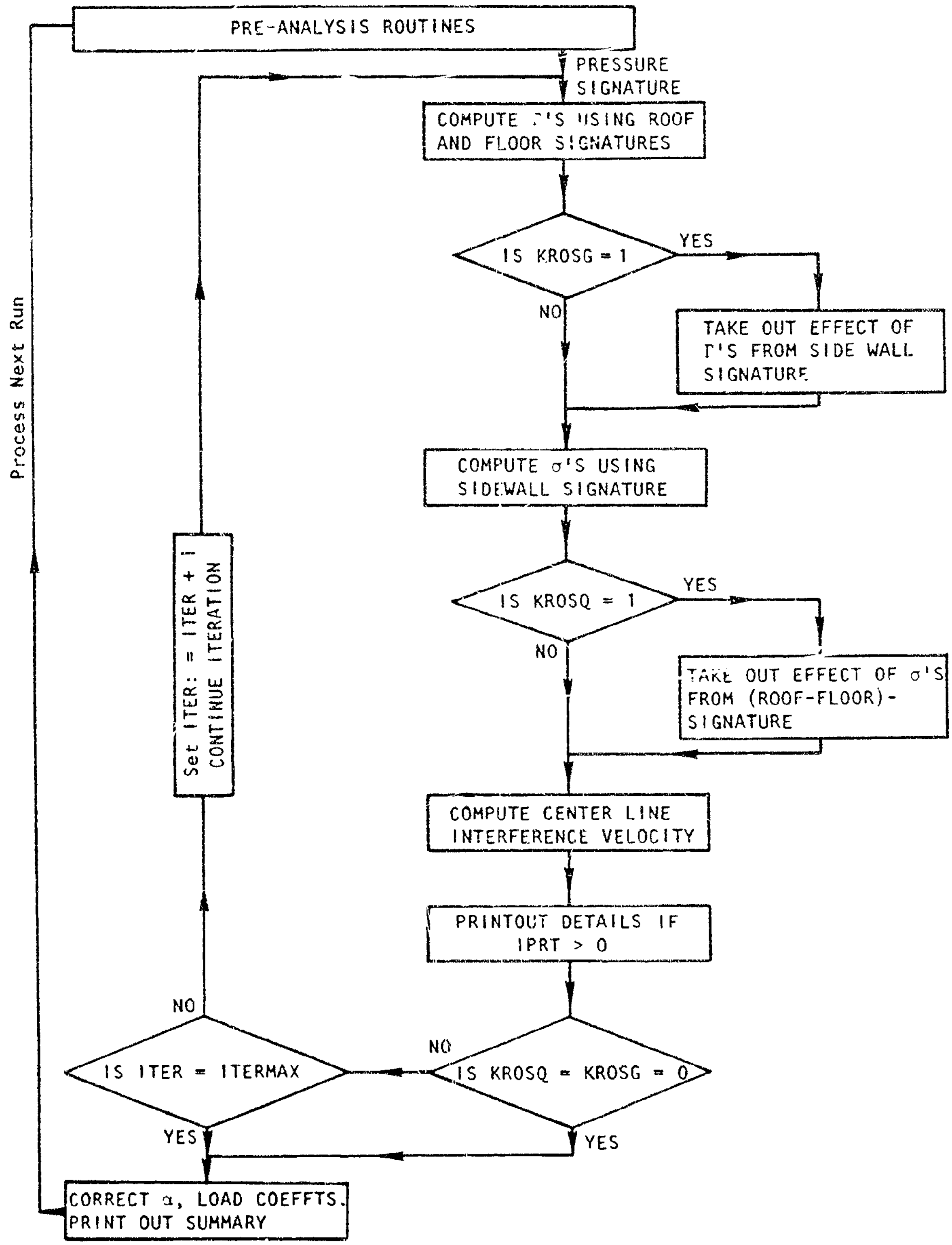

Figure A1. Flow Chart for Wall Pressure Signature-Based Tunnel Interference Program.
b) Signature Analysis and Data Correction.

available and only the signatures need be processed. (2) The matrices must be generated and saved for future use. The input sequence for these two cases are as follows. (1) Matrices available: Prepare Card Number 1 through 3 as indicated under next section. Set MATSAV=2 in Card Number 3. Skip Cards 4 through 9 and prepare Card No. 10. (2) Matrices must be generated: Prepare all cards, No. 1 through No. 10. Set MATSAV=1 in Card No. 3.

Description of Input Variables

Main Input - The main input portion consists of a title, all flag variables and a few key variables related to the model geometry as outlined below.

1 | TITLE | Format -- 80A1

TITLE: Test Description

2 | ITERMAX | MATPRT | MATSAV | IPRT | KROSG | KROSQ | ICORR | JETEFCT | Format --16I5

ITERMAX: Maximum number of iterations to be performed when cross-effect-terms are to be included in analyzing the signatures. Program automatically sets this to unity if both KROSG and KROSQ are zeros.

MATPRT: A non-zero value causes all influence coefficient matrices to be printed out.

MATSAV: Three-way flag.

=0: Generates matrices but does not save them.

=1: Generates matrices and writes them to FORTRAN unit Number 8.

=2: Implies that all required matrices are available from a previous run. They will be read from FORTRAN unit No. 8.

IPRT: Flag for printout detail.

=0: Prints out a one page summary for each tunnel test.

=1: Prints out details for each iteration.

KROSG: When non-zero, calculates and takes out the sidewall upwash due to vortices in determining the u-velocity boundary conditions on side walls from pressure coefficients.

KROSQ: When non-zero takes out the cross effect of sources/sinks from the Roof/Floor signature, before calculating the circulation strengths of the vortices. (Note: A non-zero value is meaningful only if sources/sinks are not placed symmetrically with respect to the tunnel cross section).

ICORR: The centerline interference velocities at the x-location corresponding to this index will be used in making final corrections to angle of attack and the loads.

JETEFCT: Non-zero if model includes a lifting jet. (See Part II of the report)

3

SAREA	AWB	BWB

Format--8F10.4

SAREA: Model Reference Area used in normalizing the load coefficients.

AWB
BWB: Constants in the Butler-Williams Equation for correction to angle of attack, $\Delta\alpha = AWB*CL_c/(1 + BWB*C_{\mu c})$.

Geometry Input: The input of this section pertains to the tunnel geometry and the singularity geometry.

This entire section should be skipped while preparing the input in MATSAV=2 in the Main Input which implies that all required matrices are already available.

4

LAYERS	IRF	NR	NW	NV	NS

Format--1615

LAYERS: No. of Image Layers to be used (Recommended: 5)

IRF: Flag for determining whether floor signature is to be used or not.

=0: Implies usage of roof signature only.

=1: Implies usage of (roof-floor) values.

(Note: If roof signature only is to be used, set KROSQ=1 and ITERMAX=1)

NR: No. of roof signature points.

(It is assumed No. of floor signature points is same)

NW: No. of side-wall signature points. (Both sides are assumed to have some no. of points).

NV: No. of vortex singularities

NS: No. of source/sink singularities

5

B	H	XPVOR	XPSRC

Format--8F10.4

B: Tunnel Breadth

H: Tunnel Height

XPVOR: Pivot point for pitching swept vortex, normalized w.r.t. span (See sketch). Meaningful only when the vortex is swept.

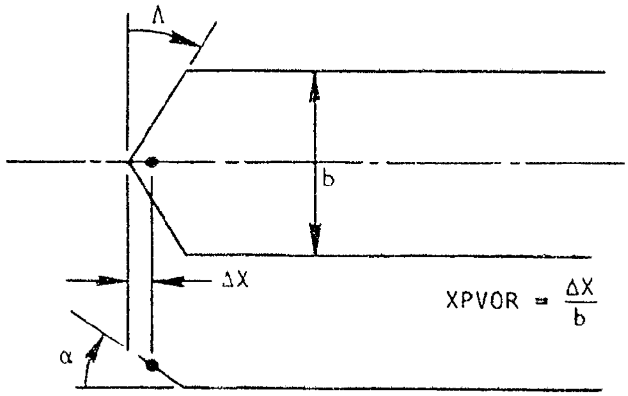

XPSRC: Pivot point for pitching swept source/sink normalized with respect to semi-span. ʋefinition is similar to XPVOR given above.

Card				Format	
6.1	XR_1	YR_1	ZR_1	Format--8F10.4	
6.2	XR_2	YR_2	ZR_2	Format--8F10.4	
	•				Non-dimensional coordinates, x/B, y/B, 2/H, of the roof/ floor signature points.
	•				
	•				
6.NR	XR_{NR}	YR_{NR}	ZR_{NR}	Format--8F10.4	

Card				Format	
7.1	XL_1	YL_1	ZL_1	Format--8F10.4	
7.2	XL_2	YL_2	ZL_2	Format--8F10.4	
	•				Non-dimensional coordinates, x/B, y/B, z/H of the side-wall signature points.
	•				
	•				
7.NW	XL_{NW}	YL_{NW}	ZL_W	Format--8F10.4	

8.1	XV_1	YV_1	ZV_1	SBV_1	$PSIV_1$	$ALFV_1$	Format--8F10.4
8.2	XV_2	YV_2	ZV_2	SBV_2	$PSIV_2$	$ALFV_2$	Format--8F10.4
•							
8.NV	XV_{NV}	YV_{NV}	ZV_{NV}	SBV_{NV}	$PSIV_{NV}$	$ALFV_{NV}$	Format--8F10.4

(XV,YV,ZV): Non-dimensional coordinate x/B, y/B, z/H of the "roof" point of horse-shoe vortices.

SBV: Vortex span normalized with B

PSIV: Sweep angle for the vortex (degrees)

ALFV: Pitch angle for the vortex (degrees)

9.1	XS_1	YS_1	ZS_1	SBS_1	$PSIS_1$	$ALFS_1$	Format--8F10.4
9.2	XS_2	YS_2	ZS_2	SBS_2	$PSIS_2$	$ALFS_2$	Format--8F10.4
•							
9.NS	XS_{NS}	YS_{NS}	ZS_{NS}	SBS_{NS}	$PSIS_{NS}$	$ALFS_{NS}$	Format--8F10.4

The definitions of these variables, defining the source/sink locations and geometries, are similar to the ones for vortices.

Test Signature Input: This last input card contains the values of key variables identifying the test, the signatures corresponding to which are to be picked up from a mass storage file. This card can be repeated as many times as desired to process all required runs. (NOTE: The user may need to replace this section of the coding. See earlier comments about subroutines READCP and INTER)

10	ITEST	IRUN	IPMIN	IPMAX	IFLOOR	IROOF	IWAL1	IWAL2	16I5

ITEST: Test Number

IRUN: Run Number

IPMIN: Point No., minimum

IPMAX: Point No., maximum

For the given run number the program will process data for all points i in the range IPMIN $\leq$ i $\leq$ IPMAX.

IFLOOR: Pressure signature rail no. for floor

IROOF: Pressure signature rail no. for roof

IWAL1: Pressure signature rail no. for first sidewall.

IWAL2: Pressure signature rail no. for second sidewall.

Mass-Storage File Requirements:

In addition to the standard input/output FORTRAN units (#5 and #6 in the coding), the coding employs four other mass-storage files, as explained below.

UNIT-7: Output file. The test no., run no., point no. are written to this file along with a summary of measured and corrected angle of attacks and load coefficients. It may be used in preparing plots if so desired.

UNIT-8: Input/Output file.

This would contain all the input data entered in the section "geometry Input", all the required influence coefft. matrices and the least square inverse matrices. This file has to be generated and saved when the program is run for the first time or whenever a change in any of the input variable described in the section "Geometry Input" is made.

UNIT-9: Output file

For each data point and for each iteration this would contain the input signatures, the recalculated boundary conditions and the centerline interference velocity components. It may be used in preparing machine plots to evaluate the program.

UNIT-10: Input file.

For each data point, this file should have the pressure signature. The structure of this file is left to the user (See comments about subroutine READCP above).

Output Format

A complete sample output follows the program listing. The output is sufficiently well annotated for easy comprehension of the print out. In the printer plots of the input signature, calculated wall supervelocities and tunnel center line velocities, the correspondence is readily established by looking for the same plot symbol under the tabulated data. In the table of corrected α and load coefficients, the values labelled "CLASSICAL" are the ones obtained using Butler-Williams equation. In the output annotations the word ROOF would mean either roof alone or (roof-floor) values depending upon how the input was arranged. Notations like "U-Q-CL" imply "u-velocity due to sources at tunnel center line."

```
EXAMPLE..KNEE_BLOWN_FLAP_TESTS..GENERATE MATRIX..EXCLUDE CROSS TERMS
    1     0     1     1     0     0     8
     80.00   0.007132   0.126970
    5     1    21    21     4     7
43.000000  30.000000   0.000000   0.000000
-0.814000   0.000000   0.500000
-0.465100   0.000000   0.500000
-0.372100   0.000000   0.500000
-0.279100   0.000000   0.500000
-0.186000   0.000000   0.500000
-0.093000   0.000000   0.500000
 0.000000   0.000000   0.500000
 0.069800   0.000000   0.500000
 0.139500   0.000000   0.500000
 0.209300   0.000000   0.500000
 0.279100   0.000000   0.500000
 0.348800   0.000000   0.500000
 0.418600   0.000000   0.500000
 0.488400   0.000000   0.500000
 0.587400   0.000000   0.500000
 0.697700   0.000000   0.500000
 0.837200   0.000000   0.500000
 0.966700   0.000000   0.500000
 1.116300   0.000000   0.500000
 1.255800   0.000000   0.500000
 1.395300   0.000000   0.500000
-0.814000   0.500000   0.000000
-0.465100   0.500000   0.000000
-0.372100   0.500000   0.000000
-0.279100   0.500000   0.000000
-0.186000   0.500000   0.000000
-0.093000   0.500000   0.000000
 0.000000   0.500000   0.000000
 0.069800   0.500000   0.000000
 0.139500   0.500000   0.000000
 0.209300   0.500000   0.000000
 0.279100   0.500000   0.000000
 0.348800   0.500000   0.000000
 0.418600   0.500000   0.000000
 0.488400   0.500000   0.000000
 0.587400   0.500000   0.000000
 0.697700   0.500000   0.000000
 0.837200   0.500000   0.000000
 0.966700   0.500000   0.000000
 1.116300   0.500000   0.000000
 1.255800   0.500000   0.000000
 1.395300   0.500000   0.000000
 0.000000   0.000000   0.000000   0.400000    25.0000    15.0000
 0.050000   0.000000   0.000000   0.400000    25.0000    15.0000
 0.200000   0.000000   0.000000   0.400000    25.0000    15.0000
 0.350000   0.000000   0.000000   0.400000    25.0000    15.0000
-69.699997  0.000000   0.000000   0.400000    25.0000    15.0000
-0.011600   0.000000   0.000000   0.400000    25.0000    15.0000
 0.069800   0.000000   0.000000   0.400000    25.0000    15.0000
 0.220900   0.000000   0.000000   0.400000    25.0000    15.0000
 0.348000   0.000000   0.000000   0.400000    25.0000    15.0000
 0.488400   0.000000   0.000000   0.400000    25.0000    15.0000
 0.628000   0.000000   0.000000   0.400000    25.0000    15.0000
   62    73     7     7     7     6     4     2
```

SAMPLE INPUT WHEN MATRICES ARE TO BE GENERATED

ORIGINAL PAGE IS OF POOR QUALITY

```
EXAMPLE..KBF_TESTS...USE AVAILABLE MATRICES..EXCLUDE CROSS TERMS
    1    Ø     2    1     Ø     Ø     8
     8Ø.ØØ  Ø.ØØ7132  Ø.12697Ø
   62   73     7    7     7     6     4     2
```

SAMPLE INPUT WHEN
MATRICES ARE AVAILABLE

```
EXAMPLE..KNEE_BLOWN_FLAP_TESTS..GENERATE MATRIX..EXCLUDE CROSS TERMS

TUNNEL GEOMETRY :
                  BREADTH:      43.000
                  HEIGHT:       30.000
                  IMAGE LAYERS: 5
```

SAMPLE OUTPUT

RUN NUMBER: 73 POINT NUMBER: 7

EXTRA OUTPUT OBTAINED BY SETTING THE FLAG IPRT = 1

INPUT BOUNDARY CONDITIONS. ROOF-FLOOR

I	X/B	Y/B	Z/H	U,R-F
1	-0.8140	0.0000	0.5000	0.0000E+00
2	-0.4651	0.0000	0.5000	0.3158E-01
3	-0.3721	0.0000	0.5000	0.5054E-01
4	-0.2791	0.0000	0.5000	0.7614E-01
5	-0.1860	0.0000	0.5000	0.1200E+00
6	-0.0930	0.0000	0.5000	0.1631E+00
7	0.0000	0.0000	0.5000	-0.1482E+00
8	0.0698	0.0000	0.5000	0.3211E+00
9	0.1395	0.0000	0.5000	0.3347E+00
10	0.2093	0.0000	0.5000	0.3353E+00
11	0.2791	0.0000	0.5000	0.2685E+00
12	0.3488	0.0000	0.5000	0.2335E+00
13	0.4186	0.0000	0.5000	0.1227E+00
14	0.4884	0.0000	0.5000	0.5940E-01
15	0.5874	0.0000	0.5000	0.4251E-01
16	0.6977	0.0000	0.5000	-0.3800E-02
17	0.8372	0.0000	0.5000	0.3020E-01
18	0.9667	0.0000	0.5000	-0.9210E-01
19	1.1163	0.0000	0.5000	-0.2400E-01
20	1.2558	0.0000	0.5000	-0.1950E-01
21	1.3953	0.0000	0.5000	0.9900E-02

INPUT BOUNDARY CONDITIONS. SIDE_WALL

I	X/B	Y/B	Z/H	U,WALL
1	-0.8140	0.5000	0.0000	0.0000E+00
2	-0.4651	0.5000	0.0000	-0.1200E-02
3	-0.3721	0.5000	0.0000	-0.3300E-02
4	-0.2791	0.5000	0.0000	-0.1100E-02
5	-0.1860	0.5000	0.0000	0.6550E-02
6	-0.0930	0.5000	0.0000	0.1515E-01
7	0.0000	0.5000	0.0000	0.2490E-01
8	0.0698	0.5000	0.0000	0.3430E-01
9	0.1395	0.5000	0.0000	0.3810E-01
10	0.2093	0.5000	0.0000	0.4135E-01
11	0.2791	0.5000	0.0000	0.3690E-01
12	0.3488	0.5000	0.0000	0.3410E-01
13	0.4186	0.5000	0.0000	0.1740E-01
14	0.4884	0.5000	0.0000	0.2900E-01
15	0.5874	0.5000	0.0000	0.2410E-01
16	0.6977	0.5000	0.0000	0.2410E-01
17	0.8372	0.5000	0.0000	0.2225E-01
18	0.9667	0.5000	0.0000	0.2145E-01
19	1.1163	0.5000	0.0000	0.2200E-01
20	1.2558	0.5000	0.0000	0.2345E-01
21	1.3953	0.5000	0.0000	0.6065E-01

ITERATION : 1

VORTEX STRENGTHS. (STR = G/(U*SQRT(B*H))

I	X/B	Y/B	Z/H	SPAN/B	SWEEP	PITCH	STR
1	Ø.ØØØØ	Ø.ØØØØ	Ø.ØØØØ	Ø.4ØØØ	25.ØØØØ	15.ØØØØ	Ø.5985E+ØØ
2	Ø.Ø5ØØ	Ø.ØØØØ	Ø.ØØØØ	Ø.4ØØØ	25.ØØØØ	15.ØØØØ	-Ø.1243E+Ø1
3	Ø.2ØØØ	Ø.ØØØØ	Ø.ØØØØ	Ø.4ØØØ	25.ØØØØ	15.ØØØØ	Ø.1438E+Ø1
4	Ø.35ØØ	Ø.ØØØØ	Ø.ØØØØ	Ø.4ØØØ	25.ØØØØ	15.ØØØØ	-Ø.5727E+ØØ
						TOTAL:	Ø.3136E+ØØ

EXTRA OUTPUT OBTAINED BY SETTING THE FLAG IPRT = 1

SOURCE STRENGTHS. (STR = Q/(U*B*H)

I	X/B	Y/B	Z/H	SPAN/B	SWEEP	PITCH	STR
1	-69.7ØØØ	Ø.ØØØØ	Ø.ØØØØ	Ø.4ØØØ	25.ØØØØ	15.ØØØØ	-Ø.4218E-Ø2
2	-Ø.Ø116	Ø.ØØØØ	Ø.ØØØØ	Ø.4ØØØ	25.ØØØØ	15.ØØØØ	-Ø.1373E-Ø1
3	Ø.Ø698	Ø.ØØØØ	Ø.ØØØØ	Ø.4ØØØ	25.ØØØØ	15.ØØØØ	Ø.24Ø7E+ØØ
4	Ø.2289	Ø.ØØØØ	Ø.ØØØØ	Ø.4ØØØ	25.ØØØØ	15.ØØØØ	-Ø.4228E+ØØ
5	Ø.348Ø	Ø.ØØØØ	Ø.ØØØØ	Ø.4ØØØ	25.ØØØØ	15.ØØØØ	Ø.3777E+ØØ
6	Ø.4884	Ø.ØØØØ	Ø.ØØØØ	Ø.4ØØØ	25.ØØØØ	15.ØØØØ	-Ø.2447E+ØØ
7	Ø.628Ø	Ø.ØØØØ	Ø.ØØØØ	Ø.4ØØØ	25.ØØØØ	15.ØØØØ	Ø.1ØØ6E+ØØ
						TOTAL:	Ø.3356E-Ø1

CROSS_EFFECT TERMS:

	U_Q_ROOF	U_G_WALL	W_G_WALL
1	Ø.ØØØØE+ØØ	Ø.ØØØØE+ØØ	Ø.ØØØØE+ØØ
2	Ø.ØØØØE+ØØ	Ø.ØØØØE+ØØ	Ø.ØØØØE+ØØ
3	Ø.ØØØØE+ØØ	Ø.ØØØØE+ØØ	Ø.ØØØØE+ØØ
4	Ø.ØØØØE+ØØ	Ø.ØØØØE+ØØ	Ø.ØØØØE+ØØ
5	Ø.ØØØØE+ØØ	Ø.ØØØØE+ØØ	Ø.ØØØØE+ØØ
6	Ø.ØØØØE+ØØ	Ø.ØØØØE+ØØ	Ø.ØØØØE+ØØ
7	Ø.ØØØØE+ØØ	Ø.ØØØØE+ØØ	Ø.ØØØØE+ØØ
8	Ø.ØØØØE+ØØ	Ø.ØØØØE+ØØ	Ø.ØØØØE+ØØ
9	Ø.ØØØØE+ØØ	Ø.ØØØØE+ØØ	Ø.ØØØØE+ØØ
1Ø	Ø.ØØØØE+ØØ	Ø.ØØØØE+ØØ	Ø.ØØØØE+ØØ
11	Ø.ØØØØE+ØØ	Ø.ØØØØE+ØØ	Ø.ØØØØE+ØØ
12	Ø.ØØØØE+ØØ	Ø.ØØØØE+ØØ	Ø.ØØØØE+ØØ
13	Ø.ØØØØE+ØØ	Ø.ØØØØE+ØØ	Ø.ØØØØE+ØØ
14	Ø.ØØØØE+ØØ	Ø.ØØØØE+ØØ	Ø.ØØØØE+ØØ
15	Ø.ØØØØE+ØØ	Ø.ØØØØE+ØØ	Ø.ØØØØE+ØØ
16	Ø.ØØØØE+ØØ	Ø.ØØØØE+ØØ	Ø.ØØØØE+ØØ
17	Ø.ØØØØE+ØØ	Ø.ØØØØE+ØØ	Ø.ØØØØE+ØØ
18	Ø.ØØØØE+ØØ	Ø.ØØØØE+ØØ	Ø.ØØØØE+ØØ
19	Ø.ØØØØE+ØØ	Ø.ØØØØE+ØØ	Ø.ØØØØE+ØØ
2Ø	Ø.ØØØØE+ØØ	Ø.ØØØØE+ØØ	Ø.ØØØØE+ØØ
21	Ø.ØØØØE+ØØ	Ø.ØØØØE+ØØ	Ø.ØØØØE+ØØ

RE_CALCULATED BOUNDARY CONDITIONS ON ROOF

I	X/B	Y/B	Z/H	U_ROOF	CP_ROOF
1	-Ø.814Ø	Ø.ØØØØ	Ø.5ØØØ	Ø.3391E-Ø2	-Ø.6794E-Ø2
2	-Ø.4651	Ø.ØØØØ	Ø.5ØØØ	Ø.1762E-Ø1	-Ø.3555E-Ø1
3	-Ø.3721	Ø.ØØØØ	Ø.5ØØØ	Ø.2736E-Ø1	-Ø.5547E-Ø1
4	-Ø.2791	Ø.ØØØØ	Ø.5ØØØ	Ø.4192E-Ø1	-Ø.8561E-Ø1
5	-Ø.186Ø	Ø.ØØØØ	Ø.5ØØØ	Ø.6229E-Ø1	-Ø.1285E+ØØ
[illegible]	[illegible]	[illegible]	[illegible]	[illegible]	[illegible]

7	0.0000	0.0000	0.5000	0.1327E+00	-0.2830E+00
8	0.0698	0.0000	0.5000	0.1917E+00	-0.4201E+00
9	0.1395	0.0000	0.5000	0.2711E+00	-0.6157E+00
10	0.2093	0.0000	0.5000	0.3304E+00	-0.7699E+00
11	0.2791	0.0000	0.5000	0.3198E+00	-0.7420E+00
12	0.3489	0.0000	0.5000	0.2386E+00	-0.5340E+00
13	0.4186	0.0000	0.5000	0.1350E+00	-0.2881E+00
14	0.4884	0.0000	0.5000	0.5520E-01	-0.1135E+00
15	0.5874	0.0000	0.5000	0.2276E-02	-0.4557E-02
16	0.6977	0.0000	0.5000	-0.9274E-02	0.1846E-01
17	0.8372	0.0000	0.5000	-0.6313E-02	0.1259E-01
18	0.9667	0.0000	0.5000	-0.3191E-02	0.6372E-02
19	1.1163	0.0000	0.5000	-0.1368E-02	0.2734E-02
20	1.2558	0.0000	0.5000	-0.6342E-03	0.1268E-02
21	1.3953	0.0000	0.5000	-0 3045E-03	0.6090E-03

EXTRA OUTPUT OBTAINED BY SETTING THE FLAG IPRT = 1

RE_CALCULATED BOUNDARY CONDITIONS ON WALL

I	X/B	Y/B	Z/H	U_WALL	W_WALL	CP_WALL
1	-0.8140	0.5000	0.0000	-0.4003E-02	0.0000E+00	0.7990E-02
2	-0.4651	0.5000	0.0000	-0.2385E-02	0.0000E+00	0.4765E-02
3	-0.3721	0.5000	0.0000	-0.1000E-02	0.0000E+00	0.1999E-02
4	-0.2791	0.5000	0.0000	0.1441E-02	0.0000E+00	-0.2885E-02
5	-0.1860	0.5000	0.0000	0.5726E-02	0.0000E+00	-0.1149E-01
6	-0.0930	0.5000	0.0000	0.1298E-01	0.0000E+00	-0.2612E-01
7	0.0000	0.5000	0.0000	0.2402E-01	0.0000E+00	-0.4862E-01
8	0.0698	0.5000	0.0000	0.3371E-01	0.0000E+00	-0.6855E-01
9	0.1395	0.5000	0.0000	0.4106E-01	0.0000E+00	-0.8380E-01
10	0.2093	0.5000	0.0000	0.4176E-01	0.0000E+00	-0.8525E-01
11	0.2791	0.5000	0.0000	0.3552E-01	0.0000E+00	-0.7229E-01
12	0.3488	0.5000	0.0000	0.2843E-01	0.0000E+00	-0.5767E-01
13	0.4186	0.5000	0.0000	0.2597E-01	0.0000E+00	-0.5262E-01
14	0.4884	0.5000	0.0000	0.2616E-01	0.0000E+00	-0.5300E-01
15	0.5874	0.5000	0.0000	0.2304E-01	0.0000E+00	-0.4661E-01
16	0.6977	0.5000	0.0000	0.2009E-01	0.0000E+00	-0.4058E-01
17	0.8372	0.5000	0.0000	0.2523E-01	0.0000E+00	-0.5110E-01
18	0.9667	0.5000	0.0000	0.2988E-01	0.0000E+00	-0.6065E-01
19	1.1163	0.5000	0.0000	0.3219E-01	0.0000E+00	-0.6541E-01
20	1.2558	0.5000	0.0000	0.3299E-01	0.0000E+00	-0.6707E-01
21	1.3953	0.5000	0.0000	0.3332E-01	0.0000E+00	-0.6775E-01

CENTER_LINE INTERFERENCE VELOCITIES

I	X/B	Y/B	Z/H	U_CNTR	W_CNTR	U_Q_CL	U_G_CL	W_Q_CL	W_G_CL
1	-0.8140	0.0000	0.0000	-0.8228E-03	-0.2422E-02	-0.8697E-03	0.4686E-04	0.2011E-04	-0.2442E-02
2	-0.4651	0.0000	0.0000	0.3530E-02	-0.1134E-02	0.3567E-02	-0.3794E-04	0.1306E-03	-0.1265E-02
3	-0.3721	0.0000	0.0000	0.5611E-02	0.2433E-03	0.5711E-02	-0.9992E-04	0.1898E-03	0.5345E-04
4	-0.2791	0.0000	0.0000	0.8228E-02	0.2475E-02	0.8422E-02	-0.1935E-03	0.2586E-03	0.2217E-02
5	-0.1860	0.0000	0.0000	0.1137E-01	0.5887E-02	0.1170E-01	-0.3295E-03	0.3235E-03	0.5563E-02
6	-0.0930	0.0000	0.0000	0.1483E-01	0.1085E-01	0.1535E-01	-0.5176E-03	0.3593E-03	0.1049E-01
7	0.0000	0.0000	0.0000	0.1823E-01	0.1774E-01	0.1899E-01	-0.7552E-03	0.3382E-03	0.1741E-01
8	0.0698	0.0000	0.0000	0.2043E-01	0.2428E-01	0.2138E-01	-0.9444E-03	0.2773E-03	0.2401E-01
9	0.1395	0.0000	0.0000	0.2214E-01	0.3187E-01	0.2324E-01	-0.1104E-02	0.1872E-03	0.3168E-01
10	0.2093	0.0000	0.0000	0.2330E-01	0.4012E-01	0.2449E-01	-0.1190E-02	0.8802E-04	0.4003E-01
11	0.2791	0.0000	0.0000	0.2399E-01	0.4842E-01	0.2516E-01	-0.1164E-02	0.2438E-05	0.4842E-01
12	0.3488	0.0000	0.0000	0.2437E-01	0.5604E-01	0.2539E-01	-0.1024E-02	-0.5528E-04	0.5609E-01
13	0.4186	0.0000	0.0000	0.2457E-01	0.6239E-01	0.2537E-01	-0.7993E-03	-0.8263E-04	0.6247E-01
14	0.4884	0.0000	0.0000	0.2471E-01	0.6716E-01	0.2525E-01	-0.5453E-03	-0.8464E-04	0.6724E-01
15	0.5874	0.0000	0.0000	0.2495E-01	0.7132E-01	0.2518E-01	-0.2299E-03	-0.5538E-04	0.7137E-01
16	0.6977	0.0000	0.0000	0.2549E-01	0.7322E-01	0.2550E-01	-0.1232E-04	0.3573E-05	0.7322E-01
17	0.8372	0.0000	0.0000	0.2671E-01	0.7347E-01	0.2662E-01	0.8975E-04	0.7010E-04	0.7340E-01

19	1.1163	Ø.ØØØØ	Ø.ØØØØ	Ø.297ØE-Ø1	Ø.721ØE-Ø1	Ø.2961E-Ø1	Ø.853ØE-Ø4	Ø.715ØE-Ø4	Ø.72Ø3E-Ø1
2Ø	1.2558	Ø.ØØØØ	Ø.ØØØØ	Ø.3Ø79E-Ø1	Ø.7145E-Ø1	Ø.3Ø72E-Ø1	Ø.72Ø3E-Ø4	Ø.4528E-Ø4	Ø.7141E-Ø1
21	1.3953	Ø.ØØØØ	Ø.ØØØØ	Ø.3155E-Ø1	Ø.7Ø95E-Ø1	Ø.3149E-Ø1	Ø.63Ø1E-Ø4	Ø.2479E-Ø4	Ø.7Ø92E-Ø1

EXTRA OUTPUT OBTAINED
BY SETTING THE FLAG
IPRT = 1

EXAMPLE..KNEE_BLOWN_FLAP_TESTS..GENERATE MATRIX..EXCLUDE CROSS TERMS TEST_62, RUN_73, POINT_ 7

POSN X/B	INPUT DU/U	WALL DU/U	WALL DV/U	WALL DW/U	C/L DU/U
-0.8140	0.0000	-0.0040	0.0000	0.0000	-0.0008
-0.4651	-0.0042	-0.0024	0.0000	0.0000	0.0035
-0.3721	-0.0033	-0.0010	0.0000	0.0000	0.0056
-0.2791	-0.0011	0.0014	0.0000	0.0000	0.0082
-0.1860	0.0066	0.0057	0.0000	0.0000	0.0114
-0.0930	0.0152	0.0130	0.0000	0.0000	0.0148
0.0000	0.0249	0.0240	0.0000	0.0000	0.0182
0.0698	0.0343	0.0337	0.0000	0.0000	0.0204
0.1395	0.0381	0.0411	0.0000	0.0000	0.0221
0.2093	0.0413	0.0418	0.0000	0.0000	0.0233
0.2791	0.0369	0.0355	0.0000	0.0000	0.0240
0.3488	0.0341	0.0284	0.0000	0.0000	0.0244
0.4186	0.0174	0.0260	0.0000	0.0000	0.0246
0.4884	0.0290	0.0262	0.0000	0.0000	0.0247
0.5874	0.0241	0.0230	0.0000	0.0000	0.0249
0.6977	0.0241	0.0201	0.0000	0.0000	0.0255
0.8372	0.0223	0.0252	0.0000	0.0000	0.0267
0.9667	0.0215	0.0299	0.0000	0.0000	0.0282
1.1163	0.0220	0.0322	0.0000	0.0000	0.0297
1.2558	0.0235	0.0330	0.0000	0.0000	0.0308
1.3953	0.0687	0.0333	0.0000	0.0000	0.0316
	X	+			O

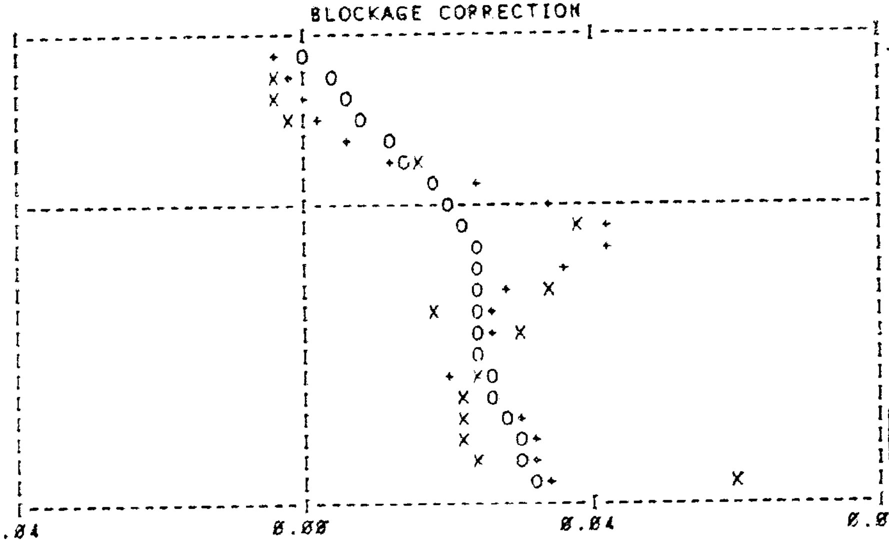

SINGULARITIES

X/B	S'
-69.7000	-0.0042
-0.0116	-0.0137
0.0698	0.2407
0.2209	-0.4228
0.3480	0.3777
0.4884	-0.2447
0.6280	0.1806

TOTAL= 0.0336

SPAN/B= 0.8000

S'=S/(U*B*H)

STANDARD OUTPUT
IPRT = 0 OR 1

POSN X/B	INPUT DU/U	WALL DU/U	WALL DV/U	WALL DW/U	C/L DW/U
-0.8140	0.0000	0.0034	0.0000	0.0030	-0.0024
-0.4651	0.0316	0.0176	0.0000	0.0040	-0.0011
-0.3721	0.0585	0.0274	0.0000	0.0000	0.0002
-0.2791	0.0761	0.0419	0.0000	0.0000	0.0025
-0.1860	0.1200	0.0623	0.0000	0.0000	0.0059
-0.0930	0.1631	0.0893	0.0000	0.0000	0.0109
0.0000	-0.1482	0.1327	0.0000	0.0000	0.0177
0.0698	0.3211	0.1917	0.0000	0.0000	0.0243
0.1395	0.3347	0.2711	0.0000	0.0000	0.0319
0.2093	0.3353	0.3304	0.0000	0.0000	0.0401
0.2791	0.2685	0.3198	0.0000	0.0000	0.0484
0.3488	0.2335	0.2786	0.0000	0.0000	0.0560
0.4186	0.1227	0.1350	0.0000	0.0000	0.0624
0.4884	0.0594	0.0552	0.0000	0.0000	0.0672
0.5874	0.0425	0.0023	0.0000	0.0000	0.0713
0.6977	-0.0038	-0.0093	0.0000	0.0000	0.0732
0.8372	0.0302	-0.0063	0.0000	0.0000	0.0735
0.9667	-0.0921	-0.0032	0.0000	0.0000	0.0729
1.1163	-0.0248	-0.0014	0.0000	0.0000	0.0721
1.2558	-0.0195	-0.0006	0.0000	0.0000	0.0715
1.3953	0.0099	-0.0003	0.0000	0.0000	0.0709
	X	+			O

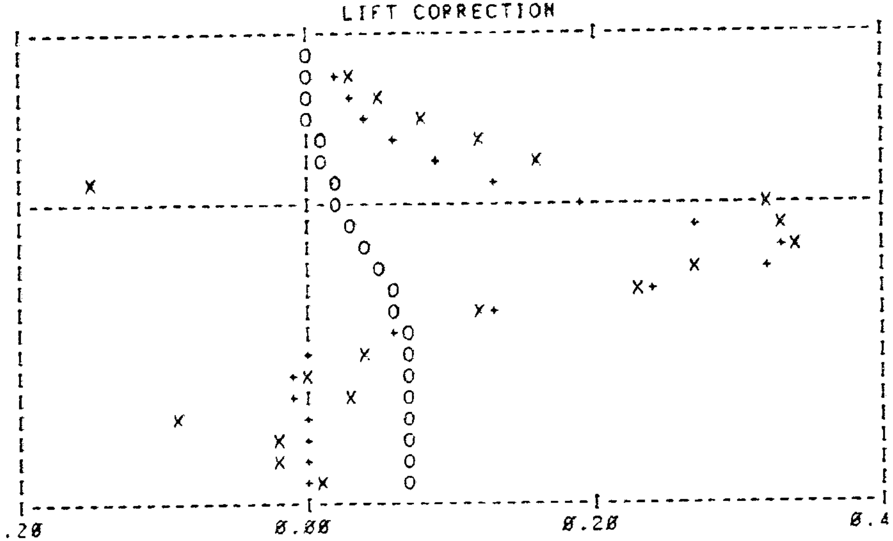

SINGULARITIES

X/B	G'
0.0000	0.6905
0.0500	-1.2426
0.2000	1.4384
0.3500	-0.5727

TOTAL= 0.3136

SPAN/B= 0.8000

G'=G/(U*SQRT(B*H))

WALL POINTS --- BLOCKAGE : Y/B= 0.5000, Z/H= 0.0000 LIFT : Y/B= 0.0000, Z/H= 0.5000
VALUES USED IN CORRECTIONS : DU/U= 0.0204, DW/U= 0.0243, DELTA-CD=-0.0182

	ALFA	PNOT	QNOT	CMU	CL	CD	CM	
MEASURED	15.9950	2048.9431	4.7220	1.0420	6.0143	1.1413	1.0417	
CORRECTED	17.3580	2048.9431	4.9169	1.0007	5.7759	1.1135	1.0004	
RESOLVED	17.3580	2048.9431	4.9169	1.0007	5.7477	1.2506	1.0004	1.3630
CLASSICAL	18.0085	2048.9431	4.9169	1.0007	5.7313	1.3238	1.0004	2.0935

APPENDIX 2

PROGRAM LISTING

```
      PROGRAM LSQITER                                                 !VAX
C-   Iterative Solution Accounting For Cross_effects Of Vortices
C-   and Sources. Least_Square Approach.
C-
C-   Version : KBF_DATA_REDUCTION.
C-   TAPE7 : Load_Coefficients. Experimental And Corrected
C_   TAPE8 : Matrix File
C_   TAPE9 : Results.  Input and Calculated Signatures, and Center_line
C-                     Interference Velocities.
C-   TAPE10: KBF Experimental Data
C-   TAPE11: Interference Velocities Due to Jets.
C-   TAPE16: INFLUENCE COEFFT MATRICES (INPUT)
C-
      COMMON/IMAT/ UGRF(25,25),UQWL(25,25),UGCL(25,25), .CL(25,25),
     *             WGCL(25,25),WQCL(25,25),UGWL(25,25),WGWL(25,25),
     *             UQRF(25,25)
      COMMON/LMAT/ AQ(25,25),AG(25,25)
      COMMON/ARR1/ XR(25),YR(25),ZR(25),XL(25),YL(25),ZL(25),
     *             XV(25),YV(25),ZV(25),XS(25),YS(25),ZS(25),
     *             SBV(25),SBS(25),PSIV(25),ALFV(25),PSIS(25),ALFS(25),
     *             CPOWL(25),UCPWL(25),UCPRF(25),UXQRF(25),UXGWL(25),
     *             WXGWL(25),ULIFT(25),UBLKG(25),GAMA(25),SIGMA(25)
      COMMON/IMAG/ B,H,LAYERS,IRF
      COMMON/SIZE/ NR,NW,NV,NS,XPVOR,XPSRC
      COMMON /BLKB/ ALFU,POU,QOU,CMUU,CLU,CDU,CMU
      DIMENSION TITLE(80),VWALL(25,3),VROOF(25,3),VCNTR(25,3)
      CHARACTER TAPE7*12,TAPE9*12                                     !VAX
      PI = 3.142592654
      RAD = PI/180.0
      DEG = 180.0/PI
C-
C-   READ INPUT
C-            ***  MAIN INPUT ***
C-
      READ (5,3000) TITLE
      READ (5,1100) ITERMAX,MATPRT,MATSAV,IPRT,KROSG,KROSQ,ICORR,JETEFCT
      READ (5,1000) SAREA,AWB,BWB
      IF(KROSG+KROSQ .EQ. 0) ITERMAX = 1
      IF(MATSAV .EQ. 2) GO TO 300
      IF(MATSAV .EQ .1) GO TO 10
      CALL TAPEIO(3,16)
      MATSAV = 1
      GO TO 95
C-
C-            *** GEOMETRY INPUT ***
C-
   10 READ (5,1100) LAYERS,IRF,NR,NW,NV,NS
      READ (5,1000) B,H,XPVOR,XPSRC
      DO 11 I = 1,NR
      READ (5,1000) XR(I),YR(I),ZR(I)
            XR(I) = XR(I)*B
            YR(I) = YR(I)*B
            ZR(I) = ZR(I)*H
   11 CONTINUE
```

```
      DO 15 I = 1,NW
      READ (5,1000) XL(I),YL(I),ZL(I)
            XL(I) = XL(I)*B
            YL(I) = YL(I)*B
            ZL(I) = ZL(I)*H
   15 CONTINUE
      DO 20 I = 1,NV
      READ (5,1000) XV(I),YV(I),ZV(I),SBV(I),PSIV(I),ALFV(I)
            XV(I) = XV(I)*B
            YV(I) = YV(I)*B
            ZV(I) = ZV(I)*H
            SBV(I) = SBV(I)*B
            PSIV(I) = PSIV(I)*RAD
            ALFV(I) = ALFV(I)*RAD
   20 CONTINUE
      DO 25 I = 1,NS
      READ (5,1000) XS(I),YS(I),ZS(I),SBS(I),PSIS(I),ALFS(I)
            XS(I) = XS(I)*B
            YS(I) = YS(I)*B
            ZS(I) = ZS(I)*H
            SBS(I) = SBS(I)*B
            PSIS(I) = PSIS(I)*RAD
            ALFS(I) = ALFS(I)*RAD
   25 CONTINUE
C-
C-  SET UP SOURCE_INFLUENCE MATRICES
C-
      MINIT = 0
      DO 60 J = 1,NS
      XPIV = XPSRC*SBS(J)
      CALL PIVOT(XS(J),YS(J),ZS(J), XPIV, SBS(J)/2.0,PSIS(J),ALFS(J),
     *             X1,Y1,Z1, X2,Y2,Z2)
C...CROSS EFFECT SOURCE/(ROOF - FLOOR)
      U3 = 0.
      U4 = 0.
      DO 40 I = 1,NR
      CALL INFLU(X1,Y1,Z1, X2,Y2,Z2, 0.5, 1, MINIT, 1,
     *             XR(I),YR(I),ZR(I), U1,V1,W1)
      CALL INFLU(X2,-Y2,Z2, X1,-Y1,Z1, 0.5, 1, MINIT, 1,
     *             XR(I),YR(I),ZR(I), U2,V2,W2)
      IF(IRF .EQ. 0) GO TO 38
      CALL INFLU(X1,Y1,Z1, X2,Y2,Z2, 0.5, 1, MINIT, 1,
     *             XR(I),YR(I),-ZR(I), U3,V3,W3)
      CALL INFLU(X2,-Y2,Z2, X1,-Y1,Z1, 0.5, 1, MINIT, 1,
     *             XR(I),YR(I),-ZR(I), U4,V4,W4)
   38 UGRF(I,J) = U1+U2-(U3+U4)
   40 CONTINUE
C...DIRECT EFFECT. SOURCE/WALL
      DO 50 I = 1,NW
      CALL INFLU(X1,Y1,Z1, X2,Y2,Z2, 0.5, 1, MINIT, 1,
     *             XL(I),YL(I),ZL(I), U1,V1,W1)
      CALL INFLU(X2,-Y2,Z2, X1,-Y1,Z1, 0.5, 1, MINIT, 1,
     *             XL(I),YL(I),ZL(I), U2,V2,W2)
      UGWL(I,J) = U1+U2
   50 CONTINUE
```

```
C...  CENTER_LINE INTERFRERNCE MATRIX.(X CORRESPONDDS TO WALL POINTS)
      DO  55 I = 1,NW
      CALL INFLU(X1,Y1,Z1, X2,Y2,Z2, Ø.5, 1, 1. 1.
     *           XL(I),Ø.Ø,Ø.Ø, U1,V1,W1)
      CALL INFLU(X2,-Y2,Z2, X1,-Y1,Z1, Ø.5, 1, 1, 1.
     *           XL(I),Ø.Ø,Ø.Ø, U2,V2,W2)
      UOCL(I,J) = U1+U2
      WOCL(I,J) = W1+W2
   55 CONTINUE
   6Ø CONTINUE
C-
C-  SET UP INFLUENCE MATRICES FOR VORTICES
C-
      DO 9Ø J = 1,NV
      XPIV = XPVOR*SBV(J)
      CALL PIVOT(XV(J),YV(J),ZV(J), XPIV, SBV(J)/2.Ø,PSIV(J),ALFV(J),
     *           X1,Y1,Z1, X2,Y2,Z2)
C...DIRECT EFFECT. VORTEX/(ROOF - FLOOR)
      U3 = Ø.
      U4 = Ø.
      DO 7Ø I = 1,NR
      CALL INFLU(X1,Y1,Z1, X2,Y2,Z2, 1.Ø, 2, MINIT, 1,
     *           XR(I),YR(I),ZR(I), U1,V1,W1)
      CALL INFLU(X2,-Y2,Z2, X1,-Y1,Z1, 1.Ø, 2, MINIT, 1,
     *           XR(I),YR(I),ZR(I), U2,V2,W2)
      IF(IRF .EQ. Ø) GO TO 68
      CALL INFLU(X1,Y1,Z1, X2,Y2,Z2, 1.Ø, 2, MINIT, 1,
     *           XR(I),YR(I),-ZR(I), U3,V3,W3)
      CALL INFLU(X2,-Y2,Z2, X1,-Y1,Z1, 1.Ø, 2, MINIT, 1,
     *           XR(I),YR(I),-ZR(I), U4,V4,W4)
   68 UGRF(I,J) = U1+U2-(U3+U4)
   7Ø CONTINUE
C...CROSS EFFECT. VORTEX/WALL
      DO 8Ø I = 1,NW
      CALL INFLU(X1,Y1,Z1, X2,Y2,Z2, 1.Ø, 2, MINIT, 1,
     *           XL(I),YL(I),ZL(I), U1,V1,W1)
      CALL INFLU(X2,-Y2,Z2, X1,-Y1,Z1, 1.Ø, 2, MINIT, 1,
     *           XL(I),YL(I),ZL(I), U2,V2,W2)
      UGWL(I,J) = U1+U2
      WGWL(I,J) = W1+W2
   8Ø CONTINUE
C...  CENTER_LINE INTERFRERNCE MATRIX.(X CORRESPONDDS TO WALL POINTS)
      DO  85 I = 1,NW
      CALL INFLU(X1,Y1,Z1, X2,Y2,Z2, 1.Ø, 2, 1. 1.
     *           XL(I),Ø.Ø,Ø.Ø, U1,V1,W1)
      CALL INFLU(X2,-Y2,Z2, X1,-Y1,Z1, 1.Ø, 2, 1, 1.
     *           XL(I),Ø.Ø,Ø.Ø, U2,V2,W2)
      UGCL(I,J) = U1+U2
      WGCL(I,J) = W1+W2
   85 CONTINUE
   9Ø CONTINUE
C-
C-  FORM [A]_INVERSE FOR SOURCE/WALL
C-
   95 EPS = Ø.Ø
```

```
      DO 110 I = 1,NS
      DO 110 J = 1,NS
      AO(I,J) = 0.0
      DO 100 K = 1,NW
      AQ(I,J) = AQ(I,J) + UQWL(K,I)*UQWL(K,J)
  100 CONTINUE
  110 CONTINUE
      IERR = 0
      CALL GJRV(AQ,NS,25,EPS,IERR)
      IF(IERR .NE. 0) GO TO 310
C-
C-   FORM [A]_INVERSE FOR VORTICES/ROOF
C-
      EPS = 0.0
      DO 210 I = 1,NV
      DO 210 J = 1,NV
      AG(I,J) = 0.0
      DO 200 K = 1,NR
      AG(I,J) = AG(I,J) + UGRF(K,I)*UGRF(K,J)
  200 CONTINUE
  210 CONTINUE
      IERR = 0
      CALL GJRV(AG,NV,25,EPS,IERR)
      IF(IERR .NE. 0) GO TO 310
C-
C-   OPTIONALLY PRINT/SAVE MATRICES
C-
  300 IF(MATSAV .NE. 0) CALL TAPEIO(MATSAV,8)
      IF(IPRT .EQ. 0) GO TO 305
      WRITE (6,3100) TITLE
      WRITE (6,3200) B,H,LAYERS
  305 IF(MATPRT .EQ. 0) GO TO 320
  310 CALL OUT(UGRF, 25,25, NR,NV, 'U_GAMA_ROOF',11)
      CALL OUT(UQWL, 25,25, NW,NS, 'U_SORC_WALL',11)
      CALL OUT(UQRF, 25,25, NR,NS, 'U_SORC_ROOF',11)
      CALL OUT(UGWL, 25,25, NW,NV, 'U_GAMA_WALL',11)
      CALL OUT(WGWL, 25,25, NW,NV, 'W_GAMA_WALL',11)
      IF(IERR .NE. 0) STOP
C-
C-           *** TEST SIGNATURE INPUT ***
C-
C-   READ_IN RUN NUMBER AND WALL SIGNATURES
C-   SET_UP BOUNDARY CONDITIONS
C-
C-   ******************************************************************!
C-       The structure of the program for INPUT'ng run identification    !
C-       and wall signatures in the next 15 statements are for the      !
C-       Knee_Blown_Flap experiments of LOCKHEED_GEORGIA.  The user     !
C-       should make appropriate changes in this section and re_write   !
C-       subroutine "READCP" to define the arrays "UCPRF" and "UCPWL"   !
C-       as indicated below:                                            !
C-             UCPRF(I) = (U,ROOF(I)-U,FLOOR(I)),  if IRF = 1           !
C-                      =  U,ROOF(I)               if IRF = 0           !
C-             UCPWL(I) = (U,WALL1(I)+U,WALL2(I))/2                     !
C-
  320    READ (5,1100,END=999) ITEST,IRUN,IPMIN,IPMAX,IFLOOR,IROOF,     !
```

```
     *                      IWAL1,IWAL2                                    !
      ENCODE(12,325,TAPE7) IRUN                                            !VAX
      ENCODE(12,326,TAPE9) IRUN                                            !VAX
 325  FORMAT ('KBFRUN',I2,'.DAT')                                          !
 326  FORMAT ('KBFSIG',I2,'.DAT')                                          !
      OPEN(UNIT=7,NAME=TAPE7,STATUS='NEW')                                 !VAX
      OPEN(UNIT=9,NAME=TAPE9,STATUS='NEW')                                 !VAX
      IPDO = IPMIN-1                                                       !
 330  IPDO = IPDO+1                                                        !
      IF(IPDO .GT. IPMAX) GO TO 600                                        !
      IP = IPDO                                                            !
      CALL READCP(UCPRF, NR, IRUN, IP, IFLOOR, IROOF, 1, IRF)              !
      IF(IRUN .LT. 0) GO TO 600                                            !
      IF(IP .EQ. 0) GO TO 330                                              !
      CALL READCP(UCPWL, NW, IRUN, IP, IWAL1,  IWAL2, 0, IRF)              !
C-                                                                         !
C-  ********************************************************************!
      IF(IPRT .NE. 0) WRITE (6,4400) IRUN,IP
      IF(IPRT .NE. 0) WRITE (6,3300)
 350  DO 370 I = 1,NR
      UXORF(I) = 0.0
      IF(IPRT .NE. 0) WRITE (6,1200) I,XR(I)/B,YR(I)/B,ZR(I)/H,
     *                               UCPRF(I)
 370  CONTINUE
C
      IF(IPRT .NE. 0) WRITE (6,3400)
      DO 380 I = 1,NW
      CPOWL(I) = 1.0-(UCPWL(I)+1.0)**2
      IF(IPRT .NE. 0) WRITE (6,1200) I,XL(I)/B,YL(I)/B,ZL(I)/H, UCPWL(I)
 380  CONTINUE
C-
C-  BEGIN ITERATIVE CYCLE
C-
      ITER = 0
 400  ITER = ITER + 1
      IF(IPRT .NE. 0) WRITE (6,3500) ITER
C-
C-  SUBTRACT CROSS_INFLUENCE OF SOURCES FROM ROOF SIGNATURE AND
C-  FORM LEAST_SQUARE COLUMN VECTOR FOR VORTICES
C-
      DO 410 I = 1,NV
      ULIFT(I) = 0.0
      DO 410 K = 1,NR
 410  ULIFT(I) = ULIFT(I) + UGRF(K,I)*(UCPRF(K)-UXORF(K) )
C-
C-  COMPUTE GAMA'S
C-
      GTOT = 0.0
      DO 425 I = 1,NV
      GAMA(I) = 0.0
      DO 420 J = 1,NV
 420  GAMA(I) = GAMA(I) + AG(I,J)*ULIFT(J)
      GTOT = GTOT + GAMA(I)/SQRT(B*H)
 425  CONTINUE
C-
```

```
C-  COMPUTE CROSS_EFFECT OF GAMA'S ON SIDE_WALL
C-
      DO 43Ø I = 1,NW
      UXGWL(I) = Ø.Ø
      WXGWL(I) = Ø.Ø
      IF(KROSG .EQ. Ø) GO TO 43Ø
      DO 43Ø J = 1,NV
      UXGWL(I) = UXGWL(I) + UGWL(I,J)*GAMA(J)
      WXGWL(I) = WXGWL(I) + WGWL(I,J)*GAMA(J)
 43Ø  CONTINUE
C-
C-  SUBTRACT CROSS_INFLUENCE OF GAMA'S FROM WALL SIGNATURE AND
C-  FORM LEAST_SQUARE COLUMN VECTOR FOR SOURCES
C-
      FACTOR = 1.Ø
 436  CONTINUE
      DO 44Ø I = 1,NS
      UBLKG(I) = Ø.Ø
      DO 44Ø K = 1,NW
      UTEMP = 1.Ø - CPOWL(K) - FACTOR*WXGWL(K)**2
      IF(UTEMP .GT. Ø.Ø) GO TO 438
      IF(FACTOR .LE. Ø.1E-Ø6) GO TO 61Ø
      FACTOR = Ø.Ø
      GO TO 436
 438  UTEMP = SQRT(UTEMP) - UXGWL(K) - 1.Ø
      UBLKG(I) = UBLKG(I) + UQWL(K,I)*UTEMP
 44Ø  CONTINUE
C-
C-  COMPUTE SIGMA'S
C-
      QTOT = Ø.Ø
      DO 455 I = 1,NS
      SIGMA(I) = Ø.Ø
      DO 45Ø J = 1,NS
      SIGMA(I) = SIGMA(I) + AQ(I,J)*UBLKG(J)
 45Ø  CONTINUE
      QTOT = QTOT + SIGMA(I)/(B*H)
 455  CONTINUE
C-
C-  PRINT OUT GAMA'S, SIGMA'S AND CROSS_EFFECT TERMS
C-
      IF(IPRT .EQ. Ø) GO TO 49Ø
      WRITE (6,36ØØ)
      WRITE (6,37ØØ)
      DO 46Ø I = 1,NV
      GP = GAMA(I)/SQRT(B*H)
      WRITE (6,13ØØ) I,XV(I)/B,YV(I)/B,ZV(I)/H,
     *                SBV(I)/B,PSIV(I)/RAD,ALFV(I)/RAD,GP
 46Ø  CONTINUE
      WRITE (6,39ØØ) GTOT
      WRITE (6,38ØØ)
      WRITE (6,37ØØ)
      DO 465 I = 1,NS
      QP = SIGMA(I)/(B*H)
      WRITE (6,13ØØ) I,XS(I)/B,YS(I)/B,ZS(I)/H,
```

```
     *                  SBS(I)/B,PSIS(I)/RAD,ALFS(I)/RAD, QP                      LSQTR  330
 465  CONTINUE                                                                    LSQTR  331
      WRITE (6,3900) QTOT                                                         LSQTR  332
      IMAX = NR                                                                   LSQTR  333
      IF(NW .GT. IMAX) IMAX = NW                                                  LSQTR  334
      WRITE (6,4300)                                                              LSQTR  335
      DO 470 I = 1,IMAX                                                           LSQTR  336
      WRITE (6,1400) I,UXQRF(I),UXGWL(I),WXGWL(I)                                 LSQTR  337
      IF((1.0 - CPOWL(I) - WXGWL(I)**2) .LT. 0.0) WRITE (6,1600)                  LSQTR  338
 470  CONTINUE                                                                    LSQTR  339
      IF(FACTOR .LE. 0.1E-06) WRITE (6,6460)                                      LSQTR  340
C-                                                                                LSQTR  341
C-   RE_CALCULATE WALL BOUNDARY CONDITIONS, U , ON ROOF                           LSQTR  342
C-                                                                                LSQTR  343
      WRITE (6,4000)                                                              LSQTR  344
 490  DO 510 I = 1,NR                                                             LSQTR  345
      VROOF(I,1) = 0.0                                                            LSQTR  346
      DO 500 J = 1,NV                                                             LSQTR  347
 500  VROOF(I,1) = VROOF(I,1) + UGRF(I,J)*GAMA(J)                                 LSQTR  348
      IF(KROSQ .EQ. 0) GO TO 506                                                  LSQTR  349
      DO 505 J = 1,NS                                                             LSQTR  350
 505  VROOF(I,1) = VROOF(I,1) + UQRF(I,J)*SIGMA(J)                                LSQTR  351
 506  CPC = -VROOF(I,1)**2 - 2.0*VROOF(I,1)                                       LSQTR  352
      IF(IPRT .NE. 0) WRITE (6,1200) I,XR(I)/B,YR(I)/B,ZR(I)/H,                   LSQTR  353
     *                                     VROOF(I,1),CPC                         LSQTR  354
 510  CONTINUE                                                                    LSQTR  355
C-                                                                                LSQTR  356
C-   RE_CALCULATE BOUNDARY CONDITIONS U & W ON SIDE WALL                          LSQTR  357
C-                                                                                LSQTR  358
      IF(IPRT .NE. 0) WRITE (6,4100)                                              LSQTR  359
      DO 530 I = 1,NW                                                             LSQTR  360
      VWALL(I,1) = 0.0                                                            LSQTR  361
      VWALL(I,3) = 0.0                                                            LSQTR  362
      DO 520 J = 1,NS                                                             LSQTR  363
 520  VWALL(I,1) = VWALL(I,1) + UQWL(I,J)*SIGMA(J)                                LSQTR  364
      IF(KROSG .EQ. 0) GO TO 528                                                  LSQTR  365
      DO 525 J = 1,NV                                                             LSQTR  366
      VWALL(I,1) = VWALL(I,1) + UGWL(I,J)*GAMA(J)                                 LSQTR  367
 525  VWALL(I,3) = VWALL(I,3) + WGWL(I,J)*GAMA(J)                                 LSQTR  368
 528  ULIFT(I) = -(FACTOR*VWALL(I,3)**2+VWALL(I,1)**2+2.0*VWALL(I,1) )            LSQTR  369
      IF(IPRT .NE. 0) WRITE (6,1200) I,XL(I)/B,YL(I)/B,ZL(I)/B,                   LSQTR  370
     *                  VWALL(I,1),VWALL(I,3),  ULIFT(I)                          LSQTR  371
 530  CONTINUE                                                                    LSQTR  372
C-                                                                                LSQTR  373
C-   OBTAIN CENTER_LINE INTERFERENCE VELOCITIES                                   LSQTR  374
C-                                                                                LSQTR  375
      IF(ITER .EQ. ITERMAX) WRITE (9,1100) IRUN,IP,NW                             LSQTR  376
      IF(IPRT .NE. 0) WRITE (6,4200)                                              LSQTR  377
      YCENTER = 0.                                                                LSQTR  378
      ZCENTER = 0.                                                                LSQTR  379
      DO 570 I = 1,NW                                                             LSQTR  380
      UQCTL = 0.0                                                                 LSQTR  381
      WQCTL = 0.0                                                                 LSQTR  382
      DO 550 J = 1,NS                                                             LSQTR  383
      UQCTL = UQCTL + UQCL(I,J)*SIGMA(J)                                          LSQTR  384
```

```
      WOCTL = WOCTL + WOCL(I,J)*SIGMA(J)
  55Ø CONTINUE
      UGCTL = Ø.Ø
      WGCTL = Ø.Ø
      DO 56Ø J = 1,NV
      UGCTL = UGCTL + UGCL(I,J)*GAMA(J)
      WGCTL = WGCTL + WGCL(I,J)*GAMA(J)
  56Ø CONTINUE
      VCNTR(I,1) = UOCTL + UGCTL
      VCNTR(I,3) = WOCTL + WGCTL
      IF(IPRT .NE. Ø) WRITE (6,12ØØ) I,XL(I)/B,YCENTER,ZCENTER,
     *                UOCTL,UGCTL,WOCTL,WGCTL
     *                VCNTR(I,1),VCNTR(I,3),
      IF(ITER .EQ. ITERMAX) WRITE (9,15ØØ) I,XL(I)/B, CPOWL(I),ULIFT(I),
     *  VCNTR(I,1), UCPRF(I), VROOF(I,1),VCNTR(I,3)
  57Ø CONTINUE
C-
C-  TERMINATE IF REQUIRED NO OF ITERARIONS HAVE BEEN PERFORMED.
C-  OTHERWISE, DETERMINE CROSS_INFLUENCE U DUE TO SOURCES ON ROOF
C-  AND CONTINUE ITERATIONS.
C-
      IF(ITER .GE. ITERMAX) GO TO 59Ø
      DO 58Ø I = 1,NR
      UXORF(I) = Ø.Ø
      IF(KROSO .EQ. Ø) GO TO 58Ø
      DO 58Ø J = 1,NS
      UXORF(I) = UXORF(I) + UORF(I,J)*SIGMA(J)
  58Ø CONTINUE
      GO TO 4ØØ
  59Ø CONTINUE
      IPASS = 1
      IF(JETEFCT .EQ. Ø) WRITE (6,61ØØ)TITLE,ITEST,IRUN,IP
      IF(JETEFCT .NE. Ø) WRITE (6,611Ø)TITLE,ITEST,IRUN,IP
  591 CALL OUTPUT(NW,NS,XS,SBS(1),Ø,
     *                UCPWL,XL,SIGMA,VCNTR,VWALL,ICORR, IPASS-1)
      CALL OUTPUT(NR,NV,XV,SBV(1),1,
     *                UCPRF,XR,GAMA, VCNTR,VROOF,ICORR, IPASS-1)
C-
C-  CORRECT ALL MEASURED QUANTITIES
C-
  592 FACT = (1.Ø+DU)**2
      QOC = QOU*FACT
      CMUC = CMUU/FACT
      CLC = CLU/FACT
      CMC = CMU/FACT
      DELA = DW/(1.Ø+DU)
      ALFC = ALFU + DELA*DEG
      BHBYS = B*H/SAREA
      DELCD = -BHBYS*QTOT**2
      CDC = (CDU-DELCD)/FACT
C-
      SINA = SIN(DELA)
      COSA = COS(DELA)
      CD = CDC*COSA + CLC*SINA
      CL = CLC*COSA - CDC*SINA
C-
```

```
      WRITE (6,6440) YL(ICORR)/B,ZL(ICORR)/H, YR(ICORR)/B,ZR(ICORR)/H,
     *               DU,DW,DELCD
      WRITE (6,6400)
      WRITE (6,6410) ALFU,POU,QOU,CMUU,CLU,CDU,CMU
      WRITE (6,6420) ALFC,POU,QOC,CMUC,CLC,CDC,CMC
      WRITE (6,6430) ALFC,POU,QOC,CMUC,CL, CD, CMC, DELA*DEG
      DELAP = AWB*CLC/(1.+BWB*CMUC)                                   WLMS&BUT
      ALFP = ALFU + DELAP*DEG
      SINA = SIN(DELAP)
      COSA = COS(DELAP)
      CDP = CDC*COSA + CLC*SINA
      CLP = CLC*COSA - CDC*SINA
      WRITE (6,6431) ALFP,POU,QOC,CMUC,CLP,CDP,CMC,DELAP*DEG
C-
C-  ADD EFFECT OF JET/S, IF PRESENT.
C-
      IF(JETEFCT .EQ. 0) GO TO 595
      IF(IPASS .EQ. 2) GO TO 595
      IPASS = 2
      CALL JETADD(NW, NR, VWALL,VROOF, VCNTR, ITEST,IRUN,IP)
      WRITE (6,6120) TITLE,ITEST,IRUN,IP
      GO TO 591
C-  WRITE FINAL RESULTS TO MASS STORAGE
C-
 595  WRITE (7,1100) ITEST,IRUN,IP
      WRITE (7,1000) ALFU,POU,QOU,CMUU,CLU,CDU,CMU
      WRITE (7,1000) ALFC,POU,QOC,CMUC,CLC,CDC,CMC
      WRITE (7,1000) ALFC,POU,QOC,CMUC,CL, CD, CMC, DELA*DEG
      WRITE (7,1000) ALFP,POU,QOC,CMUC,CLP,CDP,CMC,DELAP*DEG
C-
      GO TO 330
 600  IP = 0
      WRITE (7,1100) IP,IP,IP
      CLOSE(7)                                                          !VAX
      CLOSE(9)                                                          !VAX
      GO TO 320
 610  WRITE (6,6450)
 999  STOP
C
C
 1000 FORMAT (8F10.4)
 1100 FORMAT (16I5)
 1200 FORMAT (I4,1X,3F10.4,1X,3E12.4,2(1X,2E12.4))
 1300 FORMAT (I4,1X,6F10.4,1X, E12.4)
 1400 FORMAT (I4,1X,3E12.4)
 1500 FORMAT (I5,9E12.4)
 1600 FORMAT (1H+,42X,'****')
C
 3000 FORMAT (80A1)
 3100 FORMAT (1H1,83A1/)
 3200 FORMAT (/' TUNNEL GEOMETRY :'/18X,'BREADTH:',3X,F8.3/18X,
     *            'HEIGHT:',4X,F8.3/18X,'IMAGE LAYERS:',I2/)
 3300 FORMAT (/' INPUT BOUNDARY CONDITIONS.  ROOF-FLOOR'//
     *          3X,'I',7X,'X/B',7X,'Y/B',7X,'Z/H',8X,'U,R-F',/)
 3400 FORMAT (/' INPUT BOUNDARY CONDITIONS.  SIDE_WALL'/
```

```
     *          3X,'I',7X,'X/B',7X,'Y/B',7X,'Z/H',7X,'U,WALL'/)
 3500 FORMAT (///,13(1H-)/' ITERATION :',I2/1H ,13(1H-)/)
 3600 FORMAT (/' VORTEX STRENGTHS.  (STR = G/(U*SQRT(B*H))'/)
 3700 FORMAT (/3X,'I',7X,'X/B',7X,'Y/B',7X,'Z/H',4X,'SPAN/B',
     *          5X,'SWEEP',5X,'PITCH',10X,'STR'/)
 3800 FORMAT (/' SOURCE STRENGTHS.  (STR = Q/(U*B*H)'/)
 3900 FORMAT (/60X,'TOTAL:',E12.4/)
 4000 FORMAT (/' RE_CALCULATED BOUNDARY CONDITIONS ON ROOF'//
     *          3X,'I',7X,'X/B',7X,'Y/B',7X,'Z/H',
     *          8X,'U_ROOF',5X,'CP_ROOF'/)
 4100 FORMAT (/' RE_CALCULATED BOUNDARY CONDITIONS ON WALL'//
     *          3X,'I',7X,'X/B',7X,'Y/B',7X,'Z/H',
     *          8X,'U_WALL',6X,'W_WALL',5X,'CP_WALL'/)
 4200 FORMAT (/' CENTER_LINE INTERFERENCE VELOCITIES'//
     *          3X,'I',7X,'X/B',7X,'Y/B',7X,'Z/H',
     *          8X,'U_CNTR',6X,'W_CNTR',7X,'U_Q_CL',6X,'U_G_CL',
     *          7X,'W_Q_CL',6X,'W_G_CL'/)
 4300 FORMAT (/' CROSS_EFFECT TERMS:'// 9X,'U_Q_ROOF',3X,
     *                          'U_G_WALL',3X,'W_G_WALL'/)
 4400 FORMAT ('1RUN NUMBER:',I3,'  POINT NUMBER:',I3/1X,38(1H-)//)
C
 6100 FORMAT (1H1,80A1,'TEST_',I2,',  RUN_',I2,',  POINT_',I2)
 6110 FORMAT ('1MODEL ONLY',2X,80A1,'TEST_',I2,',  RUN_',I2,',  POINT_',
     *          I2)
 6120 FORMAT ('1MODEL WITH JET',2X,80A1,'TEST_',I2,',  RUN_',I2,
     *          ',  POINT_',I2)
 6400 FORMAT(19X,'ALFA',6X,'PNOT',6X,'QNOT',7X,'CMU',8X,
     1          'CL',8X,'CD',8X,'CM' )
 6410 FORMAT (' MEASURED    '   ,8F10.4)
 6420 FORMAT (' CORRECTED   '   ,8F10.4)
 6430 FORMAT (' RESOLVED    '   ,8F10.4)
 6431 FORMAT (' CLASSICAL   '   ,8F10.4)
 6440 FORMAT (/' WALL POINTS --- BLOCKAGE : Y/B=',F7.4,',  Z/H=',F7.4,
     1          '     LIFT : Y/B=',F7.4,',  Z/H=',F7.4/
     1          ' VALUES USED IN CORRECTIONS :  DU/U=',F7.4,',  DW/U=',
     1          F7.4,',  DELTA-CD=',F7.4)
 6450 FORMAT (///' **** SQRT OF NEGATIVE NUMBER WHILE COMPUTING'
     *                  ' U_WALL_EFFECTIVE ****'///)
 6460 FORMAT (43X,'**** : SQRT OF NEGATIVE NUMBER WHILE COMPUTING'
     *          ' U_WALL_EFFECTIVE'/50X,'CROSS_TERM W_G_WALL IGNORED'
     *          ' AT ALL POINTS'/)
C
C
      END
```

```
      SUBROUTINE PIVOT(X,Y,Z, XPIV,SP,PSI,ALFA, X1,Y1,Z1,
     *                 X2,Y2,Z2)
C
C  DETERMINES THE END POINTS OF A LINE OF LENGTH "SP",
C  WHEN IT IS PITCHED AND YAWED.
C
      TANP = TAN(PSI)
      SINA = SIN(ALFA)
      COSA = COS(ALFA)
      X1 = X + XPIV*(1.Ø-COSA)
      Y1 = Y
      Z1 = Z + XPIV*SINA
      X2 = X + XPIV*(1.Ø-COSA) + SP*TANP*COSA
      Y2 = Y + SP
      Z2 = Z - (SP*TANP-XPIV)*SINA
      RETURN
      END
```

```
      SUBROUTINE INFLU(X1,Y1,Z1, X2,Y2,Z2, STRENT,ITYP,MINIT,ITRUNC,
     1                 XP,YP,ZP, DU,DV,DW)
C
C PARAMETERS:
C        X1,Y1,Z1 : Line_singularity End Point Co_ordinates, First Point
C        X2,Y2,Z2 : Line_singularity End Point Co_ordinates, Second Point
C        STRENT   : Singularity Strength (Total for ITYP=2,3
C                                         per unit length for ITYP=2)
C        ITYP     : Type Of Singularity... 1=Source/Sink,
C                                          2=Horse_Shoe Vortex,
C                                            (GAMA +ve Y1 TO Y2)
C                                          3=Doublet.
C        MINIT    : Initial Image Layer (=0 To Include Model In Tunnel)
C        XP,YP,ZP : Calculation Point
C        DU,DV,DW : Incremental Velocity Components, RETURNed.
C
      COMMON /IMAG/ B,H,LAYERS,IRF
      COMMON /DIRC/ DCXO,DCYO,DCZO
      IBUG = 0
      IS = -1
      DU = 0.0
      DV = 0.0
      DW = 0.0
      DCX = DCXO
      XINF = 10000.0*B
      STPERL = STRENT
      IF(ITYP .EQ. 2) GO TO 5
      ELS = SQRT( (X2-X1)**2 + (Y2-Y1)**2 + (Z2-Z1)**2 )
      STPERL = STRENT/ELS
C
    5 LMAX = LAYERS + 1
      DO 30 LDO = 1,LMAX
      FAC = 1.0
      L = LDO-1
      IF(L .LT. MINIT) GO TO 30
      IF(LDO.EQ.LMAX .AND. L.GT.0) FAC = 0.5 + 1.0/FLOAT(4*L)
      IF(ITYP .NE. 2) FAC = 1.0
C
      MNDO = L*2 + 1
      NOT = L + 1
      MN1 = MNDO - 1
C
      DO 20 MDO = 1,MNDO
      M = MDO - NOT
      REVM = (IS)**(IABS(M))
      YONE = FLOAT(M)*B + REVM*Y1
      YTWO = FLOAT(M)*B + REVM*Y2
C
      NINC = MN1
      IF(MDO.EQ.1 .OR. MDO.EQ.MNDO) NINC = 1
      DO 20 NDO = 1,MNDO,NINC
      N = NDO - NOT
      REVN = (IS)**(IABS(N))
      X2IM = X2
```

```
      X1IM = X1
      Y1IM = YONE
      Y2IM = YTWO
      Z1IM = FLOAT(N)*H + REVN*Z1
      Z2IM = FLOAT(N)*H + REVN*Z2
      IF(REVM*REVN .GT. Ø) GO TO 1Ø
C
      TEMP = Y2IM
      Y2IM = Y1IM
      Y1IM = TEMP
      TEMP = Z2IM
      Z2IM = Z1IM
      Z1IM = TEMP
      TEMP = X2IM
      X2IM = X1IM
      X1IM = TEMP
C
   1Ø DCY = DCYO*REVN
      DCZ = DCZO*REVM
C
      IF(ITYP-2) 11,12,13
   11 CALL LNSCGN(X1IM,Y1IM,Z1IM, X2IM,Y2IM,Z2IM, STPERL,
     1              XP,YP,ZP, DELU,DELV,DELW)
      GO TO 16
   12 CALL LNVXGN(X1IM,Y1IM,Z1IM, XINF,Y1IM,Z1IM, STPERL,
     *              XP,YP,ZP, DUT1,DVT1,DWT1)
      CALL LNVXGN(X2IM,Y2IM,Z2IM, X1IM,Y1IM,Z1IM, STPERL,
     1              XP,YP,ZP, DUBN,DVBN,DWBN )
      CALL LNVXGN(XINF,Y2IM,Z2IM, X2IM,Y2IM,Z2IM, STPERL,
     *              XP,YP,ZP, DUT2,DVT2,DWT2)
      DELU = DUT1 + DUBN + DUT2
      DELV = DVT1 + DVBN + DVT2
      DELW = DWT1 + DWBN + DWT2
      GO TO 16
   13 CALL LNDBGN(X1IM,Y1IM,Z1IM, X2IM,Y2IM,Z2IM, STPERL,
     1              DCX,DCY,DCZ, XP,YP,ZP, DELU,DELV,DELW,
     2              VMUR, CXR,CYR,CZR)
   16 DU = DU + FAC*DELU
      DV = DV + FAC*DELV
      DW = DW + FAC*DELW
      IF(IBUG .NE. Ø) WRITE (6,6ØØ) M,N,XP,YP,ZP,DELU,DELV,DELW,DU,DV,DW
  6ØØ FORMAT (2I4,3X,3F8.3,2(2X,3E14.6))
   2Ø CONTINUE
   3Ø CONTINUE
C
C-   ADD TRUNCATION SHEET FOR SOURCE/SINK
C
      IF(ITRUNC .EQ. Ø) RETURN
      IF(LAYERS.EQ.Ø .OR. ITYP.NE.1) RETURN
      QBH = STRENT/(2.Ø*8*H)
      PI = 3.141592654
      XM = (X1+X2)/2.Ø
      XX = XP - XM
      SIGNX = SIGN(1.Ø, XX)
      IF(ABS(XX) .LT. Ø.1E-Ø6) SIGNX = Ø.Ø
```

```
      YR = LAYERS*B + B/2.
      ZU = LAYERS*H + H/2.
      YL = -YR
      ZL = -ZU
      TF =  TFUNC(XX,YP,ZP, YL,ZL, YR,ZU)
      CALL LFUNCS(XX,YP,ZP, YL,ZL, YR,ZU, FL1,FL2)
      DU = DU + QBH + QBH*(SIGNX-TF/(2.Ø*PI))
      DV = DV + QBH*FL1/(2.Ø*PI)
      DW = DW + QBH*FL2/(2.Ø*PI)
      RETURN
      END
```

```
      SUBROUTINE LFUNCS (XX,Y,Z,Y1,Z1,Y2,Z2,L1F,L2F)
C ---
C --- RETURNS L1 AND L2 FUNCTIONS FOR CALCULATION OF V AND W VELOCITIES
C --- RESPECTIVELY AT POINT XX,Y,Z DUE TO THE EDGES Y1 Z1 Y2 Z2 OF A
C --- RECTANGULAR HOLE IN AN INFINITE SHEET SOURCE AT XX=Ø
C ---
      REAL N1,N2,N3,N4,L1F,L2F
      DY=Y2-Y1
      DZ=Z2-Z1
      XQ=XX*XX
      Y1Q=(Y-Y1)**2
      Y2Q=(Y-Y2)**2
      Z1Q=(Z-Z1)**2
      Z2Q=(Z-Z2)**2
      R1=SQRT(XQ+Y1Q+Z2Q)
      R2=SQRT(XQ+Y2Q+Z2Q)
      R3=SQRT(XQ+Y2Q+Z1Q)
      R4=SQRT(XQ+Y1Q+Z1Q)
      N1=R4+R1-DZ
      N2=R2+R3+DZ
      N3=R3+R4-DY
      N4=R1+R2+DY
      D1=R4+R1+DZ
      D2=R2+R3-DZ
      D3=R3+R4+DY
      D4=R1+R2-DY
      L1F=ALOG(N1*N2/(D1*D2))
      L2F=ALOG(N3*N4/(D3*D4))
      RETURN
      END
```

```
      FUNCTION TFUNC (XX,Y,Z,Y1,Z1,Y2,Z2)
C ---
C --- RETURNS FUNCTION-T FOR COMPUTATION OF U-VELOCITY AT POINT XX,Y,Z
C --- DUE TO A FINITE RECTANGALAR SHEET S6URCE Y1 Z1 Y2 Z2 AT XX=Ø
C ---
      DIMENSION SIGN(4),YY(4),ZZ(4)
      SUM=Ø.
      IF(ABS(XX).LT..ØØØØØØØ1) GO TO 2
      SIGN(1)=1.
      SIGN(2)=-1.
      SIGN(3)=-1.
      SIGN(4)=1.
      YY(1)=Y-Y1
      YY(2)=YY(1)
      YY(3)=Y-Y2
      YY(4)=YY(3)
      ZZ(1)=Z-Z1
      ZZ(2)=Z-Z2
      ZZ(3)=ZZ(1)
      ZZ(4)=ZZ(2)
      DO 1 J=1,4
      XJ=YY(J)*ZZ(J)/(XX*SQRT(XX*XX+YY(J)*YY(J)+ZZ(J)*ZZ(J)))
      PART=SIGN(J)*ATAN(XJ)
    1 SUM=SUM+PART
    2 TFUNC=SUM
      RETURN
      END
```

```
      SUBROUTINE TAPEIO(MATSAV,IU)
C
C-    MATSAV=1 : WRITE ALL REQUIRED MATRICES
C-    MATSAV=2 : READ  ALL REQUIRED MATRICES
C-    MARSAV=3 : READ ONLY THE INFLUENCE COEFFICIENT MATRICES.
C
      COMMON/IMAT/ UGRF(25,25),UQWL(25,25),UGCL(25,25),UQCL(25,25),
     *             WGCL(25,25),WQCL(25,25),UGWL(25,25),WGWL(25,25),
     *             UQRF(25,25)
      COMMON/LMAT/ AQ(25,25),AG(25,25)
      COMMON/ARRI/ XR(25),YR(25),ZR(25),XL(25),YL(25),ZL(25),
     *             XV(25),YV(25),ZV(25),XS(25),YS(25),ZS(25),
     *             SBV(25),SBS(25),PSIV(25),ALFV(25),PSIS(25),ALFS(25),
     *             CPOWL(25),UCPRF(25),UXORF(25),UXGWL(25),WXGWL(25),
     *             ULIFT(25),UBLEG(25),GAMA(25),SIGMA(25)
      COMMON/IMAG/ B,H,LAYERS,IRF
      COMMON/SIZE/ NP,NW,NV,NS,XPVOR,XPSRC
C
      PI = 3.141592654
      RAD = PI/180.0
C
      IF(MATSAV .LE. 0) RETURN
      IF(MATSAV .EQ. 1) GO TO 30
C
      READ (IU,1100) LAYERS,IRF,NR,NW,NV,NS
      READ (IU,1000) B,H,XPVOR,XPSRC
      DO 10 I = 1,NR
      READ (IU,1000) XR(I),YR(I),ZR(I)
            XR(I) = XR(I)*B
            YR(I) = YR(I)*B
            ZR(I) = ZR(I)*H
   10 CONTINUE
      DO 15 I = 1,NW
      READ (IU,1000) XL(I),YL(I),ZL(I)
            XL(I) = XL(I)*B
            YL(I) = YL(I)*B
            ZL(I) = ZL(I)*H
   15 CONTINUE
      DO 20 I = 1,NV
      READ (IU,1000) XV(I),YV(I),ZV(I),SBV(I),PSIV(I),ALFV(I)
            XV(I) = XV(I)*B
            YV(I) = YV(I)*B
            ZV(I) = ZV(I)*H
            SBV(I) = SBV(I)*B
            PSIV(I) = PSIV(I)*RAD
            ALFV(I) = ALFV(I)*RAD
   20 CONTINUE
      DO 25 I = 1,NS
      READ (IU,1000) XS(I),YS(I),ZS(I),SBS(I),PSIS(I),ALFS(I)
            XS(I) = XS(I)*B
            YS(I) = YS(I)*B
            ZS(I) = ZS(I)*H
            SBS(I) = SBS(I)*B
            PSIS(I) = PSIS(I)*RAD
```

```
          ALFS(I) = ALFS(I)*RAD
   25  CONTINUE
C
       READ (IU,1000) ((UGRF(I,J),I=1,NR),J=1,NV)
       READ (IU,1000) ((UGWL(I,J),I=1,NW),J=1,NV)
       READ (IU,1000) ((WGWL(I,J),I=1,NW),J=1,NV)
       READ (IU,1000) ((UOWL(I,J),I=1,NW),J=1,NS)
       READ (IU,1000) ((UORF(I,J),I=1,NR),J=1,NS)
       READ (IU,1000) ((UOCL(I,J),I=1,NW),J=1,NS)
       READ (IU,1000) ((WOCL(I,J),I=1,NW),J=1,NS)
       READ (IU,1000) ((UGCL(I,J),I=1,NW),J=1,NV)
       READ (IU,1000) ((WGCL(I,J),I=1,NW),J=1,NV)
         IF(MATSAV .EQ. 3) RETURN
       READ (IU,1000) ((  AG(I,J),I=1,NV),J=1,NV)
       READ (IU,1000) ((  AQ(I,J),I=1,NS),J=1,NS)
       RETURN
C
   30  WRITE (IU,1100) LAYERS,IRF,NR,NW,NV,NS
       WRITE (IU,1000) B,H,XPVOR,XPSRC
       DO 40 I = 1,NR
       WRITE (IU,1000) XR(I)/B,YR(I)/B,ZR(I)/H
   40  CONTINUE
       DO 45 I = 1,NW
       WRITE (IU,1000) XL(I)/B,YL(I)/B,ZL(I)/H
   45  CONTINUE
       DO 50 I = 1,NV
       WRITE (IU,1000) XV(I)/B,YV(I)/B,ZV(I)/H,SBV(I)/B,
      *                PSIV(I)/RAD,ALFV(I)/RAD
   50  CONTINUE
       DO 55 I = 1,NS
       WRITE (IU,1000) XS(I)/B,YS(I)/B,ZS(I)/H,SBS(I)/B,
      *                PSIS(I)/RAD,ALFS(I)/RAD
   55  CONTINUE
C
       WRITE (IU,1000) ((UGRF(I,J),I=1,NR),J=1,NV)
       WRITE (IU,1000) ((UGWL(I,J),I=1,NW),J=1,NV)
       WRITE (IU,1000) ((WGWL(I,J),I=1,NW),J=1,NV)
       WRITE (IU,1000) ((UOWL(I,J),I=1,NW),J=1,NS)
       WRITE (IU,1000) ((UORF(I,J),I=1,NR),J=1,NS)
       WRITE (IU,1000) ((UOCL(I,J),I=1,NW),J=1,NS)
       WRITE (IU,1000) ((WOCL(I,J),I=1,NW),J=1,NS)
       WRITE (IU,1000) ((UGCL(I,J),I=1,NW),J=1,NV)
       WRITE (IU,1000) ((WGCL(I,J),I=1,NW),J=1,NV)
       WRITE (IU,1000) ((  AG(I,J),I=1,NV),J=1,NV)
       WRITE (IU,1000) ((  AQ(I,J),I=1,NS),J=1,NS)
       RETURN
C
 1000  FORMAT (5E16.8)
 1100  FORMAT (16I5)
       END
```

```
      SUBROUTINE READCP(VCP,NO,IRUN,IP,IRAIL,JRAIL,LIFT, IRF)
      COMMON /BLKB/ ALFU,POU,QOU,CMUU,CLU,CDU,CMU
      DIMENSION VCP(NO), VCPA(3Ø,8), XCP(25), XCP7(3Ø)
      DATA XCP7 / -35.Ø, -22.1, -18.3, -14.3, -1Ø.2, -6.2, -2.2, Ø.8,
     1            1.8, 2.8, 3.8, 4.8, 6.8, 9.Ø, 1Ø.8, 12.8, 15.Ø, 18.Ø,
     1           21.Ø, 24.Ø, 3Ø.Ø, 36.Ø, 42.Ø, 48.Ø, 54.Ø, 6Ø.Ø, 4*Ø.Ø /
      DATA XCP/ -35.Ø, -2Ø.Ø, -16.Ø, -12.Ø, -8.Ø, -4.Ø, Ø.Ø, 3.Ø, 6.Ø,
     *            9.Ø, 12.Ø, 15.Ø, 18.Ø, 21.Ø, 25.26, 3Ø.Ø, 36.Ø, 42.Ø,
     *           48.Ø, 54.Ø, 6Ø.Ø, 4*Ø.Ø/
C
C---RETURNS CP-VALUES FROM FILE 'TAPE1Ø'
C---PARAMETERS
C        VCP    - ARRAY OF VELOCITY VALUES FROM MEASURED CP_S
C       NOTE : AT PRESENT 'TAPE1Ø' CONTAINS VELOCITY
C              INSTEAD OF CP-S FOR KBF DATA.
C        NO     - NUMBER OF CP-VALUES
C        IRUN   - TUNNEL RUN ID NUMBER
C        IP     - POINT NUMBER
C        IRAIL  - FIRST  RAIL NUMBER FOR CP-VALUES
C        JRAIL  - SECOND RAIL NUMBER FOR CP-VALUES
C        LIFT   - Ø OR 1
C                 Ø -- VCP =(VCP(JRAIL) + VCP(IRAIL))/2, FOR SIDEWALLS
C                 1 -- VCP =(VCP(JRAIL) - VCP(IRAIL)), FOR (ROOF-FLOOR)
C        IRF    - OPTION FLAG. Ø=ROOF ONLY, 1=(ROOF-FLOOR)
C
   1Ø READ (1Ø,5ØØ,END=99) NTEST,NRUN,NPNT
      NMAX = NO
      IF(IRAIL .EQ. 7) NMAX = 26
      DO 2Ø J = 1,8
   2Ø READ (1Ø,51Ø) (VCPA(I,J), I=1,NMAX)
      READ (1Ø,52Ø) ALFU,POU,QOU,CMUU,CLU,CDU,CMU
      IF(NRUN .NE. IRUN) GO TO 1Ø
      IF(NPNT .EQ. IP) GO TO 25
      IF(NPNT .LT. IP) GO TO 1Ø
      IP = Ø
      GO TO 45
C
   25 SIGN = 1.Ø
      DENOM = 2.Ø
      IF(LIFT .EQ. Ø) GO TO 26
      SIGN = -1.Ø*FLOAT(IRF)
      DENOM = 1.Ø
   26 IRL = IRAIL
      IF(IRF .EQ. Ø) GO TO 3Ø
      IF(IRAIL .NE. 7) GO TO 3Ø
      CALL INTER (XCP7,VCPA(1,7),XCP,VCPA(1,1),26,NO)
      IRL = 1
C
   3Ø DO 4Ø I = 1,NO
   4Ø VCP(I) = (VCPA(I,JRAIL) + SIGN*VCPA(I,IRL   ))/DENOM

   45 NN = (NO+8)/9
      NN = NN*8 + 2
      DO 5Ø I = 1,NN
```

```
   5Ø  BACKSPACE 1Ø
       RETURN
C
   99  WRITE (6,6ØØ) IRUN
       IRUN = -IRUN
       RETURN
C
  5ØØ  FORMAT (16I5)
  51Ø  FORMAT (2X,9F8.4)
  52Ø  FCRMAT (7F1Ø.2)
  6ØØ  FORMAT (///' ---_ EOF ON TAPE1Ø _---'//' ** NO DATA WITH IDRUN -',
      1  I3,' **'//)
       END
```

```
      SUBROUTINE INTER(XD,FD,XI,FI,MAX,IDO)
C
C     GIVEN A SET OF VALUES IN THE ARRAY "FD" AT DATA POINTS "XD",
C     THIS SUBROUTINE INTERPOLATES THEM AT POINTS "XI"
C     THE INTERPOLATED VALUES ARE PLACED IN ARRAY "FI"
C     MAX  : NO. OF POINTS IN "XD" FOR WHICH "FD" IS DEFINED
C     IDO  : NO. OF POINTS IN "XI" FOR WHICH "FI" IS DESIRED.
C
      DIMENSION XD(1),FD(1),XI(1),FI(1)
C
      DO 4Ø I = 1,IDO
      IF(XI(I) .GT. XD(1)) GO TO 1Ø
      J = 2
      GO TO 3Ø
   1Ø DO 2Ø J = 1,MAX
      IF(XD(J) .GE. XI(I)) GO TO 3Ø
   2Ø CONTINUE
      J = MAX
   3Ø JP = J
      JM = J-1
      FI(I) = FD(JM) + (FD(JP) - FD(JM))*(XI(I)-XD(JM))/
     1        (XD(JP)-XD(JM))
   4Ø CONTINUE
      RETURN
      END
```

```
      SUBROUTINE OUTPUT(NO,NS, XM,SPAN, LIFT, VCP,XCP,SIGMA,
     *                  DC,DW, ICORR, JET)
C
C --- OUTPUT OF LIFT AND BLOCKAGE CORRECTIONS
C --- GENERATION OF LINE PRINTER PLOTS

      COMMON/IMAG/ B,H,LAYERS,IRF
      DIMENSION VCP(NO),XCP(NO),SIGMA(NS),DC(25,3),DW(25,3)
      DIMENSION XM(NS),NP(61)
C
      SPB = SPAN/B*2.Ø
C --- SET UP HEADERS AND PLOT LIMITS
      L=2*LIFT+1
      IF(LIFT.EQ.1) GO TO 1
      VALU = B*H
      WRITE(6,1Ø)
      GO TO 2
    1 WRITE(6,11)
      VALU = SQRT(B*H)
    2 CALL RLIM(VCP,DW,DC(1,L),AA,BB,CC,DD,NO)
C
      SUM = Ø.Ø
C --- CYCLE THROUGH RAIL DATA
      DO 9 N=1,NO
      X=XCP(N)/B
      CALL PPLOT(VCP(N),NP,N,AA,1,ICORR)
      WRITE(6,12) X,VCP(N),(DW(N,J),J=1,3),DC(N,L),NP
      CALL PPLOT(DW(N,1),NP,N,AA,2,ICORR)
      WRITE(6,13) NP
      CALL PPLOT(DC(N,L),NP,N,AA,3,ICORR)
      IF(N.GT.NS) GO TO 3
      X=XM(N)/B
      Q = SIGMA(N)/(VALU)
      SUM = SUM + Q
      IF(JET .EQ. Ø) WRITE(6,13) NP,X,Q
      GO TO 9
    3 K = N-NS
      IF(JET .NE. Ø) GO TO 9
      IF(K.GE.7) GO TO 8
      GO TO (4, 5, 4, 6, 8, 7), K
    4 WRITE (6,14) NP
      GO TO 9
    5 WRITE (6,15) NP,SUM
      GO TO 9
    6 WRITE (6,16) NP,SPB
      GO TO 9
    7 IF(LIFT .NE. 1) WRITE (6,17) NP
      IF(LIFT .EQ. 1) WRITE (6,18) NP
    8 WRITE (6,13) NP
    9 CONTINUE
C
C --- TERMINATION
      WRITE(6,2Ø) AA,BB,CC,DD
      RETURN
```

```
                                                                          OUTPUT 055
 10  FORMAT(/6X,4HPOSN,3X,5HINPUT,3(4X,4HWALL),5X,3HC/L,23X,              OUTPUT 056
    *        19HBLOCKAGE CORRECTION,23X,13HSINGULARITIES/                 OUTPUT 057
    *        7X,3HX/B,2(4X,4HDU/U),4X,4HDV/U,4X,4HDW/U,4X,7HDU/U   I,     OUTPUT 058
    *        3(9(2H--),2H-I),5X,3HX/B,3X,2HS' )                           OUTPUT 059
 11  FORMAT(/6X,4HPOSN,3X,5HINPUT,3(4X,4HWALL),5X,3HC/L,25X,              OUTPUT 060
    *        15HLIFT CORRECTION,25X,13HSINGULARITIES/                     OUTPUT 061
    *        7X,3HX/B,2(4X,4HDU/U),4X,4HDV/U,4X,4HDW/U,4X,7HDW/U   I,     OUTPUT 062
    *        3(9(2H--),2H-I),5X,3HX/B,3X,2HG' )                           OUTPUT 063
 12  FORMAT(2X,6F8.4,2X,61A1)                                             OUTPUT 064
 13  FORMAT(1H+,51X,61A1,    2F8.4)                                       OUTPUT 065
 14  FORMAT(1H+,51X,61A1, 8X,8(1H-) )                                     OUTPUT 066
 15  FORMAT(1H+,51X,61A1,2X,6HTOTAL=,F8.4)                                OUTPUT 067
 16  FORMAT(1H+,51X,61A1,1X,7HSPAN/B=,F8.4)                                OUTPUT 068
 17  FORMAT(1H+,51X,61A1,1X,12HS'=S/(U*B*H)   )                           OUTPUT 069
 18  FORMAT(1H+,51X,61A1,1X,18HG'=G/(U*SQRT(B*H))   )                     OUTPUT 070
 20  FORMAT(15X,1HX,7X,1H+,23X,1HO,4X,1HI,3(9(2H--),2H-I)/34X,4F20.2)     OUTPUT 071
     END                                                                  OUTPUT 072


     SUBROUTINE RLIM(X1,X2,X3,A,B,C,D,N)                                  RLIM  001
C                                                                         RLIM  002
C --- DETERMINATION OF LINE PRINTER PLOT LIMITS                           RLIM  003
C                                                                         RLIM  004
     DIMENSION X1(25),X2(25),X3(25),XN(4)                                 RLIM  005
     DATA XN/1.,2.,4.,5./                                                 RLIM  006
C                                                                         RLIM  007
     II=1                                                                 RLIM  008
     XX=-.01                                                              RLIM  009
     A=XX                                                                 RLIM  010
     D=-2.*A                                                              RLIM  011
     DO 4 I=1,N                                                           RLIM  012
   1 IF((X1(I).LT.A).OR.(X1(I).GT.D)) GO TO 2                             RLIM  013
     IF((X2(I).LT.A).OR.(X2(I).GT.D)) GO TO 2                             RLIM  014
     IF((X3(I).LT.A).OR.(X3(I).GT.D)) GO TO 2                             RLIM  015
     GO TO 4                                                              RLIM  016
C                                                                         RLIM  017
   2 II=II+1                                                              RLIM  018
     IF(II.LT.5) GO TO 3                                                  RLIM  019
     II=1                                                                 RLIM  020
     XX=10.*XX                                                            RLIM  021
   3 A=XN(II)*XX                                                          RLIM  022
     D=-2.*A                                                              RLIM  023
     GO TO 1                                                              RLIM  024
   4 CONTINUE                                                             RLIM  025
     B=0.                                                                 RLIM  026
     C=-A                                                                 RLIM  027
     RETURN                                                               RLIM  028
     END                                                                  RLIM  029
```

```
      SUBROUTINE PPLOT(X,N,L,A,K,ICORR)
C
C --- GENERATION OF PLOT BACKGROUND
C
      DIMENSION N(61),NS(3) , NP(3)
      DATA NB,NI,NL/1H ,1HI,1H-/
      DATA         NS/1HX,1H+,1HO/
C
      IF(K.EQ.3) GO TO 1
      IF(L.NE.1) GO TO 2
      B=-A/20.
      C=B/2.
      NT = NB
      GO TO 2
C
    1 IF(L.EQ.ICORR) NT=NL
C
    2 DO 3 I=1,61
    3 N(I)=NT
      NT=NB
      IF(K.LT.3) GO TO 7
C
    4 N( 1)=NI
      N(21)=NI
      N(61)=NI
C
      I1 = NP(1)
      N(I1) = NB
      I2 = NP(2)
      N(I2) = NB
C
    7 T=X-A+C
      I=T/B+1
      N(I)=NS(K)
      NP(K) = I
      RETURN
      END
```

```
      SUBROUTINE LNDBEQ(VMU2,XC,YC,ZC,VL1,DU,DV,DW,IT)
C-  LINE DOUBLET EQUATION
      PI=3.141592654
C THE VALUE OF 'IT' TAKES THE VALUE OF '2' FOR TYPE (1,2) AND '3' FOR
C TYPE (1,3).
      CONST=VMU2/(4.*PI)
      IF(IT-2)1,1,2
    2 TEMP=ZC
      ZC=YC
      YC=TEMP
    1 VL12=VL1/2.
      XCPL=XC+VL12
      XCML=XC-VL12
      TMPP=YC**2+ZC**2
      TMPN=YC**2-ZC**2
      DN1=XCML**2+TMPP
      DP1=XCPL**2+TMPP
        TEMP=Ø.1E-Ø6
        IF(IT .EQ. 1) GO TO 1ØØ
      IF(TMPP-TEMP)11,11,13
   11 TEMP=ABS(XC)-VL12
      IF(TEMP)18,18,5
   18 DU=Ø.
      DV=Ø.
      DW=Ø.
      GO TO 3
    5 DNOMP=SQRT(DP1**3)
      DNOMN=SQRT(DN1**3)
      DU=CONST*YC*(1./DNOMN-1./DNOMP)
      DV=.5*CONST*(1./XCPL**2-1./XCML**2)
      DW=Ø.
      GO TO 3
   13 DNOMP=SQRT(DP1**3)
      DNOMN=SQRT(DN1**3)
      DU=CONST*YC*(1./DNOMN-1./DNOMP)
      DV=CONST*((XCPL*(TMPN*DP1+TMPP*YC**2)/DNOMP-XCML*(TMPN*DN1+TMPP*YC
     1**2)/DNOMN)/TMPP**2)
      DW=CONST*YC*ZC*(XCPL*(2.*DP1+TMPP)/DNOMP-XCML*(2.*DN1-TMPP)/DNOMN)
     1/TMPP**2
      IF(IT-2)3,3,4
    4 TEMP=DW
      DW=DV
      DV=TEMP
    3 CONTINUE
      RETURN
C
 1ØØ     DNOMP = SQRT(DP1**3)
         DNOMN = SQRT(DN1**3)
         DU = CONST*(XCML/DNOMN - XCPL/DNOMP)
         DV = CONST*YC*(1./DNOMN - 1./DNOMP)
         DW = CONST*ZC*(1./DNOMN - 1./DNOMP)
         RETURN
C
        END
```

```
      SUBROUTINE LNDBGN(XA,YA,ZA,XB,YB,ZB,VMU,CX,CY,CZ,XP,YP,ZP,DU,DV,DW
     1,VMUR,CXR,CYR,CZR)
C-
C- GENERATES DU,DV,DW VELOCITIES DUE TO A LINE DOUBLET
C-
C DATA TO BE SUPPLIED.*****************************************************
C -----------------------------------------------------------------------
C XA,YA,ZA,XB,YB,ZB, ARE THE END COORDINATES OF THE LINE DOUBLET.
C VMU IS THE COUPLE OF THE DOUBLET.
C CX,CY,CZ ARE THE DIRECTION COSINES OF THE COUPLE VECTOR.
C CX=X/R      CY=Y/R      AND      CZ=Z/R.  R=SQRT(X**2-Y**2+Z**2)
C VL IS THE LENGTH OF THE LINE DOUBLET.
C XP,YP,ZP ARE THE COORDINATES OF ANY POINT IN SPACE.
C VALUES CALCULATED BY THE PROGPAM****************************************
C------------------------------------------------------------------------
C DU,DV,DW ARE THE VELOCITY COMPONENTS AT THE POINT 'P' IN THE (X,Y,Z)
C SYSTEM
C VMUR IS THE RESULTANT COMPONENT OF THE COUPLE OF THE DOUBLET.
C THIS COMPONENT IS NORMAL TO THE AXIS OF THE DOUBLET.
C CXR,CYR,CZR ARE THE DIRECTION COSINES OF THE COUPLE VECTOR USED IN
C CALCULATING DU,DV,DW.
C NOTE.  THE COMPONENT OF THE COUPLE VECTOR ALONG THE AXIS OF THE
C DOUBLET WAS NOT INCLUDED IN DETERMINING DU,DV,DW. THIS ELIMINATED
C POINT SOURCE AND POINT SINK EFFECTS IN THE MODELDUE TO THE LINE
C DOUBLET.***************************************************************
C************************************************************************
      TEMP=(XA+XB)/2.
      XAO=XA-TEMP
      XBO=XB-TEMP
      XPO=XP-TEMP
      TEMP=(YA+YB)/2.
      YAO=YA-TEMP
      YBO=YB-TEMP
      YPO=YP-TEMP
      TEMP=(ZA+ZB)/2.
      ZAO=ZA-TEMP
      ZBO=ZB-TEMP
      ZPO=ZP-TEMP
      IC=1
      CALL CRDTEG(XAO,YAO,ZAO,XBO,YBO,ZBO,XPO,YPO,ZPO,XPCG,YPCG,ZPCG,IC)
      CALL CRDTEG(XAO,YAO,ZAO,XBO,YBO,ZBO,CX,CY,CZ,CXG,CYG,CZG,IC)
      VMU2=VMU*CYG
      VMU3=VMU*CZG
      VMUR=SQRT(VMU2**2+VMU3**2)
      VL1=SQRT((XA-XB)**2+(YA-YB)**2+(ZA-ZB)**2)
      IT=2
      CALL LNDBEQ(VMU2,XPCG,YPCG,ZPCG,VL1,DU2,DV2,DW2,IT)
      IT=3
      CALL LNDBEQ(VMU3,XPCG,YPCG,ZPCG,VL1,DU3,DV3,DW3,IT)
      DUG=DU2+DU3
      DVG=DV2+DV3
      DWG=DW2+DW3
      CXG=0.
      TEMP=SQRT(CYG*CYG+CZG*CZG)
```

```
      CYG=CYG/TEMP
      CZG=CZG/TEMP
      IC=2
      CALL CRDTEG(XAO,YAO,ZAO,XBO,YBO,ZBO,DU,DV,DW,DUG,DVG,DWG,IC)
      CALL CRDTEG(XAO,YAO,ZAO,XBO,YBO,ZBO,CXR,CYR,CZR,CXG,CYG,CZG,IC)
      CONTINUE
      RETURN
      END
```

```
      SUBROUTINE LNVXGN(XA,YA,ZA,XB,YB,ZB,CIRC,XP,YP,ZP,DU,DV,DW)
C GENERATES INCREMENTAL VELOCITY DUE TO A LINE VORTEX.
      TEMP=(XA+XB)/2.
      XAO=XA-TEMP
      XBO=XB-TEMP
      XPO=XP-TEMP
      TEMP=(YA+YB)/2.
      YAO=YA-TEMP
      YBO=YB-TEMP
      YPO=YP-TEMP
      TEMP=(ZA+ZB)/2.
      ZAO=ZA-TEMP
      ZBO=ZB-TEMP
      ZPO=ZP-TEMP
      IC=1
      CALL CRDTEG(XAO,YAO,ZAO,XBO,YBO,ZBO,XPO,YPO,ZPO,XPCG,YPCG,ZPCG,IC)
      VL1=SQRT((XA-XB)**2+(YA-YB)**2+(ZA-ZB)**2)
      CALL LNVXEQ(CIRC,XPCG,YPCG,ZPCG,VL1,DUG,DVG,DWG)
      IC=2
      CALL CRDTEG(XAO,YAO,ZAO,XBO,YBO,ZBO,DU,DV,DW,DUG,DVG,DWG,IC)
      CONTINUE
      RETURN
      END
```

```
      SUBROUTINE LNVXEQ(CIRC,XPG,YPG,ZPG,VL,DUG,DVG,DWG)                LNVXEQ 001
C- LINE VORTEX EQUATION                                                 LNVXEQ 002
      PI=3.141592654                                                    LNVXEQ 003
      DUG=0.                                                            LNVXEQ 004
      YZ2=YPG*YPG+ZPG*ZPG                                               LNVXEQ 005
      VL2=VL/2                                                          LNVXEQ 006
      XPL2=XPG+VL2                                                      LNVXEQ 007
      XML2=XPG-VL2                                                      LNVXEQ 008
      DN=XML2**2+YZ2                                                    LNVXEQ 009
      DP=XPL2**2+YZ2                                                    LNVXEQ 010
      RDN=SQRT(DN)                                                      LNVXEQ 011
      RDP=SQRT(DP)                                                      LNVXEQ 012
      CONST=.25*CIRC/PI                                                 LNVXEQ 013
C     TEMP=.01*VL                                                       LNVXEQ 014
      TEMP=0.000001                                                     LNVXEQ 015
      IF(YZ2-TEMP)2,2,4                                                 LNVXEQ 016
    2 TEMP=ABS(XPG)-VL2                                                 LNVXEQ 017
      IF(TEMP)8,8,5                                                     LNVXEQ 018
    8 DVG=0.                                                            LNVXEQ 019
      DWG=0.                                                            LNVXEQ 020
      GO TO 7                                                           LNVXEQ 021
    5 TEMP=.5*CONST*(1./XML2**2-1./XPL2**2)                             LNVXEQ 022
      DVG=-ZPG*TEMP                                                     LNVXEQ 023
      DWG=YPG*TEMP                                                      LNVXEQ 024
      GO TO 7                                                           LNVXEQ 025
    4 TEMP=CONST*(XML2/RDN-XPL2/RDP)/YZ2                                LNVXEQ 026
      DVG=ZPG*TEMP                                                      LNVXEQ 027
      DWG=-YPG*TEMP                                                     LNVXEQ 028
    7 CONTINUE                                                          LNVXEQ 029
      RETURN                                                            LNVXEQ 030
      END                                                               LNVXEQ 031
```

```
      SUBROUTINE LNSCGN(XA,YA,ZA,XB,YB,ZB,VM,XP,YP,ZP,DU,DV,DW)
C- GENERATES INCREMENTAL VELOCITIES DUE TO LINE SOUPCE
      TEMP=(XA+XB)/2.
      XAO=XA-TEMP
      XBO=XB-TEMP
      XPO=XP-TEMP
      TEMP=(YA+YB)/2.
      YAO=YA-TEMP
      YBO=YB-TEMP
      YPO=YP-TEMP
      TEMP=(ZA+ZB)/2.
      ZAO=ZA-TEMP
      ZBO=ZB-TEMP
      ZPO=ZP-TEMP
      IC=1
      CALL CRDTEG(XAO,YAO,ZAO,XBO,YBO,ZBO,XPO,YPO,ZPO,XPCG,YPCG,ZPCG,IC)
      VL1=SQRT((XA-XB)**2+(YA-YB)**2+(ZA-ZB)**2)
      CALL LNSCEQ(VM,XPCG,YPCG,ZPCG,VL1,DUG,DVG,DWG)
      IC=2
      CALL CRDTEG(XAO,YAO,ZAO,XBO,YBO,ZBO,DU,DV,DW,DUG,DVG,DWG,IC)
      CONTINUE
      RETURN
      END
```

ORIGINAL PAGE IS
OF POOR QUALITY

```
      SUBROUTINE LNSCEQ(VM,XPG,YPG,ZPG,VL,DUG,DVG,DWG)
C- LINE SOURCE EQUATION
      PI=3.141592654
      YZ2=YPG*YPG+ZPG*ZPG
      VL2=VL/2.
      XPL2=XPG+VL2
      XML2=XPG-VL2
      DN=XML2**2+YZ2
      DP=XPL2**2+YZ2
      RDN=SQRT(DN)
      RDP=SQRT(DP)
      CONST=.25*VM/PI
      TEMP=.Ø1*VL
      IF(YZ2-TEMP)2,2,4
    2 TEMP=ABS(XPG)-VL2
      IF(TEMP)8,8,5
    8 DUG=Ø.
      DVG=Ø.
      DWG=Ø.
      GO TO 7
    5 DUG=CONST*(1./RDN-1./RDP)
      TEMP=.5*CONST*(1./XML2**2-1./XPL2**2)
      DVG=YPG*TEMP
      DWG=ZPG*TEMP
      GO TO 7
    4 DUG=CONST*(1./RDN-1./RDP)
      TEMP=CONST*(XML2/RDN-XPL2/RDP)/YZ2
      DVG=-YPG*TEMP
      DWG=-ZPG*TEMP
    7 CONTINUE
      RETURN
      END
```

```
      SUBROUTINE CRDTEG(XAO,YAO,ZAO,XBO,YBO,ZBO,XPO,YPO,ZPO,EXIP,ETAP,ZT
     1AP,IC)
C COORDINATE TRANSFORMATION 'ENGLISH TO GREEK',IC=1
C COORDINATE TRANSFORMATION 'GREEK TO ENGLISH',IC=2
C THE ORIGIN OF THE COORDINATE SYSTEM WILL BE AT THE MID-POINT OF A-B.
C SUBROUTINE TRANSFORMS (X,Y,Z) SET OF AXES TO (EXI,ETA,ZTA)AXES WITH
C THE 'EXI' AXIS PARALLEL TO THE CENTRE LINE OF THE DOUBLET.
C THE ENDS OF THE LINE DOUBLET ARE 'A' AND'B'.
C 'P' IS A GENERAL POINT IN SPACE.
C NOTE SYSTEM SET UP FOR POSITIVE_WINDING NUMBERS  FOR ROTATION OF  AXES
C EPSI AND ALFA ARE THE ANGLES OF ROTATION OF THE ETA OR (Y) AND ZTA OR
C (Z) AXES RESPECTIVELY.
      TEMP=SQRT((XAO-XBO)**2+(YAO-YBO)**2)
      IF(TEMP)4,4,5
    5 CEPSI=(XAO-XBO)/TEMP
      SEPSI=(YAO-YBO)/TEMP
      XAP=XAO*CEPSI+YAO*SEPSI
      XBP=XBO*CEPSI+YBO*SEPSI
      GO TO 6
    4 CEPSI=1.
      SEPSI=0.
      XAP=XAO
      XBP=XBO
    6 TEMP=SQRT((XAP-XBP)**2+(ZAO-ZBO)**2)
      IF(TEMP)7,7,8
    8 SALFA=(ZBO-ZAO)/TEMP
      CALFA=(XAP-XBP)/TEMP
      GO TO 9
    7 CALFA=1.
      SALFA=0.
    9 IF(IC-1)1,1,2
    1 XPP=XPO*CEPSI+YPO*SEPSI
      YPP=YPO*CEPSI-XPO*SEPSI
      ZPP=ZPO
      EXIP=XPP*CALFA-ZPP*SALFA
      ETAP=YPP
      ZTAP=XPP*SALFA+ZPP*CALFA
      GO TO 3
    2 XPP=EXIP*CALFA+ZTAP*SALFA
      YPP=ETAP
      ZPP=ZTAP*CALFA-EXIP*SALFA
      XPO=XPP*CEPSI-YPP*SEPSI
      YPO=XPP*SEPSI+YPP*CEPSI
      ZPO=ZPP
    3 CONTINUE
      RETURN
      END
```

```
      SUBROUTINE GJRV (A,N,NL,EPSIL,IERR)
C     . . . . . . . . . . . . . . . . . . . . . . . . . . . . . . . . . . .
C     .                                                                    .
C     .  MATRIX INVERSION ROUTINE                                          .
C     .                                                                    .
C     .  CALLING SEQUENCE.....                                             .
C     .  CALL          N,NL,EPSIL,IERR)                                    .
C     .  A IS THE INPUT ARRAY WHICH WILL BE DESTROYED, N IS THE RANK       .
C     .  OF A, NL IS THE ROW DIMENSION OF A, EPSIL IS THE TEST             .
C     .  VALUE FOR THE PIVOT POINT SINGULARITY CHECK,                      .
C     .  IERR IS NONZERO IF THE MATRIX IS SINGULAR                         .
C     .  IF THE MATRIX IS NONSINGULAR, A CONTAINS A-INVERSE                .
C     .                                                                    .
C     . . . . . . . . C . . . . . . . . . . . . . . . . . . . . . . . . . .
      DIMENSION A(1),B(96),C(96),IP(96),IQ(96)
      IERR=0
      DO 160 K=1,N
      PIVOT=0.
C
C     GET LARGEST ELEMENT IN MATRIX  PLACE IN PIVOT
C
      DO 30 I=K,N
      DO 20 J=K,N
      IDEX=(J-1)*NL+I
      IF (ABS(A(IDEX))-ABS(PIVOT)) 20,20,10
   10 CONTINUE
      PIVOT=A(IDEX)
      IP(K)=I
      IQ(K)=J
   20 CONTINUE
   30 CONTINUE
      IF (ABS(PIVOT)-EPSIL) 230,230,40
   40 CONTINUE
      IF (IP(K)-K) 50,70,50
   50 CONTINUE
C
C     SWAP ROWS
C
      DO 60 J=1,N
      IPX=IP(K)
      IDEX=(J-1)*NL+IPX
      KDEX=(J-1)*NL+K
      Z=A(IDEX)
      A(IDEX)=A(KDEX)
      A(KDEX)=Z
   60 CONTINUE
   70 CONTINUE
      IF (IQ(K)-K) 80,100,80
   80 CONTINUE
C
C     SWAP COLUMNS
C
      DO 90 I=1,N
      IPX=IQ(K)
```

```
      IDEX=(IPX-1)*NL+I
      KDEX=(K-1)*NL+I
      Z=A(IDEX)
      A(IDEX)=A(KDEX)
      A(KDEX)=Z
   90 CONTINUE
  100 CONTINUE
      DO 140 J=1,N
      KDEX=(J-1)*NL+K
      JDEX=(K-1)*NL+J
      IF (J-K) 120,110,120
  110 CONTINUE
      B(J)=1./PIVOT
      C(J)=1.
      GO TO 130
  120 CONTINUE
      B(J)=-A(KDEX)/PIVOT
      C(J)=A(JDEX)
  130 CONTINUE
      A(KDEX)=0.
      A(JDEX)=0.
  140 CONTINUE
      DO 150 I=1,N
      DO 150 J=1,N
      IDEX=(J-1)*NL+I
      A(IDEX)=A(IDEX)+C(I)*B(J)
  150 CONTINUE
  160 CONTINUE
      DO 220 KP=1,N
      K=N+1-KP
      IF (IP(K)-K) 170,190,170
  170 CONTINUE
      DO 180 I=1,N
      IPX=IP(K)
      IDEX=(IPX-1)*NL+I
      KDEX=(K-1)*NL+I
      Z=A(IDEX)
      A(IDEX)=A(KDEX)
      A(KDEX)=Z
  180 CONTINUE
  190 CONTINUE
      IF (IQ(K)-K) 200,220,200
  200 CONTINUE
      DO 210 J=1,N
      IPX=IQ(K)
      IDEX=(J-1)*NL+IPX
      KDEX=(J-1)*NL+K
      Z=A(IDEX)
      A(IDEX)=A(KDEX)
      A(KDEX)=Z
  210 CONTINUE
  220 CONTINUE
      GC TO 240
  230 CONTINUE
      IERP=-1
```

ORIGINAL IS
OF POOR QUALITY

```
  240 CONTINUE                                                          GJRV   110
      RETURN                                                            GJRV   111
      END                                                               GJRV   112
```

```
      SUBROUTINE OUT(A,ID,JD,MM,NN,TITL,NCAR)
C
C-  PRINTS OUT A TWO DIMENSIONAL ARRAY A(I,J), IN THE RANGE I=1 TO MM
C-  AND J=1 TO NN.  ID AND JD ARE THE ARRAY'S DIMENSION LIMITS.
C-  "TITL" is a title with "NCAR" number of characters.
C
      DIMENSION A(ID,JD)
      CHARACTER TITL(79)
      MLO = 1
      MHI = (NCAR+3)/4
      WRITE (6,600) (TITL(M),M=1,NCAR)
C
   10 MHI = MLO + 8
      IF(MHI .GT. MM) MHI = MM
      WRITE (6,610) (M,M=MLO,MHI)
      WRITE (6,612)
C
      DO 20 N = 1,NN
   20 WRITE (6,620) N,(A(M,N),M=MLO,MHI)
      MLO = MLO + 9
      IF(MLO .LE. MM) GO TO 10
C
      MLO = 1
      NLO = 1
      MHI = 1
      NHI = 1
      AHI = A(1,1)
      ALO = A(1,1)
C
      DO 50 M = 1,MM
      DO 50 N = 1,NN
      IF(A(M,N) .LE. AHI) GO TO 40
      AHI = A(M,N)
      MHI = M
      NHI = N
   40 IF(A(M,N) .GE. ALO) GO TO 50
      ALO = A(M,N)
      MLO = M
      NLO = N
   50 CONTINUE
C
      WRITE (6,630) MLO,NLO,ALO,MHI,MHI,AHI
      RETURN
C
  600 FORMAT (1H1,79A1)
  610 FORMAT (/8X,'M = ',I2,9I13)
  612 FORMAT (3X,1HN/)
  620 FORMAT (I4,1X,9E13.5)
  630 FORMAT (//' MINIMUM AND MAXIMUM :'/26X,1HM,3X,1HN,5X,5HVALUE,
     1            /(23X,2I4,E13.5))
      END
```

```
      SUBROUTINE JETADD(NW,NR, VWALL,VROOF,VCNTR, ITEST,IRUN,IP)
C-
C-  Subroutine to add the effects of jet/s.
C-
      DIMENSION VCL(3), VWALL(25,3),VROOF(25,3),VCNTR(25,3)
      NN = MAX(NW,NR)
      IREW = 0
C
   10 READ (11,1000,END=50) IT,IR,IPT
      IF(IT.NE.ITEST .OR. IR.NE.IRUN .OR. IPT.NE.IP) GO TO 40
      DO 30 I = 1,NN
      READ (11,1100) J,XOB, UWL, URF, (VCL(K),K=1,3)
      VWALL(I,1) = VWALL(I,1) + UWL
      VROOF(I,1) = VROOF(I,1) + URF
      DO 20 K = 1,3
   20 VCNTR(I,K) = VCNTR(I,K) + VCL(K)
   30 CONTINUE
C
      RETURN
C
   40 DO 45 I = 1,NN
   45 READ (11,1100)
      GO TO 10
C
   50 IF(IREW .NE. 0) GO TO 60
      IREW = 1
      REWIND 11
      GO TO 10
C
   60 WRITE (6,600) ITEST,IRUN,IP
      RETURN
C
  600 FORMAT (//' *** NO JET_EFFECT DATA FOUND IN TAPE11 FOR '
     *            'ITEST/IRUN/IPT = ',3(I3,1H/), '  ***'//)
 1000 FORMAT (16I5)
 1100 FORMAT (I5,7E15.8)
C
      END
```

APPENDIX 3

Examples of Signature Analysis

CONFIGURATION: STRAIGHT-WINGED KBF MODEL, NO TIPS.

FLAP BLOWING: $C_\mu = 2.0$

ANGLES-OF-ATTACK: 6°, 12°, 18°, 24°

PLOTTED AFTER THIRD (I.E. FINAL) ITERATION

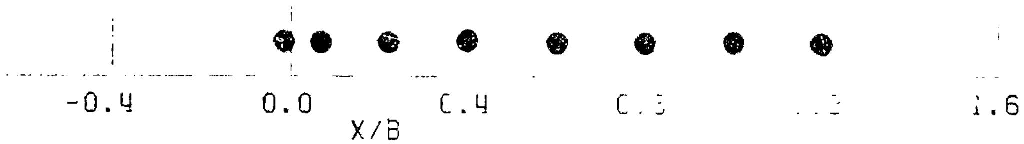

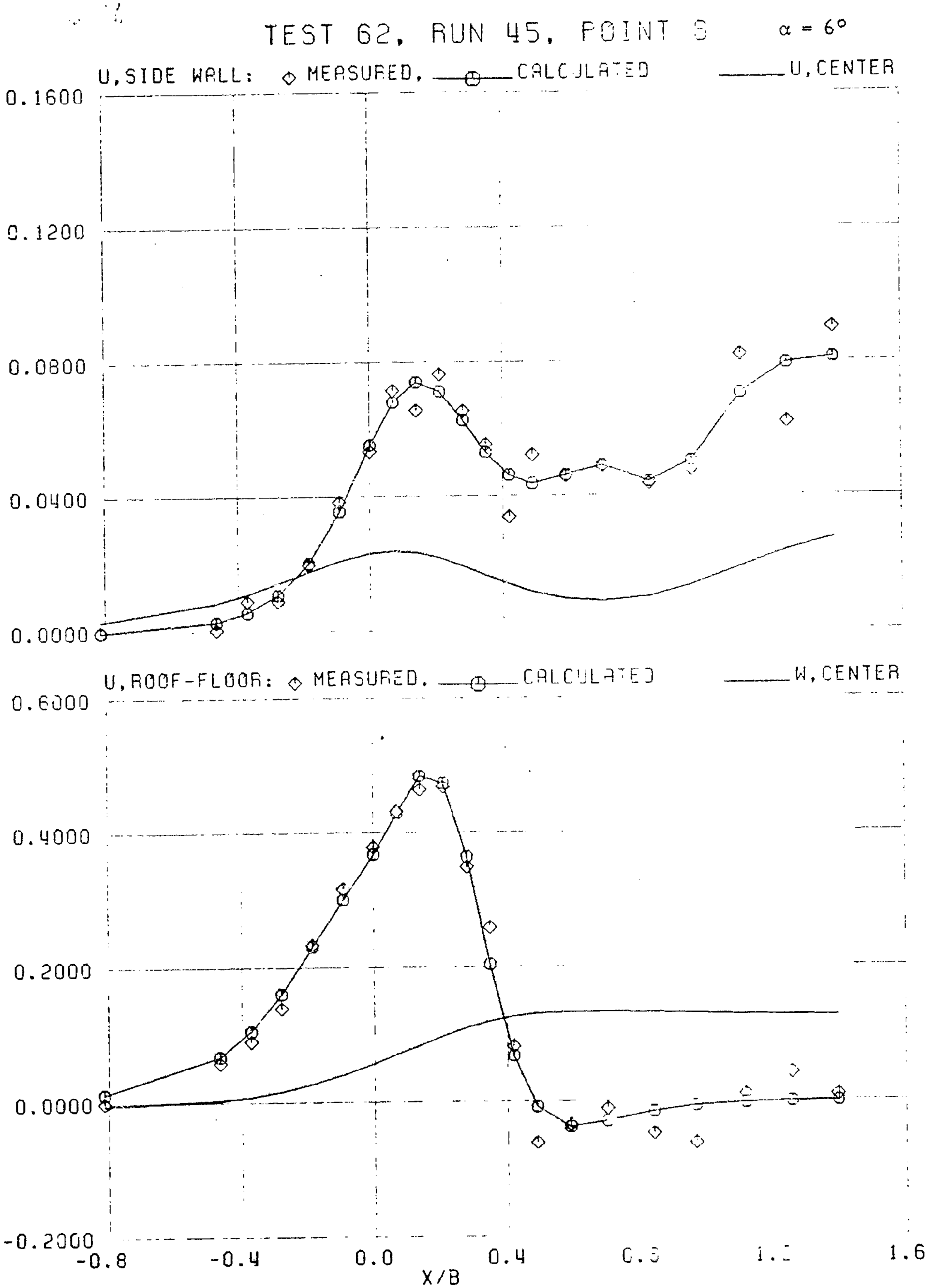

TEST 62, RUN 45, POINT 8 α = 6°
U, SIDE WALL: ◇ MEASURED, —○— CALCULATED —— U, CENTER
0.1600
0.1200
0.0800
0.0400
0.0000
U, ROOF-FLOOR: ◇ MEASURED, —○— CALCULATED —— W, CENTER
0.6000
0.4000
0.2000
0.0000
-0.2000
-0.8
-0.4
0.0
0.4
1.6
X/B

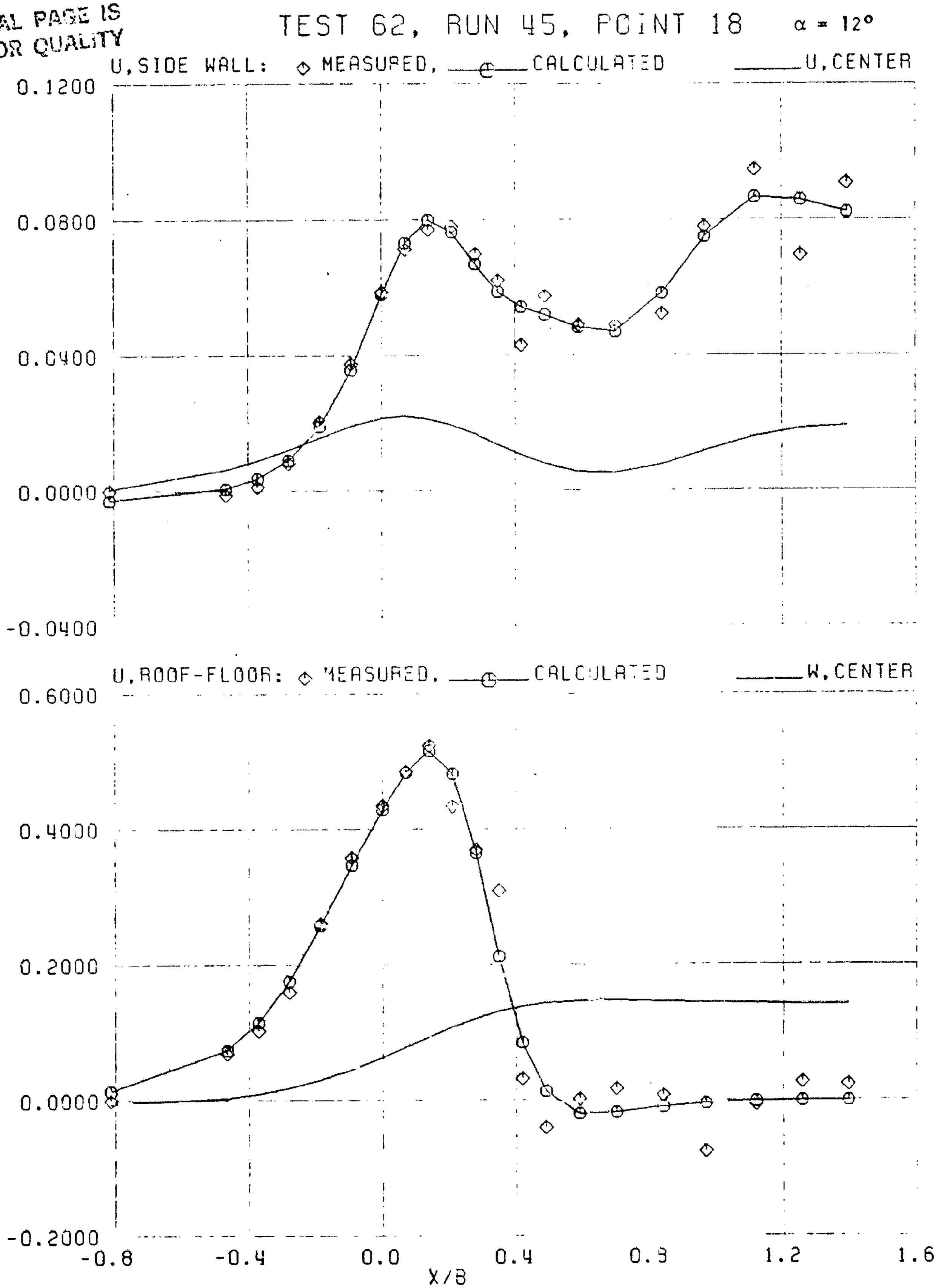
TEST 62, RUN 45, POINT 18 α = 12°
U,SIDE WALL: ◇ MEASURED, —⊖— CALCULATED
——— U,CENTER
0.1200
0.0800
0.0400
0.0000
-0.0400
U,ROOF-FLOOR: ◇ MEASURED, —⊖— CALCULATED
——— W,CENTER
0.6000
0.4000
0.2000
0.0000
-0.2000
-0.8
-0.4
0.0
0.4
0.8
1.2
1.6
X/B

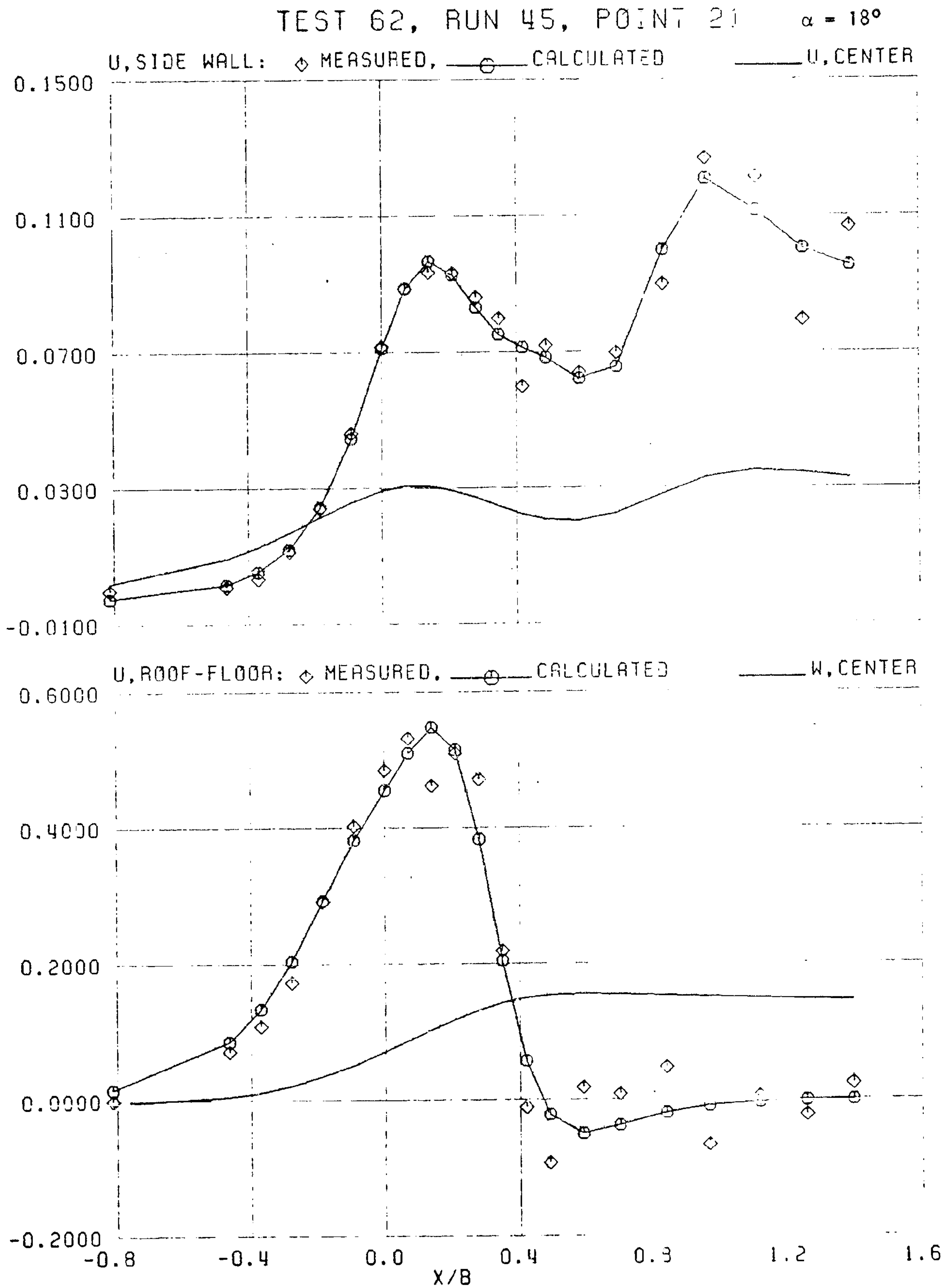

ORIGINAL PAGE IS
OF POOR QUALITY

TEST 62, RUN 45, POINT 25 α = 24°

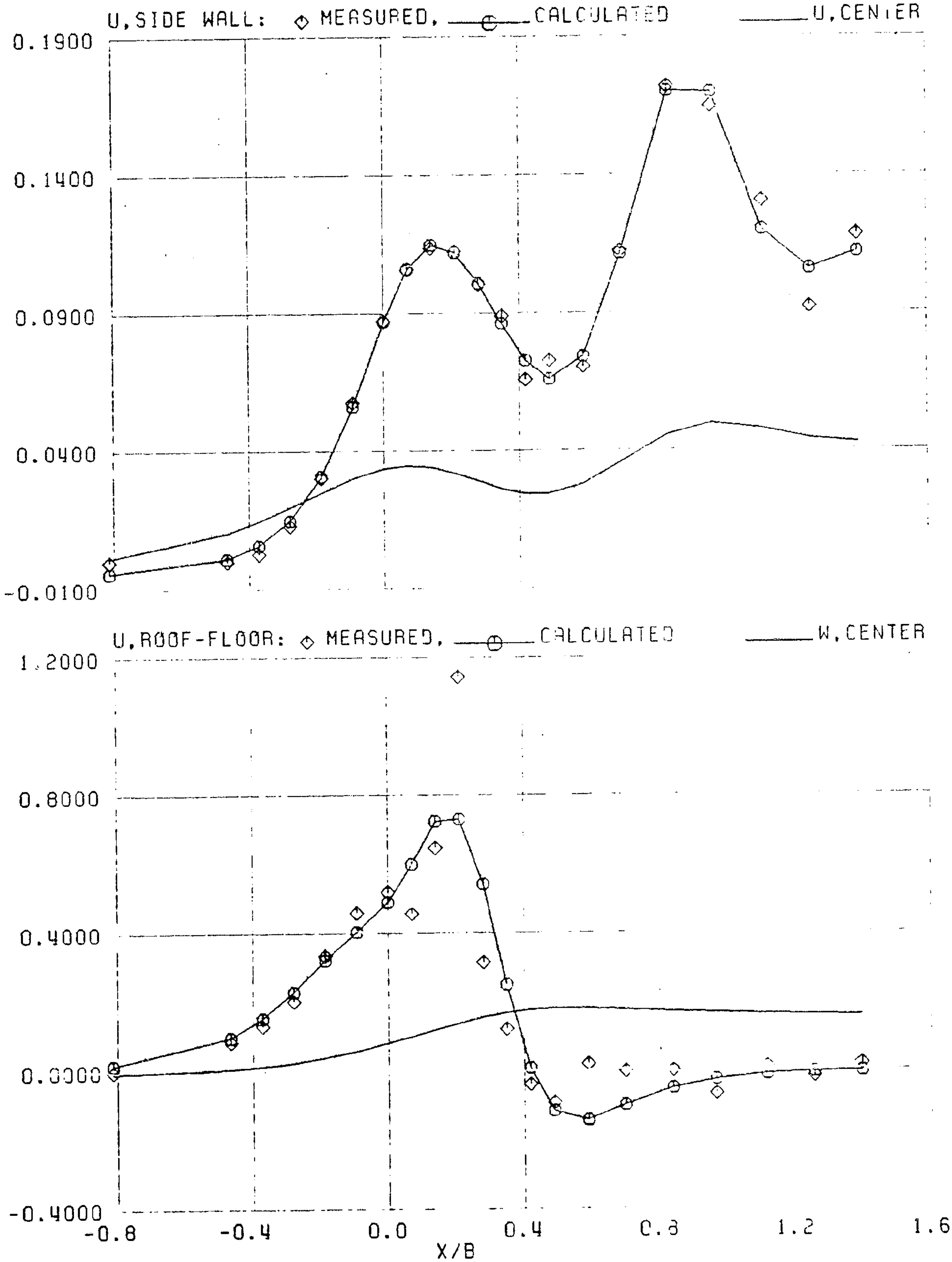

APPENDIX 4

LEAST SQUARES APPROACH FOR THE NASA 40' X 80' TUNNEL

APPENDIX 4

LEAST SQUARES APPROACH FOR THE NASA 40' X 80' TUNNEL

The image method employed by the LSQITER program cannot be applied directly to the NASA 80' x 40' tunnel because of its non-rectangular cross section. The influence coefficients required in the LSQITER program have to be generated using an alternate approach. This Appendix presents the results for interference factors for the 40' x 80' tunnel and explains how these are used to construct the influence coefficient matrices required by the LSQITER program.

Influence factors due to an isolated singularity

The influence factors due to a single horse shoe vortex or a finite length line source are obtained by using the vortex panel method described in Ref. 9. Figure A4.1 shows the theoretical flow model used to generate these factors. A length of 288' of the tunnel is panelled with vortex latices. Velocities due to a centrally located singularity are calculated at these panels. Panel circulation strengths are then obtained which satisfy the zero normal velocity condition at the tunnel surface.

Tunnel wall super velocities are then computed as the sum of panel-induced and singularity-induced effects. These calculations are done at various values of x/B at the roof, floor and the sidewall locations indicated in figure A4.1. The center-line influence factors are computed by omitting the effects of the central singularity and including only the panel circulation effects. The supervelocities thus computed are normalized by the factor Q/C for cases involving sources and by the factor $2\Gamma b/C$ for cases involving horse-shoe vortices, where C is the tunnel cross section area and b is the singularity span. The results for sources and horse shoe vortices of different spans and for both horizontal and vertical orientations are presented in Tables A4.1 through A4.6.

Generation of influence coefficient matrices

Using the normalized influence factors presented in the tables, influence coefficient matrices are constructed. The elements of these matrices are of the form a_{ij} where a is the induced velocity due to j-th singularity (of unit strength) at i-th point. Thus the influence factors given in the table must be multiplied by 1/C for sources and by 2b/C for vortices for ongoing use.

The independent variable, x/B, presented in the tables corresponds to stream-wise locations on a local coordinate system whose origin is at the singularity. Once the pressure ports locations are chosen and the positions of singularities at the tunnel centerline have been selected, the relative streamwise distance between a given singularity (j) and the pressure measurement point (i) is known. This relative distance normalized by the tunnel breadth, B, is used as the independent variable to pick values from the tables. It may be necessary to interpolate the tabulated values.

The LSQITER program has been written to handle the most general cases involving singularities that could be swept, pitched and be located off-center in the tunnel. However, due to restrictions on time and effort the influence factors for the 40' x 80' tunnel have been generated only for cases where the singularities are unswept and are placed midway between roof and floor. Consequently, many of the influence coefficient matrices required by the LSQITER program become null matrices. The following list defines the matrices required.

UGRF:	u due to Γ, (Roof-floor)	Non-zero
UGWL:	u due to Γ, (Sidewall	Zero
WGWL:	w due to Γ, Sidewall	Zero
UQWL:	u due to Q, Sidewall	Non-zero
UQRF:	u due to Q, Roof-floor	Zero
UQCL:	u due to Q, Tunnel Centerline	Non-zero
WQCL:	w due to Q, Tunnel Centerline	Zero
UGCL:	u due to Γ, Tunnel Centerline	Zero
WGCL:	w due to Γ, Tunnel Centerline	Non-zero

Note, however, that the null matrices must be made available to the LSQITER program with all elements set to zero

Data file structure for the influence coefficient matrices

The influence coefficient matrices generated for special cases like the 40' x 80' tunnel must be made available to the LSQITER program via FORTRAN input UNIT NO. 16. The structure of this data file is as follows:

The first few lines of data correspond to what was described as "Geometry Input" in the input description of the program given in detail on pages 103 through 105. Input line numbers 4 through 9 must be defined in this data file accordingly. The FORMAT s for the variables are 16I5 for integers and 5E16.8 for real numbers (see also subroutine TAPEIO in program listing, page 132). Note that the variable "LAYERS" loses its significance and that there can be no sweep or pitching of the singularities. Following these lines of input, the data file must now contain the elemenets of the matrices listed above in the same order. The elements (a_{ij}) of each matrix must be sequenced such that the subscript i varies more rapidly than the subscript j. (See program listing on page 132).

Running the LSQITER program for the 40' x 80' tunnel

Once the data file containing the influence coefficient matrices is constructed as described above, the LSQITER program can be run to process the 40' x 80' tunnel signatures. The input on UNIT 5 is identical to the rectangular tunnel case input described in pp. 101-106 with the following exceptions:

1. The program must be signalled to expect the special influence coefficient matrices. This is done by assigning a value of 3 to the flag MATSAV in input card number 2 described on page 101. This causes the program to read these matrices from FORTRAN UNIT 16 instead of calculating them through imaging techniques.
2. At present the flags KROSG and KROSQ in Card-2 must be set to zero since influence coefficients for cross effect terms are not available.

3. Omit the Geometry Input Section (Card-4 through Card-9) as these will now be read from the matrix data file via UNIT 16.

In addition to the mass storage files described on pages 106 and 107, the matrix data file described in this appendix must be pre-assigned to FORTRAN UNIT 16. For a given geometry of singularities and wall pressure points, the least square inversion process needs to be done only once. The program writes out all matrices on UNIT-8 which has to be saved for future use. Subsequent runs can be made with MATSAV=2 and the special influence coefficient matrix data file need not be made available via UNIT-16 (See comments on mass stroage file, UNIT-8 on page 106).

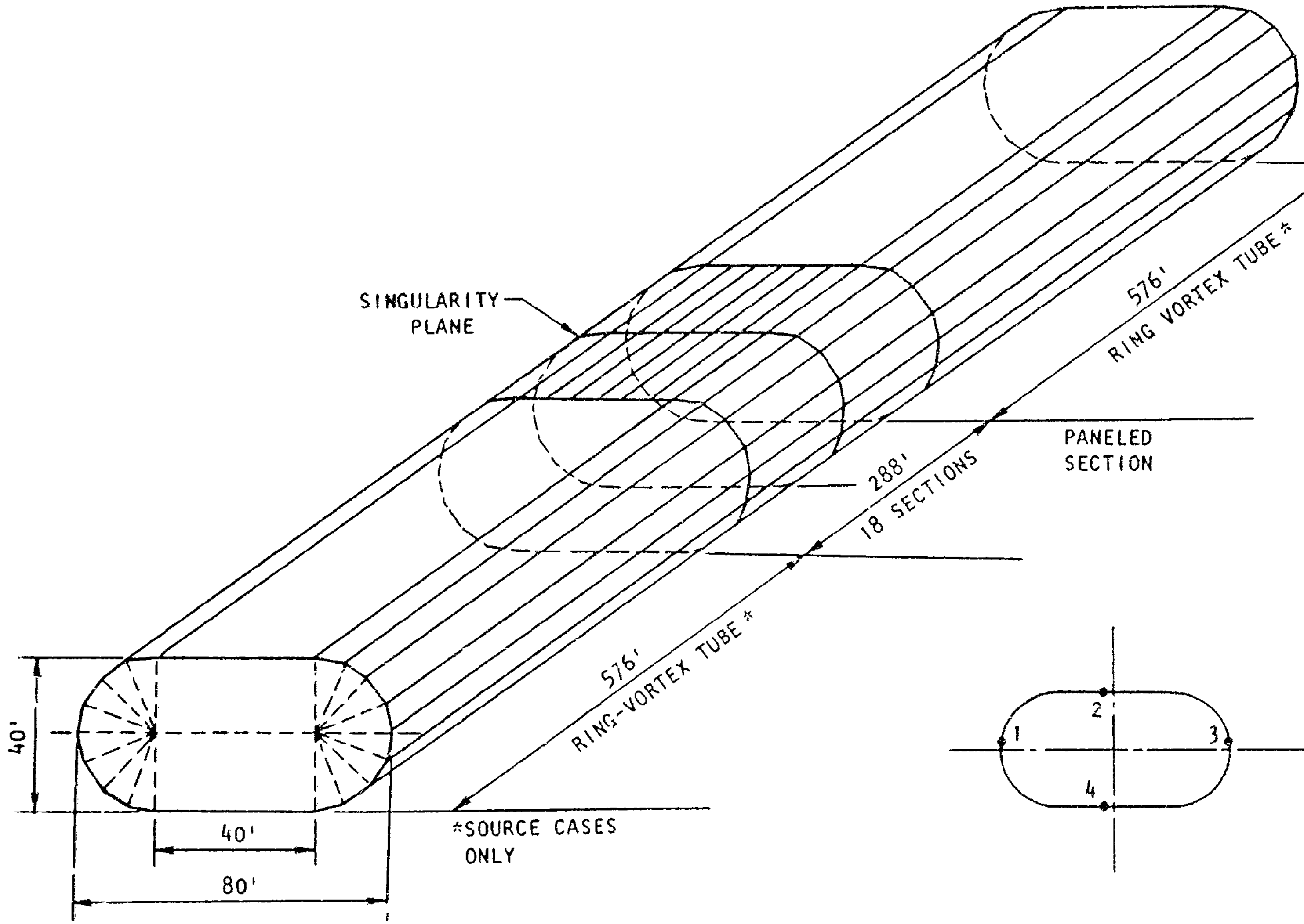

Figure A4.1 Flow model for representing the 40 x 80-foot wind tunnel.

ORIGINAL PAGE IS
OF POOR QUALITY

SOURCE SPANS

x/B	b=0.05B	b=0.10B	b=0.20B	b=0.40B	b=0.60B	b=0.70B
-1.0000	0.99999E-03	0.99999E-03	0.99999E-03	0.99999E-03	0.99999E-03	0.99999E-03
-0.8000	0.40700E-02	0.40700E-02	0.38600E-02	0.32500E-02	0.22200E-02	0.17100E-02
-0.6000	0.16230E-01	0.16120E-01	0.15200E-01	0.12020E-01	0.72200E-02	0.45700E-02
-0.4000	0.60580E-01	0.59860E-01	0.56980E-01	0.45610E-01	0.27310E-01	0.16500E-01
-0.2000	0.14812E+00	0.19677E+00	0.19122E+00	0.16636E+00	0.11470E+00	0.74100E-01
0.0000	0.50000E+00	0.50000E+00	0.50000E+00	0.50000E+00	0.50000E+00	0.50000E+00
0.2000	0.85188E+00	0.80323E+00	0.80878E+00	0.83364E+00	0.88530E+00	0.92590E+00
0.4000	0.93942E+00	0.94014E+00	0.94302E+00	0.95439E+00	0.97269E+00	0.98350E+00
0.6000	0.98377E+00	0.98388E+00	0.98480E+00	0.98798E+00	0.99278E+00	0.99543E+00
0.8000	0.99593E+00	0.99593E+00	0.99614E+00	0.99675E+00	0.99778E+00	0.99829E+00
1.0000	0.99900E+00	0.99900E+00	0.99900E+00	0.99900E+00	0.99900E+00	0.99900E+00

Table shows $\Delta u/U_\infty$ at sidewall for $Q/(U_\infty C) = 1.0$

TABLE A4/1A Tunnel-sidewall influence coefficients for horizontal line sources in the 40' x 80' tunnel.

SOURCE SPANS

x/B	b=0.05B	b=0.10B	b=0.20B	b=0.40B	b=0.60B	b=0.70B
-1.0000	0.28944E-01	0.28916E-01	0.28800E-01	0.28315E-01	0.27617E-01	0.27474E-01
-0.9000	0.32965E-01	0.32928E-01	0.32801E-01	0.32253E-01	0.31435E-01	0.31194E-01
-0.8000	0.38835E-01	0.38796E-01	0.38659E-01	0.38067E-01	0.37128E-01	0.36795E-01
-0.7000	0.50583E-01	0.50545E-01	0.50421E-01	0.49845E-01	0.48846E-01	0.48425E-01
-0.6000	0.66292E-01	0.66274E-01	0.66189E-01	0.65744E-01	0.64817E-01	0.64383E-01
-0.5000	0.91670E-01	0.91670E-01	0.91700E-01	0.91585E-01	0.90990E-01	0.90645E-01
-0.4000	0.12742E+00	0.12747E+00	0.12766E+00	0.12815E+00	0.12820E+00	0.12809E+00
-0.3000	0.18292E+00	0.18304E+00	0.18345E+00	0.18466E+00	0.18558E+00	0.18584E+00
-0.2000	0.26195E+00	0.26209E+00	0.26262E+00	0.26429E+00	0.26583E+00	0.26640E+00
-0.1000	0.37299E+00	0.37308E+00	0.37342E+00	0.37446E+00	0.37546E+00	0.37582E+00
0.0000	0.50000E+00	0.50000E+00	0.50000E+00	0.50000E+00	0.50000E+00	0.50000E+00
0.1000	0.62701E+00	0.62692E+00	0.62658E+00	0.62554E+00	0.62454E+00	0.62418E+00
0.2000	0.73805E+00	0.73791E+00	0.73738E+00	0.73571E+00	0.73417E+00	0.73360E+00
0.3000	0.81708E+00	0.81696E+00	0.81655E+00	0.81534E+00	0.81442E+00	0.81416E+00
0.4000	0.87258E+00	0.87253E+00	0.87234E+00	0.87186E+00	0.87180E+00	0.87191E+00
0.5000	0.90833E+00	0.90833E+00	0.90830E+00	0.90842E+00	0.90901E+00	0.90935E+00
0.6000	0.93371E+00	0.93373E+00	0.93381E+00	0.93426E+00	0.93518E+00	0.93562E+00
0.7000	0.94942E+00	0.94946E+00	0.94958E+00	0.95016E+00	0.95115E+00	0.95157E+00
0.8000	0.96117E+00	0.96120E+00	0.96134E+00	0.96193E+00	0.96287E+00	0.96320E+00
0.9000	0.96703E+00	0.96707E+00	0.96720E+00	0.96775E+00	0.96857E+00	0.96881E+00
1.0000	0.97106E+00	0.97108E+00	0.97120E+00	0.97168E+00	0.97238E+00	0.97253E+00

Table shows interference $\Delta u/U_\infty$, at model centerline, for $Q/(U_\infty C) = 1.0$

TABLE A4/1B Model-center interference coefficients for horizontal line sources in the 40' x 80' tunnel.

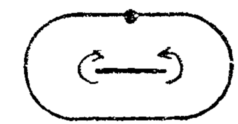

BOUND VORTEX SPANS

x/B	b=0.05B	b=0.10B	b=0.20B	b=0.40B	b=0.60B	b=0.70B
-1.0000	-0.13000E-03	-0.13000E-03	-0.13000E-03	-0.12499E-03	-0.79989E-04	-0.59992E-04
-0.8000	0.21500E-02	0.21450E-02	0.21200E-02	0.20500E-02	0.19950E-02	0.19550E-02
-0.6000	0.11855E-01	0.11810E-01	0.11650E-01	0.11100E-01	0.10400E-01	0.10010E-01
-0.4000	0.53330E-01	0.53045E-01	0.51930E-01	0.48135E-01	0.43415E-01	0.41010E-01
-0.2000	0.22515E+00	0.22297E+00	0.21475E+00	0.18880E+00	0.16059E+00	0.14785E+00
0.0000	0.49003E+00	0.48946E+00	0.46523E+00	0.39300E+00	0.32164E+00	0.29162E+00
0.2000	0.22515E+00	0.22297E+00	0.21475E+00	0.18880E+00	0.16059E+00	0.14785E+00
0.4000	0.53330E-01	0.53045E-01	0.51930E-01	0.48135E-01	0.43415E-01	0.41010E-01
0.6000	0.11855E-01	0.11810E-01	0.11650E-01	0.11100E-01	0.10400E-01	0.10010E-01
0.8000	0.21500E-02	0.21450E-02	0.21200E-02	0.20500E-02	0.19950E-02	0.19550E-02
1.0000	-0.13000E-03	-0.13000E-03	-0.13000E-03	-0.12499E-03	-0.79989E-04	-0.59992E-04

Table shows $\Delta u/U_\infty$ at roof for $\Gamma/(U_\infty C/b) = 0.50$
(Floor values have opposite signs)

TABLE A4/2A Tunnel roof influence coefficients for horizontal horseshoe vortices in the 40' x 80' tunnel.

BOUND VORTEX SPANS

x/B	b=0.05B	b=0.10B	b=0.20B	b=0.40B	b=0.60B	b=0.70B
-1.0000	-0.80465E-02	-0.80435E-02	-0.80330E-02	-0.79900E-02	-0.79205E-02	-0.78775E-02
-0.9000	-0.93465E-02	-0.93430E-02	-0.93300E-02	-0.92770E-02	-0.91915E-02	-0.91380E-02
-0.8000	-0.10708E-01	-0.10704E-01	-0.10690E-01	-0.10630E-01	-0.10531E-01	-0.10470E-01
-0.7000	-0.11900E-01	-0.11897E-01	-0.11884E-01	-0.11830E-01	-0.11734E-01	-0.11674E-01
-0.6000	-0.12322E-01	-0.12322E-01	-0.12323E-01	-0.12315E-01	-0.12276E-01	-0.12246E-01
-0.5000	-0.10861E-01	-0.10873E-01	-0.10918E-01	-0.11062E-01	-0.11214E-01	-0.11286E-01
-0.4000	-0.51910E-02	-0.52345E-02	-0.54015E-02	-0.59635E-02	-0.66390E-02	-0.69805E-02
-0.3000	0.79705E-02	0.78525E-02	0.73990E-02	0.58615E-02	0.39880E-02	0.30470E-02
-0.2000	0.33521E-01	0.33247E-01	0.32197E-01	0.28640E-01	0.24334E-01	0.22207E-01
-0.1000	0.72295E-01	0.71769E-01	0.69755E-01	0.62960E-01	0.54819E-01	0.50858E-01
0.0000	0.12410E+00	0.12321E+00	0.11981E+00	0.10838E+00	0.94844E-01	0.88347E-01
0.1000	0.17592E+00	0.17466E+00	0.16986E+00	0.15380E+00	0.13487E+00	0.12584E+00
0.2000	0.21469E+00	0.21318E+00	0.20741E+00	0.18811E+00	0.16535E+00	0.15449E+00
0.3000	0.24024E+00	0.23857E+00	0.23221E+00	0.21089E+00	0.18570E+00	0.17365E+00
0.4000	0.25339E+00	0.25165E+00	0.24501E+00	0.22271E+00	0.19632E+00	0.18367E+00
0.5000	0.25906E+00	0.25729E+00	0.25052E+00	0.22781E+00	0.20089E+00	0.18797E+00
0.6000	0.26049E+00	0.25871E+00	0.25190E+00	0.22903E+00	0.20193E+00	0.18890E+00
0.7000	0.26003E+00	0.25825E+00	0.25142E+00	0.22851E+00	0.20135E+00	0.18829E+00
0.8000	0.25874E+00	0.25695E+00	0.25012E+00	0.22721E+00	0.20004E+00	0.18699E+00
0.9000	0.25719E+00	0.25541E+00	0.24858E+00	0.22568E+00	0.19853E+00	0.18548E+00
1.0000	0.25550E+00	0.25371E+00	0.24689E+00	0.22400E+00	0.19687E+00	0.18384E+00

Table shows interference $\Delta w/U_\infty$, at model centerline, for $\Gamma/(U_\infty C/b) = 0.50$
(Values are the same as conventionally-defined δ)

TABLE A4/2B Model-center interference coefficients for horizontal horseshoe vortices in 40' x 80' tunnel.

ORIGINAL PAGE IS
OF POOR QUALITY

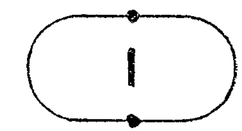

SOURCE SPANS

x/B	b = 0.05H	b = 0.10H	b = 0.20H	b = 0.40H	b = 0.60H	b = 0.70H
-1.0000	0.99999E-03	0.99999E-03	0.99999E-03	0.99999E-03	0.99999E-03	0.99999E-03
-0.8000	-0.16000E-02	-0.15000E-02	-0.16000E-02	-0.17000E-02	-0.16000E-02	-0.15000E-02
-0.6000	-0.11200E-01	-0.11100E-01	-0.11200E-01	-0.11300E-01	-0.11300E-01	-0.11000E-01
-0.4000	-0.42900E-01	-0.43100E-01	-0.43700E-01	-0.45900E-01	-0.48400E-01	-0.49000E-01
-0.2000	-0.72500E-01	-0.74300E-01	-0.81700E-01	-0.11140E+00	-0.15730E+00	-0.18180E+00
0.0000	0.50000E+00	0.50000E+00	0.50000E+00	0.50000E+00	0.50000E+00	0.50000E+00
0.2000	0.10725E+01	0.10743E+01	0.10817E+01	0.11114E+01	0.11573E+01	0.11818E+01
0.4000	0.10429E+01	0.10431E+01	0.10437E+01	0.10459E+01	0.10484E+01	0.10490E+01
0.6000	0.10112E+01	0.10111E+01	0.10112E+01	0.10113E+01	0.10113E+01	0.10110E+01
0.8000	0.10016E+01	0.10015E+01	0.10016E+01	0.10017E+01	0.10016E+01	0.10015E+01
1.0000	0.99900E+00	0.99900E+00	0.99900E+00	0.99900E+00	0.99900E+00	0.99900E+00

Table shows $\Delta u/U_\infty$ at "sidewall" for $Q/(U_\infty C) = 1.0$

TABLE A4/3A Tunnel roof influence coefficients for vertical line sources in the 40' x 80' tunnel.

SOURCE SPANS

x/B	b = 0.05H	b = 0.10H	b = 0.20H	b = 0.40H	b = 0.60H	b = 0.70H
-1.0000	[illegible]	0.28977E-01	0.24054E-01	0.29523E-01	0.31210E-01	0.33294E-01
-0.9000	0.32972E-01	0.32989E-01	0.33046E-01	0.33445E-01	0.35030E-01	0.37055E-01
-0.8000	[illegible]	0.38846E-01	0.38674E-01	0.39164E-01	0.40588E-01	0.42527E-01
-0.7000	[illegible]	0.50575E-01	0.50552E-01	0.50647E-01	0.51772E-01	0.53572E-01
-0.6000	[illegible]	0.66254E-01	0.60135E-01	0.65393E-01	0.66519E-01	0.68034E-01
-0.5000	[illegible]	0.91570E-01	0.91315E-01	0.90475E-01	0.90200E-01	0.91225E-01
-0.4000	[illegible]	0.12723E+00	0.12673E+00	0.12497E+00	0.12328E+00	0.12348E+00
-0.3000	[illegible]	0.18262E+00	0.18185E+00	0.17396E+00	0.17540E+00	0.17446E+00
-0.2000	[illegible]	0.26160E+00	0.26073E+00	0.25738E+00	0.25291E+00	0.25128E+00
-0.1000	0.37297E+00	0.37278E+00	0.37222E+00	0.37010E+00	0.36722E+00	0.36608E+00
0.0000	[illegible]	0.50000E+00	0.50000E+00	0.50000E+00	0.50000E+00	0.50000E+00
0.1000	[illegible]	0.62722E+00	0.62778E+00	0.62990E+00	0.63278E+00	0.63393E+00
0.2000	[illegible]	0.73840E+00	0.73927E+00	0.74262E+00	0.74709E+00	0.74872E+00
0.3000	[illegible]	0.81738E+00	0.81815E+00	0.82104E+00	0.82460E+00	0.82552E+00
0.4000	[illegible]	0.87277E+00	0.87327E+00	0.87503E+00	0.87672E+00	0.87652E+00
0.5000	[illegible]	0.90843E+00	0.90869E+00	0.90753E+00	0.90980E+00	0.90878E+00
0.6000	[illegible]	0.93375E+00	0.93367E+00	0.93411E+00	0.93348E+00	0.93197E+00
0.7000	[illegible]	0.94942E+00	0.94945E+00	0.94436E+00	0.94823E+00	0.94643E+00
0.8000	[illegible]	0.96115E+00	0.96113E+00	0.96084E+00	0.95941E+00	0.95747E+00
0.9000	[illegible]	0.96701E+00	0.96695E+00	0.96655E+00	0.96497E+00	0.96295E+00
1.0000	[illegible]	0.97102E+00	0.97095E+00	0.97048E+00	0.96879E+00	0.96671E+00

Table shows Interference $\Delta u/U_\infty$, at model centerline, for $Q/(U_\infty C) = 1.0$

TABLE A4/3B Model-center interference coefficients for vertical line sources in the 40' x 80' tunnel.

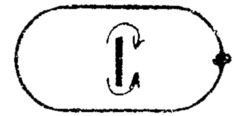

BOUND VORTEX SPANS

x/B	b = 0.05H	b = 0.10H	b = 0.20H	b = 0.40H	b = 0.60H	b = 0.70H
-1.0000	0.15050E-01	0.15050E-01	0.15040E-01	0.15005E-01	0.14960E-01	0.14950E-01
-0.8000	0.30875E-01	0.30875E-01	0.30860E-01	0.30800E-01	0.30715E-01	0.30700E-01
-0.6000	0.62030E-01	0.62025E-01	0.61990E-01	0.61860E-01	0.61685E-01	0.61650E-01
-0.4000	0.11919E+00	0.11917E+00	0.11908E+00	0.11878E+00	0.11836E+00	0.11824E+00
-0.2000	0.20101E+00	0.20096E+00	0.20076E+00	0.20004E+00	0.19905E+00	0.19871E+00
0.0000	0.24906E+00	0.24900E+00	0.24871E+00	0.24767E+00	0.24629E+00	0.24582E+00
0.2000	0.20101E+00	0.20096E+00	0.20076E+00	0.20004E+00	0.19905E+00	0.19871E+00
0.4000	0.11919E+00	0.11917E+00	0.11908E+00	0.11878E+00	0.11836E+00	0.11824E+00
0.6000	0.62030E-01	0.62025E-01	0.61990E-01	0.61860E-01	0.61685E-01	0.61650E-01
0.8000	0.30875E-01	0.30875E-01	0.30860E-01	0.30800E-01	0.30715E-01	0.30700E-01
1.0000	0.15050E-01	0.15050E-01	0.15040E-01	0.15005E-01	0.14960E-01	0.14950E-01

Table shows $\Delta u/U_\infty$ at "roof" for $\Gamma/(U_\infty C/b) = 0.50$
(Floor values have opposite signs)

TABLE A4/4A Tunnel sidewall influence coefficients for vertical horseshoe vortices in the 40' x 80' tunnel.

BOUND VORTEX SPANS

x/B	b=0.05H	b=0.10H	b=0.20H	b=0.40H	b=0.60H	b=0.70H
-1.0000	0.59175E-02	0.59175E-02	0.59160E-02	0.59110E-02	0.59080E-02	0.59200E-02
-0.9000	0.10079E-01	0.10079E-01	0.10078E-01	0.10072E-01	0.10071E-01	0.10089E-01
-0.8000	0.16100E-01	0.16100E-01	0.16099E-01	0.16096E-01	0.16100E-01	0.16131E-01
-0.7000	0.24666E-01	0.24666E-01	0.24668E-01	0.24674E-01	0.24699E-01	0.24753E-01
-0.6000	0.36706E-01	0.36708E-01	0.36716E-01	0.36750E-01	0.36825E-01	0.36929E-01
-0.5000	0.53307E-01	0.53314E-01	0.53340E-01	0.53446E-01	0.53646E-01	0.53852E-01
-0.4000	0.75781E-01	0.75799E-01	0.75868E-01	0.76145E-01	0.76639E-01	0.77068E-01
-0.3000	0.10526E+00	0.10531E+00	0.10547E+00	0.10613E+00	0.10728E+00	0.10819E+00
-0.2000	0.14250E+00	0.14259E+00	0.14293E+00	0.14435E+00	0.14684E+00	0.14876E+00
-0.1000	0.18657E+00	0.18673E+00	0.18739E+00	0.19009E+00	0.19499E+00	0.19880E+00
0.0000	0.23521E+00	0.23548E+00	0.23657E+00	0.24110E+00	0.24960E+00	0.25632E+00
0.1000	0.28378E+00	0.28415E+00	0.28567E+00	0.29204E+00	0.30412E+00	0.31376E+00
0.2000	0.32760E+00	0.32805E+00	0.32988E+00	0.33753E+00	0.35202E+00	0.36355E+00
0.3000	0.36440E+00	0.36490E+00	0.36690E+00	0.37531E+00	0.39114E+00	0.40367E+00
0.4000	0.39319E+00	0.39371E+00	0.39581E+00	0.40459E+00	0.42107E+00	0.43407E+00
0.5000	0.41465E+00	0.41518E+00	0.41732E+00	0.42626E+00	0.44302E+00	0.45623E+00
0.6000	0.42976E+00	0.43029E+00	0.43245E+00	0.44146E+00	0.45832E+00	0.47162E+00
0.7000	0.43967E+00	0.44020E+00	0.44236E+00	0.45138E+00	0.46826E+00	0.48158E+00
0.8000	0.44518E+00	0.44572E+00	0.44787E+00	0.45688E+00	0.47373E+00	0.48704E+00
0.9000	0.44686E+00	0.44740E+00	0.44954E+00	0.45851E+00	0.47531E+00	0.48858E+00
1.0000	0.44485E+00	0.44537E+00	0.44751E+00	0.45643E+00	0.47313E+00	0.48634E+00

Table shows interference $\Delta w/U_\infty$, at model centerline, for $\Gamma/(U_\infty C/b) = 0.50$
(Values are the same as conventionally-defined δ)

TABLE A4/4B Model-center interference coefficients for vertical horseshoe vortices in the 40' x 80' tunnel.

ORIGINAL PAGE IS
OF POOR QUALITY

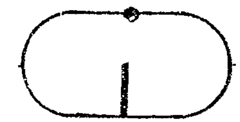

SOURCE SPANS

x/B	b=0.05H	b=0.10H	b=0.20H	b=0.40H	b=0.60H	b=0.70H
-1.0000	0.19136E-03	0.19136E-03	0.19181E-03	0.19211E-03	0.19211E-03	0.23898E-03
-0.8000	0.77981E-02	0.77057E-02	0.74677E-02	0.65588E-02	0.53260E-02	0.46591E-02
-0.6000	0.21351E-01	0.21068E-01	0.19920E-01	0.15639E-01	0.93170E-02	0.58498E-02
-0.4000	0.63769E-01	0.62770E-01	0.58860E-01	0.43251E-01	0.17584E-01	0.20927E-02
-0.2000	0.20200E+00	0.20015E+00	0.19254E+00	0.15778E+00	0.81982E-01	0.19307E-01
0.0000	0.50000E+00	0.50000E+00	0.50000E+00	0.50000E+00	0.50000E+00	0.50000E+00
0.2000	0.79800E+00	0.79985E+00	0.80746E+00	0.84222E+00	0.91802E+00	0.98069E+00
0.4000	0.93623E+00	0.93723E+00	0.94114E+00	0.95675E+00	0.98242E+00	0.99791E+00
0.6000	0.97665E+00	0.97893E+00	0.98008E+00	0.98436E+00	0.99068E+00	0.99415E+00
0.8000	0.99220E+00	0.99229E+00	0.99253E+00	0.99344E+00	0.99467E+00	0.99534E+00
1.0000	0.99981E+00	0.99981E+00	0.99981E+00	0.99981E+00	0.99981E+00	0.99976E+00

Table shows $\Delta u/U_\infty$ at sidewall for $Q/(U_\infty C) = 1.0$

TABLE A4/5A Tunnel roof influence coefficients for vertical, half-model line sources in the 40' x 80' tunnel.

SOURCE SPANS

x/B	b=0.05H	b=0.10H	b=0.20H	b=0.40H	b=0.60H	b=0.70H
-1.0000	0.50000E-02	0.50000E-02	0.50000E-02	0.50000E-02	0.50000E-02	0.50055E-02
-0.9000	0.20189E-01	0.20178E-01	0.20112E-01	0.19892E-01	0.19510E-01	0.19259E-01
-0.8000	0.39741E-01	0.39712E-01	0.39589E-01	0.39099E-01	0.38243E-01	0.37688E-01
-0.7000	0.64960E-01	0.64940E-01	0.64750E-01	0.63958E-01	0.62572E-01	0.61647E-01
-0.6000	0.97130E-01	0.97072E-01	0.96812E-01	0.95732E-01	0.93799E-01	0.92478E-01
-0.5000	0.13796E+00	0.13789E+00	0.13758E+00	0.13630E+00	0.13389E+00	0.13218E+00
-0.4000	0.18868E+00	0.18880E+00	0.18850E+00	0.18714E+00	0.18446E+00	0.18250E+00
-0.3000	0.25134E+00	0.25127E+00	0.25099E+00	0.24977E+00	0.24718E+00	0.24521E+00
-0.2000	0.32539E+00	0.32535E+00	0.32515E+00	0.32423E+00	0.32218E+00	0.32057E+00
-0.1000	0.40982E+00	0.40960E+00	0.40970E+00	0.40920E+00	0.40805E+00	0.40712E+00
0.0000	0.50000E+00	0.50000E+00	0.50000E+00	0.50000E+00	0.50000E+00	0.50000E+00
0.1000	0.59018E+00	0.59020E+00	0.59030E+00	0.59080E+00	0.59195E+00	0.59288E+00
0.2000	0.67401E+00	0.67465E+00	0.67485E+00	0.67577E+00	0.67782E+00	0.67943E+00
0.3000	0.74866E+00	0.74873E+00	0.74901E+00	0.75023E+00	0.75282E+00	0.75479E+00
0.4000	0.81112E+00	0.81120E+00	0.81150E+00	0.81286E+00	0.81554E+00	0.81750E+00
0.5000	0.86204E+00	0.86211E+00	0.86242E+00	0.86370E+00	0.86611E+00	0.86782E+00
0.6000	0.90287E+00	0.90293E+00	0.90319E+00	0.90427E+00	0.90620E+00	0.90752E+00
0.7000	0.93502E+00	0.93506E+00	0.93525E+00	0.93604E+00	0.93743E+00	0.93835E+00
0.8000	0.96026E+00	0.96029E+00	0.96041E+00	0.96090E+00	0.96176E+00	0.96231E+00
0.9000	0.97961E+00	0.97982E+00	0.97989E+00	0.98011E+00	0.98049E+00	0.98074E+00
1.0000	0.99500E+00	0.99500E+00	0.99500E+00	0.99500E+00	0.99500E+00	0.99499E+00

Table shows interference $\Delta u/U_\infty$, at model centerline, for $Q/(U_\infty C) = 1.0$

TABLE A4/5B Model center interference coefficients for vertical, half-model line sources in the 40' x 80' tunnel.

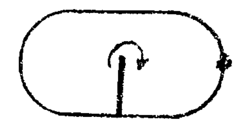

BOUND VORTEX SPANS

x/B	b=0.05H	b=0.10H	b=0.20H	b=0.40H	b=0.60H	b=0.70H
-1.0000	0.13105E-01	0.13120E-01	0.13165E-01	0.13250E-01	0.13260E-01	0.13235E-01
-0.8000	0.28565E-01	0.28585E-01	0.28660E-01	0.28795E-01	0.28800E-01	0.28750E-01
-0.6000	0.59765E-01	0.59600E-01	0.59915E-01	0.60100E-01	0.60005E-01	0.59845E-01
-0.4000	0.11851E+00	0.11857E+00	0.11874E+00	0.11890E+00	0.11835E+00	0.11780E+00
-0.2000	0.20439E+00	0.20449E+00	0.20480E+00	0.20488E+00	0.20323E+00	0.20172E+00
0.0000	0.25552E+00	0.25565E+00	0.25605E+00	0.25607E+00	0.25350E+00	0.25120E+00
0.2000	0.20439E+00	0.20449E+00	0.20480E+00	0.20488E+00	0.20323E+00	0.20172E+00
0.4000	0.11851E+00	0.11857E+00	0.11874E+00	0.11890E+00	0.11835E+00	0.11780E+00
0.6000	0.59765E-01	0.59600E-01	0.59915E-01	0.60100E-01	0.60005E-01	0.59845E-01
0.8000	0.28565E-01	0.28585E-01	0.28660E-01	0.28795E-01	0.28800E-01	0.28750E-01
1.0000	0.13105E-01	0.13120E-01	0.13165E-01	0.13250E-01	0.13260E-01	0.13235E-01

Table shows $\Delta u/U_\infty$ at roof for $\Gamma/(U_\infty C/b) = 0.50$
(Floor values have opposite signs)

TABLE A4/6A Tunnel sidewall influence coefficients for vertical, half-model horseshoe vortices in the 40' x 80' tunnel.

BOUND VORTEX SPANS

x/B	b=0.05H	b=0.10H	b=0.20H	b=0.40H	b=0.60H	b=0.70H
-1.0000	-0.34865E-02	-0.34745E-02	-0.34285E-02	-0.32720E-02	-0.30650E-02	-0.29500E-02
-0.9000	-0.15195E-02	-0.15015E-02	-0.14365E-02	-0.12190E-02	-0.93150E-03	-0.77200E-03
-0.8000	0.15875E-02	0.16115E-02	0.17015E-02	0.20050E-02	0.24050E-02	0.26280E-02
-0.7000	0.62490E-02	0.62820E-02	0.64070E-02	0.68265E-02	0.73810E-02	0.76930E-02
-0.6000	0.13006E-01	0.13052E-01	0.13221E-01	0.13791E-01	0.14550E-01	0.14984E-01
-0.5000	0.22483E-01	0.22543E-01	0.22768E-01	0.23519E-01	0.24532E-01	0.25124E-01
-0.4000	0.35396E-01	0.35474E-01	0.35758E-01	0.36702E-01	0.38001E-01	0.38787E-01
-0.3000	0.52368E-01	0.52459E-01	0.52795E-01	0.53899E-01	0.55469E-01	0.56472E-01
-0.2000	0.73772E-01	0.73871E-01	0.74231E-01	0.75401E-01	0.77158E-01	0.78376E-01
-0.1000	0.99055E-01	0.99152E-01	0.99501E-01	0.10061E+00	0.10243E+00	0.10384E+00
0.0000	0.12694E+00	0.12702E+00	0.12731E+00	0.12822E+00	0.12998E+00	0.13155E+00
0.1000	0.15475E+00	0.15483E+00	0.15508E+00	0.15578E+00	0.15747E+00	0.15920E+00
0.2000	0.17987E+00	0.17996E+00	0.18019E+00	0.18063E+00	0.18256E+00	0.18450E+00
0.3000	0.20102E+00	0.20110E+00	0.20136E+00	0.20205E+00	0.20398E+00	0.20611E+00
0.4000	0.21756E+00	0.21766E+00	0.21796E+00	0.21881E+00	0.22099E+00	0.22333E+00
0.5000	0.22984E+00	0.22995E+00	0.23031E+00	0.23133E+00	0.23378E+00	0.23629E+00
0.6000	0.23538E+00	0.23851E+00	0.23891E+00	0.24010E+00	0.24276E+00	0.24541E+00
0.7000	0.24360E+00	0.24393E+00	0.24438E+00	0.24568E+00	0.24850E+00	0.25124E+00
0.8000	0.24554E+00	0.24668E+00	0.24715E+00	0.24852E+00	0.25142E+00	0.25421E+00
0.9000	0.24697E+00	0.24705E+00	0.24753E+00	0.24892E+00	0.25184E+00	0.25462E+00
1.0000	0.24499E+00	0.24512E+00	0.24559E+00	0.24695E+00	0.24982E+00	0.25256E+00

Table shows interference $\Delta w/U_\infty$, at model centerline, for $\Gamma/(U_\infty C/b) = 0.50$
(Values are the same as conventionally-defined δ)

TABLE A4/6B Model center interference coefficients for vertical, half-model horseshoe vortices in the 40' x 80' tunnel.